The Role of Neural Stem Cells in Tumourigenesis of the Central Nervous System

---

A thesis submitted in partial fulfilment for the degree of Doctor of Philosophy to the University of London

by

Alexander George Swales BSc (Hons)

University College London

Declaration

I, Alexander George Swales, confirm that the work presented in this thesis is my own. Where information has been derived from other sources or the contributions of others are involved, I confirm that this has been indicated in the thesis.

Acknowledgements

I would like to extend my heartfelt thanks to Professor Sebastian Brandner for his role as both my supervisor and mentor. Without his tireless efforts, extraordinary knowledge base, and guidance, this project would not have been possible. Sincere thanks are also due to Heike Naumann, who was responsible for training me in the vast majority of my research techniques, as well as coordinating the day-to-day operation of a successful laboratory. I would also like to thank Dr. Nick Henriquez for his constant inspiration and advice, Dr. Tom Jacques for his co-supervision of the project, and the Wakefield Street Staff for helping me manage the animal colony. Special thanks are also due to Laura D'Castro for her comic relief and shared passion of the 4 o' clock frappuccino, Pedro Cuadrado for his morale support as my PhD buddy, Pela for trailblazing my PhD journey, Jane Ng for her always effervescent enthusiasm in my work, and my various housemates along the way with particular emphasis on Will for helping me find the hobbies that helped to distract me during my weekends.

I owe everything to my parents, without whose unyielding support for me to follow my dreams would have meant that I couldn't have afforded to do a PhD. My brother, for taking me out for the many dinner and casino trips that would have otherwise been utterly ridiculous ideas. And finally, I would like to pay the largest thanks to Kathy, without whose unconditional support in every aspect of my PhD, career, and general life would mean that I wouldn't be where I am today and I certainly wouldn't have enjoyed the journey as much as I have. I hope I have made you all proud.

Abstract

To develop targeted brain tumour therapies that carry fewer side effects it is essential to understand brain tumour histogeneiss and identify the cell of origin. It has been suggested that neoplastic transformation of neural stem/progenitor cells in the adult brain can result in the development of intrinsic brain tumours. Using the Cre-LoxP system we have developed a model that allows us to inactivate tumour suppressor genes Rb, p53 and PTEN in neural stem/progenitor cells both *in vivo* and *in vitro*.

In vivo recombination of these tumour suppressor genes in neural stem/progenitor cells resulted in the formation of intrinsic brain tumours, with the phenotype depending on the combination of recombined genes. Intracerebral engraftment of *in vitro* recombined neural stem/progenitor cells produced a similar tumour phenotype pattern. However, while *in vivo* recombination of Rb and p53 frequently caused brain tumours, *in vitro* recombined and engrafted $Rb^{-/-}$; $p53^{-/-}$ neurospheres rarely generated tumours. The converse was true following *in vivo* recombination of Rb and PTEN. These results suggest that microenvironment influences tumour formation.

An increased number of tumourigenic neural stem/progenitor cells expressed the cancer stem cell marker CD133 when compared to control cells. *In vivo* engraftment of purified CD133+ $Rb^{-/-}$; $p53^{-/-}$; $PTEN^{-/-}$ neural stem/progenitor cells resulted in the preferential development of gliomas. We also showed that astrocytes are not capable of forming tumours following either orthotopic recombination or *in vitro* recombination and engraftment.

In conclusion, we found that (i) certain phenotypes of brain tumours develop from neural stem/progenitor cells in the subventricular zone, (ii) the combination of inactivated tumour suppressor genes is the most significant but not sole determinant of *in vitro* functional profile and behaviour *in vivo*, (iii) the cellular microenvironment of neural stem/progenitor cells influences their tumourigenic profile, and (iv) terminally differentiated astrocytes do not contribute to tumour development in this model.

Table of Contents

Table of Figures

See appendix

Abbreviations

AML	acute myeloid leukemia
APC	adenomatous polyposis coli
AS	astrosphere
BCA	bicinchoninic acid
BMP	bone morphogenetic protein
BSA	bovine serum albumin
BTIC	brain tumour initiating cell
CNS	central nervous system
CSC	cancer stem cell
DAPI	4',6-diamidino-2-phenylindole
DMEM	Dulbecco's Modified Eagle Medium
EDTA	ethylenediaminetetraacetic acid
EGF	epidermal growth factor
ES	embryonic stem
FACS	fluorescence-activated cell sorting
FCS	fetal calf serum
FGF	fibroblast growth factor
GBM	glioblastoma
GFAP	glial fibrillary acidic protein
GFP	green fluorescent protein
GIC	glioma initiating cell
HIF	hypoxia-inducible factor
i.c.	intracerebral

i.c.v.	intra-cerebroventricular
IGL	internal granular layer
IHC	immunohistochemistry
LIF	leukemia inhibitory factor
LOH	loss of heterozygosity
LSM	confocal laser scanning microscopy
LV	lateral ventricles
MACS	magnetic-activated cell sorting
NSC	neural stem cell
NSCC	neural stem cell compartment
NS	neurosphere
PBS	phosphate buffered saline
PI	protease inhibitor
PNET	primitive neuroectodermal tumour
PTEN	phosphatase and tensin homologue
Rb	retinoblastoma
RIPA	radio immuno precipitation assay (buffer)
RMS	rostral migratory stream
ROS	reactive oxygen species
RT-PCR	reverse transcription polymerase chain reaction
SCZ	subcallosal zone
SGZ	subgranular zone
STAT	signal transducer and activator of transcription
SVC	subventricular zone
TGF	transforming growth factor
TSG	tumour suppressor gene
WHO	world health organisation

1 Introduction

Cancers of the central nervous system (CNS) globally account for 189,000 new cases and 142,000 deaths annually. These figures represent 1.7% of all new cancer cases and 2.1% of the total number of cancer deaths (Parkin et al., 2005). Despite these relatively low percentages, they carry a disproportionate and devastating level of morbidity and mortality. To put this into perspective, around 43,800 new brain tumour cases are diagnosed in the United States every year, and one in four of these patients will die (Buckner et al., 2007). The incidence of brain tumours in the United States is 14.8 per 100,000 person-years, and is increasing year on year (Central Brain Tumor Registry of the United States, 2006). Malignant primary brain tumours remain the leading cause of death from solid tumours in children, and the third leading cause of death from cancer in adolescents (Jemal et al., 2007). Cancer Research UK estimates that in 2005 in the United Kingdom there were around 3500 deaths from brain tumours, which accounted for 2% of all cancer deaths (Office for national statistics UK, 2008). Brain tumours are estimated to represent 1.4% of all cancers, 2.4% of all cancer deaths, ~20% of paediatric cancers, and are the commonest tumour-related cause of death in children. In addition to this, the tumour incidence is increasing by 2.7% per year in UK children (Office for national statistics UK, 2008). The survival rate in UK children is 60%, and although there is no specific clinical symptom or sign for brain tumours, slowly progressive focal neurologic signs and signs of elevated intracranial pressure can be symptomatic (Clark et al., 1985).

Brain tumours represent the most common form of solid malignancy in children and due to often innocuous sub-clinical symptoms, difficulties in diagnosis, limited treatment options, unpredictable treatment efficacy, and tumour recurrence, they remain a major cause of morbidity and mortality in adults. Despite the variation between the different tumour phenotypes they are generally extremely difficult to treat and their diagnosis often carries a poor prognosis. This is due in part to their ability to grow insidiously and diffusely throughout the brain parenchyma and to the fact they often clinically present with non-specific symptoms. The most common malignant brain tumour is glioblastoma (WHO grade IV glioma), which also accounts for 40% of all primary malignant CNS tumours (Miller and Perry, 2007). Glioblastoma patients have a median survival rate of approximately 12 months (Laks et al., 2010) despite aggressive surgical resection, chemotherapy and local radiotherapy (Krex et al., 2007; Smith and Jenkins, 2000). In order to develop effective therapeutic treatment regimens it is important to identify the

"cell of origin" from which brain tumours arise, and to define the cellular and molecular events that occur during tumourigenesis. Despite detailed genetic and morphological studies, the cell of origin of most CNS tumours is not known or has been previously assumed based on indirect inferences such as anatomical location. The differentiation stage at which a cell undergoes transformation may have important implications for the phenotype of brain tumours and it may also give important clues about the histogenesis and molecular pathogenesis of the tumours. It remains unclear as to whether brain tumour phenotype is influenced more greatly by the combination of genetic mutations a neoplastic cell contains or by the type of cell in which these mutations occur. Only a small number of models have been established in which early stages of tumourigenesis can be studied, and for which the histogenesis of brain tumours has been described.

To this end, we developed a mouse model that allows us to conditionally knock-out different combinations of the tumour suppressor genes (TSGs) Rb, p53, and PTEN in a variety of cell types both *in vivo* and *in vitro* in the aim of generating tumour-initiating cells and characterising their functional profiles. This was achieved using the Cre-LoxP system through which Adenovirus-Cre-mediated recombination allowed us to study the downstream effects of conditionally knocking-out the different TSGs with regards to tumourigenesis.

1.0 Neurogenesis

Adult neurogenesis results in the production of new functional neurons in the adult brain, produced from asymmetric cell division of neural stem and progenitor cells. After such asymmetric division, various factors such as migration, differentiation, and the cellular expression profile determine the fate of the cell. Neurogenesis applies specifically to the production of new neurons but is a term that is often used to encompass the production of glia (gliogenesis) and oligodendrocytes (oligogenesis). The work of Peter Eriksson in 1998 dispelled the dogma surrounding the lack of credibility of adult neurogenesis when he reported and characterised the birth of new neurons within the hippocampus of adult humans (Eriksson et al., 1998). At the turn of the 21st century, the heightened interest in stem cell biology, coined by many as the "stem cell revolution", drove research into developmental neurobiology and brain plasticity. Neurogenesis is fundamental to both of these topics and hence the pioneering work of Altman and Eriksson was further validated throughout the first decade of the

21st century. Although the vast majority of pioneering research into neurogenesis studied the process *in vivo*, some groups perfected the ability to study it *in vitro* (Wichterle et al., 2002) by recapitulating and characterising the regulatory processes that drive embryonic stem cells toward a neuronal phenotype. Understanding neurogenesis not only provides us with insight into neuroplastic and stem cell disorders of the brain, it potentially paves the way towards understanding the ultimate therapeutic target of the brain in neuroregeneration.

The work of His, Cajal, and Spielmeyer had never alluded to the presence of precursor cells in the brain or the ability of neurons to divide. Hence, Altman's autoradiagraphical suggestions of neurogenesis in the 1960's were met with considerable scepticism (Altman, 1963). It took additional experiments by Altman, supplemented with electron microscopy data from Kaplan (Kaplan and Hinds, 1977) before the notion of neurogenesis began to gather momentum. Despite this, scepticism remained throughout the 1980's and until the late 1990's. As interest in stem cell research grew so did the level of unorthodox research, as demonstrated by the proposal of neural transdifferentiation (Anderson et al., 2001). This concept suggested that stem cells could cross organ and germ layer borders so that NSCs could in fact migrate and divide into non-CNS cells (i.e. non-region-specific pluripotency); a hypothesis that continues to be disputed.

To be considered neurogenic, a brain region must possess a) sufficient neural stem and progenitor cells from which new neuronal cells can develop, and b) a microenvironment conducive for neurogenesis. Confirmation of the second point was first achieved in the hippocampus and the olfactory system through verifying neurogenesis following *in vivo* implantation of neural precursor cells (Gage et al., 1995; Herrera et al., 1999; Lie et al., 2002). However, it should also be noted that neurogenesis has been observed in 'non-neurogenic' areas of the brain in response to damage, such as ischemic stroke (Arvidsson et al., 2002).

1.1 Brain Tumours

A brain tumour is any intracranial neoplasm created by abnormal and uncontrolled cell division. Primary brain tumours are derived from neural cells intrinsic to the brain (i.e. neurons, astrocytes, ependymal cells, oligodendrocytes and their progenitors), the brain envelopes (meninges), skull, pituitary or pineal gland, or even the from the portion of

cranial nerves that are myelinated by Schwann cells. Secondary brain tumours are those that have metastasised from cancers primarily located in other organs (Louis et al., 2007). Brain tumours are named and classified according to the cell type that the tumour mass most closely resembles. For example, most primary brain tumours share features with glial cells (globally termed 'gliomas') and can be further classified as astrocytomas, oligodendrogliomas, or ependymomas depending on the cell they most closely resemble (e.g. astrocytes, oligodendrocytes, or ependymal cells). There are also mixed forms with, for example, both an astrocytic and an oligodendroglial cellular resemblance (an oligoastrocytoma).

1.1.1 Classification of human brain neoplasms

In 2007, the World Health Organisation (WHO) published a collaborative classification of tumours of the nervous system (Louis et al., 2007). This classification provides histopathological, immunohistochemical, and anatomical criteria to classify and grade brain tumours and predict their biological behaviour thus allowing for a standardised means of diagnosis/prognosis. This WHO classification grades tumours based on their malignancy in a scale from I to IV (Louis et al., 2007; Kleihues et al., 1993). For example, grade I glioma lesions are generally benign tumours with a low proliferative potential and can typically be cured with surgical resection alone. Grade II gliomas also proliferate slowly but show abnormal nuclei (atypia) and in case of intrinsic tumours, often grow infiltrativey. These tumours tend to recur after surgical resection, often transforming to higher grades. Patients exhibiting grade II tumours typically survive for more than 5 years. Grade III gliomas show histological signs of malignancy including enhanced mitotic activity and nuclear atypia, with a median survival rate of 2-3 years. Grade IV gliomas are of the most malignant grade and are histologically defined by atypical nuclei, highly enhanced mitotic activity as well as necrosis and/or microvascular proliferation (Kleihues and Sobin, 2000). These tumours are rapidly fatal if untreated and the projected survival rate can be as little four months depending on the available treatment regimens (Louis et al., 2007).

The most common intrinsic tumours of the CNS are gliomas. They occur in a variety of different tumour forms ranging from grade I to IV (Daumasduport et al., 1988). Astrocytic tumours represent the most common form of glioma and comprise pilocytic astrocytoma (grade I), diffuse astrocytoma (grade II), anaplastic astrocytoma (grade III)

and glioblastoma (grade IV). Glioblastomas account for 12-15% of all intracranial neoplasms and 60-75% of all astrocytic tumours. They can arise *de novo* (95%) or from the malignant progression of a lower grade glioma (5%) (Ohgaki et al., 2004). The incidence rate in the USA is 2.96 new cases per 100,000 population per year and slightly higher in Europe with 3.55 new cases. Glioblastomas are highly infiltrative and completely resection risks serious brain damage. The same is true for grade II and III gliomas which are also diffusely infiltrative but just to a lesser extent.

Ependymomas (WHO grade I–III) are primarily composed of glial tumour cells but are distinct from gliomas. They are relatively rare (accounting for 2-9% of all neuroepithelial tumours) and typically occur within the posterior fossa in children under 4 years of age, while in adults they usually arise in the spinal canal. The five-year survival is 60%, however, the prognosis is much worse in children as the location is mostly intracranial (Auguste and Gupta, 2006).

Medulloblastoma (WHO grade IV) is the most common malignant brain tumour of childhood, affecting 1 in 200,000 children less than 15 years old (Central Brain Tumor Registry of the United States, 1995). Medulloblastomas are referred to as embryonal tumours as they are comprised of undifferentiated cells that amass to resemble embryonic brain structures. It typically arises in the cerebellum and has a tendency to metastasise along the craniospinal axis (but not systemically). There have been significant advances in the treatment of childhood medulloblastoma which have seen 5-year survival rise from 30% to 60-70% in recent years, but most patients suffer from severe long-term side effects (Central Brain Tumor Registry of the United States, 2005), mostly as a consequence of radiotherapy.

There has been progress (albeit limited) in the treatment of brain tumours over the last ten years, with the introduction of concomitant adjuvant temozolomide into the established chemo/radiotherapy treatment regimes being the most notable advancement in glioma treatment. And as a result, the overall 3 year survival rate of newly diagnosed glioblastoma patients has increased four-fold from ~4% to ~16% (Scott et al., 1998; Stupp et al., 2009). However, surgical resection in combination with chemotherapy and radiotherapy remains the mainstay for many types of brain tumour. And although such a treatment stragtegy may provide the patient with a period of clinical remittance, ranging from 5 years in the case of diffuse astrocytoma (grade II) to as little as 4 months in glioblastoma (grade IV), clinically progressive relapse remains inevitable in many cases. This issue highlights the high levels of morbidity and mortality associated with

brain tumours and the current socio-economic burden they place on the healthcare systems around the world as “the fourth greatest impacting cancer” (Royds and Iacopetta, 2006).

Hostorically, brain tumours were thought to derive from the neoplastic transformation of mature cell types such as astrocytes and oligodendrocytes. This was a result of the belief that the brain was a mitotically quiescent tissue with negligible neurogenesis. This model however failed to adequately explain the development of some tumours i.e. the mixed gliomas. There is now a growing body of evidence suggesting that brain tumours potentially originate from neoplastically transformed populations of stem/precursor cells that persist within the adult brain (Dirks, 2008; Zheng et al., 2008). This may ultimately explain why certain brain neoplasms show reproducible patterns of genetic mutations or why alterations in specific pathways are often associated with certain histological types of tumour.

1.2 Stem Cells

All of the organs in the body are primarily composed of terminally differentiated cells that perform specialised functions. These cells can stop functioning if they enter senescence or undergo apoptosis in response to stress. An homeostatic mechanism exists to regulate the replacement of these lost cells in order to maintain the functionality of the particular organ (Miller et al., 2005). This mechanism is governed by primitive progenitor cells, which are able to reproduce for the life of the organ. These cells can be characterised by several hallmark features: stem cells are (i) localised to specific niches capable of cell genesis, (ii) represent a very small subpopulation of cells within an organ, (iii) are undifferentiated and ultrastructurally unspecialised, (iv) are capable of self-renewal, (v) mostly multipotent (the ability to generate a diversity of differentiated cells), (vi) are slow cycling and divide infrequently, and (vii) have a proliferative capacity that exceeds the life of the organ (Miller et al., 2005).

Stem cells must maintain their own population in addition to those of the terminally differentiated cell type lineages (Watt and Hogan, 2000). This can be achieved through symmetrical (producing two clonal stem cells) or asymmetrical (producing one clonal stem cell and one daughter cell programmed to differentiate into a non-stem cell fate) cell division. Asymmetrical cell division allows stem cells to both self-renew and regulate the different cell populations of the stem cell niche. It involves the stepwise

generation of daughter cells that are progressively and irreversibly committed to differentiation along non-stem cell lineages. In a simplified model system, a stem cell will typically divide to produce two daughter cells, one of which will remain as a true stem cell in the stem cell niche, and the other may leave the niche as a more differentiated progenitor cell. This progenitor may not be capable of self-renewal but is highly proliferative and can undergo further reproductive divisions through which an exponentially increasing number of increasingly differentiated daughter cells can be generated (Figure 1). These daughter cells progressively lose their stem cell characteristics and acquire lineage-specific fates until they become terminally differentiated mature cells (Vescovi et al., 2006).

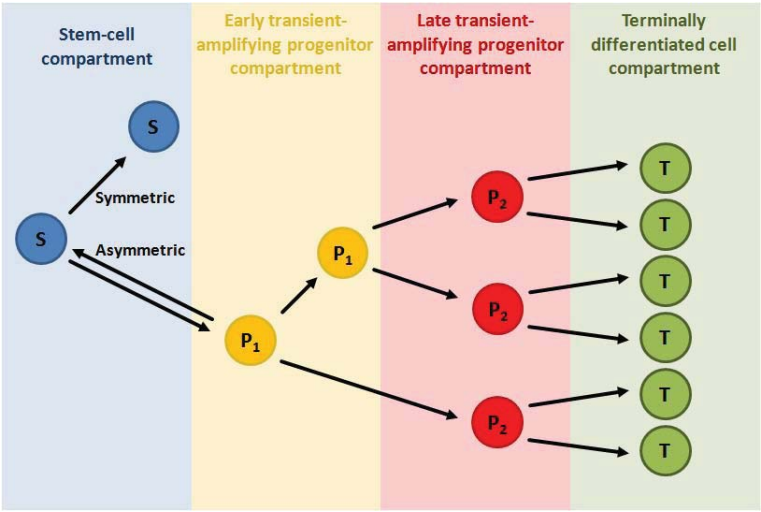

Figure 1: Stem cell compartment hierarchy. S: neural stem cell, P_1: early transient-amplifying progenitor cell, P_2: late transient-amplifying progenitor cell, T: terminally differentiated cell.

Mounting evidence suggests that extrinsic factors, such as microenvironment (e.g. growth factors), play a critical role in the regulation and coordination of asymmetrical stem cell division, rather than the intrinsic properties of the cells themselves (Alvarez-Buylla and Lim, 2004).

Embryonic stem (ES) cells are pluripotent (the ability to generate all the cells of the body) and exist within the inner cell mass of the blastocyst. ES cells can be propagated *in vitro* and would provide an excellent cellular model for human disease but their derivation from human embryos raises ethical concerns. However, the pluripotency of ES cells means that they can generate tumours containing cells of all three germ layers such as teratomas and teratocarcinomas *in vivo* (Reubinoff et al., 2000; Asano et al.,

2003). Neural precursor cells have been successfully generated from ES cells *in vitro* (Brustle et al., 1999; Lee et al., 2000; Zhang et al., 2001). These precursor cells behave like NSCs *in vivo* as they are capable of developing into functioning neurons and glia (Brustle et al., 1999). The restricted neural differentiation portfolio (e.g. neurons, glia, and oligodendrocytes) makes NSCs multipotent rather than pluripotent.

1.3 Neural Stem Cells

In recent times, the opinion over the regenerative capacity of the adult mammalian brain has changed dramatically. Historically the brain was thought of as an end-point in neurodevelopment whereby it was composed of postmitotic, fully differentiated cells. Although a few reports in the 1950s – 1970s described mitotic activity as a hypothetical measure of neurogenesis in the postnatal rodent brain (Messier et al., 1958; Altman and Das, 1965; Dacey and Wallace, 1974), it wasn't until the 1990's that it was convincingly proven that neurogenesis occurs in the adult brain of rats (Luskin, 1993; Lois and Alvarezbuylla, 1993), canaries (Alvarez-Buylla et al., 1998), monkeys (Gould et al., 1998), and humans (Kirschenbaum et al., 1994; Eriksson et al., 1998; Kukekov et al., 1999). The brain is therefore no more an exception to general rules governing most of the other adult tissues, where reservoirs of self-renewing and multipotent cells are involved in the generation and repair of differentiated cells (Merkle and Alvarez-Buylla, 2006).

Neural stem cells (NSCs) can be defined by their unlimited ability to self-renew and give rise to at least one identical copy of the mother cells and/or daughter cells that are more determined for a particular differentiation lineage (Weissman et al., 2001), and by their multipotency. NSCs properties can be investigated *in vitro* by growing them in non-adherent conditions in medium rich in mitogens such as EGF and FGF-II (Gritti et al., 1996; Gritti et al., 1999; Doetsch et al., 2002). An interesting property of NSCs when grown *in vitro* is their propoensity to grow as spherical aggregates, termed neurospheres (NS). NSCs can be serially passaged and upon the removal of growth factors NSCs they differentiate into neurons, astrocytes and oligodendrocytes. These respective self-renewal and multipotency capacities are the primary indicators that a cell possesses stem-like characteristics.

1.3.1 Anatomical location of neural stem cells in the adult brain

To date, five separate populations of NSCs have been characterised within the adult brain (Figure 2). They remain localised to specific regions, principally around the lateral ventricles (Alvarez-Buylla et al., 2002). The primary neural stem cell compartment (NSCC) is the subventricular zone (SVZ), a subependymal layer of cells (3-4 cells deep) that lines the walls of the lateral ventricles (Doetsch et al., 1999). The other germinal zones are located in the subcallosal zone (SCZ) between the corpus callosum and the hippocampus (Seri et al., 2006), the subgranular zone (SGZ) within the dentate gyrus of the hippocampus (Seri et al., 2001), between the internal granular layer (IGL) and the white matter of the cerebellum (Lee et al., 2005), and along the length of the rostral migratory stream (Pencea et al., 2001) (Figure 2).

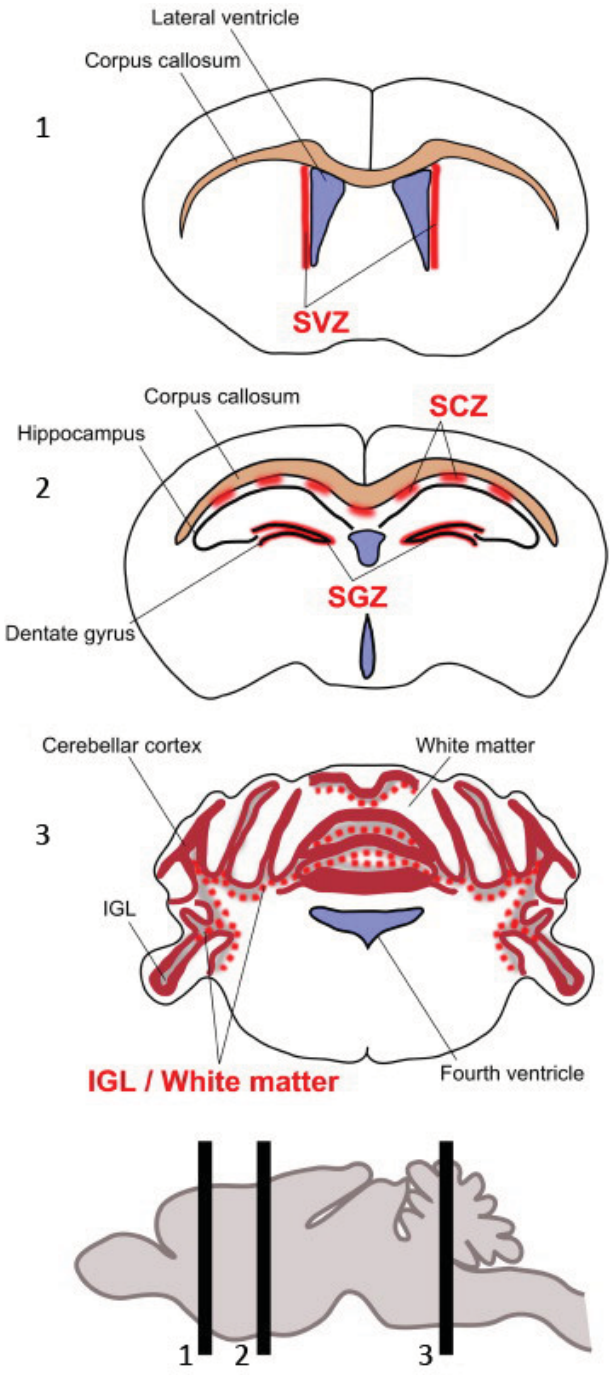

Figure 2: Anatomical location of NSCs in the adult mouse brain (adapted from (Sutter et al., 2007). (1) The subventricular zone (SVZ) of the rostral portion of the lateral ventricles. (2) The subcallosal zone (SCZ) found between the corpus callosum and the hippocampus, and the subgranular zone (SGZ) within the dentate gyrus of the hippocampus. (3) Between the internal granular layer (IGL) and the white matter of the cerebellum (red dots).

The largest of these areas is the SVZ (Figure 3) within which a structural hierarchy of NSC sub-classes has been characterised according to a proposed pinwheel architecture (Doetsch et al., 1999; Mirzadeh et al., 2008).

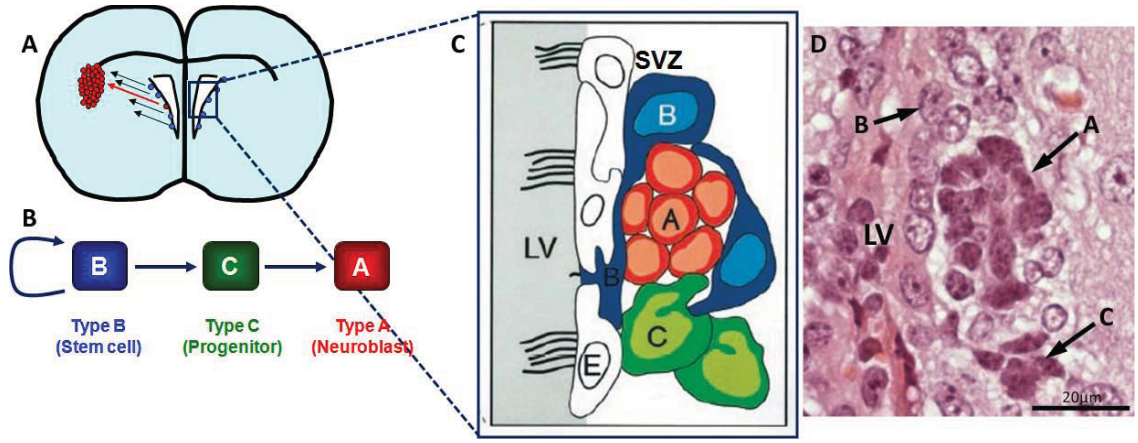

Figure 3: Hierarchical cellular organisation of the subventricular zone in the adult mouse. (A) Coronal cross-section of the mouse brain: NSCs (shown as blue circles) are located in the SVZ and can undergo neoplastic transformation resulting in the development of a brain tumour (shown as red circles). (B) Differentiation hierarchy of the NSC sub-classes within the SVZ. (C) Schematic representation of the spatial organisation of the NSC sub-classes within the SVZ (Alvarez-Buylla and Lim, 2004). (D) H&E stain of the wild-type mouse SVZ depicting the spatial organisation of the NSC sub-classes. H&E image was taken using a ColorView III digital camera mounted on a Zeiss Axioskop 2 MOT microscope with a 40x objective and using the AnalySIS software package. E: ependymal cells, A: Type A neuroblasts, B: Type B astrocytes, C: Type C transient-amplifying progenitor cells, LV: lateral ventricles.

The type B astrocytes represent the least differentiated form of NSC and are thought to be slow-growing, derived from radial glia (Merkle et al., 2004), and responsible for the generation of all neuroblasts and new neurons in the adult mouse forebrain (Denise et al., 2004). Although their specific origin remains unclear it has been postulated that they could originate from radial glial cells (Vescovi et al., 2006; Doetsch, 2003). These type B type cells divide slowly and can undergo asymmetric division to differentiate into highly proliferative transiently amplifying type C progenitor cells, which proliferate rapidly and can in turn can differentiate into type A young neuroblasts (Alvarez-Buylla et al., 2002). Type A cells are restricted to a neuronal fate and migrate along the rostral migratory stream (RMS) until they reach the olfactory bulb where they differentiate into interneurons (Kornack and Rakic, 2001; Lois and Alvarez-Buylla, 1994).

1.3.2 Parallels between neural stem cells and central nervous system tumour cells

Brain tumours have been shown to a) exhibit histological features similar to undifferentiated neural stem/progenitor cells (Zaidi et al., 2009), and b) originate from the SVZ (Quinones-Hinojosa and Chaichana, 2007; Chaichana et al., 2008; Jacques et al., 2010). In addition, the cellular and molecular mechanisms relevant to early brain development can also contribute to tumourigenesis when functioning aberrantly. Also, brain tumours are often heterogeneous and can contain immature, undifferentiated cells that resemble neural progenitor-like cells (Sutter et al., 2007). Therefore, it is somewhat paradoxical to think that brain tumours could arise from fully differentiated postmitotic cells, as the likelihood of them accumulating enough genetic mutations by chance to undergo neoplastic transformation is exceptionally low. Nevertheless, this remains an alternative hypothesis to that of NSCs being the brain tumour cell of origin.

There are numerous examples of the parallels between NSCs and CNS tumour cells. Firstly, many CNS tumours exhibit differentiation along several neural lineages, suggestive of a multipotent cell of origin (Zaidi et al., 2009). Also, CNS tumourigenesis involves many of the same pathways as NSC regulation (sonic hedgehog, notch, Akt), and many CNS tumours express known NSC markers (e.g. GFAP, Nestin, Sox-2, Notch, Olig-2) (Dirks, 2008). Targeted overexpression of oncogenes in Nestin-positive cells leads to the development of malignant glial tumours (Sutter et al., 2007). And cells with stem-like characteristics have been identified in biopsies of glioblastoma and medulloblastoma grown in mitogen-enriched medium *in vitro* (Ignatova et al., 2002; Hemmati et al., 2003). These cells also formed neurospheres that could be serially passaged and differentiated along neuronal and glial lineages. Furthermore, intracerebral engraftment of these *in vitro* grown glioblastoma cells into nude mice reproduced the original tumour (Galli et al., 2004). Notably, neurosphere-forming cells could once again be isolated from these secondary tumours and serially re-grafted to recapitulate the original glioblastoma, illustrating the *in vivo* self-renewal potential of these cells. The intrinsic behavioural similarities between NSCs and CNS tumour cells, however, are a good indication that similar growth, survival and proliferation pathways are active in both types of cells.

1.3.3 Parallels between neural stem cells and astrocytes

Historically, glial cells and neurons were thought to be derived from two separate pools of progenitor cells. However, when the primary progenitor cells of the SVZ were first identified they were shown to exhibit both structural and biological markers of astrocytes (Doetsch et al., 1999). Subsequent cytoarchitectural analysis of the brain's germinal regions including its pattern of NSC sub-population division has raised fundamental questions about the mechanism of adult neurogenesis. Astrocytic NSCs belong to a developmental lineage that includes the neuroepithelium, radial glia and germinal astrocytes. There is mounting evidence to suggest that adult NSCs are strongly influenced by their local microenvironment (Calabrese et al., 2007). To this end, non-germinal astrocytes can be oncogenically induced to de-differentiate into a stem-like state (Lee et al., 2008b), but environmental factors alone seem to be insufficient to inducing astrocytes to behave like NSCs (Alvarez-Buylla and Lim, 2004). Further characterisation of these cells may reveal a role in brain development and disease. We aim to test this hypothesis by examining whether non-germinal terminally differentiated astrocytes can contribute towards tumour development.

1.4 Cancer Stem Cells

Historically, two hypotheses have existed to explain how tumours arise and develop; the stochastic model and the hierarchical model (Figure 4). The stochastic model predicts that tumour cells are heterogeneous and can all induce tumour formation due to a combination of intrinsic and/or extrinsic variables. The hierarchical model predicts that only a small subset of cells in a tumour is capable of re-generating the bulk of the tumour, with the rest being more differentiated (Vescovi et al., 2006).

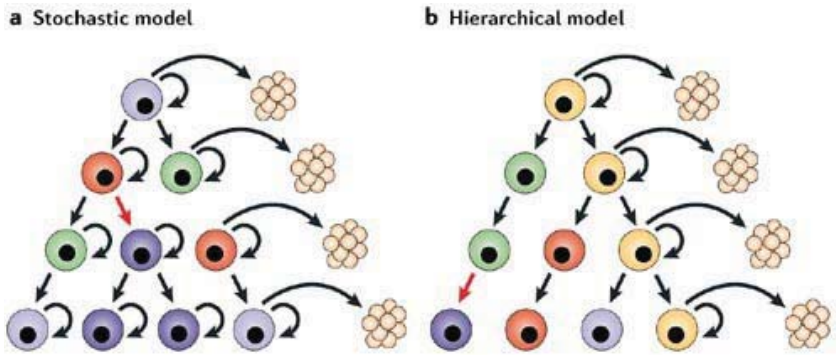

Figure 4: A schematic representation of the (a) stochastic vs. (b) hierarchical model of tumourigenesis (adapted from (Vescovi et al., 2006). The stochastic model proposes that all tumour cells can sustain the growth of a tumour whereas the hierarchical model proposes that only a small subset of tumour cells possess this ability.

The latter model has received more attention and resulted in the coining of the "cancer stem cell hypothesis" (Bonnet and Dick, 1997). This hypothesis suggests that tumours are initiated and maintained by a subpopulation of cells, with similar properties to adult stem cells, termed cancer stem cells (CSC). The first of these cells to be described was the SCID leukaemia-initiating cell (SL-IC) in 1997 (Bonnet and Dick, 1997). However, the fact that only a few blood cells isolated from leukemic patients had the ability to proliferate *in vivo* was noted some 40 years earlier (Bruce and Vanderga.H, 1963). Similarly CSCs have been identified in breast, pancreatic, and colon cancer and it is widely thought that the same may be true for most if not all cancers (Al Hajj et al., 2003; O'Brien et al., 2007; Ricci-Vitiani et al., 2007; Esposito et al., 2002).

Assuming the hierarchical model for tumour development, cancer stem cells (CSCs) are believed to represent a sub-population of neoplastic cells found within tumours or haematological cancers that possess characteristics normally associated with stem cells (Bao et al., 2006). They can account for 3% of cancerous cells in leukaemia and up to 30% in glioblastoma (Miller et al., 2005). It is hypothesised that only the CSCs within a tumour bulk drive tumourigenesis and are responsible for repopulating the bulk of the tumour stroma following surgical resection and/or chemo/radiotherapy (Zaidi et al., 2009; Huntly and Gilliland, 2005) (Figure 5).

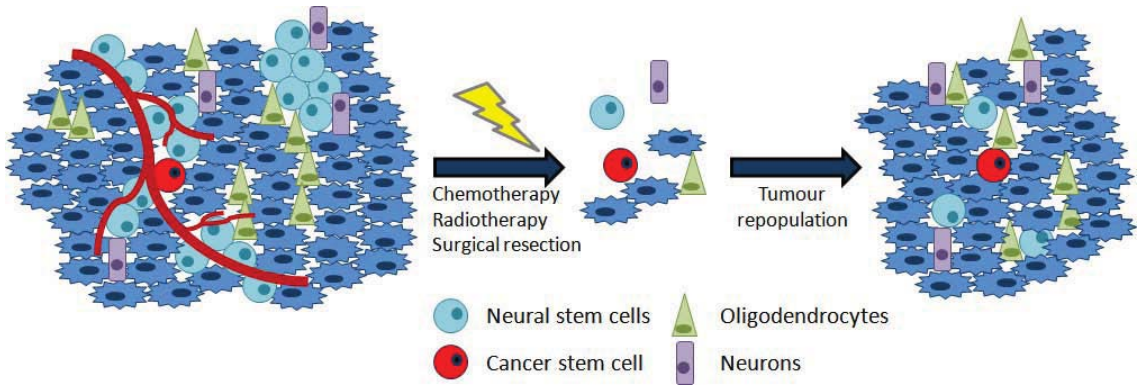

Figure 5: Schematic representation of the cancer stem cell hypothesis. According to the hierarchical model, only a small subset of tumour cells has the ability, as cancer stem cells, to drive tumour repopulation following surgical resection and chemo/radiotherapy. The phenotype of the repopulated tumour does not always perfectly recapitulate that of the original tumour.

CSCs typically persist in a variety of tumours as a distinct and very small subpopulation of cells (1-5%). They are responsible for initiating and maintaining the growth of neoplastic tissue as it has been repeatedly shown that they can induce tumourigenesis when transplanted into a receptive host (Lowry and Temple, 2009). In one extreme example, only around 1 in 1,000,000 cells in some human acute myeloid leukemia (AML) samples can seed tumour growth when transplanted into severe combined immunodeficient (*scid*) mice (Hope et al., 2004). In the other extreme, it has been shown that primary pre-B/B lymphoma cells isolated from Eμ-myc transgenic mice induced lymphoma development when injected into congenic mice regardless of cell number (Kelly et al., 2007). However, this finding is not representative of the heterogeneity of tumours observed in the majority of cancers.

The properties of CSC can sometimes be used to deduce their origin. For example, both epithelial tissue stem cells and their CSC counterparts contain lower levels of reactive oxygen species (ROS) than their terminally differentiated progeny; an essential requirement for maintaining their proliferative capacity, and a similarity that reinforces a theoretical step-wise link between the two cell types (Diehn et al., 2009). Low levels of ROS have also been observed in CNS stem/progenitor cells (Tsatmali et al., 2005) perhaps due to endogenously elevated levels of the antioxidant enzyme copper/zinc superoxide dismutase (SOD1), which is a known correlate of NSC proliferation (Takemura et al., 2006). Enhanced antioxidant levels and increased expression of free radical scavenging systems is one mechanism by which both normal and cancer stem cells can protect themselves against DNA damage (i.e. become radioresistant) and

maintain their stem-related proliferative capacity. And indeed, pharmacologicalical depletion of free radical scavenging systems in CSCs makes them more radiosensitive and reduces their proliferative capacity (Diehn et al., 2009). It is therefore plausible that the enhanced activity/protection against ROS observed in CSCs is a retained property from their origins as CNS stem/progenitor cells. A second mechanism by which cells can demonstrate radioresistance against ionising radiation is through enhanced DNA damage repair. And glioma CSCs have been shown to possess such a hyperactivated DNA damage response mechanism as a result of preferential phosphorylation activation of the Chk1 and Chk2 checkpoint proteins and subsequent prevention of G2-S cell cycle progression (Bao et al., 2006; Ward, 1985). And once again, pharmacological inhibition of Chk1/2 with debromohymenaildisine enhanced the radiosensitivity of the CSCs, but this time without affecting their proliferative capacity (Bao et al., 2006). The presence of these two separate pathways by which CSCs protect themselves against cytotoxic therapy highlights the need to identify further disease-specific CSC resistance mechanisms in order to develop effective therapeutic regimens.

CSCs are known to characteristically resemble normal stem cells of the corresponding tissue of origin. For example, neural CSCs express the neural stem cell markers GFAP, Nestin, and CD133 (Galli et al., 2004; Singh et al., 2004). Until recently it was also not known whether CSCs remain dependent upon the same niche microenvironments that regulate normal NSCs. However, endothelial cells interact selectively with neural CSCs in order to maintain them in stem cell-like state (Sneddon and Werb, 2007). Also, increasing the vascularity within brain tumour xenografts expands the number of CSCs and accelerates tumour growth. Disruption of this vascular niche microenvironment ablated CSC numbers and arrested tumour growth (Calabrese et al., 2007). These data suggest that brain tumours orchestrate niche microenvironments that maintain CSCs.

We know that CSCs can resemble normal tissue stem cells based on their expression profile, ability to self-renew, and ability to differentiate into all of the appropriate cellular lineages. However, it remains unknown as to whether CSCs arise from normal stem cells that have lost their growth control or from later-stage progenitor cells that have de-differentiated and acquired stem-like characteristics. In the case of intestinal cancer the former has been proven to be the case as stem-cell-specific loss of APC induced neoplasia (Barker et al., 2009). Despite this finding, it is likely that CSCs will have to be characterised in a tissue-dependant manner as this scenario may not be applicable to all cancer types.

The identity of the neural CSC has yet to be defined; a question that we aim to address with our model system. The potential therapeutic value of defining the CSC is enormous as (i) treatments could be designed to specifically target tumour growth thus minimising the cytotoxic side-effects seen with traditional chemo/radiotherapy methods, and (ii) it would allow us to understand the aetiology of tumourigenesis and develop ways to prevent tumour formation/recurrence.

1.4.1 Brain Tumour Initiating Cells (BTICs)

With the exception of hematopoeitic stem cells, more is known about the development of embryonic and adult NSCs than any other tissue-specific stem cell. CNS malignancies have become widely studied to test the CSC hypothesis. None more so than gliomas, from which glioblastoma-initiating cells (GICs) have been identified (Singh et al., 2004). GICs have been shown to possess a number of parallels with normal adult NSCs from their self-renewal and multi-lineage differentiation potential to their similar transcriptomic profiles (Lee et al., 2008a). Further comparisons of NSCs and GICs will provide us with an insight into the mechanism of fate determination and tumourigenesis. A linear relationship of NSC progression to GIC seems unlikely when considering the heterogeneity of gliomas. A more likely scenario of fate determination would be a contextually dependent progression whereby NSCs can give rise to an array of GIC sub-types (all of which could have different response to the same signalling pathway) based on the spatial and developmental qualities of the target NSC.

It has long been thought that the regulatory cytokine transforming growth factor beta (TGF-β) exerts tumour-suppressing signals that must be avoided for a cell to become cancerous. However, TGF-β is commonly overexpressed in malignant glioma and has been variously implicated in glioma cell proliferation, migration, immune regulation, and microenvironment modulation (Bodmer et al., 1989). As such, the TGF-β receptor has been highlighted as a potentially promising therapeutic target. TGF-β has been shown to induce increased self-renewal, whilst preventing the differentiation, of GICs but not normal human neuroprogenitors. It does so through the Smad-dependent activation of leukemia inhibitory factor (LIF) and the subsequent downstream activation of the JAK-STAT pathway, and ultimately promotes tumourigenesis (Penuelas et al., 2009). The Smad complex also has a range of cofactors with which it can interact to achieve differential gene expression/repression in a cell context-dependent manner

(Fine, 2009). TGF-β is also known to inhibit Wnt-mediated self-renewal and proliferation in midbrain-derived NSCs but to have no effect on forebrain-derived NSCs (Falk et al., 2008). This is further proof of the contextual nature of stem cell signalling. In addition, a distance of 1mm between NSCs of the adult SVZ is sufficient to impart a spatial restriction between the cells in terms of their fate determination.

This supports our previous statement that fate determination may be influenced by NSCs microenvironment, and that the resulting heterogeneous pool of GICs may preclude the efficacy of single pathway therapeutics such as in the case of the TGF-β receptor. For example, there is a sub-population of BMPR1b-methylated GICs that are unresponsive to LIF as they cannot mediate the phosphorylation of STAT3 (Lee et al., 2008a). Conversely, during development STAT3 inhibition is required for cells to stop proliferating and differentiate, meaning that TGF-β inhibition and the subsequent activation of STAT3 would counter-intuitively expand the GIC pool (Fine, 2009). It is plausible that targeting of stem cell pathways may hold therapeutic promise but a combination therapy / surgery approach tailored to each patient and specific to the tumour remains the best option currently available.

In the case of medulloblastomas, the most common paediatric brain tumour, an association has been identified between the aberrant activation of Shh signalling and loss of function in the *Ptch* gene (Vorechovsky et al., 1997; Stone et al., 1996). The neural progenitor cells of $Ptc^{+/-}$ mice exhibit an increased rate of proliferation and around 20% of the mice themselves develop medulloblastomas (Goodrich et al., 1997; Galvin et al., 2007). Medulloblastomas derived from these mice are propagated by cells expressing the progenitor markers Math1 and CD15, and interestingly not by cells expressing the NSC marker CD133. These CD15+ cells were not able to form neurospheres *in vitro*, and were incapable of multilineage differentiation. CD15 has since been found to be expressed in a subset of human medulloblastomas and is associated with poor prognosis (Read et al., 2009). This suggests that BTICs do not have to exclusively belong to the NSC lineage and can also lack CD133 expression (Wang et al., 2008).

Much work has focussed on attempting to identify and characterise BTIC, with nestin (Dahlstrand et al., 1992) and CD133 receiving much of the attention based on the association of their expression with increased tumour malignancy (Thon et al., 2010). Nestin is an intermediate filament produced by both neural stem and progenitor cells during embryongenesis (Zimmerman et al., 1994; Galli et al., 2004; Hemmati et al.,

2003). Its expression is thought to correlate with the "stemness" of NSCs with a decrease in its expression correlated with a progression towards a more differentiated cell phenotype (Vescovi et al., 1993). Elevated nestin immunoreactivity has also been observed across a large number of brain tumours including astrocytomas, oligodendrogliomas, and glioblastomas (Almqvist et al., 2002). This finding was taken further by Calabrese et al who went on to show that nestin-positive brain tumour cells were located significantly closer to tumour vasculature than nestin-negative cells, with the greatest association observed in oligodendrogliomas and glioblastomas (Calabrese et al., 2007). The same group also showed that nestin-positive/CD133-positive tumour cells include the self-renewing tumourigenic CSC fraction and interact selectively with the endothelial cells of the tumour vasculature. The importance of this interaction was highlighted by treatment with antiangiogenic therapies, which were shown to arrest tumour growth as a result of depleting tumour vasculature and its associated pool of nestin-positive/CD133-positive cells (Calabrese et al., 2007). This was the first study to suggest a perivascular niche for the BTIC. CD133 itself has had a wealth of interest as a stand-alone and co-expressed marker of BTIC. Another less well studied potential BTIC marker is Musashi-1, an RNA-binding protein expressed by proliferating and multipotent neural progenitor cells of the SVZ (Sakakibara and Okano, 1997; Okano et al., 2002). Similarly to nestin and CD133, elevated Musashi-1 expression has been correlated with increased tumour malignancy and grade in human glioma (Toda et al., 2001).

We aim to address the relative likelihoods of BTIC originating from: a) NSCs which undergo neoplastic transformation, b) neural progenitor cells which have acquired mutations that cause them to de-differentiate into a stem-like state with unregulated growth control, or c) terminally differentiated cells (e.g. glia) which have acquired mutations that cause them to de-differentiate into a stem-like state with unregulated growth control.

1.4.2 CD133 (Prominin-1) as a marker of cancer stem cells

Human CD133 belongs to a family of 5-transmembrane (5-TM) proteins with extracellular N-termini and cytoplasmic C-termini. It is a single chain polypeptide of 856 amino acids and a molecular weight of 120kD and its precise function remains relatively unclear (Miraglia et al., 1997). In 1997, a monoclonal antibody was developed

which recognised the glycosylation-dependent epitope of CD133 (AC133) and was used to show that AC133 protein expression was restricted to CD34+ haemapoietic stems cells (Yin et al., 1997). However, it was later shown that AC133 mRNA expression was present in the adult brain, heart, kidney, liver, lung, and placenta (Miraglia et al., 1997).

In a similar manner, a monoclonal antibody developed against murine CD133 (prominin-1) was later used to identify murine CD133 as a 5-TM protein with the same topology as human CD133 (Weigmann et al., 1997). However, they only share 60% amino acid sequence homology with murine CD133 being an 858 amino acid, 115kD glycoprotein with an even more diverse distribution of expression (Corbeil et al., 1998).

Both CD133 epitopes are present as plasma membrane protrusions on epithelial microvilli and are thought to act as regulators of the plasma membrane (Mizrak et al., 2008). CD133-containing membrane particles are present in the ventricular fluid of the developing mouse neural tube in a temporal relationship with the development of protuberances on the embryonic neuroepithelium (Marzesco et al., 2005). Furthermore, CD133 has been shown to be downregulated in the plasma membrane of Caco2 human epithelial cells in response to enterocytic differentiation (Corbeil et al., 2000). Taking both of these findings into account it appears that CD133 may actively play a role in maintaining the phenotype of the NSC niche.

CD133 antibodies have been used to isolate human NSCs from fetal brain (Uchida, 2000), and more recently putative CSCs from glioblastomas (Singh et al., 2003). This finding has caused much excitement in the field of cancer research with CD133 expression often being associated with multipotent and self-renewing BTICs (Gunther et al., 2008). This statement was initially validated by two separate publications that respectively showed that CD133+ cells contribute to radioresistance and tumour repopulation, and that *in* vivo delivery of bone morphogenetic proteins block tumour growth by depleting the pool of CD133+ BTICs (Bao et al., 2006; Piccirillo et al., 2006). However, there have been several recent studies in which CD133- cells have also been found to be tumourigenic (Shmelkov et al., 2008; Wang et al., 2008; Ogden et al., 2008). The argument becomes even less clear-cut when we consider the dynamic nature of CD133 expression and the fact that CD133- cells may reflect a loss of expression rather than derivation from a CD133- cell. In addition to this, increased CD133 expression has been associated with bioenergetic stress induced by hypoxia and mitochondrial dysfunction and may therefore simply be a marker of tumour microenvironment rather than tumourigenicity (Griguer et al., 2008). These

contradictory findings highlight the current lack of understanding in the behaviour of CSCs. We aim to further characterise CD133+/- NSCs in terms of their relative contributions to tumourigenesis.

Since the implication of CD133 expression as a marker of CSCs in brain tumours, its potential as a marker of CSCs in other tumour types have been exhaustively investigated. Using a range of isolation techniques, such as cell sorting, CD133+ CSCs have been identified in a range of different cancers including breast cancer (Wright et al., 2008). However, the unpredictable variability in CD133 expression leaves the field open for debate. An assumption of the CSC hypothesis is that the clinical behaviour of a brain tumour should correlate with the relative presence and biological state of the CSC population. Despite growing ambiguity, increased CD133 expression in glioma has in fact been found to correlate with decreased survival independent of tumour grade, extent of resection, and patient age. And interestingly, the proportion of CD133+ cells was also found to be associated with an increased risk of tumour re-growth (Zeppernick et al., 2008). This is a particularly important finding considering that it fits with the CSC hypothesis in that it implies the ability of CD133+ cells to proliferate and re-populate the tumour. A similar finding has been made in neuroblastoma and ganglioneuroblastoma where patients with CD133- tumours had an increased chance of survival over those with CD133+ tumours, and increased CD133 expression was found to correlate with increased malignancy (Tong et al., 2008). Similarly, CD133 expression has been used to predict decreased survival in glioblastoma patients treated with concomitant chemo/radiotherapy, suggesting that a CD133+ CSC population is responsible for the treatment resistance of glioblastoma (Murat et al., 2008). These correlations between increased CD133 expression and decreased survival and/or increased malignancy have also been observed in astrocytomas (Ma et al., 2008; Rebetz et al., 2008) and oligodendroglioma (Beier et al., 2008).

1.5 Cell Cycle Regulation and Tumourigenesis

Uncontrolled cellular proliferation is a hallmark feature of almost all malignant cancers, including brain tumours, and typically results from the neoplastic transformation of cells following loss of regulatory control over the cell cycle. This can lead to a decrease in apoptosis and/or an increase in cellular proliferation that may clinically manifest as a tumour mass. The cell cycle is regulated by four categories of genes/proteins: proto-

oncogenes, tumour suppressor genes, DNA repair enzymes, and cyclins / cyclin-dependent kinases (CDKs). Mutations in these genes, leading to a loss/gain of function, can result in deregulation of the cell cycle and subsequently lead to tumourigenesis. Proto-oncogenes can positively regulate the cell cycle upon activation by mediating the transduction of mitogenic signals which lead to an increase in cell proliferation (e.g. EGF signalling cascade). Aberrant oncogenic gain of function effects can be brought about by: (i) mutation in the gene coding sequence leading to a constitutively active protein made in normal amounts, (ii) gene amplification leading to the over production of normal protein or (iii) by chromosomal rearrangement resulting in the over production of a protein via by gene fusion with a strong and constitutively active promoter (Lozano, 2010).

Under normal conditions, progression through the cell cycle is regulated by the protein kinase activities of CDKs. However, the catalytic capability of a CDK is only activated when in the form of a heterodimer with a bound cyclin molecule. These activated heterodimers have the ability to regulate key substrates through phosphorylation and facilitate the passage of a cell through the cell cycle. Cyclins are classified according to the phase of the cell cycle they regulate. For example, transition through the G1-S-G2-M phases is controlled by cyclins D, E, A and B respectively (Obaya et al., 2002). Cyclins are regulatory proteins and must form an active heterodimer with a CDK in order to exert a catalytic function. Cyclin D is a G1 phase cyclin that couples with CDK4 and CDK6 to regulate the tranition of cells from G0 to G1. Cyclin D levels are controlled through the Ras GTPase signaling pathway and when present it binds to existing CDK4 to form the active heterodimer cyclin D-CDK4. This complex hypophosphorylates pRb, which subsequently binds to and inhibits E2F transcription factors resulting in the downstream facilitation of cyclin E expression (Zhang et al., 2000). Cyclin E (and cyclin A) is then able to bind to CDK2 and facilitate transition from G1 to S-phase. This is achieved through cyclin E-CDK2 / cyclin A-CDK2-mediated hyperphosphorylation, and subsequent inactivation, of pRb in late G1 phase (Akiyama et al., 1992). Hyperphosphorlyated (inactivated) pRb has an altered molecular conformation and is no longer able to inhibit the E2F transcription factors (Weinberg, 1995). The resulting increase in E2F levels results in the transcription of a range of essential proteins involved in cell prolieration (e.g. cyclins E/A and DNA polymerases), which ultimately shunt the cell from G1 into S-phase. During S-phase cyclin E interacts with Cdc6 to stimulate replication complex assembly and cyclin A activates the

complex to promote DNA synthesis. The final transition of the cell cycle from G2 to mitosis is regulated by the complex formed between cyclins B1/ B2 and CDK1 (cdc2). Cyclin B-cdc2 forms part of the M-phase maturation promoting factor (MPF) that mediates assembly of the mitotic spindle, and conversely, deactivation of this complex results in the cell exiting mitosis (O'Farrell, 2001). Uncontrolled cellular proliferation and tumourigenesis can result when the above mechanism begins to function aberrantly. In addition to gene amplification / mutation (as described above), abnormal CDK activity can also be achiebed through inactivation of inhibitors. The cip/kip and INK4a/ARF families of genes downregulate progression through the cell cycle by inactivating cyclin-CDK complexes, and their loss-of-function is frequently observed in human tumours (Ivanchuk et al., 2001). To this end, many of the current cancer therapies in development focus on cell cycle regulation through the use of small molecule inhibitors and gene therapy. For example, although most interphase CDKs are dispensable for mouse development, their inhibition may prevent DNA replication in some types of tumour cells (Vermeulen et al., 2003).

1.5.1 The role of Rb, p53, and PTEN in CNS tumourigenesis

Our model reproduces known mechanisms of CNS tumourigenesis by conditionally knocking out the tumour suppressor genes (TSGs) Rb, p53, and PTEN. This allows us to examine the putative interactions between these pathways as well as the ways in which they may differentially influence tumourigenesis both *in vitro* and *in vivo*. One particular function of tumour suppressor genes is to negatively regulate progression through the cell cycle. The majority of TSGs are haplosufficient, i.e. as long as one allele remains unaffected then there is no overall effect on the function of the gene. In relation to our work there are three particular TSGs whose function in which we are interested.

The retinoblastoma gene (RB1) was the first TSG identified in humans and Rb1 the first TSG to be knocked-out by targeted deletion in mice (Jacks et al., 1992; Clarke et al., 1992; Lee et al., 1992). It is ubiquitously expressed and its protein product, pRb, binds and inhibits many cellular proteins implicit in the regulation of cell cycle progression (Friend et al., 1986). Rb tumour suppressor function was originally thought to be exclusively attributed the ability of hypophosphorylated pRb to arrest cells in G1 by inhibiting the activity of E2F transcription factors. E2F transcription factors positively

regulate genes whose activation is required for entry into the S-phase of the cell cycle (Hanahan and Weinberg, 2000). However, it is now known that Rb binds to over 100 protein partners resulting in the transcriptional regulation of hundreds of target genes which in turn mediate a vast array of downstream effects ranging from cell cycle arrest to apoptosis, differentiation, angiogenesis, and metastasis (Burkhart and Sage, 2008). As such, homozygous knockout of Rb ($Rb^{-/-}$) in mice results in embryonic lethality (Zhang et al., 2004). Rb was originally identified in families with a history of retinoblastoma and it is accepted that Rb loss is the most common initiating genetic event in retinoblastoma (Knudson, 1984). Rb inactivation/loss has also been implicated as a major contributing factor in a many other cancers such as osteosarcomas in children (Friend et al., 1986), and various carcinomas in adults (Burkhart and Sage, 2008). It is now known that Rb is directly or indirectly inactivated in nearly all human cancers. However, it is still unclear as to which cell type (stem cells, progenitors, differentiated cells) is responsible for cancer initiation following Rb loss. It is postulated that Rb loss could induce cell cycle re-entry and subsequent differentiation in type B NSCs, hyperproliferation in progenitors, and de-differentiation in differentiated cell types (Burkhart and Sage, 2008). All of these mechanisms could potentially contribute towards tumourigenesis. Rb loss is relatively rare in human gliomas (15-30%), and as of yet there has been no mouse model developed to specifically examine the consequence of Rb loss alone in brain tumour progression (Burkhart and Sage, 2008). In our model we aim to address this current knowledge gap.

p53 was first described in 1979 by Arnold Levine, David Lane, and Lloyd Old and was originally considered to be an oncogene based on the finding that over 50% of all cancer cells were observed to exhibit increased p53 levels (Deleo et al., 1979; Lane, 1992). However, this elevation was later found to be due to increased levels of a mutant p53 isoform that was interacting with, and inhibiting, the function of the endogenous p53. It was not until 1989 that p53 was revealed as a TSG (Nigro et al., 1989), with subsequent work leading to the identification of the p53 gene (TP53) as a critical element in the signal transduction pathway of DNA damage repair (Kastan et al., 1991). Described as the “guardian of the genome”, p53 is a ubiquitously expressed transcription factor that negatively regulates the cell cycle (Lane, 1992). Under unperturbed conditions p53 is expressed at low levels (Bourdon, 2007). However activation by phosphorylation, resulting from various genotoxic stress factors such as oncogene activation, hypoxia and DNA damage causes p53 to target and regulate genes that induce apoptosis and cell

cycle arrest (Maltzman and Czyzyk, 1984). p53 mutations have been implicated in brain tumour progression. Specifically, germ line mutations of the gene encoding p53 (TP53), located at 17p13.1 cause a rare familiar cancer disorder called Li-Fraumeni syndrome. This disorder includes 55 different inherited mutations of TP53 because of which the subsequently altered p53 isoform cannot bind to DNA and therefore loses its function. These mutations typically occur within the sequence-specific DNA-binding domain which contains a zinc ion and is responsible for DNA binding. Those affected are predisposed to the development of brain tumours such as astrocytomas (Srivastava et al., 1990). TP53 mutations have been reported in 28% of primary glioblastomas (WHO grade IV) and in 59% of low grade astrocytomas (WHO grade II) (Ohgaki and Kleihues, 2007). In the mouse, disruption of TP53 alone is not sufficient to result in astrocytoma formation, suggesting that additional genetic events are required (Zhu et al., 2002). Although it cannot be considered haploinsufficient, p53 heterozygosity predisposes the carrier to a vastly increased chance of developing tumours in early life. This is because loss of heterozygosity (LOH), or the loss of both alleles, confers this cancerous predisposition.

Following the identification of Rb as the most common initiating genetic event in retinoblastoma in the 1980's, genetic evidence suggested the presence of an additional TSG on chromosome 10, as loss of heterozygosity (LOH) at this location had been seen in a variety of cancers (Li et al., 2003). The subsequent characterisation of Cowden disease, caused by a germline mutation in 10q23, validated this finding (Liaw et al., 1997). Sequence analysis revealed a phosphatase domain and a large region of homology to chicken tensin at this chromosomal location, hence PTEN (Phosphatase and Tensin homologue). In 1997, Li et al. confirmed the existence of PTEN at 10q23 when screening 12 primary breast tumours. They also showed that PTEN was absent in 31% of glioblastoma (GB) cell lines and 17% of primary glioblastomas, and that LOH is also a frequent event in the progression of low-grade to high grade glioma (Li et al., 1997). PTEN is now known to be a dual lipid and protein phosphatase involved in the regulation of apoptosis, metabolism, cell proliferation, and cell growth through the PI3K/AKT pathway. As a phosphatidylinositol phosphate (PIP) phosphatase, PTEN can de-phosphorylate PI(3)P and PI(3,4)P2 but its main substrate is thought to be PIP3 which is the product of PI3K (Blanco-Aparicio et al., 2007; Maehama and Dixon, 1998). The activity of PTEN antagonises that of PI3K by lowering the levels of PIP3, therefore decreasing Akt activity, and subsequently enhancing the rate of apoptosis and

lowering cell motility/migration through a series of downstream effectors (i.e. PDK1, AKT/PKB, Rac1/cdc42, small G proteins, FAK) (Datta et al., 1999; Liliental et al., 2000; Tamura et al., 1998; Blanco-Aparicio et al., 2007). PTEN activation promotes cell cycle arrest at G1, and increases the level of apoptosis. For example, exogenous PTEN causes GB cells to arrest at G1 (enhanced by G2 blocker nocodazole) and can be rescued by p-Akt expression. Also involved in PTEN-mediated cell death is an up-regulation of p27 and down regulation of cyclin D1 (Weng et al., 2001). Homozygous knockout of PTEN ($PTEN^{-/-}$) in mice results in embryonic lethality with the mice exhibiting abnormal differentiation and poor cellular organisation in all of the three germ layers. Mice heterozygous for PTEN ($PTEN^{+/-}$) are viable but have a reduced rate of Fas-mediated apoptosis and a high incidence of lethal polyclonal autoimmune disorder (Di Cristofano et al., 1998; Di Cristofano et al., 1999). Mice in which PTEN is conditionally knocked out in neural precursor cells by using the Cre-LoxP system and a nestin promoter driven Cre transgene demonstrate a profound phenotype in which they are born with open eyes and enlarged brains, and die shortly after birth. Cell migration is impaired in these mice and an increased level of proliferation can be seen in cells of the SVZ (Groszer et al., 2001). In addition to this model, PTEN has also been conditionally knocked out under the control of a GFAP, En2, or L7 promoters in which neural precursor cells, cells of the midbrain-hindbrain junction at embryonic day 9.5, and mature Purkinje cells were targeted respectively. All of these mice, with the exception of the L7-Cre mice, exhibited cellular disorganisation, increased proliferation, decreased apoptosis, and increased cell/brain size in the affected tissues with seizures, ataxia, and death (Backman et al., 2001; Marino et al., 2002a). The L7-Cre mice had almost normal appearing Purkinje cells, but which showed signs of chronic neurodegeneration. Taken together these findings suggest that PTEN is does not play a major role in lineage determination but is implicitly involved in the regulation of cell motility, migration, and regulation of the SVZ neural stem cell compartment.

1.6 Model System

There are many well-established animal model systems that enable the studying of CNS tumourigenesis and its molecular aetiology. However, they vary enormously depending on the research topic being investigated, e.g. the tumour cell of origin, the role of specific signalling pathways and/or the role of the cell cycle, or therapeutic strategies. A selection of the most commonly used such model systems are summarised below:

Tumour Type	Model System	Target Effect	Target Cell	Reference
Astrocytoma / Glioblastoma	v-src kinase transgenic mice	Non-specific (some VEGF expression)	GFAP-expressing astrocyte	Weissenberger et al, 1997
Neuroblastoma	K/o transgenic mice	MYCN (myc) expression	Developing neural crest cells	Weiss et al, 1997
Oligodendroglioma / Glioblastoma / PNET	Retrovirus	PDGF	Non-specific neural cell	Uhrbom et al, 1998
Oligodendroglioma	K/o transgenic mice	$p19^{ARF}$ loss	Non-specific neural cell	Kamijo et al., 1999
Medulloblastoma	Cre-LoxP	Rb and p53 loss	External granular layer cells	Marino et al, 2000
Glioblastoma	Cre-LoxP	K-ras and Akt expression	Nestin-expressing stem/progenitor cells	Holland et al, 2000
Astrocytoma / Glioblastoma	K/o transgenic mice	Nf1 (Ras) and p53 loss	Non-specific neural cell	Reilly et al, 2000
Oligoastrocytoma / Oligodendroglioma	MTA gene transfer	Non-specific	GFAP-expressing astrocyte	Holland et al, 2000
Astrocytoma	K/o transgenic mice	H-ras	GFAP-expressing astrocytes	Ding et al, 2001
Glioblastoma	Ectopically transfected cell line	E6/E7-mediated p53/Rb loss with hTERT and H-ras expression	Astrocytes	Sonoda et al, 2001
Glioblastoma	Ectopically transfected cell line	SV40 T/t-ag-mediated p53/Rb with c H-ras and hTERT	Astrocytes	Rich et al, 2001

Medulloblastoma	K/o transgenic mice	Ptch heterozygosity and p53 loss	Granule cell progenitors	Wetmore et al, 2001
Medulloblastoma	K/o transgenic mice / pharma. inhibition	p53 and Parp loss	Granule cell progenitors	Tong et al, 2003
Oligodendroglioma	K/o transgenic mice	v-erbB (EGFR) expression with Ink4a/Arf or p53 heterozygosity	S100β-expressing neural cells	Weiss et al, 2003
Glioblastoma	Ntv-a transgenic mice	Akt and Kras expression with Arf loss	Nestin-expressiing glial progenitors and GFAP-expressing astrocytes	Uhrbom et al, 2005
Astrocytoma (low grade)	K/o transgenic mice	Ink4a/Arf and Bmi1 loss with mutant EGFR expression	Nestin-expressing GFAP-negative progenitor cells	Bruggeman et al, 2007
Astrocytoma	Cre-LoxP	Nf1 and p53 loss (+ PTEN heterozygosity)	GFAP-expressing SVZ neural stem/progenitor cells	Kwon et al, 2008
Astrocytoma	Cre-LoxP	PTEN and p53 loss	GFAP-expressing SVZ neural stem/progenitor cells	Zheng et al, 2008
Glioma	Cre-LoxP	Nf1 and p53 and PTEN loss	Nestin-expressing neural stem/progenitor cells	Alcantara Llaguno et al, 2009

Table 1: Summary table of established animal models of CNS tumourigenesis.

1.6.1 Modelling gene loss-of-function through the generation of knock-out mice

Mice are widely used to model human diseases due to their genetic similarity and large array of genetic techniques available. One of the greatest breakthroughs in disease modelling was the cellular targeting of genes to ablate their function. This was achieved by 'homologous recombination', which involves the recombination between two homologous DNA sequences. In this manner, targeting vectors can recombine with homologous sequences in the genome to replace key exons or to disrupt expression through the insertion of mutations.

Embryonic stem cells (see section 1.2 for a description) cells can be maintained in an undifferentiated state *in vitro*, therefore retaining their pluripotency when returned to the environment of the early embryo. In this manner, ES cells in which genes have been ablated / inserted can be injected into the inner cell mass of murine blastocysts where they contribute to the development of the embryo (Figure 6). Incorporation of these cells into the germline allows the gene deletions / insertions to be inherited so that stable knock-out mouse lines can be established.

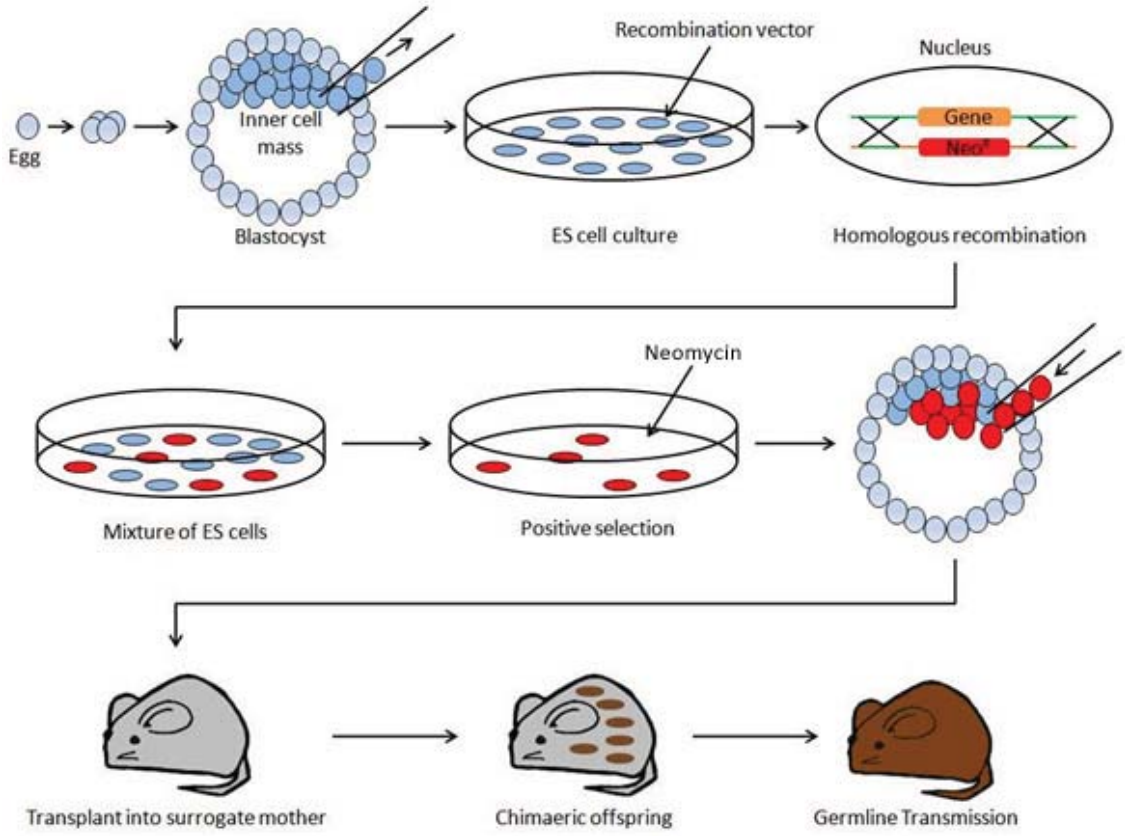

Figure 6: Generation of knock-out mice. Embryonic stem (ES) cells are derived from the blastocyst inner cell mass and expanded *in vitro*. The required genetic material (gene) is then introduced into the ES cells, along with the neomycin resistance gene (Neo^R), by homologous recombination. The *in vitro* culture is then treated with neomycin to positively select those ES cells containing the required genetic material, which are then transplanted back into the inner cell mass of a blastocyst. This blastocyst is then implanted in a surrogate mother who produces chimaeric (mice that developed from both genetically manipulated and normal ES cells) offspring. These chimaeras are then crossed against one another to achieve germline transmission so that the artificially inserted genetic material is expressed by all cells of the body (used with permission from Pedro Cuadrado).

1.6.2 Modelling conditional gene loss-of-function using the Cre-LoxP system

Conditional gene inactivation enables the inactivation of genes in a time/tissue-specific manner (Gu et al., 1993). This process uses enzymes that recombine specific DNA sequences with high fidelity. The most commonly used system for conditional gene inactivation is the Cre-LoxP system, first identified within yeast (Sauer and Henderson, 1988). Cre-recombinase is a bacteriophage P1 enzyme that belongs to a large family of DNA recombinases. It recognises sequences called ‘locus of crossover in P1’ (LoxP), which consist of two palindromic 13 base pair inverted repeats separated by an 8 base

pair asymmetric spacer. Cre-recombinase binds to these two LoxP sites and mediates strand cleavage, exchange and ligation (homologous recombination) at the asymmetric spacer (Hoess et al., 1982).

By controlling Cre-recombinase expression it is therefore possible to conditionally inactivate gene function in a time-specific manner. The most common method for controlling Cre-recombinase expression is by generating mice that express the enzyme under the control of a specific promoter. As a result, only the cells in which the promoter is active will express Cre-recombinase and subsequently undergo recombination. The limitation of this approach is the requirement of multiple tissue-specific Cre-recombinase-expressing mice in order to study the effect of gene inactivation in different cell populations.

Cre-recombinase expression can also be controlled by inducible systems such as the Cre-tamoxfin system. This system relies on the synthetic oestrogen receptor antagonist tamoxifen (commonly used to treat early breast cancer) to achieve inducible recombination. In this model system, the transgenic mice express a Cre-recombinase-oestrogen receptor binding-domain fusion protein (Cre-ER), rather than just Cre-recombinase. When tamoxifen (however administered) binds to these oestrogen receptors the Cre-ER protein is translocated into the nucleus where it targets LoxP sites for recombination. This method is highly versatile as the timing and route of tamoxifen administration can be used to achieve temporal and spatial recombination specificity.

Adenoviral vectors expressing Cre-recombinase can also be used to mediate inducible LoxP site recombination. In this system, Adenoviral vectors can be administered (*in vitro* and *in vivo*) in a time/tissue-specific manner whereby all the infected cells transiently express Cre-recombinase and undergo irreversible recombination at the target LoxP sites. It is this method that our model system uses to model the loss-of-function of the tumour suppressor genes (TSGs) Rb, p53, and PTEN.

1.6.3 Creation of a novel mouse model system

The selection of a model system, or the creation of a new one, depends on the research aims being addressed. For example, although human xenograft model systems most accurately reproduce the human clinical condition, and are the most robust models for pre-clinical therapeutic testing, they are less suitable when attempting to investigate the molecular events of early tumourigenesis. And conversely, although there are a wealth

of transgenic mouse models that recapitulate the tumourigenic process for a variety of tumour phenotypes, they carry the risk of reduced homology to the human condition as signalling pathways are often unequally represented between the endogenous biologies of mice and humans. In addition, the vast majority of transgenic mouse models of CNS tumourigenesis are oncogenically driven (Table 1) in the aim of expediting the tumourigenic process by reducing tumour latencies allowing for more cost/time-effective research.

In our research we aim, amongst other things (refer to section 1.8), to characterise the brain tumour initiating cell (BTIC) by delineating and defining the early molecular events of tumourigenesis in relation to phenotype commitment. For this reason, we must use a model system that: a) accurately and naturally reproduces the full tumourigenic process, b) allows for the development of multiple tumour phenotypes and c) allows for the identification, isolation, and functional characterisation of potential BTICs.

No existing model sufficiently addresses all of these requirements. And to this end, we developed a new mouse model that uses tumour suppressor gene (TSG) ablation, rather than one that is actively driven by oncogenic processes, to subtely predispose mice to developing intrinsic tumours. Although this means that the tumour latencies in our model are often considerably longer than those seen in other similar models, our model more naturally reproduces the early stages of tumourigenesis and allows for multiple phenotype determination as the mice must accrue additional (chance) mutations to the initial genetic lesion before neoplastic transformation can take place. This controls against the concern that oncogenically driven models force the tumour phenotype and render genotype-phenotype relationship analysis null and void. As previously discussed, we selected the three TSGs (Rb, p53, PTEN) based on their widespread loss of function in a variety of brain tumours. However, as homozygous deletion of Rb and PTEN is embryonically lethal (and all are haplosufficient) we incorporated the Cre-LoxP system in order to allow for conditional knock-out of the genes (refer to sections 1.6.1 and 1.6.2). In addition to the Cre-LoxP system allowing for temporal control of gene loss we can also control the spatial perspective through targeted delivery of Cre-recombinase or by putting it under the control of a regionally-specific promoter. For example, we can target the NSC compartment *in vivo* by injecting Adenovirus-Cre into the lateral ventricles of the “conditional knock-out” mice. And finally, the Cre-LoxP system also allows for gene ablation (with subsequent functional profiling) to be conducted *in vitro* following *ex vivo* isolation of target neural cells. We can derive primary NSC or other

specific cell cultures (i.e. astrocytes) from the brains of conditional knock-out mice, and induce *in vitro* recombination of the TSGs by transduction with Adenovirus-Cre. This model system allows us not only to study which cell types possess tumourigenic potential, but also the downstream effects of knocking-out these particular TSGs in relation to tumourigenesis.

1.6.4 Generation of transgenic mouse lines

The TSGs Rb, p53 and PTEN were each modified in the germline by inserting a 34 base pair sequence termed a LoxP site into an intron either side of one or more exons of the coding sequence. These LoxP sites have no effect on gene function but serve as recognition sites for the enzyme Cre-recombinase. Cells infected with an adenovirus expressing Cre-recombinase synthesise the enzyme, which binds to the nuclear LoxP recognition sequences and results in the excision, or "conditional knock-out", of the genetic material in between; a process termed "floxing". Mice carrying LoxP sites flanking Rb, p53 or PTEN alone were bred together in order to produce various genotype combinations. In addition, a so-called "reporter" gene was crossed into the background of the mice, termed ROSA26R$^{Lox/Lox}$. This allows for Cre-mediated recombination, and subsequent LacZ expression (Figure 7), to be visualised with a β-Galactosidase assay.

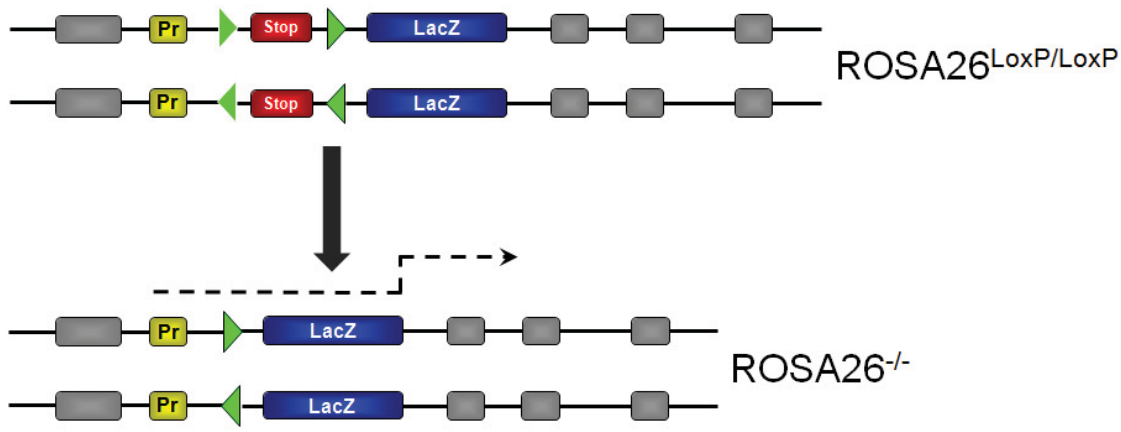

Figure 7: Cre-mediated recombination of the stop codon in between the LoxP sites results in the expression of LacZ, which can be detected by β-galactosidase staining.

1.6.5 *In vivo* model system

Using the Adenovirus-mediated Cre-LoxP system we are able to model the loss-of-function of the tumour suppressor genes (TSGs) Rb, p53, and PTEN in the subventricular zone (SVZ) of adult mice. This is achieved by intracerebroventricular (i.c.v.) injection of Adenovirus expressing Cre-recombinase (Adenovirus-Cre), which infects SVZ cells and targets them for recombination (Figure 8). This method can be used to study whether *in vivo* recombination of TSGs in SVZ cells results in the development of brain tumours.

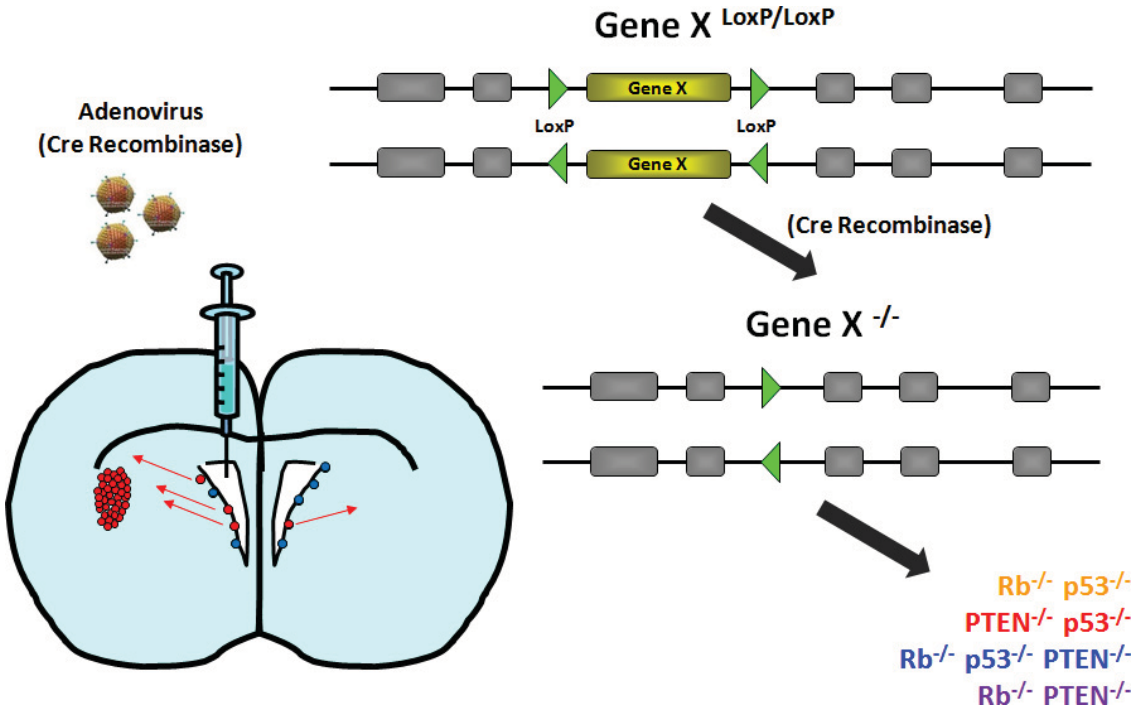

Figure 8: Schematic of the experimental procedure used to achieve *in vivo* recombination of the TSGs. I.c.v. administration of Adenovirus-Cre targets SVZ cells for LoxP site recombination and subsequent TSG loss.

1.6.6 *In vitro* model system

NSCs and astrocytes are derived from the brains of 5-12 week and two day old mice respectively. NSCs are derived from microdissection and dissociation of the SVZ, and astrocytes are derived from dissociation of the cortices. NSCs are grown as free-floating aggregates, termed "neurospheres" (NS) *in vitro*, whereas astrocytes are grown as an adherent monolayer. Prior to splitting for passage two these cells are separated into three treatment groups: untreated, Adenovirus-GFP-infected (control), and Adenovirus-

Cre-infected and recombined (experimental). The cells are then expanded for further passages until sufficient cells are yielded for a) *in vitro* functional characterisation (usually passage three or four), and b) intracerebral engraftment into recipient mice to characterise their ability to form tumours *in vivo* (Figure 9).

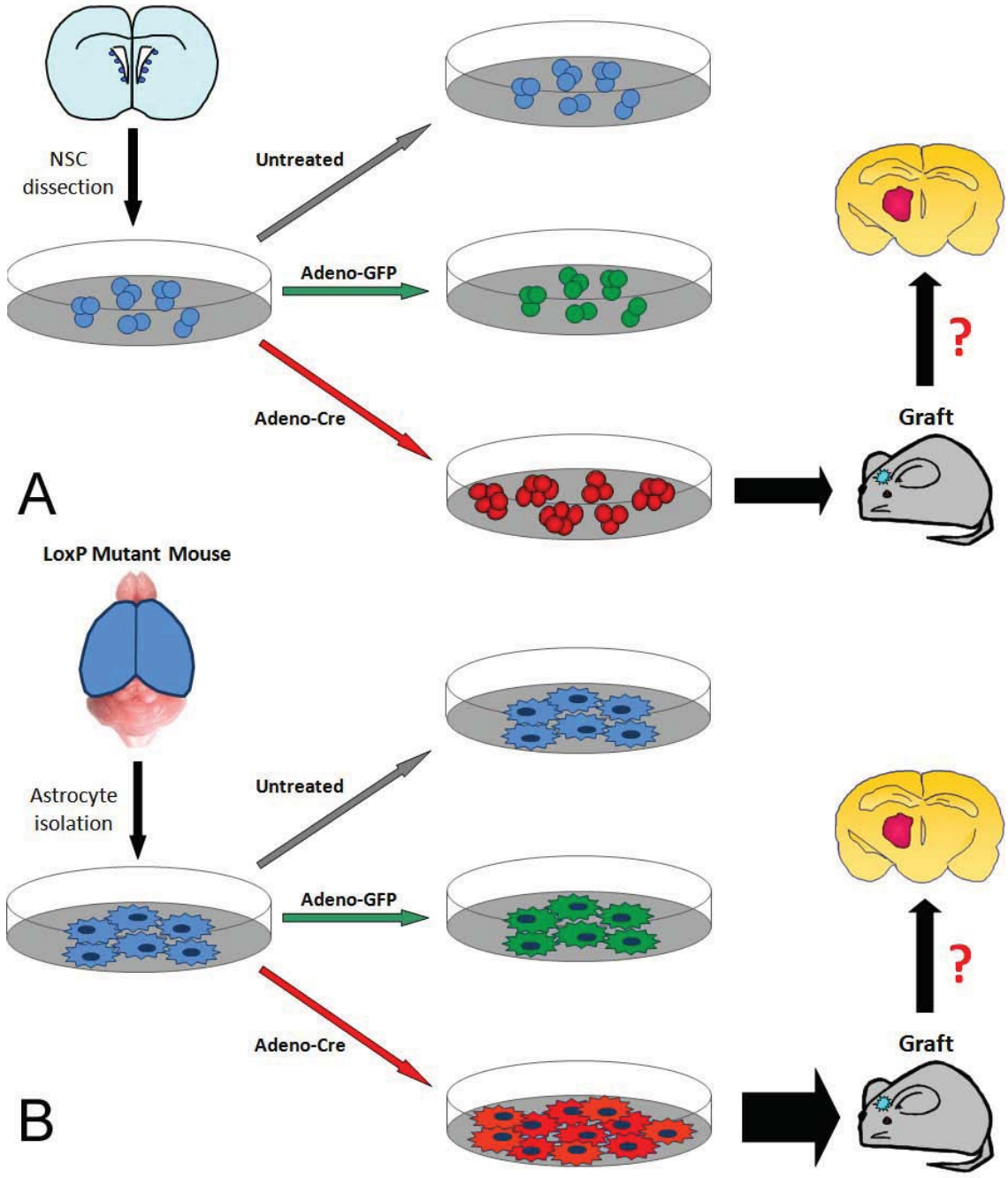

Figure 9: Schematic of the experimental procedure used for the derivation and generation of *in vitro* recombined NSCs and astrocytes. NSCs (A) and astrocytes (B) are derived from the SVZ or cortices, respectively of mice and grown *in vitro*. Prior to splitting for passage two these cells are separated into three treatment groups: untreated, Adenovirus-GFP-infected (control), and Adenovirus-Cre-recombined (experimental). They are then further expanded to allow for functional characterisation and testing of their tumourigenicity through intracerebral engraftment.

1.7 Model Validation

1.7.1 Intracerebroventricular Adenovirus-Cre administration targets neurosphere-forming subventricular zone cells for recombination

ROSA26R$^{Lox/Lox}$ reporter mice (R26R), which express LacZ upon Cre-mediated recombination, were given an intra-cerebroventricular (i.c.v.) injection of 5µl Adenovirus-Cre. The subsequent localisation and distribution of the cells targeted for recombination was examined by β-galactosidase staining *in situ*. As a control, wild-type mice were injected with Adenovirus-GFP. Both the Cre/GFP-infected mice were culled at 7 days post-injection, their brains removed and stained for β-galactosidase or GFP respectively. I.c.v. Adenovirus-Cre administration induced recombination, and subsequent β-galactosidase expression, in cells within the SVZ of the lateral ventricles (Figure 10: A,B). This SVZ-targeted effect was validated by GFP-expression in an equivalent population in the control mice (Figure 10: C). Furthermore, SVZ cells (containing NSCs) derived from the brains of R26R mice at 7 days post-infection were observed to form neurospheres (NS) *in vitro*. Some of these NS expressed β-galactosidase, suggesting that i.c.v. Adenovirus-Cre injection target NS-forming SVZ cells for recombination.

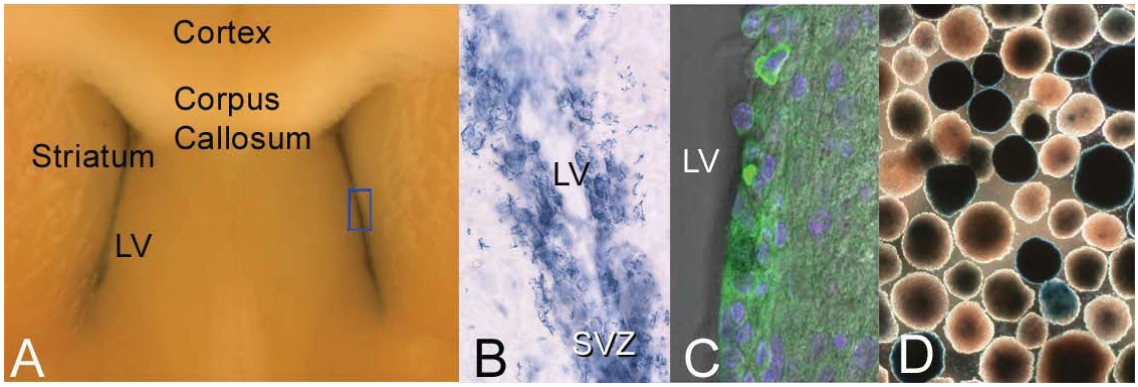

Figure 10: R26R mice given an intra-cerebroventricular (i.c.v.) injection of Adenovirus-Cre exhibit a reproducible pattern of recombination in the 4-5 cell thick periventricular layer that includes the SVZ and ependymal layer (A,B). These cells include NS-forming cells as evidence by their β-galactosidase-positivity (D). An equivalent population of cells was targeted in control wild-type mice injected with Adenovirus-GFP (C) (adapted from (Jacques et al., 2010).

Using confocal microscopy and immunofluorescence staining we examined the SVZs of the Adenovirus-GFP infected control mice to identify the types of cells targeted for recombination. The GFP-expression of infected SVZ cells was observed to co-localise with GFAP and nestin. This suggests that Adenvirus infection targets both the GFAP+ / nestin+ type B astrocytes and GFAP- / nestin+ transiently amplifying type C progenitor cells of the SVZ (Doetsch et al., 1999) (Figure 11: A-D).

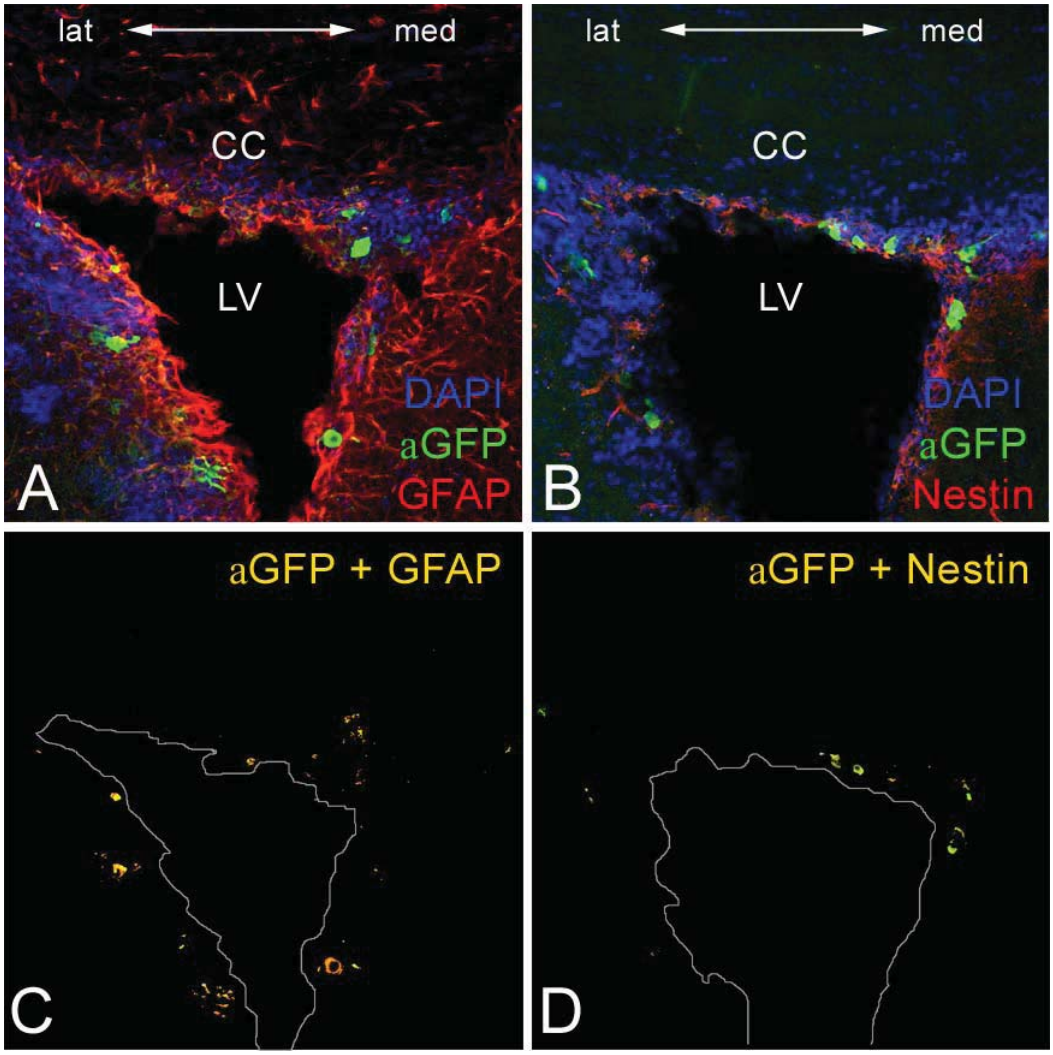

Figure 11: The GFP-expression of infected SVZ cells was observed to co-localise with GFAP (A,C) and nestin (B,D), suggesting that Adenovirus infection targets the NSCs of the SVZ (adapted from (Jacques et al., 2010). Representative images of R26R wild-type SVZ 7 days post-i.c.v. Adenovirus-GFP administration immunofluorescently stained for GFP and GFAP (A-C) or nestin (B,D) with a Hoechst 33342 (DAPI) counterstain. Blue: excitation at 405nm, green: excitation at 488nm, red: excitation at 546nm. Images were taken using a 10x objective on a Zeiss LSM510 META confocal laser scanning microscope with the LSM software.

1.7.2 Inactivation of tumour suppressor genes in the stem cell compartment of the subventricular zone causes brain tumours

In order to determine whether tumours could arise from SVZ cells, i.c.v. Adenovirus-Cre was administered into R26R mice carrying further homozygous LoxP alleles for three different combinations of the tumour suppressor genes Rb, p53, and PTEN. These different combinations were $Rb^{Lox/Lox}$; $p53^{Lox/Lox}$, $Rb^{Lox/Lox}$; $p53^{Lox/Lox}$; $PTEN^{Lox/Lox}$, and $PTEN^{Lox/Lox}$; $p53^{Lox/Lox}$. Each of these genotypes exhibited foci of atypical pre-neoplastic lesions as shown by time culls performed at 14-18 weeks post-injection (Figure 12: A-C). Mice that were left for a longer time post-injection exhibited intrinsic tumours that manifested clinically with phenotypes (Figure 12: D-R) and latencies (Figure 12: S) that were dependent on the genotype and highly reproducible.

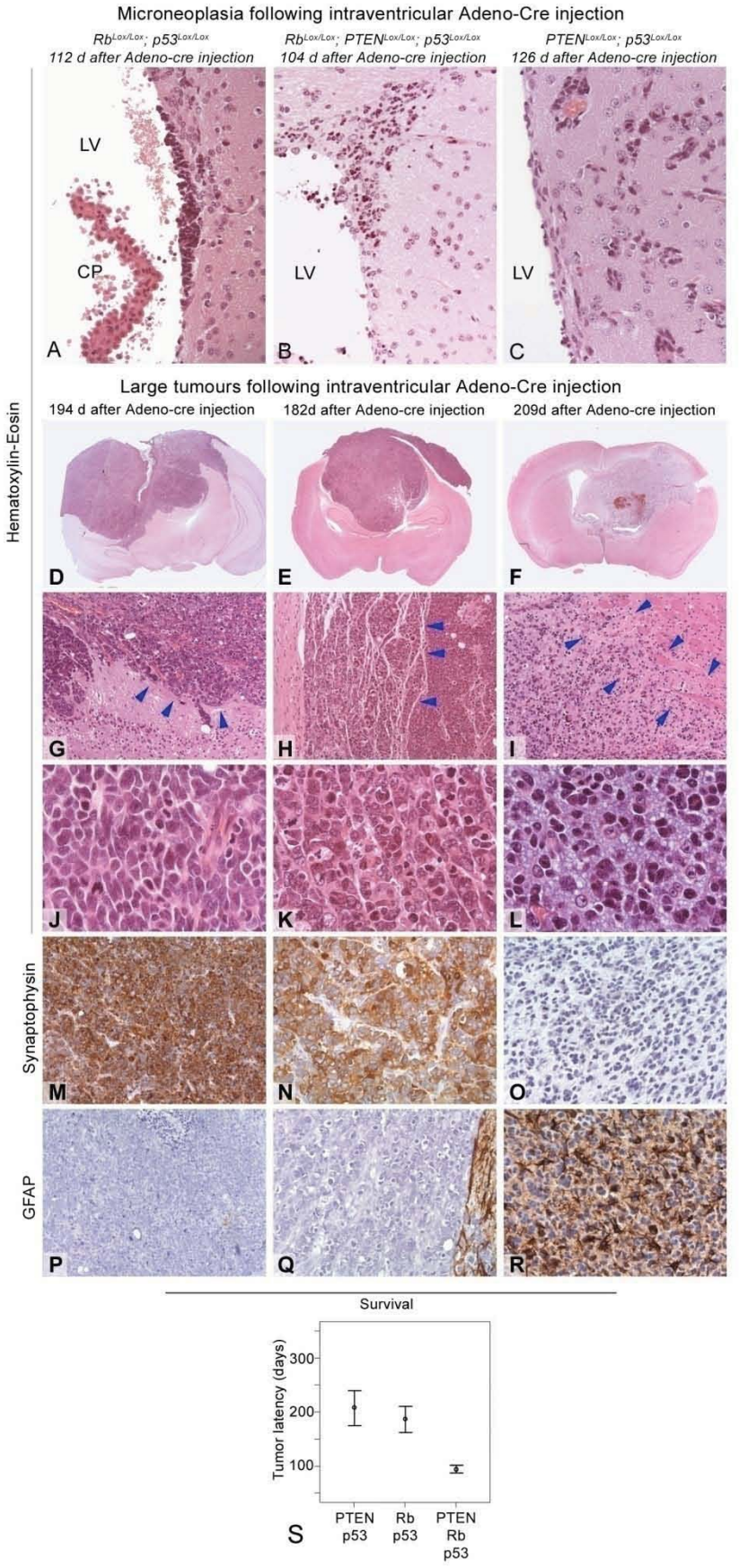

Figure 12: *In vivo* recombination of NSCs induces tumour formation. The development of microneoplasias were observed in the $Rb^{Lox/Lox}$; $p53^{Lox/Lox}$ (A), $Rb^{Lox/Lox}$; $p53^{Lox/Lox}$; $PTEN^{Lox/Lox}$ (B), and

$PTEN^{Lox/Lox}$; $p53^{Lox/Lox}$ (C) genotypes at 112, 104, and 126 days post i.c.v. Adenovirus-Cre administration respectively. Fully developed large intrinsic tumours were observed to develop in the same genotypes (D,E,F) at 194, 182, and 209 days respectively, with means of 190, 95, and 210 (S). In the case of the $Rb^{Lox/Lox}$; $p53^{Lox/Lox}$ genotype the tumour appeared to clinically resemble that of a PNET (G,J,M,P), this was also the case for the $Rb^{Lox/Lox}$; $p53^{Lox/Lox}$; $PTEN^{Lox/Lox}$ genotype (H,K,N,Q). However, the $PTEN^{Lox/Lox}$; $p53^{Lox/Lox}$ genotype appeared to give rise to a glioma-like tumour (I,L,O,R) (adapted from (Jacques et al., 2010).

The $Rb^{Lox/Lox}$; $p53^{Lox/Lox}$ mice developed solid malignant tumours, which morphologically resembled that of human primitive neuroectodermal tumours (PNET), after a latency of 6 months (Figure 12: S). $Rb^{Lox/Lox}$; $p53^{Lox/Lox}$; $PTEN^{Lox/Lox}$ mice also developed PNETs but after a significantly reduced latency of 3 months. Confirmation of the PNET-like phenotype of the tumours was observed from the synaptophysin-positive and GFAP-negative staining patterns (Figure 12: M,N,P,Q) (Louis et al., 2007). The $PTEN^{Lox/Lox}$; $p53^{Lox/Lox}$ mice developed highly malignant infiltrative tumours that morphologically resembled human high-grade gliomas, as also seen in the literature (Llaguno et al., 2009), and confirmed by their synaptophysin-negative and GFAP-positive expression profile (Figure 12: O,R) (Louis et al., 2007). The latency of tumour development in these mice was 6 months, similar to that of the $Rb^{Lox/Lox}$; $p53^{Lox/Lox}$ mice.

1.7.3 Microneoplasia arises from recombined subventricular zone cells and precedes brain tumours

To trace the origin of the tumours observed following i.c.v. Adenovirus-Cre administration1 4x $Rb^{-/-}$; $p53^{-/-}$, 6x $Rb^{-/-}$; $p53^{-/-}$; $PTEN^{-/-}$, and 14x $PTEN^{-/-}$; $p53^{-/-}$ mice were culled prior to the expected the expected latency of tumour formation and their brains processed for haematoxylin and eosin paraffin immunohistochemistry. Small clusters of morphologically atypical cells were observed in areas that contained the neural stem and progenitor cells (Figure 13). These neoplastic lesions were observed to be β-galactosidase-positive, thereby confirming their development as a result of Cre-mediated recombination.

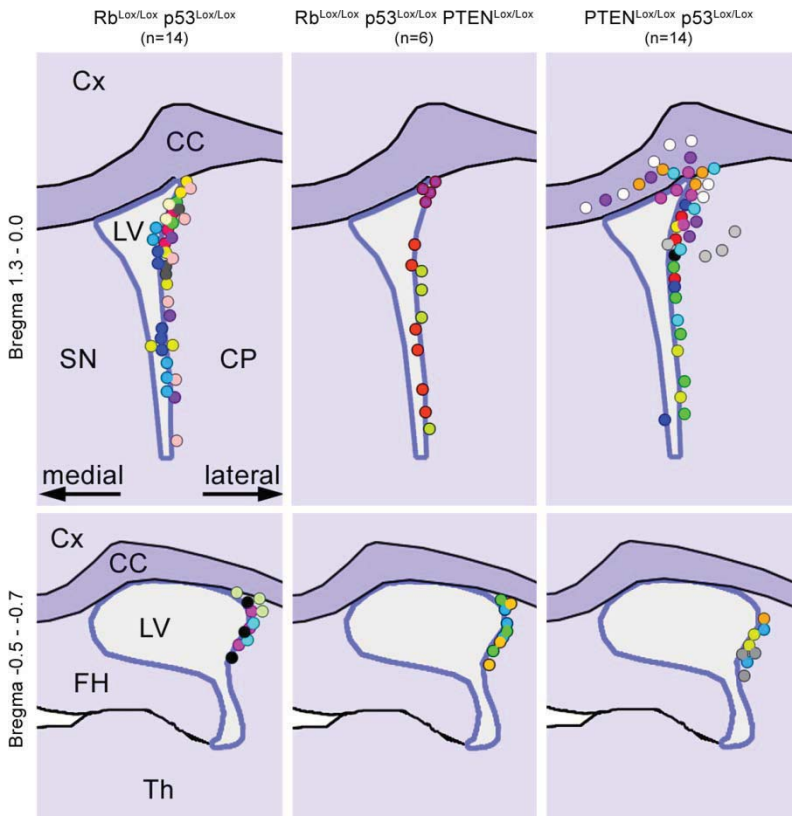

Figure 13: *In vivo* inactivation of TSGs results in the development of small neoplastic lesions in the SVZ prior to tumour formation. The location of precursor lesions from 14x $Rb^{-/-}$; $p53^{-/-}$, 6x $Rb^{-/-}$; $p53^{-/-}$; $PTEN^{-/-}$, and 14x $PTEN^{-/-}$; $p53^{-/-}$ were identified using haematoxylin and eosin paraffin immunohistochemistry and schematically plotted to verify their origin.

The predominant location of the precursor lesions in the lateral and rostral portion of the SVZ suggests that this area contains the stem / progenitor cells that initiate tumourigenesis in our model.

1.7.4 *In vitro* recombined and engrafted neural stem / progenitor cells generate tumours that resemble those induced by intracerebroventricular Adenovirus-Cre administration

In order to confirm that the *in vivo* generated tumours were derived from neural stem / progenitor cells of the SVZ we derived and expanded SVZ cells *in vitro*, recombined the TSGs using Adenovirus-Cre, and engrafted them into the striata of non-recombined mice of a similar genetic background.

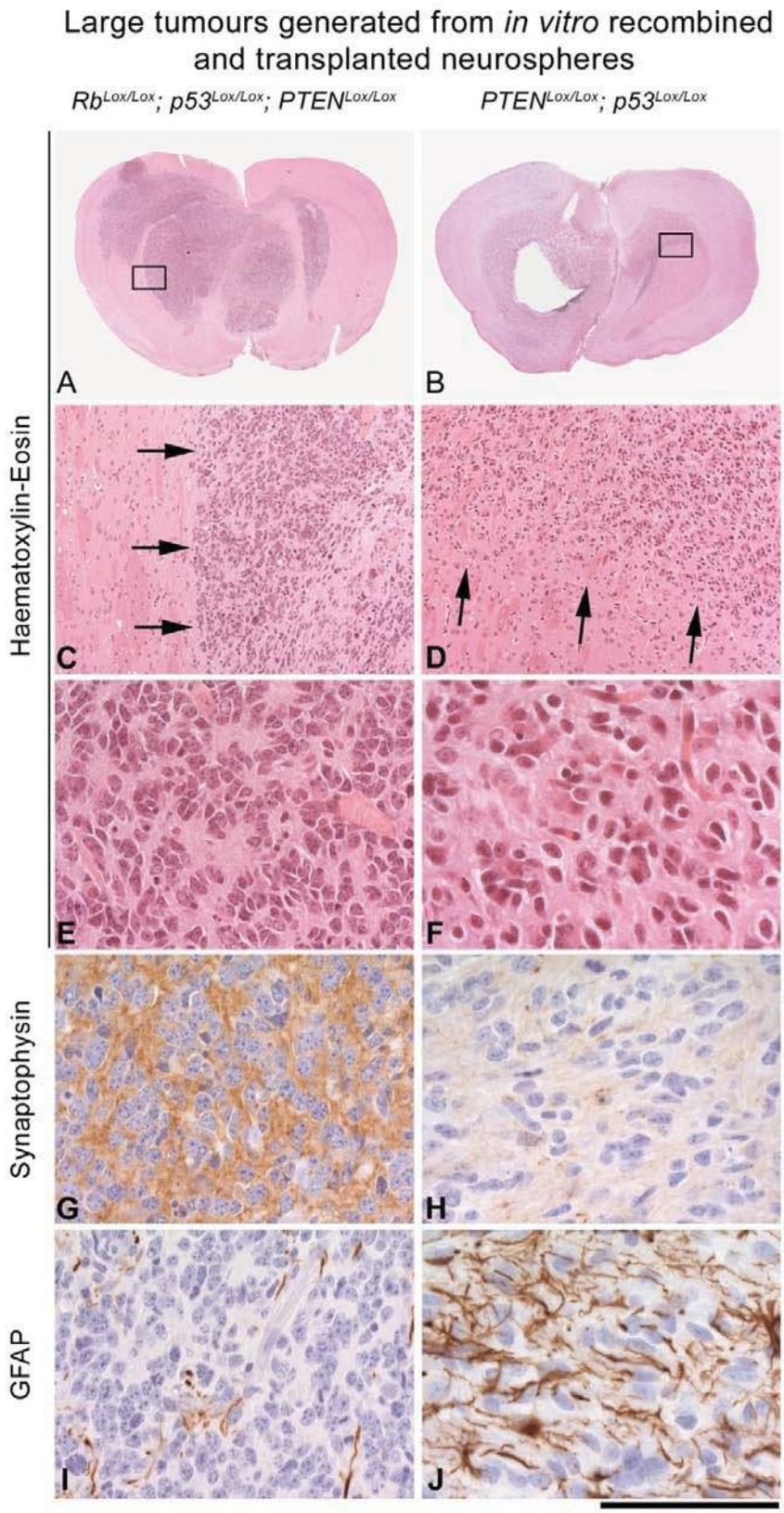

Figure 14: *In vitro* recombined and engrafted NS generate tumours. As with i.c.v. Adenvirus-Cre administration, *in vitro* recombined $Rb^{-/-}$; $p53^{-/-}$; $PTEN^{-/-}$ NS were observed to generate synaptophysin-positive (G) and GFAP-negative (I) PNET-like tumours (A,C,E) whereas the $PTEN^{-/-}$; $p53^{-/-}$ NS were observed to generate synaptophysin-negative (H) and GFAP-positive (J) glioma-like tumours (B,D,F) (adapted from (Jacques et al., 2010).

The engrafted $Rb^{-/-}$; $p53^{-/-}$; $PTEN^{-/-}$ (13/13), and to a lesser extent the $Rb^{-/-}$; $p53^{-/-}$ (2/32), NS gave rise to tumours (Figure 14: A,C,E) that resembled PNETs similar to the coprresponding i.c.v. Adenovirus-Cre-induced tumours (Figure 12), and also displayed the same synaptophysin-positive and GFAP-negative expression profile (Figure 12: G,I). Likewise, the engrafted $PTEN^{-/-}$; $p53^{-/-}$ NS gave rise to infiltrative gliomas (8/23) (Figure 14: B,D,F) that displayed the same synaptophysin-negative and GFAP-positive expression profile as those tumours observed after i.c.v. Adenovirus-Cre-mediated recombination of the same TSGs (Figure 12 and Figure 14: H,J). These findings demonstrate that *in vitro* recombined and grafted neural stem/progenitor cells, grown as NS, generate tumours that are phenocopies of those generated following i.c.v. *in vivo* recombination. This suggests that SVZ NSCs may represent the brain tumour initiating cell (BTIC). However, these results do not exclude the possibility that other more mature cell types (e.g. terminally differentiated astrocytes) were ectopically targeted for recombination during i.c.v. Adenvirus-Cre delivery and contributed toward the observed tumourigenesis.

1.8 Model System Aims

1. Characterise the *in vitro* functional profiles of neural stem cells and their transformed counterparts based on the combination of tumour suppressor genes inactivated;
    a. Verify that *in vitro* NSCs cultures contain the same SVZ NSCs that are targeted by i.c.v. Adenovirus-Cre administration.
    b. Characterise the effect of Rb, p53, and PTEN loss on the growth rate, self-renewal, multipotency and biomarker expression of NSCs *in vitro*.
    c. Examine whether the *in vitro* functional properties of NSCs correlate with *in vivo* tumour hit rate and/or latency.
    d. Identify surrogate markers of tumour phenotype.

2. Characterise the brain tumour initiating cell;
    a. Verify that brain tumour development following i.c.v. Adenovirus-Cre administration is initiated and driven by SVZ NSCs.
    b. Examine whether NSCs exist in the brain tumour bulk as brain tumour initiating cells (BTICs).
    c. Refine the BTIC to a more specific sub-type of SVZ NSC.
    d. Identify whether NSCs exist in different states dependent on their environment and whether these have altered tumour hit rates, latencies, and phenotype propensities.
    e. Functionally characterise these different states *in vitro*.

3. Investigate CD133 (Prominin-1) as a marker brain tumour initiating cells;
    a. Verify that SVZ NSCs express CD133 both *in vivo* and *in vitro*.
    b. Characterise the CD133 expression pattern in wild-type and recombined tumourigenic NSCs.
    c. Characterise the functional differences of tumourigenic CD133+ and CD133- NSCs *in vitro*.
    d. Characterise the *in vivo* tumour hit rates, latencies, and phenotype propensities of tumourigenic CD133+ and CD133- NSCs and assess whether CD133 expression can be used as a predictive indicator.
    e. Identify novel markers of BTICs.

4. Assess the relative contribution of terminally differentiated astrocytes to the development of brain tumours in our model system.
    a. Verify whether i.c.v. Adenovirus-Cre administration targets terminally differentiated astrocytes, outside of the SVZ, for TSG recombination.
    b. Assess whether TSG loss in terminally differentiated astrocytes induces a transformation in function and/or differentiation state of the cells.
    c. Examine whether these hypothetically transformed astrocytes can generate tumours *in vivo*.

2 Materials and Methods

2.1 *In Vivo* Experimental Procedures

2.1.1 Mice

The following mouse genotypes were used: $Rb^{LoxP/LoxP}$; $p53^{LoxP/LoxP}$; $R26R^{LoxP/LoxP}$ (short: Rb/p53), $PTEN^{LoxP/LoxP}$; $p53^{LoxP/LoxP}$; $R26R^{LoxP/LoxP}$ (short: PTEN/p53), $Rb^{LoxP/LoxP}$; $PTEN^{LoxP/LoxP}$; $R26R^{LoxP/LoxP}$ (short: Rb/PTEN), or $Rb^{LoxP/LoxP}$; $p53^{LoxP/LoxP}$; $PTEN^{LoxP/LoxP}$; $R26R^{LoxP/LoxP}$ (short: Rb/p53/PTEN). All mice were inter-crossed from single mutant conditional knockout mice generated with the same strain ES cells (129 Ola). After generating double, triple, or quadruple homozygous mouse lines, they were kept homozygous for all alleles and in-bred within the same colony. Further description of $PTEN^{LoxP/LoxP}$ mice is given in (Marino et al., 2002b), $Rb^{LoxP/LoxP}$, and $p53^{LoxP/LoxP}$ mice in (Marino et al., 2000) and $R26R^{LoxP/LoxP}$ reporter mice are described in (Soriano, 1999). Genotyping was carried out from tail DNA using standard PCR reactions. Primers are as published: Rb18 and Rb19, p53–int10–fwd and p53 int10–rev (Marino et al., 2000), PTEN A and S (Marino et al., 2002b), ROSA26-1, 2 3 (Soriano, 1999), LZ1 and LZ2 (Marino et al., 2000). The mice were kept, and all procedures were carried out, according to institutional and UK Home Office guidelines (Project license 70/5540 and 70/6603). All mice were housed and maintained in the MRC Biological Services Facility (BSF), Wakefield Street, London under specific pathogen-free conditions in accordance with the UK Animals (Scientific Procedures) Act 1986. They were kept on a 12hr light-dark cycle and given food and water *ad libitum*.

2.1.2 Anaesthesia

Prior to all stereotaxic surgery mice were anaesthetised intraperitoneally (i.p.) using Hypnorm / Hypnovel (Hypnorm : Hypnovel : H_2O; 1:1 :3) at 10µl/g bodyweight with the males receiving a slightly lower dose of ca. 8µl/g, or with Ketaset / Rompun at 100mg/kg bodyweight / 16mg/kg body weight (150-200µl).

2.1.3 Preparation and administration of Adenovirus-Cre for i.c.v. delivery

The HindIII fragment of pBS185 containing the Cre ORF under control of the hCMV immediate early promoter and the metallothionein I polyadenylation signal was inserted into the HindIII site of pdE1spIA and co-transfected with pJM17 into HEK293 cells. The viruses were plaque purified and re-analysed prior to preparation of large scale stocks. The recombinant adenoviral vector was propagated in HEK293 cells and the titre was determined by a plaque formation assay.

Viral infection of SVZ cells was achieved by unilateral stereotaxic injections of 10^9 plaque-forming units (5µl) of Adenovirus-Cre in 10mMTris-HCl directly through the skull into the left cerebral hemisphere of anaesthetised mice placed in a stereotaxic frame (Narishige SR 6N). The coordinates of the injection site in relation to bregma were: anterior 0 mm; lateral 0.5 mm, ventral 2.5 mm and was performed with a Hamilton syringe (701RN) and 26G needle.

2.1.4 Intracerebral engraftment of cells

NS and astrocytes were taken for engraftment/transplantation at passage 3-5. NS were collected in a 15/50ml tube and allowed to settle before being resuspended in 0.5ml DMEM/HAM F12 (BioWhittaker) NS growth medium. Astrocytes were trypsinised with trypsin-EDTA solution (Invitrogen), spun at 300 x g for 5 min (room temperature) and collected in 100µl DMEM high glucose astrocyte growth medium (BioWhittaker).

Intracerebral engraftment of NS/astrospheres was performed by injecting 5-15µl of concentrated NS/astrosphere suspension sediment into the left striatum of genetic background-matched adult mice (bregma, 1.5 mm lateral, 2 mm ventral) using a 22G needle attached to a 25µl Hamilton syringe (RN1702). A 15µl injection was found to contain 1202 +/- 147 NS/astrospheres or $1.38x10^6$ +/- $0.12x10^6$ NSCs.

Intracerebral injection of astrocytes was achieved by injecting 5-12.5µl glial cell suspension sediment ($1x10^5$ - $1x10^6$ cells) into the left striatum (bregma, 1.5 mm lateral, 2 mm ventral) genetic background-matched or nude adult mice using a 22G needle attached to a 25µl Hamilton syringe (RN1702).

2.1.5 BrdU injections

To label proliferating cells, mice were given intraperitoneal (i.p.) injections of BrdU at a concentration of 50μg per gram of body weight. Being a base analogue of thymidine, BrdU substitutes for thymidine during DNA synthesis and incorporates into the newly synthesized DNA. Therefore by BrdU administration, dividing (stem) cells are labelled. BrdU positive cells can be detected on brain sections by immunohistochemical techniques using an antibody detecting the BrdU residues incorporated into nuclear DNA.

2.1.6 Culling and brain removal

For the purposes of primary cell culture the mice were culled by cervical dislocation, their brains removed under sterile conditions, collected in ice-cold HEPES buffer and subsequently processed in accordance with the required protocol.

For histology purposes the mice were culled by asphyxiation in rising levels of CO_2 in order to retain the structural integrity of the entire brain. Following this the brains were removed and left to fix in 10% buffered formalin for 30 minutes at room temperature after which they were either stained for β-galactosidase or processed for paraffin histology.

2.2 Cell Culture

2.2.1 Derivation and growth of neural stem cells

All surgical instruments were surgically sterilised. A minimum of four mice were used and were killed by cervical dislocation. The brain was removed and placed in a 10cm dish containing ice-cold HEPES buffer in order to preserve the tissue. Each brain was transferred out of the HEPES buffer and onto the sterile side of a dry petri dish lid and processed sequentially. Using a stereo microscope, along with surgical forceps and a razor blade, the anterior portion (bregma 2 to -2) of the SVZ-containing lateral ventricles was microdissected (Figure 15).

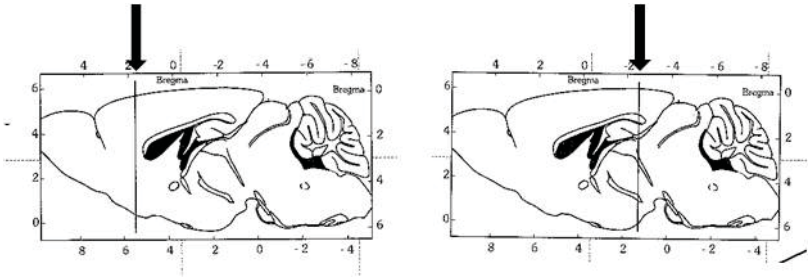

Figure 15: Bregma coordinates of the brain region microdissected for lateral ventricle acquisition.

This 4mm coronal slice was then trimmed further (Figure 16), using micro-scissors, to eliminate surplus tissue leaving an area that specifically encompassed the lateral ventricles.

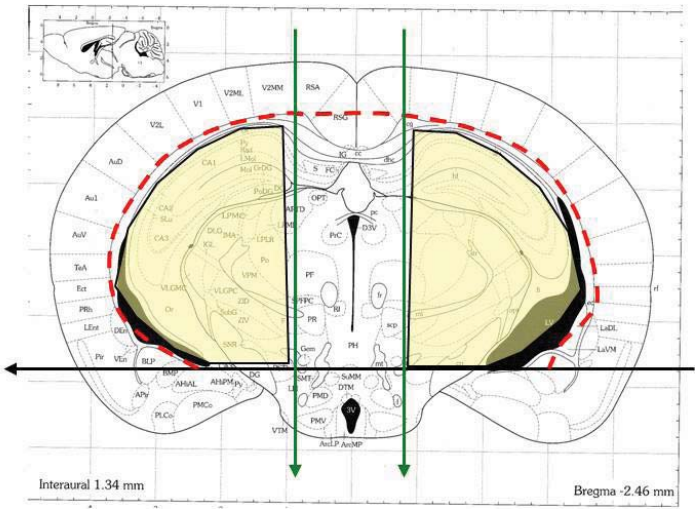

Figure 16: Coronal schematic showing the two lateral SVZ-containing lateral ventricle regions (yellow) targeted for microdissection. Black line: first plane used to trim tissue, dashed red line: second plane used to trim tissue, green lines: third planes used to trim tissue.

The two resulting segments of tissue were transferred back into ice-cold HEPES buffer. These SVZ-containing tissue segments were transferred onto a sterile Teflon disk and minced using a Tissue Chopper (McIlwain) set to 400µm and cut in 5 planes. The tissue was then dissociated by treatment with Papain (Worthington, USA), and mechanically dissociated into a single cell suspension. The cells were pelleted by centrifugation at 300 x g for 5min (room temperature). In order to purify the sample and remove debris the cell pellet was reconstituted in a DNAse-albumin-inhibitor mixture and spun in a discontinuous density dependant gradient over an albumin-inhibitor mixture at 70g for

6min (room temperature). The purified cell pellet was then resuspended in the pro-mitogenic Dulbecco's modified Eagle's medium/Ham F12 medium (DMEM/Ham F12, Sigma) supplemented with 1 ml B27, 500ml P/S, EGF and bFGF (both 20ng/ml). The cells were plated out and initially left for five days before replacing the medium. Following this media changes were performed every three days. The cells grew as free-floating aggregates (neurospheres) and were passaged when deemed large enough (ca. 12 days) by incubation in Accumax (Chemicon) for 45 minutes at 37°C followed by mechanical dissociation into single cells at which point they could be re-plated.

All cultures were maintained at 37°C in an atmosphere of 5.0% CO_2 and 95% rH (Hareaeus), and all experiments were performed between passages 2 and 4.

2.2.2 Derivation and growth of glial cells

Neonatal mice (P2-P5) were killed by decapitation. The brain was removed and placed in cold (4°C) HEPES buffer on ice. Using a dissecting stereo-microscope, meninges and blood vessels were separated from the cortex, which were then collected in 6cm sterile dishes containing cold HEPES buffer. The tissue was minced with a mechanical tissue shopper (400μm thickness) and digested for 12 minutes at 37°C in a solution of HEPES buffer and trypsin containing trypsin-EDTA and Dnase I. The digestion was terminated by adding a Trypsin stopper solution containing trypsin-inhibitor soybean (Boehringer Mannheim), $MgSO_4$ $7H_2O$ and Dnase I. Subsequently, tissue suspension was fractionated by centrifugation for 30 seconds at 3300 rpm (room temperature). The fraction was resuspended in a small volume of pre-warmed trypsin solution, triturated with an 18G syringe and spun once more for 12 minutes at 1000 rpm (room temperature). The cell suspension was plated out in 10cm dishes (NUNC) with growth medium (DMEM high glucose with L-glutamine supplement (BioWhittaker), 10% FCS (Invitrogen, #10106-169) and 1% P/S (Invitrogen). Medium was replaced every 3 days. Prior to infection, the cells were passaged once confluent using trypsin-EDTA solution (Invitrogen) and re-plated at half of their original density (1 in 2 dilution) in growth medium.

All cultures were maintained at 37°C in an atmosphere of 5.0% CO_2 and 95% relative humidity (Heraeus), and all experiments were performed between passages 2 and 3. In order to calculate cell numbers for the purpose of experiments, astrocytes were trypsinised with trypsin-EDTA solution (Invitrogen), spun for 5 min at 1000rpm and

resuspended in 5ml fresh medium. A 20µl aliquot was taken from this cell suspension to perform the cell count (as described in section 2.2.3).

2.2.3 Adenovirus-Cre/GFP-infection of neurospheres and astrocytes

NS were collected in a 15/50ml tube and allowed to settle. All but 1ml media was aspirated and a 50µl aliquot was taken, incubated in 350µl AccuMax (Chemicon, #SCR006) at 37^0C for 20 minutes (as the NS are smaller), and then mechanically dissociated into single cells. A 20µl aliquot was taken from these single cells and mixed 1:1 with 20µl of Trypan Blue (Sigma, T8154) so that the cells could be visualised. The solution was then loaded onto a haemocytometer where a cell count was performed. Using a multiplicity of infection (MOI) of 5, the required volume of Adenovirus-Cre / Adenovirus-GFP required for infection was calculated (both viral titres were ~$2.5x10^9$ pfu/ml). The original population of NS were separated with a ratio of 0.1 : 0.55 : 0.35 for Adenovirus-Cre : Adenovirus-GFP : Untreated and placed in separate 10cm plates. The NS were then infected with the required volume of Adenovirus-Cre / Adenovirus-GFP virus. The NS medium was changed 2 days after infection, and then the NS were passaged after 3 days. Infection efficacy was determined by examining and recording the 509nm emission of the Adenovirus-GFP treated cells 2 days post-infection under a Zeiss Axiovert 200 fluorescence microscope (excitation wavelength 488nm). Pictures were obtained using a Nikon Coolpix 995 3 Megapixel digital camera mounted on the microscope.

In contrast to NS, astrocytes were grown as an adherent culture. Using the same multiplicity of infection (MOI) of 5, the required volume of Adenovirus-Cre / Adenovirus-GFP required for the infection of astrocytes was calculated. Based on both viral titres being ~$2.5x10^9$ pfu/ml this volume was ~2µl per 80-90% confluent 10cm plate. As the number of cells in an 80-90% confluent 10cm plate was highly repeatable, a standardised volume of 2µl Adenovirus-Cre/GFP was used for the infection of each 10cm plate for all astrocytic cultures. Six 10cm plates were infected with a ratio of 1 : 3 : 2 for Adenovirus-Cre : Adenovirus-GFP : Untreated astrocytes. The medium was changed 2 days after infection, and then the astrocytes were passaged after 3 days. Infection efficacy was determined by examining and recording the 509nm emission of the Adenovirus-GFP treated cells 2 days post-infection under a Zeiss Axiovert 200

fluorescence microscope (excitation wavelength 488nm). Pictures were obtained on a Nikon Coolpix 995 3 Megapixel digital camera mounted on the microscope.

2.3 *In vitro* Functional Characterisation Assays

2.3.1 β-Galactosidase staining

Upon Cre-recombination, the LacZ reporter gene in the ROSA26 locus expresses β-Galactosidase and can therefore be used as a marker to estimate the efficiency of Cre-recombination.

This technique can be performed *in situ* on *ex vivo* brain slices, i.e. to macroscopically observe any Adenovirus-Cre-mediated recombination. Mice were culled by CO_2, their brains removed and left to fix in 10% formaldehyde (formalin) for 30 minutes at room temperature. Using a razor blade, brain slices encompassing the necessary regions (rostral section of the LV and SVZ) were cut and further fixed in formalin for 30 minutes (room temperature) on an orbital shaker. The brain slices were then permeabilised by incubation in permeabilisation buffer (10mM Phosphate buffer, 150mM NaCl, 3mM $MgCl_2$, 3.3mM $K_4Fe(Cn)_6$ x $3H_2O$, 3.3 $K_3Fe(CN)_6$, 0.02% NP40, 0.01% sodium deoxycholate) for 30 minutes (room temperature) on an orbital shaker. The buffer was then changed to permeabilisation buffer containing 1mg/ml BlueGal (Merck) and the slices were left to incubate o/n at 37°C on an orbital shaker. BlueGal is cleaved by β-galactosidase expressed by the LacZ gene yielding galactose and 5-bromo-4-chloro-3-hydroxyindole. This compound is then oxidized into 5,5'-dibromo-4,4'-dichloro-indigo, an insoluble blue product. Once successfully stained, these slices were then post-fixed for 24 hours in formalin and either immediately imaged or processed for paraffin immunohistochemistry.

For NS, a 1ml aliquot of was taken directly from a NS culture at around 10 days post-infection. In contrast, astrocytes which had been trypsinised at confluence and plated out at $0.3x10^5$ cells/ml in a 4-well plate, were once again allowed to grow to confluence prior to being stained. Both preparations were washed once with PBS followed by fixation with 0.5% Glutaraldehyde for 5 minutes at room temperature. After two more PBS washing steps the cells were incubated with staining solution (10mM Phosphate

buffer, 150mM NaCl, 1mM $MgCl_2$, 3.3mM $K_4Fe(CN)_6$ x $3H_2O$, 3.3 $K_3Fe(CN)_6$) containing 1mg/ml BlueGal (Merck) overnight at 37°C.

The brain slices and the cells were checked for β-galactosidase staining using a Zeiss Stemi SV11 microscope or a Zeiss Axiovert 200 microscope respectively, and images were captured using a mounted Nikon Coolpix 995 3.34 mega pixels digital camera.

2.3.2 WST-1 proliferation assay

The WST-1 assay is used to measure the relative proliferation of cells *in vitro*. The assay principle is based on the conversion of the tetrazolium salt WST-1 into an orange coloured dye (formazan salt) by mitochondrial dehydrogenase enzymes. Over time this reaction produces a colour change of the medium which is directly proportional to the amount of mitochondrial dehydrogenase, and therefore cell number/activity, in a given culture.

This analysis was performed in a 96-well plate. NS were dissociated by Accumax and seeded at $6x10^4$ cells/well in 10 wells each containing 100µl medium. Astrocytes were trypsinised at confluence and seeded at $5x10^3$ cells/well in 10 wells each containing 100µl. NS were left for 3 days, and astrocytes for 2, before the addition of 10µl WST-1 reagent per well and taking readings at 0, 4, 6 and 8 hours.

Samples were run in groups of 10 repeats, and corrected against background fluorescence, on a Tecan Sunrise microplate reader with XFluor 4 software using a detection wavelength of 440nm and a reference of 620nm.

2.3.3 Neurosphere size and neurosphere-forming clonogenicity assay

For the NS size assay, NSCs were taken at passage 3 were seeded at $0.5x10^6$ cells/well in 1 well of a 6-well plate containing 3ml NS media. On day 3 an additional 4ml of media was added to the well, and full media changes (4ml) were carried out on days 5 and 7. On day 8 the diameter of the cells was visualised using a Zeiss Axiovert 135 microscope and recorded using the Openlab 5 software. An average was calculated from ≥100 cells with the cell diameter being measured twice per cell.

For the NS-forming clonogenicity assay NSCs taken at passage 3 were seeded at $0.5x10^6$ cells/well in 1 well of a 6-well plate containing 3ml NS media and the number of neurospheres that formed was measured after 8 days. To measure the NS-forming

ability of the NSCs a representative 0.5ml aliquot was taken from the NS culture and transferred into a 4-well plate for counting. Two NS counts were performed and the average was extrapolated, depending on the total volume of the NS culture, in order to generate an estimation of the total number of NS in the culture.

2.3.4 Self-renewal assay

Neurospheres were collected and, if these were non-*in vitro* recombined, the percentage of recombined neurospheres was calculated by staining for β-Galactosidase activity and counting the number of positive (blue) neurospheres. The neurospheres were then dissociated into single NSCs by complete aspiration of any media (including a wash of the cells in PBS) and incubation in 500µl (per half 10cm plate) Accumax (Chemicon) for 45mins at 37°C followed by mechanical dissociation. The Accumax was diluted out by transferral into NS medium at a ratio of 1:3. The NSC-containing medium was then passed through a sterile 40µm nylon mesh to remove any multi-cell aggregates, collected in an Eppendorf tube and transferred onto ice. The single cells were then adjusted to a concentration of $1x10^6$ cells/ml, transferred to the Flow Cytometry Core Facility (UCL Institute of Child Health) for single cell sorting into individual wells of 96-well plates (2x plates per genotype) using the MoFlo XDP FACS machine (Beckman Coulter) with IntelliSort software. 200µl of NS medium was added to each of the wells of the 96-well plates for cell collection (less liquid causes NSCs to be reflected out of the wells and lost). The forward/side scatter gating and both forward scatter and side scatter height-width plots were respectively used to exclude dead cells and for doublet discrimination to maximise efficient single cell sorting (Figure 17). One well of each 96-well plate used was designated to receive 100 cells as a positive control. Once the single NSCs had been collected in the 96-well plates they were kept on ice until they could be transferred back into an incubator maintained at 37°C in an atmosphere of 5.0% CO_2 and 95% relative humidity. As a post-hoc measure of verifying the viability of the NSCs used for sorting the DNA binding dye Hoechst 33342 (Sigma) was added at a concentration of 5µg/ml to the original NSC samples and left to incubate for 5 minutes before being re-run through the FACS machine.

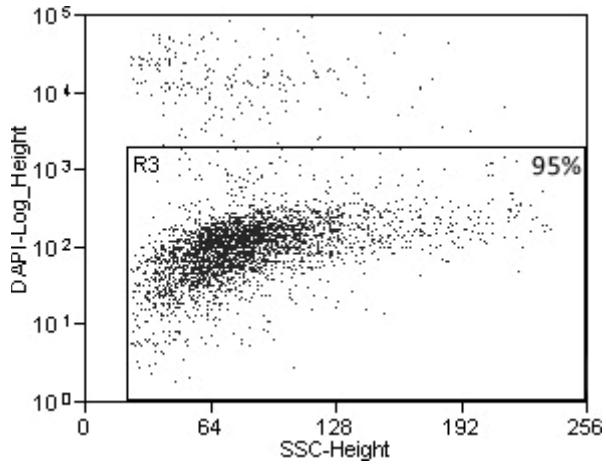

Figure 17: 95% of NSCs used for single cell sorting (self-renewal assay) were viable. Representative DAPI fluorescence (y-axis) vs. side scatter (x-axis) FACS plot of a NSC sample used for single cell sorting into individual wells of a 96-well plate using a MoFlo XDP FACS machine.

The number of cells present in each of the wells was then counted to verify the success and accuracy of the single cell sorting process and to record the starting number of single cells. The plates were then incubated for nine days with medium changes of 250µl taking place after four and seven days (only 80% of the medium was removed with each change to prevent aspirating the neurospheres). The self-renewal and growth of the single NSCs into neurospheres was monitored over the nine days by taking images with a Nikon Coolpix 995 3 Megapixel digital camera mounted on a Zeiss Axiovert 200 fluorescence microscope. After nine days the number of neurospheres that had grown from single NSCs in both 96-well plates was counted and the percentage of NSCs capable of self-renewal was calculated. If the percentage of recombined neurospheres calculated at the start of the assay was less than 100% then a repeat β-Galactosidase activity stain was performed *in situ* on all the neurospheres in one of the two 96-well plates so that the self-renewal data could be split into non-recombined vs. recombined NSCs.

If desired, the secondary self-renewal of the NSCs could be tested for by repeating the protocol described above (minor changes detailed below) on the neurospheres yielded from the primary self-renewal assay (Figure 18). Special care was taken for the secondary self-renewal assay with respect to dissociating the neurospheres as they had to be dealt with individually to maintain the clonal identity of the neurospheres. The neurospheres were therefore randomly selected and dissociated into single NSCs in the individual wells of the 96-well plates *in situ* by complete aspiration of any media and

incubation in 100µl Accumax (Chemicon) for 20mins at 37°C followed by gentle mechanical dissociation. The Accumax was diluted out by transferral into 300µl NS medium. The NSC-containing medium was then passed through a sterile 40µm nylon mesh to remove any multi-cell aggregates, collected in an Eppendorf tube and transferred onto ice. The final concentration was calculated but not adjusted as the estimated ~1000 cells/neurosphere ($0.25x10^4$ cells/ml) is already below the optimum concentration of cells for sorting with the MoFlox XDP FACS machine. To compensate for this, only half of a 96-well plate was used to receive the sorted single NSCs from each of the secondary neurospheres, with a single designated well receiving 10 cells as a positive control. A minimum of six individual neurospheres totalling three 96-well plates were used for the secondary self-renewal assay.

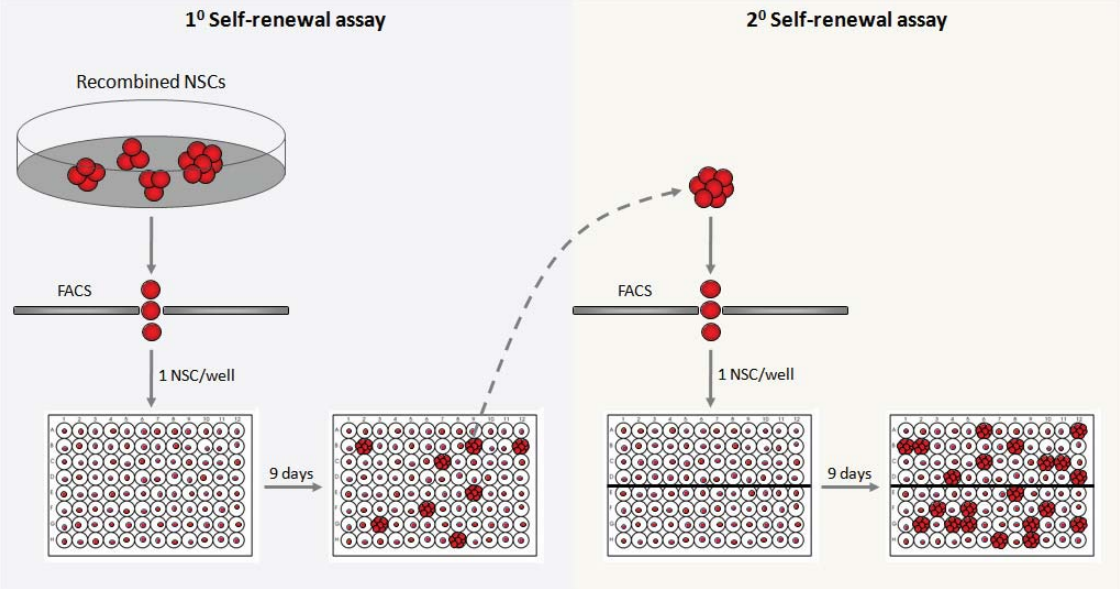

Figure 18: Schematic representation of the primary and secondary phases of the self-renewal assay protocol.

2.3.5 Neurosphere differentiation

Neurosphere differentiation was induced by plating NS on laminin-coated (1mg/ml) glass coverslips (13mm) contained in 24-well plates or chamber slides in DMEM/Ham F12 (Sigma) with 1% FCS for 5 days. A partial medium change was carried out after 3 days. The differentiated cells were then washed in PBS and fixed in 4% formaldehyde for 30 minutes (room temperature) before being processed for immunohistochemistry.

2.3.6 Plating glia on coverslips

To prepare for immunohistochemistry, cells were trypsinised using trypsin-EDTA solution (Invitrogen) and plated at a density of $1x10^5$cells/ ml on sterile 13mm glass cover slips contained in the wells of 24-well plates in DMEM high glucose with L-glutamine (Sigma) with 10% FCS for 5 days. The differentiated cells were then washed in PBS and fixed in 4% formaldehyde for 30 minutes (room temperature) before being processed for immunohistochemistry.

2.4 Expression Analysis

2.4.1 cDNA Expression analysis with Superarray RT^2 Profiler

Total RNA was extracted from samples using the Qiagen RNeasy Mini Kit in accordance with the manufacturer's instruction. The yield and purity of a 1µl sample of the total RNA was assessed using the UV/VIS NanoDrop spectrophotometer (ND-3300, NanoDrop Technologies, USA) to measure the concentration (A_{260}: ng/µl), the level of protein contamination (A_{260}:A_{280}), and the level of general contamination (A_{260}:A_{230}). Only samples with concentrations greater than 500 ng/µl, A_{260}:A_{280} ratios greater than 2.0, and A_{260}:A_{230} ratios greater than 1.7 were considered suitable for downstream use. The ribosomal RNA band integrity of these samples was then assessed using a 2100 BioAnalyzer (Agilent Technologies, USA) to verify that that had been no 18s or 28s ribosomal RNA (rRNA) degradation. All the samples that passed the NanoDrop purity test were found to have high quality non-degraded rRNA as shown by the presence of two well-defined peaks without any smearing corresponding to 18S and 28S rRNA on the electropherograms (Figure 19).

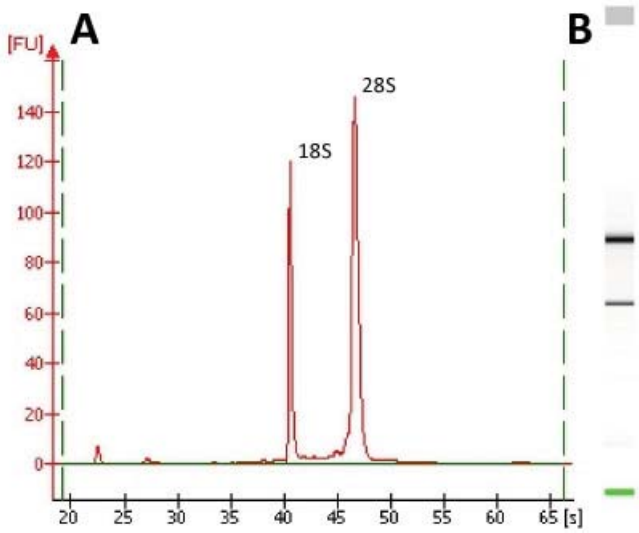

Figure 19: All samples that passed the NanoDrop purity test were found to have high quality non-degraded rRNA. (A) Representative BioAnalyzer electropherogram of a total RNA sample taken from *in vitro* neurospheres showing well-defined sharp peaks for both the 18S and 28S ribosomal RNA. (B) Sharp pseudo-agarose gel electrophoresis bands demonstrate minimal degradation.

A quantitative RT-PCR was performed using the manufacturer's protocols for the Mouse Cancer PathwayFinder RT^2 Profiler PCR Superarray (APMM-033C, SA Biosciences, USA). The Mouse Cancer PathwayFinder PCR Superarray is a 96-well plate containing RT^2 qPCR Primers for a set of 84 genes representative of six cancer pathways (cycle control and DNA damage repair, apoptosis and cell senescence, signal transduction molecules and transcription factors, adhesion, angiogenesis, invasion and metastasis), plus five housekeeping genes (β-glucuronidase, hypoxanthine guanine phosphoribosyl transferase 1, heat shock protein 1 beta, glyceraldehydes-3-phosphate dehydrogenase, β-actin), a mouse genomic DNA contamination control, three reverse transcription controls, and three positive PCR controls.

First strand cDNAs were prepared from 1µg of total RNA from each sample using the RT^2 First Strand Kit according to the maunfacturer's instructions (C-03, SA Biosciences, USA). Following this, the cDNA for each sample was added to the ready-to-use RT^2 SYBR green qPCR mastermix and, with one sample corresponding to one 96-well PCR Superarray plate, 25µl of the experimental cocktail was added to each well (containing the predispensed gene-specific primer sets) of the plate. The plate was sealed with optical adhesive film and a two-step cycling program (Figure 20) was loaded onto the ABI 7500 FAST Real-Time PCR System (Applied Biosystems).

Cycles	Duration	Temperature
1	10 minutes	95^0C
40	15 seconds	95^0C
	1 minute	60^0C

Figure 20: Two-step cycling program used to run the Mouse Cancer PathwayFinder RT^2 Profiler PCR Superarray on the ABI 7500 FAST Real-Time PCR System.

The instrument's software was used to automatically set the baseline (start cycle: 3, end cycle: 15) and the threshold cycle (C_t) was set manually by adjusting it above the background signal but within the lower half to one-third of the linear phase on the log view of the amplification plot. The resulting C_t values for all the genes across each of the four experimental genotypes (n=2 each) were exported into the Superarray 'Data Analysis Template Excel File' for analysis against the control genotype (n=2).

Relative gene expressions were calculated using the $2^{-\Delta\Delta Ct}$ method (Pfaffl, 2001) and an average of all five of the housekeeping genes for normalisation. Any C_t values greater than 35 were considered to be negative and only samples that were passed for all the internal/external controls were analysed (none failed). Fold change values were then presented as average fold change = 2(average $^{\Delta\Delta Ct}$) for each of the genes relative to the control samples and converted into fold changes (up- or down-regulation). The statistical significance of differences in gene expression between the experimental samples (n=2) and the controls (n=2) was calculated using a two-tailed student's *t*-test ($P < 0.05$).

The Superarray assay was carried out for a total of two experimental repeat samples for each of the non-recombined Adenvirus-GFP-infected control, $Rb^{-/-}$; $p53^{-/-}$, $PTEN^{-/-}$; $p53^{-/-}$, $Rb^{-/-}$; $p53^{-/-}$; $PTEN^{-/-}$, and $Rb^{-/-}$; $PTEN^{-/-}$ genotypes (n=10 overall).

2.4.2 Reverse-transcriptase polymerase chain reaction analysis of CD133 RNA expression

Total RNA was extracted from samples using the Qiagen RNeasy Mini Kit in accordance with the manufacturer's instructions. Total RNA was transcribed using SuperScript II Reverse Transcriptase (Invitrogen) according to the manufacturer's instructions. Filtered pipette tips were used throughout to prevent contamination. cDNA samples were pre-warmed to 37°C. GoTaq Flexi DNA polymerase kit (Promega) was

used and kept on ice at all times. All PCR primers were obtained from MGW Biotech, dissolved in sterile water to a concentration of 100pmol/µl and dissolved for 8' at 65°C with shaking. A mastermix containing 5xGreen GoTaq Flexi Buffer (1x final concentration), $MgCl_2$ (1.5mM), GoTaq DNA polymerase (1U), dNTPs (0.25mM)(PCR nucleotide mix [Promega]), primers (0.5pmol/µl)(MGW Biotech) was made. Per sample, 1µl of DNA was dissolved in 24µl of mastermix and heated according to the type of PCR (see below) using an AB Applied Biosystems GeneAmp PCR System 9700. All PCRs have a common initial heating phase of 94°C for 2min to activate the Taq polymerase and a final phase of 72°C for 7' to complete extension of products and annealing of single-stranded complementary products. The PCR samples were subsequently stored at 4°C for up to 2 days or at -20°C until used.

Mouse Prominin-1

Primers:	RT Prominin-1-F:	5' GGA GCT GAC TTG AAT TGA GG 3'	
	RT Prominin-1-R:	5' ACC AAC ACC AAG AAC AAG GC 3'	
	Actin-F:	5' GAT GAC GAT ATC GCT GCG CTG GTC G 3'	
	Actin-R:	5' GCC TGT GGT ACG ACC AGA GGC ATA CAG 3'	
Band:	Prominin-1:	349bp	
	β-actin:	1kb (internal control)	
Program:	Denaturing:	94^0C 30''	
	Annealing:	60^0C 45''	35 cycles
	Extension:	72^0C 45''	

The PCR samples were separated by agarose gel electrophoresis. 1.5%-2% Agarose (Sigma) was dissolved in 1x TAE buffer (Sigma) in the microwave. 1.5µl of 10 mg/ml ethidium bromide (Sigma) was added per 200ml of Agarose gel. The gel was poured into a mould and allowed to solidify. It was then transferred to a running chamber and filled with enough 1xTAE buffer to completely submerge the gel. 10µl of PCR samples were pipetted into the wells. 6µl of 100bp ladder (Promega) was loaded as a marker and the gel was run at 100V for ~1 hour. The bands were then visualised with a BioRad Gel Doc 1000 and QuantityOne software.

2.4.3 Protein extraction from neurospheres

NS were collected in a 1.5ml Eppendorf tube and washed in PBS whilst kept on ice. All of the liquid was aspirated and 200µl RIPA buffer (50mM Tris pH: 7.4, Sigma; 1% Igepal, Fluka BioChemika; 0.25% Sodium Deoxycholate, Sigma; 150mM NaCl, Fisher Chemicals; 1mM EGTA, Sigma) containing Protease Inhibitor (1 tablet in 7ml RIPA buffer, Roche) was added to the neurospheres and left on ice for 20mins before either being mechanically homogenised by passing them through a 21g needle for immediate protein determination or transferred to a -80^{0}C freezer for storage.

2.4.4 Protein determination assay

Bovine serum albumin (BSA) standards of 0.0mgl/ml to 1.2mg/ml (in 0.2mg/ml increments) were prepared by diluting BSA (2mg/ml) with RIPA buffer. The NS homogenates were diluted 20-fold and 10-fold respectively with RIPA/PI. BCA protein assay reagent A and B (Pierce) were mixed in a 50:1 ratio and 200µl were pipetted into the wells of a 96-well plate. 10µl of each sample were added in duplicates and the plate was incubated at 37°C for 30'. The plate was then analysed using the Tecan Sunrise microplate reader with XFluor 4 software. The detection wavelength was set to 570nm with a reference of 690nm. The protein concentration of the NS sample homogenates was then back-calculated off the BSA standard curve.

2.4.5 Western blot of CD133 and HIF1α proteins

0.75mm discontinuous "Laemmli" polyacrylamide gels were made up with 10% separating gel (dH_2O, 10% Bis-acrylamide, separating gel buffer (0.38M Tris-base, 1.4mM SDS, pH8.8), APS, TEMED) and 5% stacking gel (dH_2O, 5% Bis-acrylamide, stacking gel buffer (0.13M Tris-base, 3.5mM SDS, traces of Bromphenolblue, pH6.8), APS, TEMED) for the wells. Prior to loading, the protein samples were made up to 1.25mg/ml with dH_2O, 1x XT sample buffer (BioRad) and 0.35M Dithiothreitol (DTT) to reduce the disulphide bridges. They were then boiled for 5' at 95°C to denature the proteins. 10µl corresponding to 12.5µg of protein were loaded into each well. Two different protein markers were used, biotinylated protein ladder (Cell Signalling) and Precision Plus protein ladder (BioRad). Empty wells were loaded with 10µl 1x XT

sample buffer (BioRad) to ensure even running of the bands. The gel was then run at 200V for ~35' in 'running buffer' (250mM Tris, 1.92M Glycine, 1 % SDS). The stacking gel and any unused wells were then removed.

Immobilon-P membrane (Millipore) and gel blotting paper (Schleicher & Schuell) were cut to match the gel size. The membrane was then dipped in 100% methanol for 15'' washed in dH_2O and equilibrated in cold 'transfer buffer' (dH_2O, 20% methanol, 25mM Tris, 0.2M Glycine) for 15'. The gel, filter paper and two foam pads were also equilibrated in cold 'transfer buffer' for 15'. The blot was then assembled as follows: 1x foam pad, 2x filterpaper, equilibrated gel, Immobilon-P membrane, 2x filterpaper, 1x foam pad. A glass tube was used to gently roll air bubbles trapped in between the layers to prevent them interfering with the transfer of proteins. This was placed in a cassette and transferred to a mini-trans blot cell (BioRad) filled with cold 'transfer buffer'. The cell was then run for 1h at 100V. The membrane was air-dried to improve protein binding, dipped in 100% methanol for 10'' and air dried again. After drying the blot was washed in TBST (1mM Tris pH7.8, 0.1M NaCl, 0.05% Tween-20) and blocked overnight in 5% milkpowder (Marvel, Premier International Foods)/TBST (w/v) at 4°C on an orbital shaker. After washing, the blot was incubated overnight with primary antibody (see below) in 1% milkpowder/TBST at 4°C on an orbital shaker. Excess antibody was washed off with 3x rinses in TBST and the blot was incubated for 1h with horse radish peroxidase (HRP)-conjugated secondary antibody (see below)/1% milkpowder/TBST. Again, excess antibody was washed off with 3x rinses in TBST, and the blot was incubated with SuperSignal WestPico Chemiluminescent substrate (Pierce) to enhance the HRP signal. The bands were finally visualised with an Image Station 440 (Kodak) with Kodak 1D v3.6 software.

Antibodies: anti-CD133 (Prominin-1) (rabbit polyclonal, 1:500 [1µg/ml], Abcam ab66141), anti-HIF1α (mouse monoclonal, 1:400 [3.25µg/ml], Abcam ab1), anti-β-actin (mouse monoclonal, 1:1000, Sigma A5441), goat anti-rabbit IgG-HRP (Sigma, A6667), goat anti-mouse IgG-HRP (Sigma, A9917).

2.4.6 Semi-quantitative analysis of Western blot bands

Using the KODAK 1D Image Analysis software package band areas of 814 pixels were assigned around each of the bands and set so that the peak of the intensity profiles fell centrally. The net intensity was then calculated as the sum of the background-subtracted

pixel intensity values within the band area defined. The corrected intensity was calculated as: (Net CD133 Intensity / Net β-actin Intensity)*1000.

2.5 Magnetic/Fluorescence-Activated Cell Sorting

2.5.1 Magnetic-activated cell sorting of neural stem cells into CD133-negative and CD133-positive populations

Neurospheres were collected and dissociated into single cells by complete aspiration of any media (including a wash of the cells in PBS) and incubation in 500µl (per half 10cm plate) Accumax (Chemicon) for 45mins at 37°C followed by mechanical dissociation. The Accumax was diluted out by transferral into NS medium at a ratio of 1:3. The NSC-containing medium was then passed through a sterile 40µm nylon mesh to remove any multi-cell aggregates, collected and transferred onto ice. The MACS separation was achieved using the Miltenyi Biotec MiniMACS Starting Kit (130-090-312), mouse anti-CD133 MicroBeads (130-092-33) and mouse anti-CD133-PE-conjugated antibody in accordance with the manufacturer's instructions. Keeping all the cells and reagents on ice the concentration of NSCs was adjusted to $1x10^7$ per ml in NS medium. The cell suspension was centrifuged at 300g for 10 minutes at 4^0C and the supernatant was removed. The cell pellet was then re-suspended in 80µl of MACS buffer (PBS pH7.2, 0.5% BSA, 2mM EDTA) per 10^7 cells and 20µl of anti-CD133 MicroBeads were also added per 10^7 cells. This suspension was then mixed and left to incubate for 15 minutes at 4^0C. 10µl of mouse anti-CD133-PE conjugated staining antibody was then added to the suspension per 10^7 cells and left to incubate for 10 minutes in the dark at 4^0C (in order to permit downstream FACS analysis). The cells were then washed by adding 1.5ml of MACS buffer per 10^7 cells, centrifugating them at 300g for 10 minutes at 4^0C, removing the supernatant, and then re-suspending them in 500µl MACS buffer. An MS column was placed in the magnetic field of the MACS separation unit (magnet) and mounted on the MACS multistand. The column was prepared by running 500µl of MACS buffer through it under gravity, ensuring that the column did not dry out, after which the 500µl of cell suspension was subsequently applied. The unlabelled cells passed through the column, whilst the labelled cells were retained within the magnetic field, and collected in a 15ml falcon tube. The column was

then washed by running 500µl of MACS buffer through it three times to fully elute the unlabelled cells. The total collected effluent represented the unlabelled CD133-negative NSC population. The column was then removed from the magnetic field of the MACS separation unit and placed over a separate 1.5ml Eppendorf collection tube. 1ml of MACS buffer was pipetted onto the column and immediately flushed through by applying a plunger in order to elute the magnetically labelled CD133-positive NSC population. This CD133-positive NSC fraction was obtained after passing the cells through a single column, rather than the manufacturer's recommendation of two columns, because the further enrichment a second column provides was negligible when compared to its significant reduction in yield (~50%). However, as the yield of CD133-negative NSCs from the MACS separation is relatively high we carried out this further enrichment by running those cells over a second MS column (using the same protocol as above) after re-labelling them with the MicroBeads and the antibody. The second CD133-negative/positive fractions eluted were respectively added to the first. The two cell fractions were then either used immediately for downstream experiments or transferred back into NS medium for subsequent culturing (Figure 57 and Figure 60).

2.5.2 Fluorescence-activated cell sorting of neural stem cells into CD133-negative and CD133-positive populations

Neurospheres were collected and dissociated into single cells by complete aspiration of any media (including a wash of the cells in PBS) and incubation in 500µl (per half 10cm plate) Accumax (Chemicon) for 45mins at 37°C followed by mechanical dissociation. The Accumax was diluted out by transferral into NS medium at a ratio of 1:3. The NSC-containing medium was then passed through a sterile 40µm nylon mesh to remove any multi-cell aggregates, collected and transferred onto ice. The cell suspension was then split into two tubes each containing a total of $1x10^7$ cells in 1ml of NS medium. The cell suspensions were centrifugated at 300g for 10 minutes at 4^0C and the supernatants were removed. The cell pellets were re-suspended in 100µl of MACS buffer per 10^7 cells and 10µl of mouse anti-Prominin-1-PE conjugated staining antibody was added to the suspensions per 10^7 cells and left to incubate for 10 minutes in the dark at 4^0C. The cells were then washed by adding 1.5ml of MACS buffer per 10^7 cells, centrifuging them at 300g for 10 minutes at 4^0C, removing the supernatants, and re-suspending them in 500µl MACS buffer. The NSC-containing solutions were then split

into 10 tubes each containing an adjusted concentration of $2x10^6$ cells in 1ml of MACS buffer and kept on ice. These samples were run through a high speed MoFlo XDP cell sorter (Beckman Coulter) with the gates set for FSC-SSC, FSC-Pulse Width, PE-positive, and PE-negative in order to specifically sort viable and single PE-positive (CD133-positive) NSCs. The CD133-negative/positive fractions were eluted into NS medium on ice and their concentrations were calculated prior to being injected into the brains of recipient mice.

2.5.3 Fluorescence-activated cell sorting analysis of neural stem cell CD133 expression

Neurospheres were collected and dissociated into single NSCs by complete aspiration of any media (including a wash of the cells in PBS) and incubation in 500µl (per half 10cm plate) Accumax (Chemicon) for 45mins at 37°C followed by mechanical dissociation. The Accumax was diluted out by transferral into NS medium at a ratio of 1:3. The NSC-containing medium was then passed through a sterile 40µm nylon mesh to remove any multi-cell aggregates, collected and transferred onto ice. The concentration of the NSC-containing medium was adjusted to $1x10^7$ cells in 1ml of NS medium. The cell suspension was centrifuged at 300g for 10 minutes at 4^0C and the supernatant was removed. The cell pellet was then resuspended in 100µl of MACS buffer per 10^7 cells and 10µl of mouse anti-Prominin-1-PE conjugated staining antibody was added to the suspension per 10^7 cells and left to incubate for 10 minutes in the dark at 4^0C. The cells were then washed by adding 1.5ml of MACS buffer per 10^7 cells, centrifuging them at 300g for 10 minutes at 4^0C, removing the supernatant, and resuspending them in 500µl MACS buffer. The cell concentrations to be FACS analysed were adjusted to $1x10^6$ cells/ml in MACS buffer and 1ml was run through a FACScalibur (Becton-Dickinson) flow cytometer using CellQuest software. A control population of unlabelled and unsorted NSCs were FACS-analysed in order to set a side scatter vs. forward scatter gate that would only allow the detection of viable and non-aggregated single NSCs. The same population of cells was also used to set the M1 fluorescence threshold for PE(CD133)-positivity to include a false-positive detection of ~3%, which was then corrected to a 0% baseline. The expression intensity of CD133 was then calculated as the integration of the fluorescence plot greater than the M1 fluorescence threshold.

2.6 Immunostaining

2.6.1 Paraffin immunohistochemistry

Brains were fixed in 10% formaldehyde (formalin), processed through graded alcohols and xylene into paraffin wax (Tissue processor Tissue-Tek VIP or Vision Biosystem Peloris), then embedded in paraffin (LECA Tissue embedding station) and 3µm sections were taken and processed for staining after antigen retrieval by boiling for 2 minutes in citrate buffer and a 1 hour incubation in SuperBlock (Pierce): haematoxylin-eosin (H&E), anti-β-galactosidase (Cre-recombined cells; Chemicon AB1211, rabbit polyclonal, 1:500), anti-GFAP (glial fibrillary acidic protein; DAKO Z0334, rabbit polyclonal, 1:1000), anti-synaptophysin (neuronal synapse; Zymed 080130, rabbit polyclonal, prediluted), anti-NeuN (neuronal nuclei; Chemicon MAB377, mouse monoclonal, 1:2000), anti-Nestin (intermediate filament of neuroepithelial stem cells; BD Pharmingen 556309, mouse monoclonal IgG1, 1:100), anti-MAP2 (microtubule associated protein-2; Chemicon MAB3418, mouse monoclonal IgG1, 1:200), BrdU (proliferating cells; Abcam ab6326, rat monoclonal, 1:100), anti-Sox2 (embryonic stem cell transcription factor; Chemicon AB5603, rabbit polyclonal, 1:500), anti-Sox-9 (neural crest cell transcription factor; National Institute for Medical Research – London, rabbit polyclonal, 1:200), anti-phospho-Histone H3 (proliferating cells; Cell Signaling, rabbit polyclonal, 1:50), anti-Olig2 (oligodendrocyte transcription factor 2; Abcam ab33427, rabbit polyclonal, 1:500), anti-EGFR (epidermal growth factor receptor; R&D Systems MAB1280, rat monoclonal IgG1, 1:500). All primary antibody incubations were for 1 hour at room temperature. Biotinylated secondary antibodies were incubated for 1 hour at room temperature, and visualisation was carried out using the horseradish peroxidase-conjugated streptavidin system with diaminobenzidine as a chromogen.

All immunostaining was carried out using the automated Benchmark XT machine in accordance with the manufacturer's guidelines. Analysis of the sections was performed under a Zeiss Axioskop 2 MOT microscope. Images were captured using a ColorView III digital camera with the AnalySIS software package.

2.6.2 Immunofluorescence staining

Immunofluorescence was conducted on cells plated on coverslips, chamber slides (see sections 2.3.7 and 2.3.8), vibratome sections, and free-floating NS. Vibratome (Vibratome 1500, Vibratome Instruments # GS-044026) sections of 40-50um thickness were sectioned from formalin fixed, agarose-embedded and coronally orientated brains. The staining protocol was carried out on parafilm for coverslips, 24-well plates for vibratome sections, or in 1.5ml Eppendorf tubes for free-floating NS collected from culture. The cells were washed with PBS three times in between each protocol step. All cell containing media were permeabilised by incubation in 0.1% TritonX100 / PBS for 10 minutes at room temperature. Non-specific binding to endogenous proteins was blocked by incubation in 0.1% BSA / PBS for 15 minutes (room temperature). Cells were then incubated with primary antibodies overnight at 4^0C: anti-β-galactosidase (Cre-recombined cells; Abcam ab616, rabbit polyclonal, 1:500), anti-GFAP (glial fibrillary acidic protein; Abcam ab4674, chicken polyclonal, 1:1000), anti-Nestin (intermediate filament of neuroepithelial stem cells; BD Pharmingen 556309, mouse monoclonal, 1:400), anti-Sox2 (embryonic stem cell transcription factor; Chemicon AB5603, rabbit polyclonal, 1:500), anti-CD133 (putative cancer stem cell marker; Abcam ab31448, rabbit polyclonal, 1:500), anti-MAP2 (microtubule associated protein-2; Abcam ab5392, chicken polyclonal, 1:1000), anti-O4 (oligodendrocyte progenitor marker; Chemicon MAB345, mouse monoclonal IgM, 1:400), anti-βIII-tubulin (neuronal microtubule marker; Chemicon MAB1637, mouse monoclonal, 1:1000), anti-GFP (green fluorescent protein; Abcam ab290, rabbit polyclonal, 1:500). Visualisation was achieved by incubation for 1 hour (protected from light) with directly conjugated Alexa Fluor secondary antibodies (Molecular Probes) carrying fluorochromes 488, 546, or 633nm. Hoechst 33342, a DNA-binding fluorescent molecule (405nm), was included in the secondary antibody incubation to achieve nuclear counterstaining. Secondary antibody only control stains were carried out by omitting the primary antibody incubation step in order to test for non-specific staining. All cell containing media were then mounted onto glass slides with coverslips (if required) using Dako fluorescent mounting medium. Sections were then left for 1hr for the mounting medium to set and imaged with either an AxioCam MRm camera mounted on a Zeiss Axioplan 2 microscope using the Axiovision software or a Zeiss LSM510 META confocal laser scanning microscope with the LSM software.

2.6.3 Preparation of cytoblocks for paraffin immunohistochemistry

Cytoblock is a method to embed cells in a wax-block that allows the cells to be cut into sections and processed for immunohistochemistry. NS or astrocytes were collected in 1.5ml Eppendorf tubes, mixed 1:1 with 10% buffered formal saline (formalin) overnight at room temperature. A cytoblock kit (#74010159, Shandon) was used in accordance to the manufactures instructions. The resulting cytoblocks were processed in a tissue processor (Tissue-Tek VIP) and embedded in paraffin wax. Cytoblocks were cut with a nominal thickness of 3µm and were stained using the same antibodies and equipment referenced in section 2.3.4. Analysis of the cytoblock sections was performed under a Zeiss Axioskop 2 MOT microscope. Images were captured using a ColorView III digital camera with the AnalySIS software.

2.7 Statistical Analysis

For assays where multiple NSC genotypes were compared based on a single output (e.g. WST-1 proliferation assay, neurosphere size assay, neurosphere-forming clonogenicity assay, self-renewal assay) we used a one-way repeated measures ANOVA with a Bonferroni's multiple comparison correction (*: $P<0.05$, **: $P<0.01$, ***: $P<0.001$). In cases where the number of repeated measures was not equal per group then a normal one-way ANOVA with a Bonferroni's multiple comparison correction was used.

For assays where multiple NSC genotypes were compared on multiple outputs (e.g. neurosphere differentiation assay) we used a two-way ANOVA with a Bonferroni's multiple comparison correction (*: $P<0.05$, **: $P<0.01$, ***: $P<0.001$).

When comparisons were made between multiple NSC genotypes each with more than one output (e.g. comparing the tumour latencies of *in vitro* recombined and engrafted NS versus *in vivo* recombined, derived *in vitro* and engrafted NS both within and between the different NSC genotypes), a two-way ANOVA with no repeated measures and a Bonferroni's multiple comparison correction was used (*: $P<0.05$, **: $P<0.01$, ***: $P<0.001$).

When a direct comparison of a single output, and with matching data points, between two NSC genotypes was required (e.g. HIF1α expression intensity in $Rb^{-/-}$; $PTEN^{-/-}$ vs. $Rb^{-/-}$; $p53^{-/-}$ NS) a one-tailed paired Student's t-Test was used (*: $P<0.05$).

When a direct comparison of a single output, but with unequal data points, between two NSC genotypes was required (e.g. mean tumour latency of $PTEN^{-/-}$; $p53^{-/-}$ NS vs. $PTEN^{-/-}$; $p53^{-/-}$ TS) a two-tailed unpaired Student's t-Test was used (*: $P<0.05$).

When comparing the fit of two data sets (e.g. CD133 vs. HIF1α expression intensity) a linear regression was used to determine the goodness of the fit (R^2) and a two-tailed Pearson's correlation test was used to measure the level of correlation (*: $P<0.05$, **: $P<0.01$, ***: $P<0.001$).

3 *In Vitro* Functional Characterisation of Neural Stem Cells Based on Genotype

3.1 Introduction

In vitro methods of studying neural stem cells (NSCs) are a valid complement to *in vivo* studies as they allow for the controlled analysis of NSC behaviour in a context-dependent manner. One of the defining features of stem cells is their ability to self-renew. Expansion of NSCs *in vitro* has enabled downstream analysis of their function, expression profile, and proteome (Maurer et al., 2004). This has led to the widespread *in vitro* analysis of both primary NSCs (Tropepe et al., 1999; Engstrom et al., 2002) and tumour cells (Ignatova et al., 2002; Hemmati et al., 2003; Singh et al., 2003) derived from the brains of mice and humans. Such previous research has focussed on the study of specific tumour cell subtypes, such as CD133+ glioblastoma cells (Liu et al., 2009). However, our model system generates multiple tumour types allowing for a functional comparison between multiple tumour cell subtypes. In addition, our model system also allows for a baseline functional comparison by using non-recombined NSCs as non-tumour cell controls.

By deriving SVZ NSCs from the brains of conditional knock-out adult mice we are able to generate primary *in vitro* cultures. These cultures can be expanded over serial passages *in vitro* (Conti and Cattaneo, 2010) allowing for downstream functional analysis of the NSCs with regards to their growth rate, multipotency, self-renewal, and mRNA expression profiles following inactivation of the TSGs Rb, p53, and PTEN. These *in vitro* expanded NSCs can then be engrafted into the brains of mice to examine their *in vivo* tumour hit rate, latency, and phenotype (addressed in Chapter Four).

In this chapter we use this approach to address the following aims:

Aims

1. Verify that *in vitro* NSCs cultures contain the same SVZ NSCs that are targeted by i.c.v. Adenovirus-Cre administration.
2. Characterise the effect of Rb, p53, and PTEN loss on the growth rate, self-renewal, multipotency and biomarker expression of NSCs *in vitro*.

3. Examine whether the *in vitro* functional properties of NSCs correlate with *in vivo* tumour hit rate and/or latency.
4. Identify surrogate markers of tumour phenotype.

3.2 Materials and Methods

Refer to the main materials and methods section (Chapter Two).

3.3 Results and Discussion

NSCs are possible candidates for brain tumour initiating cells (Sutter et al., 2007; Dirks, 2008). Previous work has extensively verified the *in vivo* tumourigenicity of NSCs but less has been done to characterise their behaviour *in vitro*. Using our model system we aim to characterise the behavioural profile of NSCs with regards to their growth rate, self-renewal, and multipotency capabilities following inactivation of the TSGs Rb, p53, and PTEN.

3.3.1 Cells derived from the subventricular zones of ROSA26R$^{Lox/Lox}$ mice following intracerebroventricular Adenovirus-Cre become enriched in neurosphere cultures over serial passages

In order to examine whether i.c.v. administration of Adenovirus-Cre targets NSCs, four separate cohorts (3-6 mice in each) of ~4 week old ROSA26R$^{Lox/Lox}$ reporter mice (R26R) received injections. After an incubation period of seven days, NSC were prepared from the SVZ and expanded *in vitro* where they formed neurospheres. The proportion of NS that had been targeted by Adenovirus-Cre for recombination was then determined at passages 0, 1, 2, and 3 by β-galactosidase staining (Figure 21).

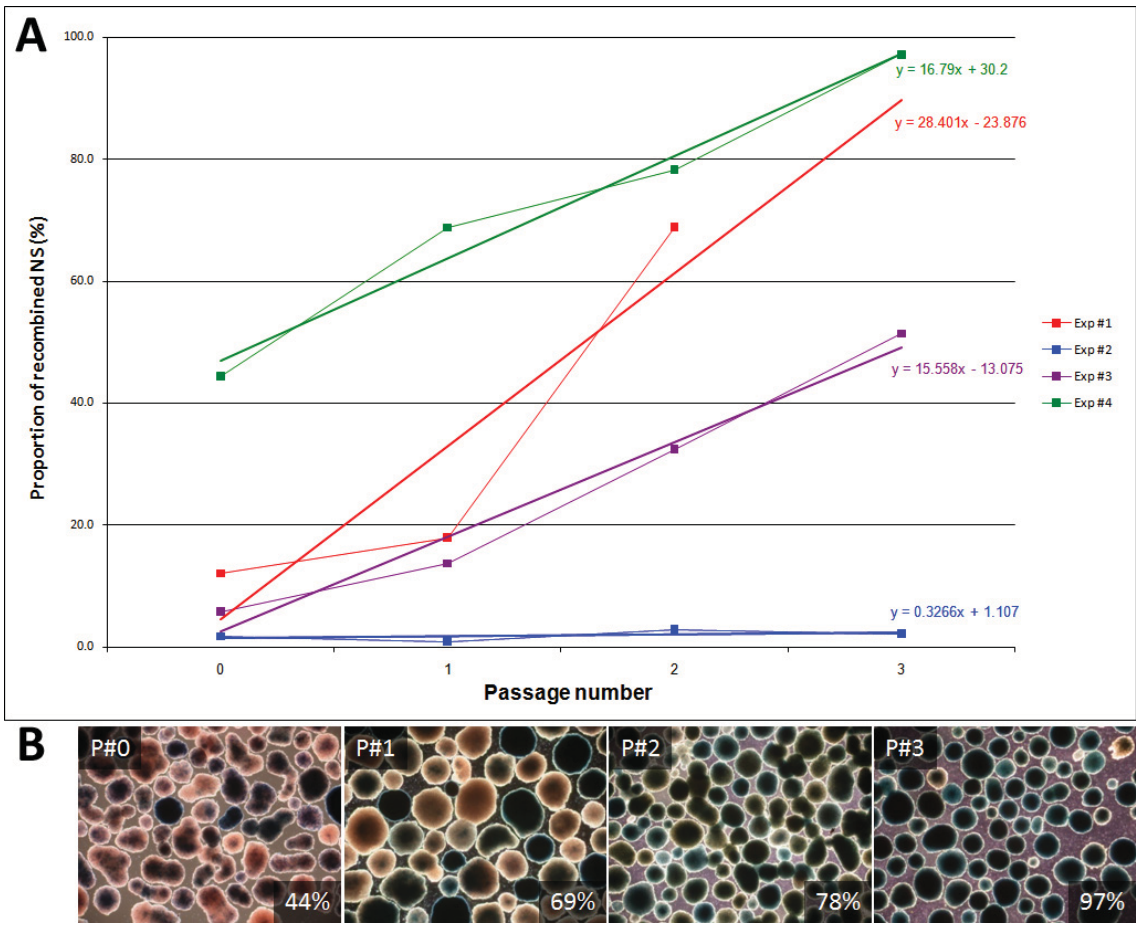

Figure 21: The proportion of recombined β-galactosidase-positive R26R NS increases over serial passages *in vitro*. (A) Each line (with their associated linear trendlines) on the graph represents an independent experiment in which NSCs (grown as NS) were derived from the brains of ROSA26R$^{Lox/Lox}$ reporter mice 7 days post i.c.v. Adenovirus-Cre administration and grown as NS *in vitro*. The percentage of recombined NS was calculated at passages 0, 1, 2, and 3 by way of β-galactosidase staining and counting the positive NS. (B) Representative serial images taken at passages 0, 1, 2, and 3 for experiment 4 (green line) and used to calculated the proportion of recombined β-galactosidase-positive R26R NS. The percentages given were generated from an average count taken from three randomly selected fields of vision captured through a 10x objective on a Zeiss Axiovert 200 microscope.

The fraction (passage zero) of β-galactosidase-positive NS derived in four separate experiments was 12%, 1.7%, 5.8%, and 44.4% (Figure 21: A). Irrespective of the initial starting percentage, the number of β-galactosidase-positive recombined NS increased in a linear manner when serially passaged. In the case of experiment four the percentage of β-galactosidase-positive NS rose from 44.4% at passage zero to 97.2% by passage three (Figure 21: A). It is thought that only the most immature NSCs are capable of self-renewal, although it has been suggested that the transiently amplifying neural progenitor cells can also form NS (Reynolds and Rietze, 2005). Therefore, only self-renewing

NSCs should be able to persist in a culture that is serially passaged. Our finding therefore suggests that *in vitro* NS cultures become enriched for NSCs and their transient amplifying progenies over serial passages. Experiment two (Figure 21: A, blue line) represents an experiment in which almost no SVZ NSCs were targeted by i.c.v. Adenovirus-Cre administration, as a negligible proportion of <2% β-galactosidase-positive NS were identified *in vitro*.

Neurospheres are a heterogeneous population of stem, transiently amplifying stem-like progenitor, and supporter cells (Ahmed, 2009). Over serial passages we would expect that the culture would become enriched for the self-renewing type B astrocytes and transiently amplifying type C progenitors of the SVZ. Assuming that a) i.c.v. administration of Adenovirus-Cre infects SVZ cells in a stochastic manner (four independent experiments generated four different starting percentages of recombined NS at passage 0), b) Adenovirus-Cre is not selective towards the type of cell it infects (Akagi et al., 1997), and c) β-galactosidase-positive ROSA26R$^{-/-}$ NSCs do not possess any growth advantage over their non-recombined NSC counterparts, we should expect to see a proportional quantity of β-galactosidase-negative NS persist with the β-galactosidase-positive NS after three passages *in vitro*. This was not the case, as shown by experiment four (Figure 21: A) in which the percentage of recombined NS was observed to reach 97% by passage 3.

The linear increase in the proportion of β-galactosidase-positive NS had a slope that ranged from 15.6 to 28.4 across the viable experiments (Figure 21: Exp#1, 3, and 4). The relative similarity of these slopes suggests that the same mechanism is responsible for driving the increase. This mechanism can be explained by a phenomenon known as "NS aggregation" whereby NS in bulk culture can fuse together or even swap matter (Singec et al., 2006; Mori et al., 2007; Coles-Takabe et al., 2008). The blue colour of the recombined NSCs could drown out the colourless appearance of the non-recombined NSCs when matter is aggregated or exchanged between NS. This would mean that NS deemed β-galactosidase-positive could in fact be 50% positive and 50% negative, and would explain the increase of β-galactosidase-positive NS in a linear fashion over serial passages. It would also explain why some NS exhibit patches of blue staining and why some NS of the same size appear to carry different shade depths of blue.

3.3.2 Intracerebroventricular administration of Adenovirus-Cre targets subventricular zone neural stem cells that are capable of self-renewal and are multipotent

To specifically determine the self-renewal ability and to examine the multipotency of the cells constituting a NS culture we performed self-renewal and differentiation assays. Three separate cohorts (3-6 mice in each) of ~4 week old ROSA26R$^{Lox/Lox}$ reporter mice (R26R) received injections and were left for four days prior to SVZ cell preparation and expansion *in vitro*. The NS were then dissociated into single cells and individually FACS-seeded into single wells of a 96-well plate (in accordance with the protocol given in section 3.2.1). The number of these cells, at passage one, that had self-renewed to form neurospheres after nine days was used to estimate what percentage of SVZ cells were capable of self-renewal and could be classed as NSCs. This percentage was then used in conjunction with β-galactosidase staining to calculate the original *in vivo* proportion of SVZ cells targeted by i.c.v. Adenovirus-Cre that were self-renewing NSCs (Figure 22).

	Exp #1	Exp #2	Exp #3	Average	SE
No. single cells plated	51	139	101	97.0	25.5
No. single cells that formed NS	12	24	25	20.3	4.2
% Self-renewing NSCs	**23.5**	**17.3**	**24.8**	**21.8**	**2.3**
No. B-gal +ve NS derived from single cells	8	22	21	17.0	4.5
% Self-renewing NSCs targeted by i.c.v. Adenovirus-Cre	**66.7**	**91.7**	**84.0**	**80.8**	**7.4**
% SVZ cells targeted by i.c.v. Adenovirus-Cre that were self-renewing NSCs	**15.7**	**15.8**	**20.8**	**17.4**	**1.7**

Figure 22: Table of the data generated from the three separate self-renewal assays conducted on SVZ cells, grown as NS *in vitro*, derived from the brains of ROSA26R$^{Lox/Lox}$ control mice (R26R) four days post-i.c.v. Adenovirus-Cre administration.

Across these three separate experiments, a total of 291 single cells were seeded into individual wells, from which 61 (21.8% +/- 2.3) self-renewed to form NS (Figure 22). Of these 61 self-renewing cells, 51 (17.4% +/- 1.7 of all single seeded cells) were uniformly β-galactosidase-positive (Figure 23: A, representative example). This suggests that 21.8% of SVZ cells were NSCs capable of self-renewal and that 17.4% of SVZ cells were self-renewing NSCs targeted by i.c.v. Adenovirus-Cre (i.e. i.c.v.

Adenovirus-Cre administration had a 80.8% +/- 7.4 success rate of targeting self-renewing NSCs). The accepted architecture and cellular hierarchy of the SVZ predicts that type B astrocytes, thought to represent NSCs, represent a minority of the cell population (Doetsch et al., 1997). However, this relatively high percentage (21.8%) of self-renewing cells suggests that additional NSC subtypes may also possess the ability to self-renew, such as the transiently amplifying type C progenitors.

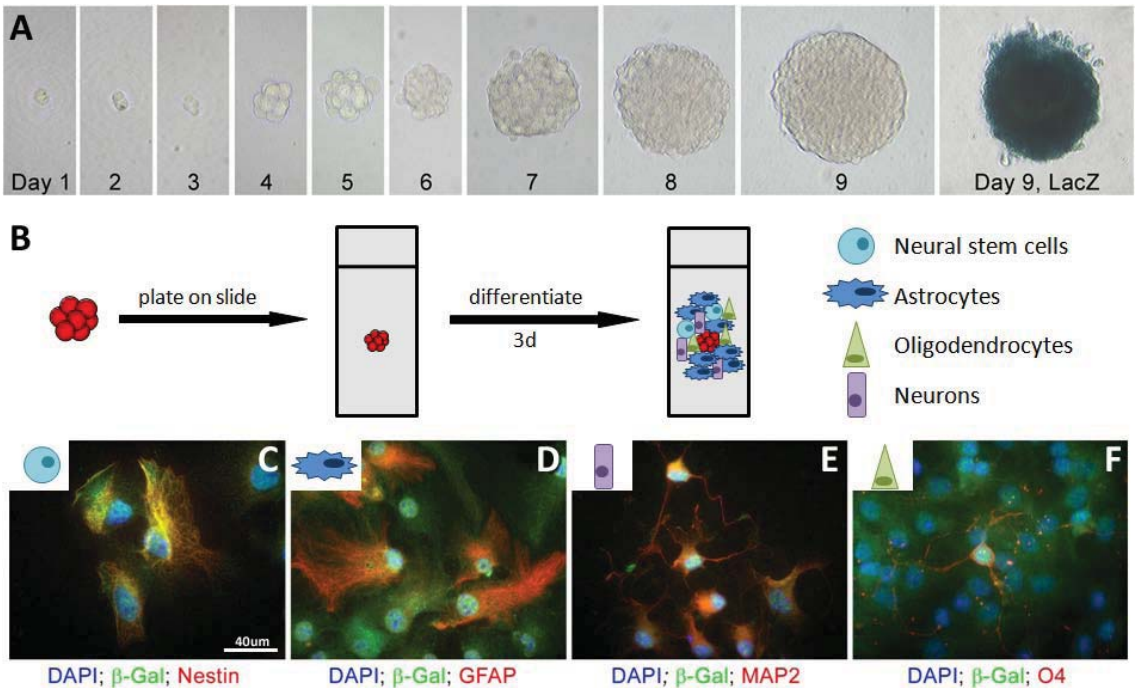

Figure 23: I.c.v. Adenovirus-Cre administration targets self-renewing and multipotent SVZ NSCs that can be propagated *in vitro*. (A) Representative image series taken of the same NSC/NS over 9 days showing the monoclonal self-renewal ability of a single *in vivo* recombined NSC as it develops into a NS *in vitro*. The β-galactosidase-positive stain at day 9 (Day 9, LacZ) demonstrates that Adenovirus-Cre administration targets these self-renewing SVZ NSCs. (B) Monoclonal NS generated from the self-renewal assay were allowed to differentiate on glass slides for 3 days before their cells were examined for markers of NSCs (Nestin: C), astrocytes (GFAP: D), neurons (MAP2: E), and oligodendrocytes (O4: F). DAPI: Hoechst 33342 nuclear marker, β-gal: β-galactosidase. Blue: excitation at 405nm, green: excitation at 488nm, red: excitation at 546nm. Images were taken using a 63x objective with oil immersion on a Zeiss Axioplan 2 microscope and captured using a mounted AxioCam MRm camera and the Axiovision software.

Individual monoclonal NS generated from the self-renewal assay, but not used for β-galactosidase staining, were then allowed to differentiate on laminin-coated glass chamber slides (Figure 23: B). These NS were observed to differentiate into glial,

neuronal, and oligodendrocytic lineages, demonstrating their multipotency (Figure 23: C-F).

These experiments confirm that i.c.v. Adenovirus-Cre-mediated recombination targets self-renewing and multipotent SVZ NSCs that can be propagated *in vitro*.

3.3.3 The combination and number of TSGs lost determines the growth rates and neurosphere-forming ability of neural stem cells *in vitro*

The effect of inactivation of the TSGs Rb, p53, and PTEN on the *in vitro* growth rate of NSCs was determined by the WST-1 proliferation assay. This assay measures the cumulative mitochondrial activity (as a surrogate marker for growth) of NSCs at 0, 4, 6, and 8 hours after a 3 day incubation period.

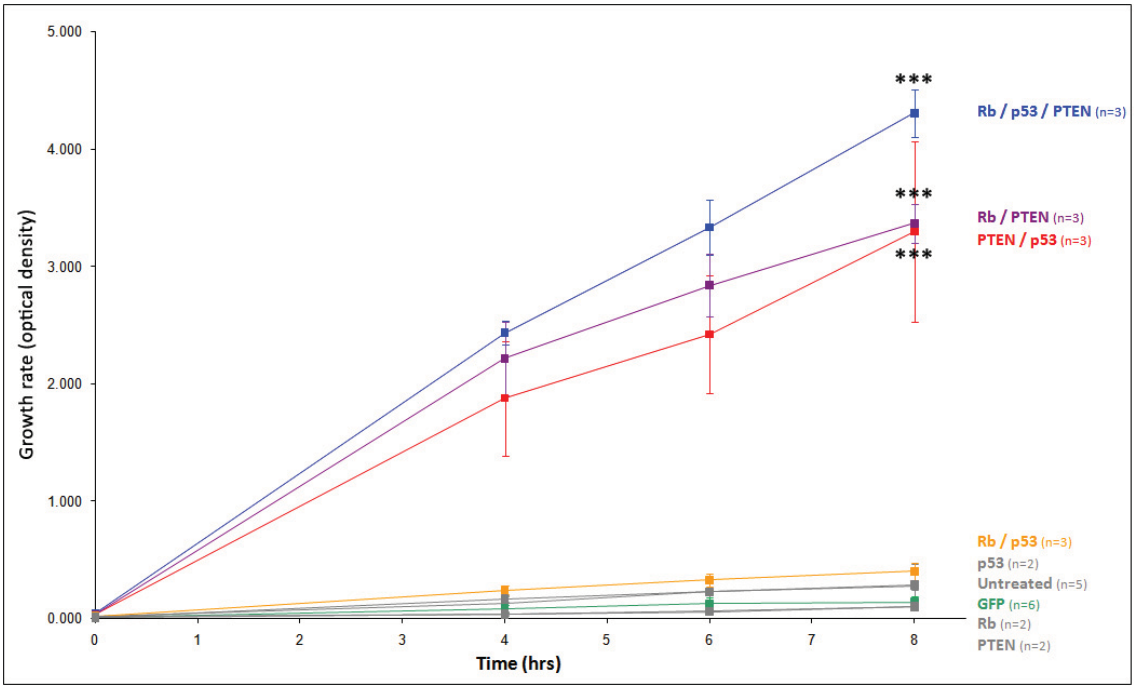

Figure 24: The growth rates of *in vitro* recombined Rb$^{-/-}$; p53$^{-/-}$; PTEN$^{-/-}$, Rb$^{-/-}$; PTEN$^{-/-}$, and PTEN$^{-/-}$; p53$^{-/-}$ NSCs (grown as NS) at passage 3 are significantly higher than that of non-recombined Adenovirus-GFP-infected NSCs. The growth rates of the Rb$^{-/-}$; p53$^{-/-}$ NSCs and the single TSG knock-out Rb$^{-/-}$, p53$^{-/-}$, and PTEN$^{-/-}$ NSCs are not different to those of both the non-recombined-untreated and Adenovirus-GFP-infected control NSC groups. Using the WST-1 assay the growth rate (y-axis) of NSCs (growing as NS) was measured at 0, 2, 4, and 8hrs (x-axis) after a 3 day incubation period. Growth rate of *in vitro* recombined Rb$^{-/-}$; p53$^{-/-}$; PTEN$^{-/-}$ (blue: n=3; 4.31 +/- 0.20; 8hrs) vs. Rb$^{-/-}$; PTEN$^{-/-}$ (purple: n=3; 3.37 +/- 0.17; 8hrs) vs. PTEN$^{-/-}$; p53$^{-/-}$ (red: n=3; 3.30 +/- 0.77; 8hrs) vs. Rb$^{-/-}$; p53$^{-/-}$ (orange: n=3; 0.40 +/- 0.07; 8hrs) vs. Rb$^{-/-}$ (grey: n=2; 0.10 +/- 0.02; 8hrs) vs. p53$^{-/-}$ (grey: n=2; 0.28 +/-

0.03; 8hrs) vs. $PTEN^{-/-}$ (grey: n=2; 0.10 +/- 0.003; 8hrs) vs. non-recombined Adenovirus-GFP-infected (green: n=6; 0.14 +/- 0.05; 8hrs) vs. non-recombined untreated (grey: n=5) NSCs. Error bars: standard errors. ***: P<0.001 vs. GFP control at 8hrs (one-way ANOVA with Bonferroni's multiple comparison correction).

Two different controls were used for this experiment with the slightly decreased growth rate of the non-recombined Adenovirus-GFP-infected NSCs (Figure 24: green data set) compared to non-recombined untreated NSCs (Figure 24: grey data set), suggesting a possible effect of Adenovirus infection. This difference was not significant but to compensate for any possible Adenovirus-mediated effects the Adenovirus-GFP-infected control was used as the baseline control. The $Rb^{-/-}$; $p53^{-/-}$; $PTEN^{-/-}$ NSCs grew faster than the $Rb^{-/-}$; $PTEN^{-/-}$ and $PTEN^{-/-}$; $p53^{-/-}$ NSCs, all of which grew significantly faster than the $Rb^{-/-}$; $p53^{-/-}$ NSCs which were found to grow at a statistically similar rate to the $Rb^{-/-}$ alone, $p53^{-/-}$ alone, $PTEN^{-/-}$ alone, and Adenovirus-GFP-infected NSCs. These results suggest that the growth rates of the different *in vitro* recombined NSC genotypes increase with the number of TSGs lost. The $Rb^{-/-}$; $p53^{-/-}$ NSC growth rate appears to be a combination of the $Rb^{-/-}$ alone and $p53^{-/-}$ alone levels, and highlights a potential PTEN-loss-mediated growth advantage. Interestingly, PTEN loss alone had no effect on the growth rate of NSCs but appeared to have a disproportionally large effect on increasing the growth rate of NSCs in which Rb or p53 had already been lost. For example, the $Rb^{-/-}$; $PTEN^{-/-}$ and $PTEN^{-/-}$; $p53^{-/-}$ NSCs grew significantly faster than the $Rb^{-/-}$; $p53^{-/-}$ NSCs, in which the additional loss of PTEN resulted in the $Rb^{-/-}$; $p53^{-/-}$; $PTEN^{-/-}$ genotype which had the fastest growth rate of all. This finding that PTEN loss alone is not sufficient to confer increased NSC proliferation contradicts the findings of other groups (Groszer et al., 2001; Stiles et al., 2004; Groszer et al., 2006). This discrepancy can be explained by several differences: (i) Groszer et al, 2001 used neural progenitor cells derived from brains of E14.5 or P0 mice whereas we used adult stem cells, and consequently (ii) loss of PTEN has different effects on neural progenitor populations than on adult NSC.

Interestingly, as described in section 3.3.1 *in vitro* recombined and engrafted $Rb^{-/-}$; $p53^{-/-}$ NS very rarely give rise to tumours (9.6%), suggesting that there is a correlation between *in vitro* growth rate and tumourigenicity. This potential correlation is addressed in section 3.3.5.

To further delineate the differential growth patterns of the NSC genotypes we used two additional assays. Firstly, the NS size assay (Figure 25) was used to measure the proliferative capacity of NSCs, and secondly, the NS-forming clonogenicity assay (Figure 26) was used, as an interpretation of the neurosphere formation assay originally described by Reynolds in 1992 (Reynolds and Weiss, 1992; Reynolds et al., 1992), to measure the NS-forming ability of NSCs.

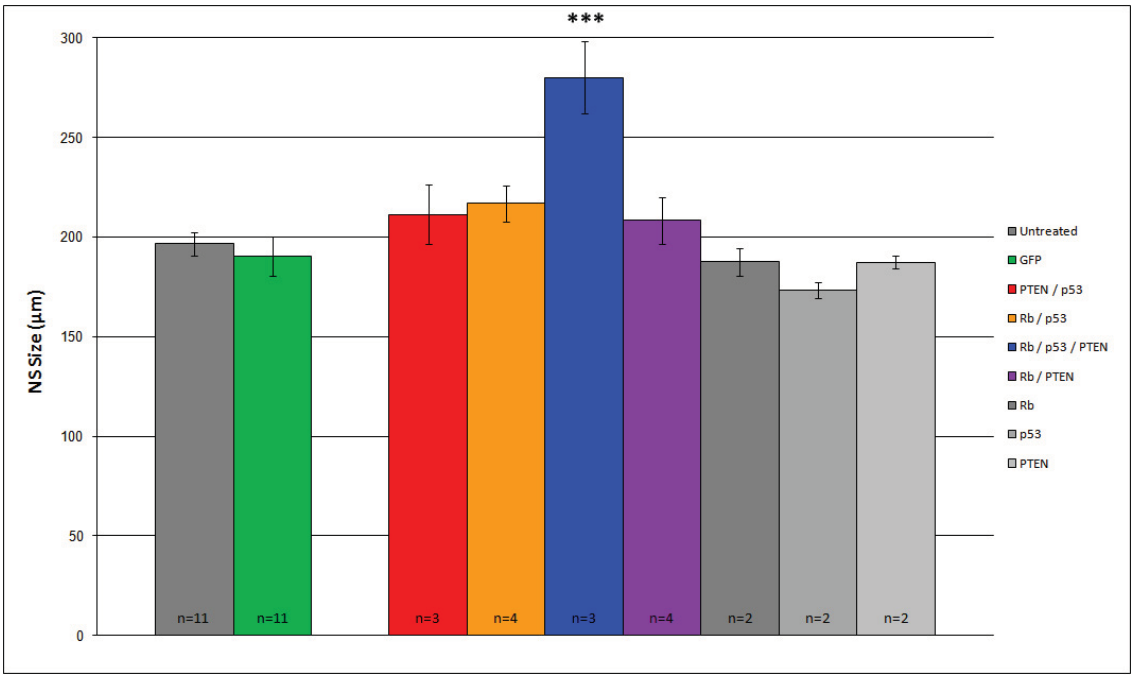

Figure 25: The Rb$^{-/-}$; p53$^{-/-}$; PTEN$^{-/-}$ NSCs at passage 3 form significantly larger NS than the rest of the experimental genotypes, all of which form NS of the same size as the Adenovirus-GFP-infected control NSCs. NSCs were seeded into NS medium and left to grow as NS for eight days before their diameters were measured using a Zeiss Axiovert 135 microscope and the Openlab 5 software package. NS size of non-recombined untreated (grey: n=11) vs. non-recombined Adenovirus-GFP-infected (green: n=11; 190.5 +/- 10.0) vs. *in vitro* recombined PTEN$^{-/-}$; p53$^{-/-}$ (red: n=3; 211.3 +/- 14.8) vs. Rb$^{-/-}$; p53$^{-/-}$ (orange: n=4; 216.9 +/- 9.2) vs. Rb$^{-/-}$; p53$^{-/-}$; PTEN$^{-/-}$ (blue: n=3; 280.1 +/- 18.2) vs. Rb$^{-/-}$; PTEN$^{-/-}$ (purple: n=4; 208.2 +/- 11.7) vs. Rb$^{-/-}$ (grey: n=2; 187.5 +/- 7.0) vs. p53$^{-/-}$ (grey: n=2; 173.2 +/- 4.0) vs. PTEN$^{-/-}$ (grey: n=2; 187.3 +/- 3.2) NSCs. Error bars: standard errors. ***: P<0.001 vs. GFP control (one-way ANOVA with Bonferroni's multiple comparison correction).

The NS size assay confirmed our finding from the WST-1 assay, but was less apparent. The Rb$^{-/-}$; p53$^{-/-}$; PTEN$^{-/-}$ NSCs formed significantly larger NS than the rest of the experimental genotypes (P<0.001), from which the PTEN$^{-/-}$; p53$^{-/-}$, Rb$^{-/-}$; p53$^{-/-}$ and Rb$^{-/-}$; PTEN$^{-/-}$ NSCs appeared to form larger NS than the Rb$^{-/-}$ alone, p53$^{-/-}$ alone, PTEN$^{-/-}$

alone, and Adenovirus-GFP-infected control NSCs, but did so in a statistically non-significant manner (Figure 25). This suggests that either a) the NS size assay was not as sensitive as the WST-1 assay in delineating the proposed additive effect of additional TSG loss on growth rate advantage, or b) that the size of NS formed is not a suitable surrogate marker of growth rate.

The growth rate of the $Rb^{-/-}$; $p53^{-/-}$ NSCs was significantly lower than the other double knock-out genotypes, but they formed NS of a statistically similar size. This finding reinforces the earlier proposal that "the size of NS formed is not a suitable surrogate marker of growth rate".

In addition to growth rate, self-renewal is a key characteristic of NSCs. To see if the loss of the different combinations of TSGs had an effect on self-renewal we measured the NS-forming ability of the same NSC genotypes.

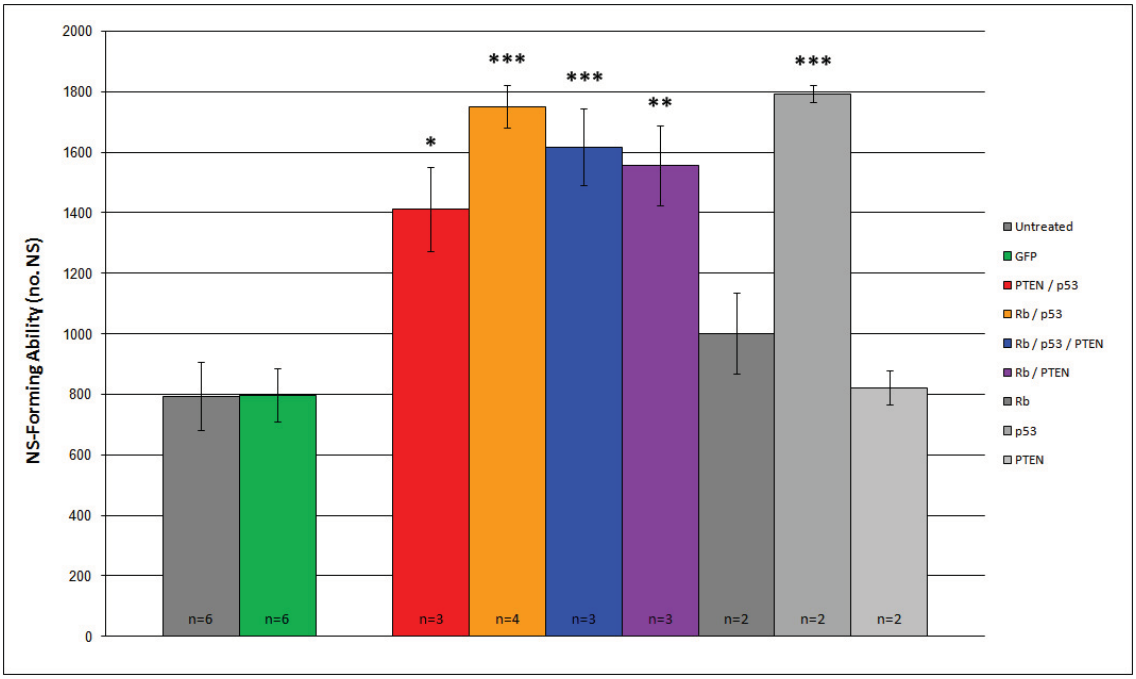

Figure 26: All of the experimental NSC genotypes, with the exception of the $Rb^{-/-}$ and $PTEN^{-/-}$ NSCs, form significantly more NS at passage 3 than the Adenovirus-GFP-infected control NSCs. Interestingly, the $p53^{-/-}$ NSCs appear to form the most NS, but at a level that is not significantly more than the $Rb^{-/-}$; $p53^{-/-}$ or $Rb^{-/-}$; $p53^{-/-}$; $PTEN^{-/-}$ NSCs. NSCs were seeded into NS medium and left to grow as NS for eight days before the number of NS formed was counted. NS size of non-recombined untreated (grey: n=6) vs. non-recombined Adenovirus-GFP-infected (green: n=6; 797.7 +/- 87.1) vs. *in vitro* recombined $PTEN^{-/-}$; $p53^{-/-}$ (red: n=3; 1411.3 +/- 138.6) vs. $Rb^{-/-}$; $p53^{-/-}$ (orange: n=4; 1750.5 +/- 70.1) vs. $Rb^{-/-}$; $p53^{-/-}$; $PTEN^{-/-}$ (blue: n=3; 1617.3 +/- 127.2) vs. $Rb^{-/-}$; $PTEN^{-/-}$ (purple: n=3; 1556.8 +/- 131.2) vs. $Rb^{-/-}$ (grey: n=2; 1001.1 +/- 134.0) vs. $p53^{-/-}$ (grey: n=2; 1793.4 +/- 28.5) vs. $PTEN^{-/-}$ (grey:

n=2; 822.5 +/- 57.2) NSCs. Error bars: standard errors. *: P<0.05 vs. GFP control, **: P<0.01 vs. GFP control, ***: P<0.001 vs. GFP control (one-way ANOVA with Bonferroni's multiple comparison correction).

Unlike in the WST-1 and NS size assays (where the $Rb^{-/-}$; $p53^{-/-}$; $PTEN^{-/-}$ NSCs had the highest growth rates and formed the largest NS), the triple mutant $Rb^{-/-}$; $p53^{-/-}$; $PTEN^{-/-}$ NSCs formed similar numbers of NS compared to the $PTEN^{-/-}$; $p53^{-/-}$, $Rb^{-/-}$; $p53^{-/-}$, $Rb^{-/-}$; $PTEN^{-/-}$, and $p53^{-/-}$ NSCs, all of which formed significantly more NS than the Adenovirus-GFP-infected controls (Figure 26). The only similar finding from this NS-forming clonogenicity assay (when compared to the WST-1 and NS size assays) was the lack of any statistically significant difference observed between the $Rb^{-/-}$ and $PTEN^{-/-}$ NSCs and the Adenovirus-GFP-infected controls. Whereas we suggested that a) the NS size assay might not be sensitive enough to delineate the proposed additive effect of additional TSG loss on growth advantage, or b) that the size of NS formed is not a suitable surrogate marker of growth rate, it appears that the number of NS formed can be used as a measure of delineating the growth patterns of the different NSC genotypes. However, these data do not match the growth data trends observed from the WST-1 assay, as illustrated by the $p53^{-/-}$ NSCs forming the most significantly large (P<0.001) number of NS (1793.4 +/- 28.5), suggesting that different growth mechanisms were examined. A possible explanation is that the number of NS formed is a measure of self-renewal and not of growth rate. However, it could also be argued that this NS-forming clonogenicity assay does not strictly measure the self-renewal ability of NSCs as single NSCs are not studied in isolation. In addition, the mass seeding of NSCs could mean that NS aggregation could occur, as previously described. To illustrate this point, the large number of NS formed by the $p53^{-/-}$ NSCs (Figure 26) could be as a result of their increased ability to self-renew following p53 loss (Meletis et al., 2006), and the small size of the NS formed (Figure 25) could be due to a low level of NS aggregation. In contrast, the comparatively larger but smaller number of NS formed by the $Rb^{-/-}$; $p53^{-/-}$; $PTEN^{-/-}$ NSCs may be due to increased NS aggregation. Transcriptionally inactive p53 downregulates E-cadherin (calcium-dependent adhesion molecule) expression in the colon carcinoma cell line HCT116 (Roger et al., 2010) and may explain the low level of NS aggregation observed with $p53^{-/-}$ NSCs. For this reason we proposed that there may be a correlation between the number and size of the NS formed, which could be interpreted as a coefficient of NS aggregation. However, despite some instances of correlation (e.g. $p53^{-/-}$ and $Rb^{-/-}$; $p53^{-/-}$) the overall correlation between the NS size and

NS-forming clonogenicity for all the genotypes was not significant at R^2=0.145 (data not shown).

Taken together, the WST-1 proliferation assay (Figure 24), NS size assay (Figure 25), and NS-forming clonogenicity assay (Figure 26) were able to delineate the *in vitro* growth profiles of the different NSC genotypes. The WST-1 and NS size assays highlighted an additive effect of additional TSG loss on growth advantage, and a potential PTEN-loss-mediated growth advantage. And the NS-forming clonogenicity assay highlighted a similar additive effect but on the number of NS formed, and a potential relationship between p53 loss and reduced NS aggregation through the downregulation of cell adhesion molecules. However, we identified that the NS-forming clonogenicity assay could be measuring the self-renewal of NSCs rather than their outright growth rate, and that self-renewal can only be truly measured by studying single NSCs in isolation. As previously stated, NSCs can be defined by their self-renewal and multipotency. To assess the self-renewal of our genetically modified NSC *in vitro*, we performed a self-renewal assay.

3.3.4 *In vitro* recombined NSCs possess increased self-renewal in a genotype-dependent manner and with an additive effect of additional TSG loss

We tested the primary and secondary *in vitro* self-renewal ability of all our NSC genotypes in order to characterise the effect of inactivating the TSGs Rb, p53, and PTEN. NS at passage two were dissociated into single cells (passage three), FACS-seeded into 96-well plates, and incubated for nine days before the number of NS that formed were counted to assess the primary self-renewal ability. NS were then randomly selected, individually dissociated into single cells, and re-FACS-seeded into 96-well plates and left to assess the secondary self-renewal ability. The efficiency of the MoFlox XDP FACS machine at seeding single cells into single 96-well plate wells was verified at >99% and therefore no correction was applied to the self-renewal data.

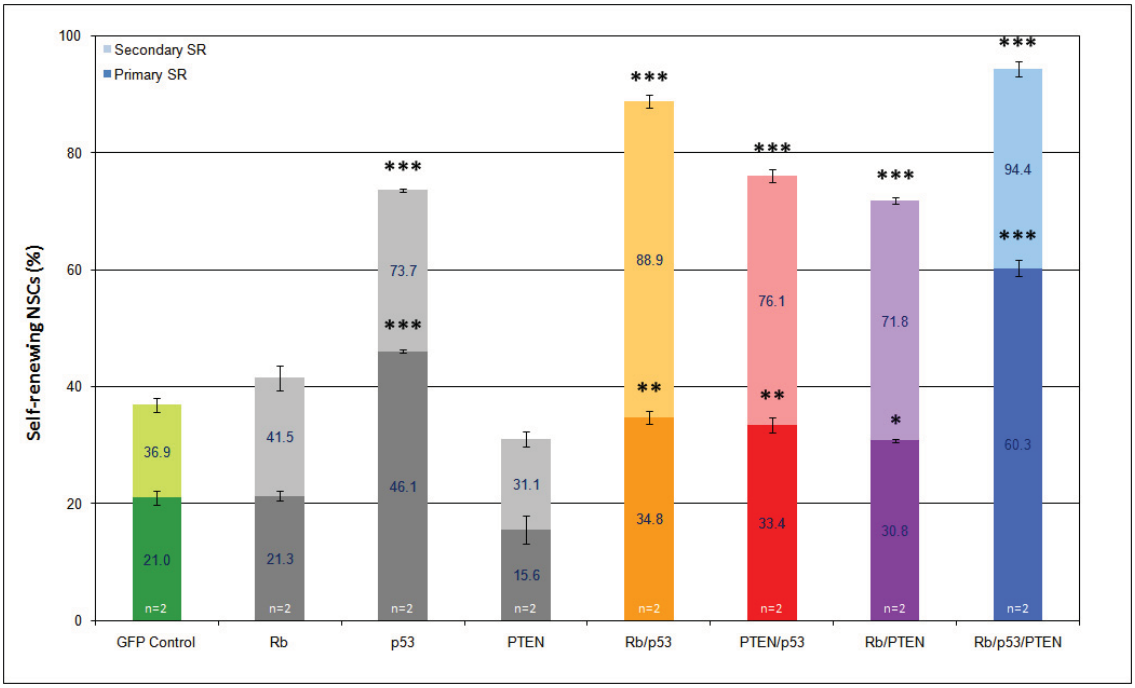

Figure 27: All genotypes, with the exception of the Rb$^{-/-}$ and PTEN$^{-/-}$ NSCs, have a significantly increased self-renewal ability at passages 3 and 4 compared to the Adenovirus-GFP-infected control NSCs. Interestingly, increase in self-renewal appears to be an additive result of additional TSG loss, with the exception that the p53$^{-/-}$ NSCs possess a significantly elevated self-renewal ability. NS at passage 2 were dissociated into single NSCs and individually seeded, using a MoFlo XDP FACS machine, into single wells of a 96-well plate containing 200µl NS medium and left to grow for nine days before the number of NS formed was counted and interpreted as the primary self-renewal ability. The process was then repeated for a selection of these monoclonal NS, chosen at random, to assess the secondary self-renewal ability. Primary/secondary self-renewal of non-recombined Adenovirus-GFP-infected (green: n=2) vs. *in vitro* recombined Rb$^{-/-}$ (grey: n=2) vs. p53$^{-/-}$ (grey: n=2) vs. PTEN$^{-/-}$ (grey: n=2) vs. Rb$^{-/-}$; p53$^{-/-}$ (orange: n=2) vs. PTEN$^{-/-}$; p53$^{-/-}$ (red: n=2) vs. Rb$^{-/-}$; PTEN$^{-/-}$ (purple: n=2) vs. Rb$^{-/-}$; p53$^{-/-}$; PTEN$^{-/-}$ (blue: n=2) NSCs. Primary self-renewal is shown as the solid bars and secondary self-renewal is shown as the paler-coloured bars on top of the primary self-renewal bars. Error bars: standard errors. *: P<0.05 vs. GFP control, **: P<0.01 vs. GFP control, ***: P<0.001 vs. GFP control (one-way repeated measures ANOVA with Bonferroni's multiple comparison correction).

Only the Rb$^{-/-}$ and PTEN$^{-/-}$ NSCs generated similar numbers of primary (21.3% +/- 0.8 and 15.6% +/- 2.4) and secondary (41.5% +/- 2.1 and 31.1% +/- 1.3) self-renewing NSCs as the Adenovirus-GFP-infected controls (Figure 27). All of the double knock-out genotypes generated significantly more primary self-renewing NSCs (>30%) compared to GFP-infected non-recombined controls (21.0% +/- 1.2). The triple knock-out Rb/p53/PTEN NSCs showed the most significant increase of primary self-renewing cells (60.3% +/- 1.4), once again suggesting an additive effect of TSG loss on self renewal. Interestingly, the significantly increased number of primary self-renewing p53^{-}

$^{/-}$ NSCs (46.1% +/- 0.3) was as significant as the $Rb^{-/-}$; $p53^{-/-}$; $PTEN^{-/-}$ NSCs ($P<0.001$). This validates the same finding from the NS-forming clonogenicity assay (Figure 26).

The secondary self-renewal patterns of significance remained similar to those observed with the primary self-renewal. However, the number of secondary self-renewing $Rb^{-/-}$; $p53^{-/-}$ (88.9% +/- 1.05), $PTEN^{-/-}$; $p53^{-/-}$ (76.1% +/- 1.05) and $Rb^{-/-}$; $PTEN^{-/-}$ (71.8% +/- 0.5) NSCs cells had increased to the same level as the $p53^{-/-}$ (73.7% +/- 0.25) and $Rb^{-/-}$; $p53^{-/-}$; $PTEN^{-/-}$ (94.4% +/- 1.3) NSCs (Figure 27).

The increase in self-renewal upon p53 loss in NSC is in keeping with recent studies that p53 is a key determinant of the transcriptional activation of *Nanog* (Lin et al., 2005; Hong et al., 2009; Kawamura et al., 2009; Po et al., 2010; Zbinden et al., 2010). *Nanog* itself is an intrinsic determinant of stemness and self-renewal with its expression is downregulated upon differentiation (Mitsui et al., 2003; Boiani and Scholer, 2005; Pan and Thomson, 2007). In addition, *Nanog* is reactivated in glioma and prostate cancer cells (Clement et al., 2007; Jeter et al., 2009; Ji et al., 2009; Zbinden et al., 2010). Taken together, these studies confirm our finding that p53 loss has a significant effect on increasing the self-renewal of NSCs. It has been proposed that PTEN loss increases the *in vitro* self-renewal capacity of NSCs by enhancing G_0 cell cycle exit (Groszer et al., 2006). However, other groups did not verify this finding experimentally and have shown that PTEN loss alone is not sufficient to confer an increase in self-renewal but that the additional loss of p53 is required (Zheng et al., 2008). Also, downregulation of Rb has been correlated with increased self-renewal of mouse NSCs, but only as a result of Ink4a-Arf deletion (Molofsky et al., 2005).

It therefore appears that only p53 loss has a direct effect on increasing the self-renewal capacity of NSCs and that additive effects of Rb and PTEN loss can only be seen, through indirect mechanisms, when both are lost together. The additive effect of additional TSG loss on increased growth (section 3.3.3) and self-renewal (Figure 27) suggests that these functional qualities may be indicators of *in vivo* tumourigenicity and/or tumour latency.

3.3.5 The *in vitro* growth rate of neural stem cells is a positive predictive indicator of *in vivo* tumour hit rate and an inverse predictive indicator of *in vivo* tumour latency

In order to test whether the *in vitro* growth (Figure 24 and Figure 25) or self-renewal (Figure 27) properties of NSCs could be used as indicators of *in vivo* tumour hit rate and/or tumour latency we performed a multiple correlation analysis of the various data sets using data from the non-recombined Adenovirus-GFP-infected control, $Rb^{-/-}$; $p53^{-/-}$, $PTEN^{-/-}$; $p53^{-/-}$, $Rb^{-/-}$; $PTEN^{-/-}$, and $Rb^{-/-}$; $p53^{-/-}$; $PTEN^{-/-}$ NSCs (Figure 28).

	Hit Rate	Latency	WST-1	NS Size
Latency	* (R^2= 0.7741)			
WST-1	*** (R^2= 0.9924)	ns (R^2= 0.7661)		
NS Size	ns (R^2= 0.4242)	ns (R^2= 0.4367)	ns (R^2= 0.4216)	
Self-renewal	ns (R^2= 0.4708)	ns (R^2= 0.5112)	ns (R^2= 0.4616)	*** (R^2= 0.9913)

Figure 28: Summary table of the correlation statistical analyses between the hit rate (*in vivo* tumour incidence), latency (*in vivo* tumour latency), WST-1 (growth assay), NS size (growth assay), and self-renewal data sets for the non-recombined Adenovirus-GFP-infected control, $Rb^{-/-}$; $p53^{-/-}$, $PTEN^{-/-}$; $p53^{-/-}$, $Rb^{-/-}$; $PTEN^{-/-}$, and $Rb^{-/-}$; $p53^{-/-}$; $PTEN^{-/-}$ NSCs. Linear regression was used to determine the goodness of the fit (R2), and a two-tailed Pearson's correlation test was used to measure the level of correlation (*: P<0.05, ***: P<0.001).

A statistically significant negative correlation was observed between the *in vivo* tumour hit rate and the *in vivo* tumour latency (R^2=0.7741, P<0.05) (Figure 28). This implies that tumour development follows a stochastic model whereby the more aggressive and faster growing tumours carry a higher chance of development. If we also take into account the highly significant positive correlation between the *in vivo* tumour hit rate and the WST-1 *in vitro* growth rate data (R^2=0.9924, P<0.001) we can revise this statement to read: those NSCs that exhibit the fastest growth rate *in vitro* possess the highest likelihood of generating tumours *in vivo*, and do so with the shortest latency. In other words, the *in vitro* growth rate of NSCs can be used as a positive predictive indicator of *in vivo* tumour hit rate. No correlation was observed between the NS size

and *in vivo* hit rate data (R^2=0.4242). This further validates our earlier proposal that "the size of NS formed is not a suitable surrogate marker of growth rate" (section 3.3.3).

A significant positive correlation was also observed between the NS size and self-renewal data (R^2=0.9913, P<0.001). This finding suggests that NS size may indirectly infer self-renewal and supports our proposal "that there may be a correlation between the number and size of the NS formed, which could be interpreted as a coefficient of NS aggregation" (section 3.3.3). No significant correlations were observed between any of the other data sets. No significant correlation was observed between the NS-forming clonogenicity data and any of the other data sets, including self-renewal. The latter highlights the deficiency of using an NS-forming assay to infer self-renewal.

3.3.6 Qualitative immunohistochemical biomarker analysis of *in vitro* recombined neurospheres yields few notable differences in expression levels

Adenovirus-Cre-infected control $Rosa^{Lox/Lox}$ and *in vitro* recombined $Rb^{-/-}$; $p53^{-/-}$, $PTEN^{-/-}$; $p53^{-/-}$, $Rb^{-/-}$; $PTEN^{-/-}$, and $Rb^{-/-}$; $p53^{-/-}$; $PTEN^{-/-}$ NS were taken at passage three and prepared in cytoblocks for paraffin immunohistochemistry (sections 2.3.6 and 2.3.4) and qualitative biomarker expression analysis (Figure 29).

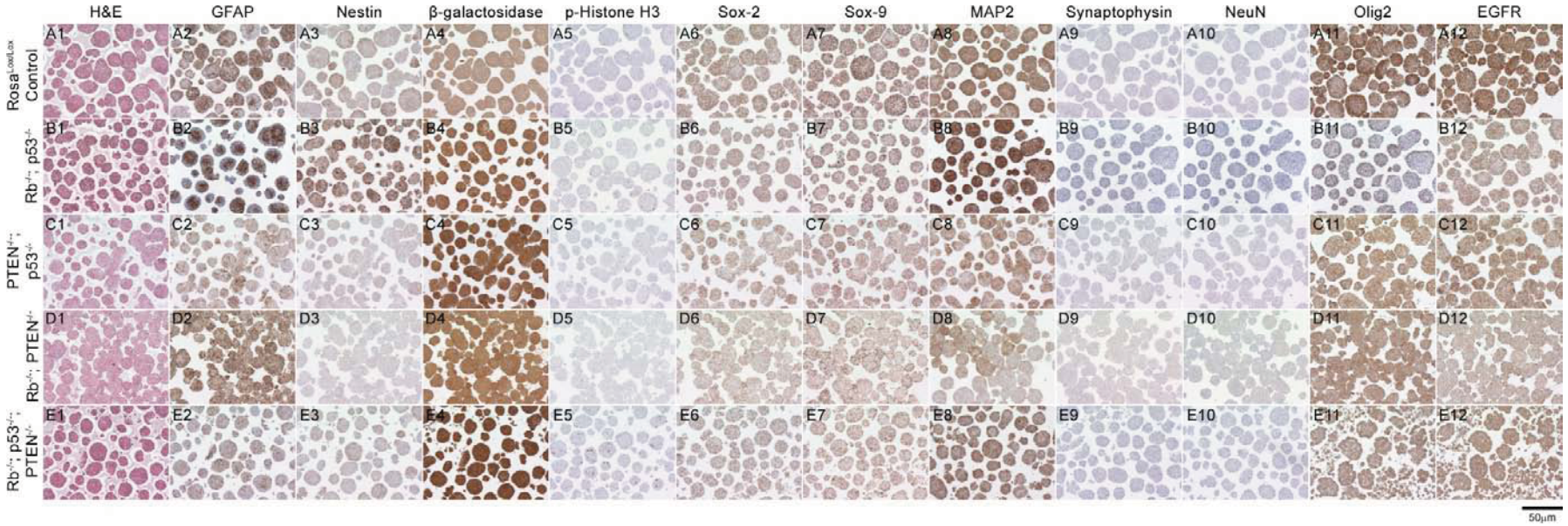

Figure 29: Only the PNET-generating Rb$^{-/-}$; p53$^{-/-}$ NS showed an expression profile different from all other *in vitro* recombined NS genotypes and controls. Representative images taken from cytoblocks of Adenovirus-Cre-infected control Rosa$^{Lox/Lox}$ (A1-A12) vs. Rb$^{-/-}$; p53$^{-/-}$ (B1-B12), PTEN$^{-/-}$; p53$^{-/-}$ (C1-C12), Rb$^{-/-}$; PTEN$^{-/-}$ (D1-D12), and Rb$^{-/-}$; p53$^{-/-}$; PTEN$^{-/-}$ (E1-E12) NS stained for haematoxylin-eosin, GFAP, nestin, β-galactosidase, phospho-Histone H3, Sox-2, Sox-9, MAP2, synaptophysin, and NeuN, Olig2, and EGFR. Images were taken using a ColorView III digital camera mounted on a Zeiss Axioskop 2 MOT microscope with a 5x magnification and using the AnalySIS software package.

Due to the variable nature of staining intensity in cytoblocks, immunohistochemistry is only suitable for semiquantitative analysis. No opposites in expression patterns were observed between any of the NS genotypes, however, reductions of Olig2 expression in $Rb^{-/-}$; $p53^{-/-}$ NS and of nestin expression in $Rb^{-/-}$; $PTEN^{-/-}$ NS were observed. To improve this semiquantitative expression analysis we carried out immunofluorescence staining of NS grown as differentiating cells on coverslips.

3.3.7 Expression of the biomarkers GFAP, Sox-2, and nestin by *in vitro* recombined and differentiated neurospheres are significantly altered in a genotype-dependent manner

NS at passage three from our four double and triple knockout genotypes were plated onto laminin-coated glass coverslips and allowed to differentiate for five days. Following fixation, they were double-labelled with antibodies against GFAP and CD133 (Figure 30: A-E), Sox-2 and Nestin (Figure 30: F-J), MAP2 and βIII-tubulin (Figure 30: K-O) and Hoechst 33342 (DAPI) was used as a nuclear counterstain. Adenovirus-GFP-infected NS fluoresce when excited by a 488nm laser, which can interfere with confocal microscopy image acquisition. For this reason, non-recombined untreated NS were used as the controls as no Adenovirus-mediated effect on the biomarker expression levels was observed (data not given).

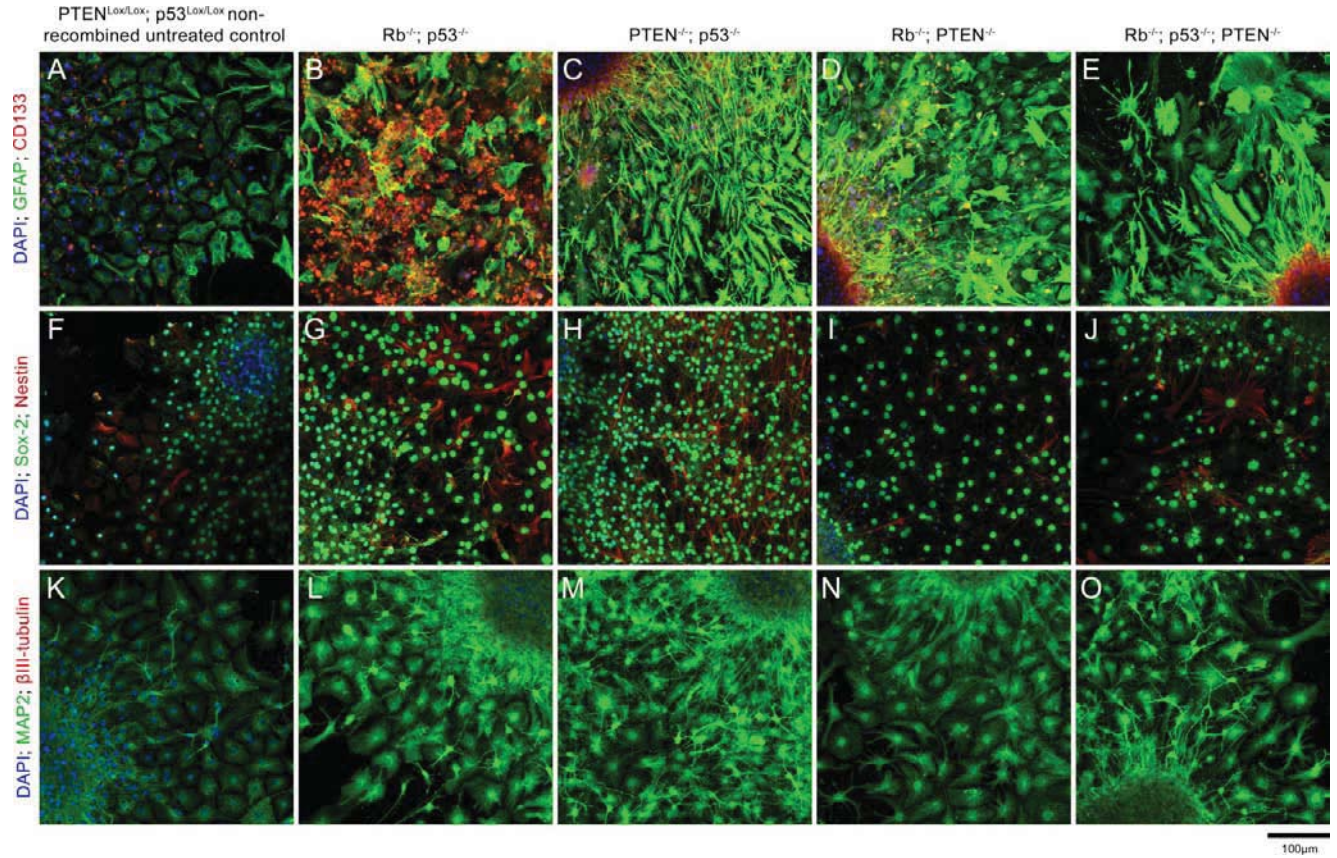

Figure 30: The expression of differentiation biomarkers varies significantly, and in a genotype-dependent manner, following *in vitro* inactivation of the TSGs Rb, p53, and PTEN. Representative images of PTEN$^{Lox/Lox}$; p53$^{Lox/Lox}$ non-recombined untreated control (A,F,K) vs. Rb$^{-/-}$; p53$^{-/-}$ (B,G,L) vs. PTEN$^{-/-}$; p53$^{-/-}$ (C,H,M) vs. Rb$^{-/-}$; PTEN$^{-/-}$ (D,I,N) vs. Rb$^{-/-}$; p53$^{-/-}$; PTEN$^{-/-}$ (E,J,O) NS that were left to differentiate on laminin-coated glass coverslips for 5 days before being fixed and immunofluorescently dual-stained for GFAP and CD133 (A-E), Sox-2 and Nestin (F-J), MAP2 and βIII-tubulin (K-O), and Hoechst 33342 (DAPI: A-O). Blue: excitation at 405nm, green: excitation at 488nm, red: excitation at 546nm. Images were taken using a 20x objective on a Zeiss LSM510 META confocal laser scanning microscope with the LSM software.

Three differentiated NS (per stain per genotype) were randomly selected under the microscope, and a field of view that encompassed both the edge of the NS and the spreading of the cells was imaged using a Zeiss LSM510 META confocal laser scanning microscope with the LSM software. The number of cells that were positive for the marker of interest were counted from the three images (taken from 425µm x 425µm = 0.181mm^2 fields of view), averaged, and expressed as a percentage against the total number of cells as measured by the number of Hoechst (or DAPI) positive nuclei (Figure 31 & Figure 32). This staining and counting was then repeated three times (to give an experimental n=3) using NS derived from separate cohorts of mice. Although an internal experimental control (PTEN$^{Lox/Lox}$; p53$^{Lox/Lox}$ non-recombined untreated control) was used to allow for expression comparison between the genotypes, no positive or negative control was directly incorporated into the experimental design (antibody specificity was validated using paraffin immunohistochemistry but not immunofluorescence). For this reason, the results detailed in section 3.3.7 (Figure 30, Figure 31, Figure 32, Figure 33) should be considered with caution on the basis that the staining patterns have not been sufficiently controlled against non-specific antibody-mediated effects. Positive controls could have taken the form of cell lines with known expression, and negative controls as knock-out cell lines. Additionally, incorporation of isotype controls would have enabled better (than secondary antibody only controls) control against: a) non-specific binding of the primary antibodies to cellular proteins, lipids, surface antigens (e.g. Fc receptors), and b) cellular autofluorescence.

Genotype		GFAP			CD133			Sox-2			Nestin			MAP2			βIII-tubulin		
Non-recombined (untreated)	No. positive cells	61	66	51	38	22	37	147	105	96	47	40	45	137	111	119	0	0	0
	Total no. DAPI-positive cells	74	82	59	74	82	59	149	110	96	149	110	96	137	111	119	137	111	119
	Positivity (%)	82.4	80.5	86.4	51.4	26.8	62.7	98.7	95.5	100.0	31.5	36.4	46.9	100.0	100.0	100.0	0.0	0.0	0.0
	Average Positivity (%)		**83.1**			**47.0**			**98.0**			**38.3**			**100.0**			**0.0**	
	SE		**1.8**			**10.6**			**1.3**			**4.5**			**0.0**			**0.0**	
	Expression intensity	++	++	++	++	++	++	++	++	++	++	++	++	++	++	++	-	-	-
Rb/p53	No. positive cells	70	66	71	89	95	80	101	85	74	75	49	44	152	84	70	0	0	0
	Total no. DAPI-positive cells	89	101	88	89	101	88	105	87	82	105	87	82	152	84	70	152	84	70
	Positivity (%)	78.7	65.3	80.7	100.0	94.1	90.9	96.2	97.7	90.2	71.4	56.3	53.7	100.0	100.0	100.0	0.0	0.0	0.0
	Average Positivity (%)		**74.9**			**95.0**			**94.7**			**60.5**			**100.0**			**0.0**	
	SE		**4.8**			**2.7**			**2.3**			**5.5**			**0.0**			**0.0**	
	Expression intensity	+++	+++	+++	++++	++++	++++	+++	+++	+++	+++	+++	+++	+++	+++	+++	-	-	-
PTEN/p53	No. positive cells	115	77	88	66	32	48	127	127	99	100	122	86	93	139	94	0	0	0
	Total no. DAPI-positive cells	121	81	97	121	81	97	138	157	106	138	157	106	93	139	94	93	139	94
	Positivity (%)	95.0	95.1	90.7	54.5	39.5	49.5	92.0	80.9	93.4	72.5	77.7	81.1	100.0	100.0	100.0	0.0	0.0	0.0
	Average Positivity (%)		**93.6**			**47.8**			**88.8**			**77.1**			**100.0**			**0.0**	
	SE		**1.4**			**4.4**			**4.0**			**2.5**			**0.0**			**0.0**	
	Expression intensity	++++	++++	++++	++	++	++	+++	+++	+++	+++	+++	+++	++++	++++	++++	-	-	-
Rb/PTEN	No. positive cells	112	113	99	88	64	60	39	48	44	22	16	27	77	81	69	0	0	0
	Total no. DAPI-positive cells	112	113	99	112	113	99	75	70	84	75	70	84	77	81	69	77	81	69
	Positivity (%)	100.0	100.0	100.0	78.6	56.6	60.6	52.0	68.6	52.4	29.3	22.9	32.1	100.0	100.0	100.0	0.0	0.0	0.0
	Average Positivity (%)		**100.0**			**65.3**			**57.7**			**28.1**			**100.0**			**0.0**	
	SE		**0.0**			**6.7**			**5.5**			**2.7**			**0.0**			**0.0**	
	Expression intensity	++++	++++	++++	++	++	++	+++	+++	+++	++	++	++	+++	+++	+++	-	-	-
Rb/p53/PTEN	No. positive cells	149	167	120	34	30	41	84	61	84	59	43	37	148	140	121	0	0	0
	Total no. DAPI-positive cells	149	167	120	149	167	120	89	71	92	89	71	92	148	140	121	148	140	121
	Positivity (%)	100.0	100.0	100.0	22.8	18.0	34.2	94.4	85.9	91.3	66.3	60.6	40.2	100.0	100.0	100.0	0.0	0.0	0.0
	Average Positivity (%)		**100.0**			**25.0**			**90.5**			**55.7**			**100.0**			**0.0**	
	SE		**0.0**			**4.8**			**2.5**			**7.9**			**0.0**			**0.0**	
	Expression intensity	++++	++++	++++	+	+	+	+++	+++	+++	+++	+++	+++	++++	++++	++++	-	-	-

Figure 31: Table of results of the counts (n=3), their averages, and the expression intensities recorded for all the differentiation biomarkers across all the different genotypes.

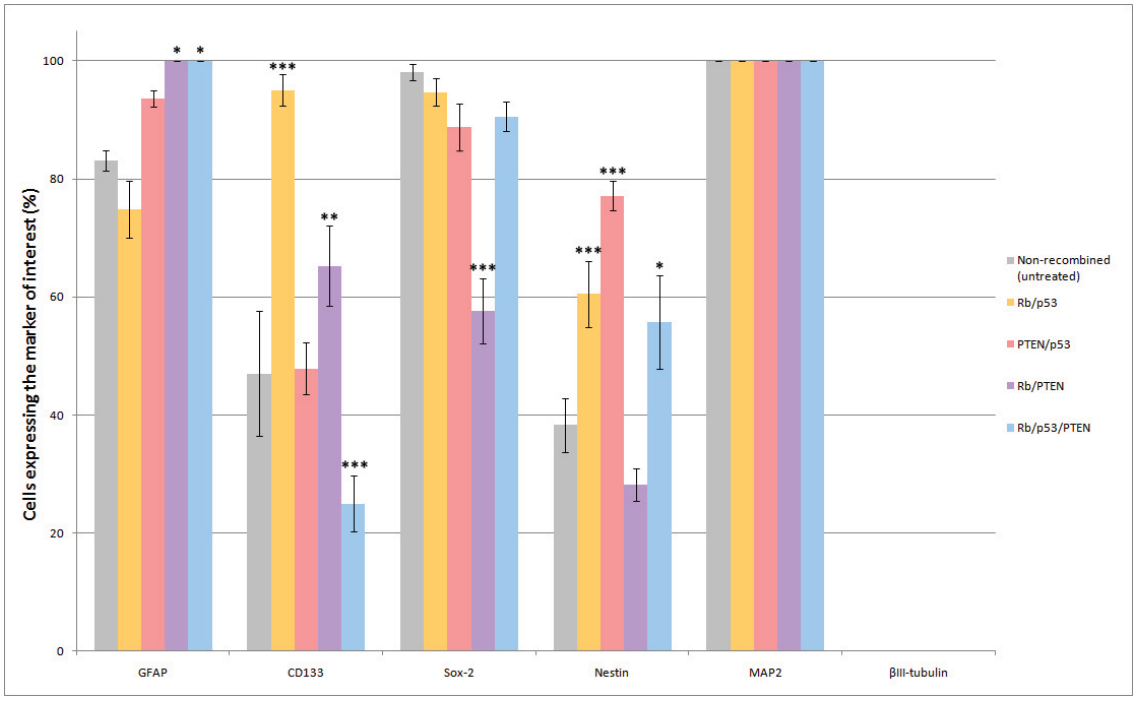

Figure 32: The expression of the biomarkers GFAP, CD133, Sox-2, and Nestin are significantly altered, in a genotype-dependent manner, following *in vitro* inactivation of the TSGs Rb, p53, and PTEN in differentiated neurospheres when compared against non-recombined untreated controls. The expression of MAP2 and βIII-tubulin was respectively ubiquitous and absent across all the genotypes, and the $Rb^{-/-}$; $PTEN^{-/-}$ glioblastoma-generating NS exhibits the most altered / unique expression profile when compared against the other *in vitro* recombined NS genotypes. Percentage of cells expressing the differentiation biomarkers GFAP, CD133, Sox-2, Nestin, MAP2, and βIII-tubulin from $PTEN^{Lox/Lox}$; $p53^{Lox/Lox}$ non-recombined untreated control vs. $Rb^{-/-}$; $p53^{-/-}$ vs. $PTEN^{-/-}$; $p53^{-/-}$ vs. $Rb^{-/-}$; $PTEN^{-/-}$ vs. $Rb^{-/-}$; $p53^{-/-}$; $PTEN^{-/-}$ NS that were left to differentiate on laminin-coated glass coverslips for 5 days before being fixed and immunofluorescently stained. Error bars: standard errors. *: P<0.05 vs. non-recombined untreated control, **: P<0.01 vs. control, ***: P<0.001 vs. control (two-way ANOVA with Bonferroni's multiple comparison correction).

GFAP was observed to be expressed by significantly more cells in both the $Rb^{-/-}$; $PTEN^{-/-}$ (100% +/- 0: P<0.05) and $Rb^{-/-}$; $p53^{-/-}$; $PTEN^{-/-}$ (100% +/- 0: P<0.05) NS when compared against the non-recombined untreated control (83.1% +/- 1.8). CD133 was seen to be expressed by significantly more cells in the $Rb^{-/-}$; $p53^{-/-}$ (95.0% +/- 2.7: P<0.001) and $Rb^{-/-}$; $PTEN^{-/-}$ (65.3% +/- 6.7: P<0.01) NS, but by significantly less cells in the $Rb^{-/-}$; $p53^{-/-}$; $PTEN^{-/-}$ (25.0% +/- 4.8: P<0.001) NS when compared against the control (47.0% +/- 10.6) (Figure 32). The only change in Sox2 expression was observed with the $Rb^{-/-}$; $PTEN^{-/-}$ (57.7% +/- 5.5: P<0.001) NS in which significantly less cells expressed Sox2 when compared against the control (98.0% +/- 1.3). Nestin was observed to be expressed by significantly more cells in the $Rb^{-/-}$; $p53^{-/-}$ (60.5% +/- 5.5:

P<0.001), PTEN$^{-/-}$; p53$^{-/-}$ (77.1% +/- 2.5: P<0.001), and Rb$^{-/-}$; p53$^{-/-}$; PTEN$^{-/-}$ (55.7% +/- 7.9: P<0.05) NS when compared against the non-recombined untreated control (38.3% +/- 4.5). MAP2 was found to be expressed by 100% of the cells in both the non-recombined control and all the *in vitro* recombined genotypes. Conversely, no βIII-tubulin expression was observed in any of the genotypes (Figure 32).

As expected, the number of *in vitro* GFAP-expressing cells in PNET-generating Rb$^{-/-}$; p53$^{-/-}$ NS was not significantly different from the control, in line with the fact that PNETs express GFAP at endogenously low levels (section 4.3.2). However, the PTEN$^{-/-}$; p53$^{-/-}$, Rb$^{-/-}$; PTEN$^{-/-}$, and Rb$^{-/-}$; p53$^{-/-}$; PTEN$^{-/-}$ NS predominantly generated high GFAP-expressing glioma, glioblastoma, and PNET + glioma tumours respectively following intracerebral engraftment, which all showed more GFAP-expressing cells *in vitro*. This correlation highlights the potential use of the *in vitro* NS differentiation expression profile as a predictor of the *in vivo* tumour expression profile. Additionally, this model system may possibly be used to manipulate (e.g. shRNA silencing) the *in vitro* differentiation expression profile to identify determining factors of tumour phenotype and identify therapeutic targets. A cellular pattern of CD133 staining was expected; in line with the *in vivo* staining pattern we observed (section 5.3.1). However, the pattern was overly granular and therefore probably a result of cross-reactivity with cellular debris. In chapter five we show that 12.5% of Rb$^{-/-}$; p53$^{-/-}$; PTEN$^{-/-}$ NSCs express CD133 whereas only 2.5% of wild-type untreated control NSCs express CD133 (sections 5.3.2 and 5.3.3), a result not mirrored by the differentiation expression profile detailed here. Taken together, we believe that the CD133 staining was non-specific and subsequently void for analysis. As previously discussed, the incorporation of an isotype control into the experimental design would have effectively controlled against this outcome and allowed for a better understanding of the antibody reliability. Sox-2 is expressed by all the intrinsic brain tumours generated by our model, and also in human glioblastomas (Schmitz et al., 2007; Eschbacher et al., 2008). It has also been shown that miRNA silencing of Sox-2 in human glioblastoma-initiating cells reduces their proliferation and tumourigenicity in nude mice (Gangemi et al., 2009). A significant reduction of Sox-2-expressing cells was seen in the glioblastoma-generating Rb$^{-/-}$; PTEN$^{-/-}$ NS; a result which contradicts the literature but suggests that the expression profile of differentiated NS may not always accurately predict the expression profile of the tumours they generate *in vivo*. Nestin is variably expressed across the different tumour phenotypes, but particularly strong immunoreactivity was seen in the

undifferentiated PNET tumours. Despite this, nestin expression is not restricted to undifferentiated tumours with expression also observed in high and low-grade malignant gliomas (Almqvist et al., 2002). MAP2, a marker of immature neurons, is highly expressed by all the intrinsic brain tumours generated by our model. This pattern of expression was not changed in the expression profile of the differentiated NS. The lack of any βIII-tubulin positive cells highlights the fact that the *in vitro* differentiation conditions we used were not permissive to the generation of mature neurons and should be altered if required. However, the possibility that this observation was as a result of a lack of antibody specificity could have been effectively controlled aginst through the inclusion of a positive control into the experimental design.

In addition to the number of positive cells, the expression intensity of the different markers across the genotypes was also graded. This was achieved by comparative confocal laser scanning imaging whereby the experimental genotype images were taken using identical imaging parameters as used for the control NS (Figure 33).

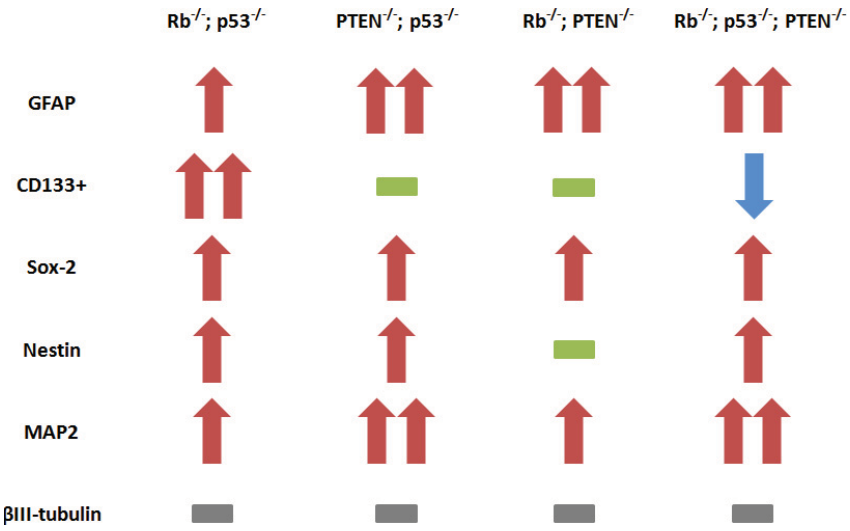

Figure 33: The qualitative expression intensities of the differentiation biomarkers GFAP, CD133, Sox-2, Nestin, and MAP2 following *in vitro* inactivation of the TSGs Rb, p53, and PTEN correlate with the changes in the number of respective biomarker-expressing cells when compared against non-recombined untreated controls. Matrix of the expression intensity changes observed across the *in vitro* recombined $Rb^{-/-}$; $p53^{-/-}$, $PTEN^{-/-}$; $p53^{-/-}$, $Rb^{-/-}$; $PTEN^{-/-}$, and $Rb^{-/-}$; $p53^{-/-}$; $PTEN^{-/-}$ NS when compared against the $PTEN^{Lox/Lox}$; $p53^{Lox/Lox}$ non-recombined untreated control. Red up-arrow: increased expression intensity, double red up-arrow: vastly increased expression intensity, blue down-arrow: decreased expression intensity, green dash: no change, grey dash: no expression observed.

The qualitative expression intensity levels of GFAP, Sox-2, and MAP2 were higher across all of the experimental genotypes. Interestingly, an increase in Sox-2 expression intensity was observed in the $Rb^{-/-}$; $PTEN^{-/-}$ NS, despite having demonstrated a significantly reduced number of cells expressing Sox-2. Also, no change in the number of cells expressing MAP2 could be observed between any of the genotypes as the figure was always 100%. However, this expression intensity measurement method, highlighted a potential difference in MAP2 expression with the $PTEN^{-/-}$; $p53^{-/-}$ and $Rb^{-/-}$; $p53^{-/-}$; $PTEN^{-/-}$ NS appearing to express it at a higher intensity than the $Rb^{-/-}$; $p53^{-/-}$ and $Rb^{-/-}$; $PTEN^{-/-}$ NS, despite 100% of the cells expressing MAP2 in all of the cases. The CD133 expression intensity was disregarded due to its non-specific nature as previously described. The expression intensity of nestin was seen to be increased in the $Rb^{-/-}$; $p53^{-/-}$, $PTEN^{-/-}$; $p53^{-/-}$, and $Rb^{-/-}$; $p53^{-/-}$; $PTEN^{-/-}$ NS (Figure 33). These findings suggest that biomarker expression intensity correlates with the number of biomarker-expressing cells, but also highlights the potential of qualitative data in adding to quantitative data sets. However, in light of the lack of experimental controls within this design, as previously discussed, the deduced results from this immunofluorescence data should be taken with caution.

3.3.8 Quantitative real-time PCR identifies differentially expressed cancer genes between genotypes

Using the Cancer PathwayFinder RT^2 Profiler PCR Superarray system we were able to examine the mRNA expression profiles of NSCs for 84 genes (representative of six cancer pathways) of NSCs. RNA was extracted from each of the $Rb^{-/-}$; $p53^{-/-}$, $PTEN^{-/-}$; $p53^{-/-}$, $Rb^{-/-}$; $p53^{-/-}$; $PTEN^{-/-}$, and $Rb^{-/-}$; $PTEN^{-/-}$ NS genotypes (n=2 for each, passage 2-5) to compare their mRNA expression profiles in the aim of identifying the effects of TSG loss in the different combinations. These profiles were corrected against RNA taken from Adenovirus-GFP-infected control NS (n=2, passage 3) and five housekeeping control genes.

Symbol	Description	Rb-p53		PTEN-p53		Rb-p53-PTEN		Rb-PTEN	
Akt1	Thymoma viral proto-oncogene 1	0.12	0.4806	1.56	0.0790	1.88	0.3844	1.53	0.0966
Akt2	Thymoma viral proto-oncogene 2	0.53	0.0463	0.83	0.6245	0.70	0.1870	0.65	0.7268
Angpt1	Angiopoietin 1	3.03	0.3760	1.00	0.9885	2.23	0.2613	0.85	0.8347
Apaf1	Apoptotic peptidase activating factor 1	0.59	0.4179	0.55	0.2802	0.69	0.5923	1.20	0.7933
Atm	Ataxia telangiectasia mutated homolog (human)	1.39	0.2161	1.35	0.1420	1.87	0.4691	1.29	0.5871
Bad	Bcl-associated death promoter	0.74	0.6306	0.90	0.8227	0.94	0.9293	0.69	0.3427
Bax	Bcl2-associated X protein	0.33	0.1371	0.32	0.0963	0.40	0.2746	1.17	0.7155
Bcl2	B-cell leukemia/lymphoma 2	0.71	0.4030	0.78	0.5010	0.74	0.6137	0.84	0.8182
Bcl2l1	Bcl2-like 1	0.62	0.5272	0.88	0.8506	0.76	0.7316	2.28	0.3197
Birc5	Baculoviral IAP repeat-containing 5	1.16	0.6952	0.38	0.4174	0.89	0.8539	0.19	0.1746
Brca1	Breast cancer 1	1.09	0.7108	0.42	0.4010	0.89	0.6718	0.29	0.0634
Casp8	Caspase 8	3.51	0.0849	1.59	0.5979	2.97	0.0991	5.07	0.0440
Ccnd1	Cyclin D1	0.46	0.2335	0.46	0.5158	0.29	0.1162	0.74	0.6418
Ccne1	Cyclin E1	1.23	0.4999	1.01	0.9774	1.60	0.2427	3.24	0.1253
Cdc25a	Cell division cycle 25 homolog A (S. pombe)	1.87	0.0352	1.28	0.4465	2.45	0.0882	1.26	0.5349
Cdh1	Cadherin 1	0.23	0.4200	0.90	0.9555	0.33	0.5693	0.39	0.5441
Cdk2	Cyclin-dependent kinase 2	1.38	0.6015	0.83	0.8484	1.79	0.4855	1.18	0.7886
Cdk4	Cyclin-dependent kinase 4	0.86	0.7196	0.78	0.5407	0.92	0.8616	0.72	0.4555
Cdkn1a	Cyclin-dependent kinase inhibitor 1A (P21)	0.10	0.0798	0.06	0.1202	0.17	0.1793	1.66	0.5772
Cdkn2a	Cyclin-dependent kinase inhibitor 2A	5.38	0.0389	6.52	0.0148	11.59	0.0120	3.52	0.0470
Cflar	CASP8 and FADD-like apoptosis regulator	0.75	0.6789	0.90	0.8604	1.12	0.9034	0.82	0.7574
Chek2	CHK2 checkpoint homolog (S. pombe)	0.99	0.9876	1.17	0.8626	1.04	0.9733	0.90	0.8989
Col18a1	Procollagen, type XVIII, alpha 1	0.59	0.6070	0.78	0.7022	0.65	0.3517	0.51	0.1512
Ctnnb1	Catenin (cadherin associated protein), beta 1	0.66	0.4331	0.81	0.5210	0.87	0.7781	0.69	0.2975
E2f1	E2F transcription factor 1	3.38	0.0598	1.82	0.4287	3.68	0.0225	2.41	0.0636
Egfr	Epidermal growth factor receptor	0.82	0.2790	1.11	0.4654	1.13	0.8662	0.73	0.6310
Ets2	E26 avian leukemia oncogene 2, 3' domain	0.84	0.7433	1.20	0.7268	1.36	0.7335	1.19	0.7415
Fas	Fas (TNF receptor superfamily member)	0.40	0.7493	1.10	0.9660	1.51	0.8754	14.54	0.3157
Fgf1	Fibroblast growth factor 1	0.96	0.7704	0.61	0.1894	0.47	0.0696	1.07	0.6276
Fgfr2	Fibroblast growth factor receptor 2	0.94	0.9492	1.11	0.8790	0.90	0.9258	1.24	0.7553
Figf	C-fos induced growth factor	0.33	0.5298	0.90	0.9555	0.38	0.6342	0.39	0.5441
Fos	FBJ osteosarcoma oncogene	0.52	0.6127	0.54	0.5993	0.40	0.5227	1.66	0.6497
Grb2	Growth factor receptor bound protein 2	0.85	0.8766	0.90	0.9000	1.08	0.9524	0.76	0.7453
Hgf	Hepatocyte growth factor	1.04	0.9768	0.95	0.9697	0.67	0.8390	1.99	0.6964
Ifnb1	Interferon beta 1, fibroblast	0.23	0.4200	1.23	0.8981	0.68	0.8740	0.39	0.5441
Igf1	Insulin-like growth factor 1	0.93	0.9574	1.96	0.6321	2.96	0.4730	0.91	0.9523
Itga2	Integrin alpha 2	1.95	0.6717	4.49	0.3423	5.17	0.2441	3.11	0.3531
Itga3	Integrin alpha 3	1.01	0.9769	1.55	0.3134	0.88	0.9190	2.86	0.1200
Itga4	Integrin alpha 4	0.40	0.0812	0.42	0.3743	0.76	0.4201	0.35	0.1320
Itgav	Integrin alpha V	0.31	0.2651	0.75	0.7410	0.62	0.5454	0.90	0.8760
Itgb1	Integrin beta 1 (fibronectin receptor beta)	0.93	0.8896	0.97	0.9507	1.08	0.9047	0.82	0.7107
Itgb3	Integrin beta 3	1.05	0.9326	0.89	0.7120	0.43	0.0988	0.82	0.5473
Jun	Jun oncogene	0.58	0.3400	0.41	0.1972	0.40	0.1761	0.66	0.4827
Kiss1	KiSS-1 metastasis-suppressor	0.54	0.7200	1.16	0.9141	0.45	0.7260	0.57	0.6488
Map2k1	Mitogen activated protein kinase kinase 1	0.82	0.5594	1.00	0.9888	1.15	0.7720	1.25	0.5980
Mcam	Melanoma cell adhesion molecule	0.78	0.7535	0.71	0.6877	0.62	0.5819	1.20	0.8584
Mdm2	Transformed mouse 3T3 cell double minute 2	0.23	0.4200	0.90	0.9555	0.33	0.5693	0.39	0.5441
Met	Met proto-oncogene	3.91	0.0028	3.99	0.0732	4.16	0.3858	16.12	0.0318
Mmp2	Matrix metallopeptidase 2	0.07	0.1258	0.10	0.1223	0.05	0.1042	4.73	0.1993
Mmp9	Matrix metallopeptidase 9	1.57	0.5477	2.86	0.0313	1.29	0.5024	1.29	0.0438
Mta1	Metastasis associated 1	0.77	0.5610	0.81	0.6136	0.88	0.8141	0.64	0.3832
Mta2	Metastasis-associated gene family, member 2	0.68	0.4506	0.93	0.8764	0.98	0.9672	0.65	0.3894
Muc1	Mucin 1, transmembrane	0.90	0.8708	1.32	0.5688	0.86	0.8729	1.09	0.8562
Myc	Myelocytomatosis oncogene	0.84	0.5183	0.64	0.2389	0.69	0.5936	0.82	0.6525
Ncam1	Neural cell adhesion molecule 1	0.97	0.9670	1.21	0.7446	1.47	0.6989	1.09	0.8860
Nfkb1	Nuclear factor of kappa light chain gene enhance	0.90	0.9040	1.03	0.9730	1.13	0.9110	1.09	0.9125
Nfkbia	Nuclear factor of kappa light chain gene enhance	1.47	0.3980	2.17	0.3000	2.37	0.3200	4.33	0.1691
Nme4	Expressed in non-metastatic cells 4, protein	0.69	0.2939	0.67	0.3397	0.68	0.2817	0.92	0.8318
Pdgfa	Platelet derived growth factor, alpha	0.63	0.5121	1.24	0.7374	1.08	0.9130	4.16	0.1143
Pdgfb	Platelet derived growth factor, B polypeptide	1.28	0.8281	1.10	0.9457	1.22	0.8722	2.42	0.4761
Pik3r1	Phosphatidylinositol 3-kinase, regulatory subunit	0.72	0.7663	1.60	0.5819	1.58	0.7745	1.09	0.9232
Plau	Plasminogen activator, urokinase	0.26	0.1649	0.12	0.0910	0.18	0.1339	0.93	0.9483
Plaur	Plasminogen activator, urokinase receptor	1.73	0.6046	1.76	0.6324	1.50	0.6691	1.10	0.9365
Pten	Phosphatase and tensin homolog	0.55	0.0902	0.00	0.0126	0.00	0.0117	0.00	0.0007
Raf1	V-raf-leukemia viral oncogene 1	0.62	0.0609	1.29	0.2043	1.34	0.6028	0.93	0.5964
Rb1	Retinoblastoma 1	0.00	0.0126	1.37	0.2510	0.00	0.0278	0.00	0.0010
S100a4	S100 calcium binding protein A4	2.38	0.3112	1.79	0.2667	1.51	0.4492	17.85	0.0396
Serpinb2	Serine (or cysteine) peptidase inhibitor, clade B,	0.23	0.4200	0.90	0.9555	0.33	0.5693	0.39	0.5441
Serpine1	Serine (or cysteine) peptidase inhibitor, clade E,	0.81	0.8893	1.98	0.6501	0.62	0.7627	1.23	0.8906
Syk	Spleen tyrosine kinase	0.53	0.5387	0.56	0.6795	1.16	0.9031	0.24	0.2173
Tek	Endothelial-specific receptor tyrosine kinase	0.77	0.7461	1.31	0.7988	0.54	0.5341	1.20	0.8554
Tert	Telomerase reverse transcriptase	2.13	0.2744	1.43	0.6349	2.34	0.2420	70.61	0.3265
Tgfb1	Transforming growth factor, beta 1	2.69	0.1475	2.85	0.3142	2.28	0.3327	4.12	0.1634
Tgfbr1	Transforming growth factor, beta receptor I	1.41	0.5284	1.29	0.1127	1.95	0.1805	0.80	0.4927
Thbs1	Thrombospondin 1	1.24	0.6370	1.92	0.2966	2.42	0.4315	2.28	0.1920
Timp1	Tissue inhibitor of metalloproteinase 1	2.71	0.1762	3.38	0.0578	4.24	0.0279	42.36	0.0450
Tnf	Tumor necrosis factor	0.23	0.4200	1.72	0.7194	0.65	0.8547	0.64	0.7759
Tnfrsf10b	Tumor necrosis factor receptor superfamily, mem	0.17	0.0346	0.15	0.1586	0.38	0.3947	2.31	0.3144
Tnfrsf1a	Tumor necrosis factor receptor superfamily, mem	0.44	0.0953	0.93	0.7454	0.86	0.4868	2.07	0.1178
Trp53	Transformation related protein 53	0.00	0.0164	0.00	0.0145	0.00	0.0133	1.35	0.3827
Twist1	Twist gene homolog 1 (Drosophila)	2.12	0.0173	3.33	0.0326	9.52	0.0014	1.65	0.8412
Vegfa	Vascular endothelial growth factor A	1.17	0.6804	0.63	0.3255	1.18	0.5989	0.31	0.0489
Vegfb	Vascular endothelial growth factor B	1.46	0.0383	1.88	0.1159	2.14	0.0273	1.57	0.2147
Vegfc	Vascular endothelial growth factor C	0.93	0.9753	0.24	0.3704	6.08	0.2890	0.47	0.6436
Gusb	Glucuronidase, beta	0.69	0.3926	1.03	0.8415	0.87	0.7293	0.75	0.4748
Hprt1	Hypoxanthine guanine phosphoribosyl transferas	0.73	0.2735	1.06	0.8824	1.18	0.8028	0.95	0.9285
Hsp90ab1	Heat shock protein 90kDa alpha (cytosolic), class I	1.46	0.0843	1.37	0.1785	1.59	0.0677	1.25	0.1874
Gapdh	Glyceraldehyde-3-phosphate dehydrogenase	1.64	0.3225	0.91	0.6266	1.02	0.9749	1.29	0.2366
Actb	Actin, beta, cytoplasmic	0.83	0.1234	0.74	0.0928	0.60	0.3404	0.86	0.3843

Figure 34: Average mRNA expression fold changes (2(average $^{\Delta\Delta Ct}$)) and associated P-values for the full set of 84 experimental genes (and 5 additional housekeeping control genes: given at the bottom) examined. For each genotype the left-hand column represents the mRNA fold change and the right-hand

column represents the P-value. Gene (symbol) column colour key - orange: upregulated in all genotypes, red: upregulated in three genotypes, olive: upregulated in two genotypes, yellow: downregulated in three genotypes, green: single genotype differential expression. Fold change column colour key – blue font: <0.33, red font: >2. P-value column colour key – red font: P<0.05. Genotype fold change and P-value dual column colour key – highlighted blue box: dual-significant downregulation, highlighted orange box: dual-significant upregulation.

Rb, p53, and PTEN were observed to be completely knocked-out with a fold change of 0.00 (where 1.00 = no change) in all the corresponding genotypes in which they were lost, therefore validating the assay. In addition, it should be noted that no significant fold changes were observed in non-recombined Rb, p53, or PTEN genes as a compensation of the others being lost (Figure 34). Any significant up/downregulation of these 84 experimental genes was highlighted so that comparisons could be made between the different genotypes. Genes that were differentially expressed to a significant level were then used to generate a 'hit list' (Figure 35).

Symbol	Description	Rb-p53		PTEN-p53		Rb-p53-PTEN		Rb-PTEN	
Casp8	Caspase 8	3.51	0.0849	1.59	0.5979	2.97	0.0991	5.07	0.0440
Cdkn2a	Cyclin-dependent kinase inhibitor 2A	5.38	0.0389	6.52	0.0148	11.59	0.0120	3.52	0.0470
E2f1	E2F transcription factor 1	3.38	0.0598	1.82	0.4287	3.68	0.0225	2.41	0.0636
Met	Met proto-oncogene	3.91	0.0028	3.99	0.0732	4.16	0.3858	16.12	0.0318
Mmp9	Matrix metallopeptidase 9	1.57	0.5477	2.86	0.0313	1.29	0.5024	1.29	0.0438
S100a4	S100 calcium binding protein A4	2.38	0.3112	1.79	0.2667	1.51	0.4492	17.85	0.0396
Timp1	Tissue inhibitor of metalloproteinase 1	2.71	0.1762	3.38	0.0578	4.24	0.0279	42.36	0.0450
Tnfrsf10b	Tumor necrosis factor receptor superfamily, mem	0.17	0.0346	0.15	0.1586	0.38	0.3947	2.31	0.3144
Twist1	Twist gene homolog 1 (Drosophila)	2.12	0.0173	3.33	0.0326	9.52	0.0014	1.65	0.8412
Vegfa	Vascular endothelial growth factor A	1.17	0.6804	0.63	0.3255	1.18	0.5989	0.31	0.0489
Vegfb	Vascular endothelial growth factor B	1.46	0.0383	1.88	0.1159	2.14	0.0273	1.57	0.2147

Figure 35: Differentially expressed gene 'hit list'. For each genotype the left-hand coloum represents the mRNA fold change and the right-hand column represents the P-value. Gene (symbol) column colour key - orange: upregulated in all genotypes, red: upregulated in three genotypes, olive: upregulated in two genotypes, green: single genotype differential expression. Fold change column colour key – blue font: <0.33, red font: >2. P-value column colour key – red font: P<0.05. Genotype fold change and P-value dual column colour key – highlighted blue box: dual-significant downregulation, highlighted orange box: dual-significant upregulation.

Previous work has shown that conditional knockout of TSGs *in vivo* results in the development of brain tumours whose phenotype is strongly influenced by genotype (Jacques et al., 2010). For example, the conditional *in vivo* knockout of Rb and p53 resulted in the development of intrinsic tumours which phenotypically resembled human

primitive neuroectodermal-like tumours (PNETs), whereas the knockout of PTEN and p53 resulted in the development of gliomas. For this reason, the mRNA expression profiles of these two genotypes were compared. In *in vitro* cultures, the only significantly differentially expressed gene between those two genotypes was Mmp9 (matrix metalloproteinase 9: 2.86-fold significant up-regulation in $PTEN^{-/-}$; $p53^{-/-}$ vs. 1.57-fold non-significant upregulation $Rb^{-/-}$; $p53^{-/-}$), which was relatively overexpressed in the $PTEN^{-/-}$; $p53^{-/-}$ glioma-generating genotype. This was interesting as Mmp-9 has been shown to play a major role in the migration and invasion of tumour cells, with elevated Mmp-9 levels being associated with the enhanced progression of glioma in humans (Lakka et al., 2002). In addition, downregulation of Mmp-9 has been shown to inhibit the adhesion, migration and invasive potential of human glioma xenografts in nude mice. It is thought that this is achieved by downregulating integrins and associated signaling molecules (Veeravalli et al., 2010). These findings highlight Mmp-9 expression as a potential correlate of glioma invasiveness (Figure 35).

Other genes that were differentially expressed between the genotypes were S100a4 (S100 calcium binding protein A4) with 17.85-fold upregulation in $Rb^{-/-}$; $PTEN^{-/-}$ vs. non-significant upregulation in all other genotypes) and Timp1 (tissue inhibitor of metalloproteinase 1 with 42.36-fold significant upregulation in $Rb^{-/-}$; $PTEN^{-/-}$ & 4.24-fold significant upregulation in $Rb^{-/-}$; $p53^{-/-}$; $PTEN^{-/-}$ vs. non-significant upregulation in $Rb^{-/-}$; $p53^{-/-}$ and $PTEN^{-/-}$; $p53^{-/-}$). These were interesting because they were up/downregulated to a particularly large extent in the $Rb^{-/-}$; $PTEN^{-/-}$ glioblastoma-generating genotype. In the case of S100a4, it is known that increased expression in rat C6 glioma cells correlates with the progression of low-grade astrocytic tumours to high-grade glioblastomas, as well as increased migration throughout white matter in humans (Takenaga et al., 2007). This finding has also been verified in xenografted human glioblastoma cell lines and primary human glioma tissues, in addition to which S100a4-expressing tumour cells were found to possess enhanced tumour-initiating capacity, self-renewal, and multipotency (Harris et al., 2008). Taken in combination with our findings, these data suggest S100a4 to be a potential marker of GICs. Timp1 is thought to be involved in tumour invasion, proliferation, and apoptosis across a range of different cancers. And it has been shown that a low Timp1 expression predicts longer overall survival in glioblastoma, but not grade II or III astrocytoma patients (Aaberg-Jessen et al., 2008; Aaberg-Jessen et al., 2009). The decreased survival associated with increased Timp1 expression could be as a result of its anti-apoptotic effects preventing

chemo/radiotherapy-induced apoptosis. Timp1 may, therefore, represent a potential therapeutic target in the treatment of glioblastoma (Figure 35).

Genes that were found to be consistently, overexpressed in all of our tumourigenic NSC genotypes were Cdkn2a (cyclin-dependent kinase inhibitor 2A: 3.52-11.59-fold significant upregulation across all genotypes), Met (Met proto-oncogene: upregulated across all genotypes with a 16.12-fold significant upregulation in $Rb^{-/-}$; $PTEN^{-/-}$), and Twist1 (Twist gene homolog1: 2.12-9.52-fold significant upregulation across all genotypes except $Rb^{-/-}$; $PTEN^{-/-}$). It has long been known that the Cdkn2a gene is lost or deleted in a wide variety of human tumours, including glioblastoma (Moulton et al., 1995; Nobori et al., 1994). However, we observed an overexpression of Ckn2a in our model but propose that this is due to an overcompensation following the intrinsic loss of Rb, p53, and/or PTEN. Hence the $Rb^{-/-}$; $p53^{-/-}$; $PTEN^{-/-}$ NSC genotype demonstrated the largest overexpression. Met expression is strongly increased in glioblastomas, in which it is believed to promote tumour proliferation, migration, invasion, and angiogenesis. And based on this belief it has been shown that the *in vivo* growth of glioblastoma xenografts in nude mice is inhibited by intratumoural treatment with an anti-c-Met antibody (Martens et al., 2006). Considering that we found Met expression to be most significantly upregulated in the $Rb^{-/-}$; $PTEN^{-/-}$ glioblastoma-generating genotype, we can be confident in our suggestion of Met as a therapeutic target in the treatment of glioblastoma. Twist1 has been shown to significantly increase the *in vivo* invasion of human glioblastoma cells following orthotopic xenotransplantation in nude mice. Inhibiting Twist1 has also been shown to decrease the invasion and growth of human glioblastoma cells *in vitro* (Mikheeva et al., 2010). Although Twist1 was not seen to be overexpressed in our $Rb^{-/-}$; $PTEN^{-/-}$ glioblastoma-generating genotype, we propose that its consistent overexpression across the other genotypes is suggestive of a role in general tumour progression and cell migration (Figure 35).

One anomaly can be seen in the downregulated expression of Vegfa (vascular endothelial growth factor A) in the $Rb^{-/-}$; $PTEN^{-/-}$ glioblastoma-generating genotype. Vegfa is overexpressed in grade IV glioblastomas, particularly in areas surrounding necrosis (Johansson et al., 2002). However, the expression of the angiogenesis factor Vegfa is strongly correlated with the hypoxic conditions of *in vivo* environment. As such we believe that the relatively non-hypoxic conditions of *in vitro* cell culture effectively drive the downregulation of Vegfa (Figure 35).

Other genes found to be differentially expressed (to lesser degrees) between the different genotypes were Casp8, E2f1, Tnfrsf10b (most likely to be as a direct result of p53 loss), and Vegfb (Figure 35).

3.4 Conclusion

In this chapter we demonstrated that i.c.v. administration of Adenovirus-Cre targets self-renewing and multipotent SVZ NSCs that become enriched in neurosphere cultures over serial passages. This verified that the *in vitro* model system is an effective surrogate of the *in vivo* model system and allowed us to characterise the effect of Rb, p53, and PTEN loss on the growth rate, self-renewal, multipotency and biomarker expression of NSCs *in vitro*. The combination and number of TSGs lost was seen to determine the growth rates of NSCs *in vitro*, with an additive effect of additional TSG loss on increased growth rate. *In vitro* recombined NSCs also possessed increased self-renewal in a genotype-dependent manner, in addition to possessing altered expression levels of GFAP, Sox-2, and nestin. We also identified that the *in vitro* growth rate, but not the *in vitro* self-renewal ability, of NSCs is a positive predictive indicator of *in vivo* tumour hit rate and an inverse predictive indicator of *in vivo* tumour latency. Finally, Mmp-9, S100a4, and Timp1 were identified as differentially expressed cancer genes between the NSC genotypes and hypothetical surrogate markers of tumour phenotype.

We hypothesise that the different NSC genotypes possessed functional differences in growth rate, NS-forming ability, self-renewal, and differentiation expression profiles *in vitro* because they are composed of different NSC sub-populations with different functional properties. Cancer stem cells are dependent on their microenvironment (Calabrese et al., 2007) and we therefore hypothesise that the NSC sub-populations of the different genotypes exist in different states dependent on their *in vitro* or *in vivo* microenvironment. In the next chapter we aim to address this hypothesis and also examine a) whether these NSC states can be manipulated by switching between microenvironments and b) whether these states influence their *in vivo* tumour hit rate, latency, or phenotype.

3.5 Future Work

Expansion of the sample numbers and/or number of genes tested across all of the functional assays would allow for a more robust analysis and the potential identification of additional *in vitro* predictive indicators of *in vivo* behaviour. In addition, the functional assay portfolio would benefit from the inclusion of multipotency profiles for the NSC genotypes. By studying the differentiation expression profiles of additional biomarkers (e.g. Sox-9, NeuN, Olig2 and an optimised CD133) we may elucidate further *in vitro* predictive indicators of *in vivo* behaviour. However, the methodological rigour of the differentiation analysis by immunofluorescence should be strengthened through the inclusion of positive and negative controls. The mRNA / cDNA expression analysis, although successful in identifying differentially expressed genes, would benefit from validation at the protein level by Western blot.

Rather than correlating the functional properties of *in vitro* recombined NSCs directly to their behaviour *in vivo*, it would be interesting to observe the behaviour of the NSCs when grown in 3-D matrices as this may act as a better system for modelling *in vivo* behaviour without the need for lengthy *in vivo* studies.

4 Characterisation of the Brain Tumour Initiating Cell

4.1 Introduction

This chapter is separated into three parts, the first of which is covered by sections 4.3.1, 4.3.2, and 4.3.3 in which we aim to confirm that the tumours generated by i.c.v. Adenovirus-Cre administration (section 1.7.2) were derived from SVZ NSCs and/or their immediate progeny. We aim to address this by deriving neurosphere cultures from the SVZs of $Rb^{Lox/Lox}$; $p53^{Lox/Lox}$, $PTEN^{Lox/Lox}$; $p53^{Lox/Lox}$, $Rb^{Lox/Lox}$; $PTEN^{Lox/Lox}$, and $Rb^{Lox/Lox}$; $p53^{Lox/Lox}$; $PTEN^{Lox/Lox}$ mice and inducing recombination *in vitro* before engrafting these neurospheres into the brains of recipient mice to compare the tumour hit rate, latency, and phenotype profiles against those observed following i.c.v. Adenovirus-Cre administration. We also cultured and re-grafted 'tumourspheres' (TS) derived from a glioma generated by intracerebrally engrafted $Rb^{-/-}$; $p53^{-/-}$ NS to examine whether the brain tumour initiating cell (BTIC) phenotype is maintained and refined through serial passages.

Secondly, in section 4.3.4 we aim to address whether BTIC status can be refined to a specific SVZ NSC sub-type. We have previously demonstrated that i.c.v. Adenovirus-CMV-Cre-mediated recombination of TSGs in cells of the SVZ NSC compartment results in the development of malignant brain tumours. However, the variability in tumour hit rate and phenotype suggests that we may not be exclusively targeting the BTIC population for recombination; plausible considering the widespread expression of the CMV promoter. Methods by which Cre-mediated recombination can be targeted within specific cell types or anatomical locations are commonly available. Nestin-Cre transgenic mouse lines were developed to study the effect of gene loss in nestin-expressing stem cells during development whilst bypassing embryonic lethality (Betz et al., 1996). Using the same approach, cell-specific mutations have been achieved in Purkinje cells of the cerebellum and in the mid-hindbrain cerebellar region during development by expressing Cre-recombinase under the control of the L7 and Engrailed2 promoters respectively (Barski et al., 2000; Song and Joyner, 2000). Here we use i.c.v. Adenovirus-GFAP-Cre administration to more specifically target the GFAP-expressing type B astrocytes of the SVZ (Garcia-Verdugo et al., 1998) for recombination. Using this approach we aim to address the relative contribution of the type B astrocytes to tumourigenesis.

Finally, in sections 4.3.5, 4.3.6, and 4.3.7 we aim to address whether the environment (*in vivo* versus *in vitro*) of the SVZ NSCs at the time of recombination has an influence on the tumour hit rate, latency, and/or phenotype profile for each of the different genotypes. The rationale being that in section 4.3.2 we highlight that some genotypes of *in vitro* recombined and intracerebrally engrafted NS do not recapitulate the tumour phenotypes seen following *in vivo* recombination of the same TSGs by i.c.v. Adenovirus-Cre administration. For example, *in vivo* recombination of Rb and p53 in $Rb^{Lox/Lox}$; $p53^{Lox/Lox}$ mice resulted in the development of brain tumours, whereas *in vitro* recombined and engrafted $Rb^{-/-}$; $p53^{-/-}$ NSCs did not generate tumours. The converse was observed with the $Rb^{Lox/Lox}$; $PTEN^{Lox/Lox}$ genotype. We propose that such discrepancies could be because a) *in vivo* Adenovirus-Cre targets a cell population that is not present *in vitro*, and vice versa, or b) the act of deriving *in vivo* NSCs and putting them in culture alters the phenotype of the cells. In order to address these hypotheses, we will recombine NSCs *in vivo* by i.c.v. Adenovirus-Cre administration and then derive and expanded them *in vitro* at 2 weeks (early), 2 months (middle), or >3.5 months (late) post-recombination. These NSCs will then be characterised *in vitro* and intracerebrally engrafted back into the brains of recipient mice to observe whether the hit rates, latencies, and phenotypes of the resulting brain tumours more closely resemble those generated by *in vivo* recombination or *in vitro* recombined and engrafted NS. Using this approach we aim to further characterise the *in vivo* tumourigenic transformation process and refine our knowledge of the BTIC.

Aims

1. Verify that brain tumour development following i.c.v. Adenovirus-Cre administration is initiated and driven by SVZ NSCs.
2. Examine whether NSCs exist in the brain tumour bulk as brain tumour initiating cells (BTICs).
3. Refine the BTIC to a more specific sub-type of SVZ NSC.
4. Identify whether NSCs exist in different states dependent on their environment and whether these have altered tumour hit rates, latencies, and phenotype propensities.
5. Functionally characterise these different states *in vitro*.

4.2 Materials and Methods

Refer to the main materials and methods section (Chapter Two).

4.3 Results and Discussion

4.3.1 Inactivation of tumour suppressor genes in subventricular zone cells causes them to proliferate and migrate into the brain parenchyma where they generate tumours

A cohort of five $Rb^{Lox/Lox}$; $p53^{Lox/Lox}$; $PTEN^{Lox/Lox}$ mice received i.c.v. Adenovirus-Cre and were culled after 60 days (mean tumour latency: 101 days) with the aim of observing a developing tumour prior to clinical manifestation.

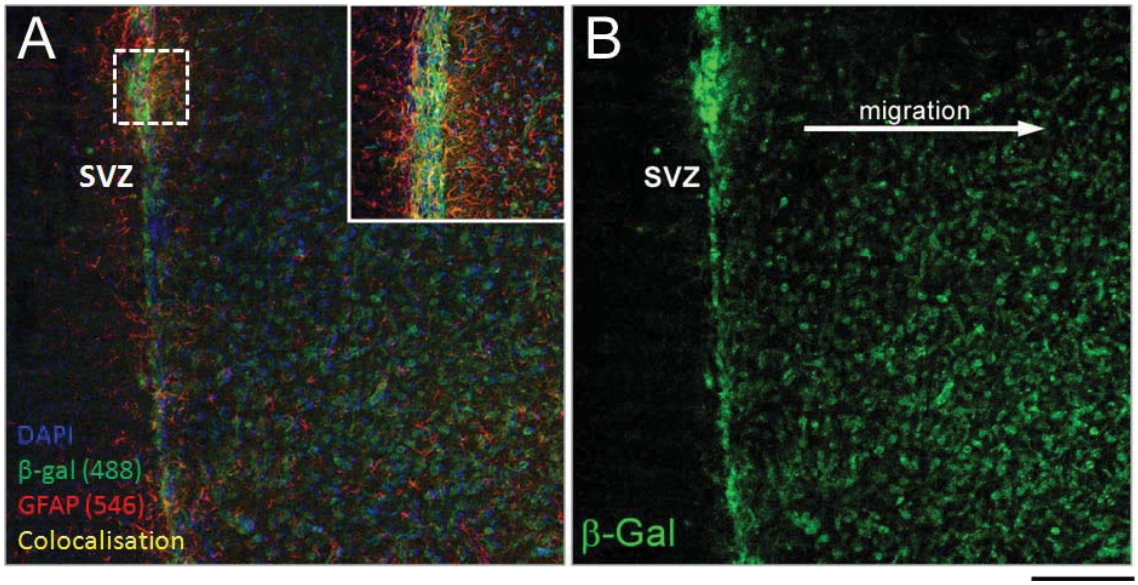

Figure 36: SVZ cells targeted for inactivation of the TSGs Rb, p53 and PTEN proliferate and migrate away from the SVZ into the brain parenchyma where they generate tumours.
Representative images of a $Rb^{Lox/Lox}$; $p53^{Lox/Lox}$; $PTEN^{Lox/Lox}$ mouse 60 days post-i.c.v. Adenovirus-Cre administration immunofluorescently stained for β-galactosidase and GFAP with a Hoechst 33342 (DAPI) counterstain (A,B). Blue: excitation at 405nm, green: excitation at 488nm, red: excitation at 546nm. Images were taken using a 10x (inset: 20x) objective on a Zeiss LSM510 META confocal laser scanning microscope with the LSM software. Scale bar: 100µm (main images) or 50µm (inset).

After 60 days a large number of β-galactosidase-positive recombined cells, including the GFAP-expressing type B astrocytes, could be seen in the SVZ (Figure 36: A, inset). These recombined cells were proliferating and migrating laterally away from the SVZ into the brain parenchyma where we would expect them to generate a PNET tumour after a mean latency of 101 days. This highlights that the highly proliferative cells responsible for forming the bulk of brain tumours can originate from the SVZ.

4.3.2 *In vitro* recombined and intracerebrally engrafted neurospheres derived from the subventricular zone neural stem cell compartment recapitulate the tumour phenotype observed following intracerebroventricular Adenovirus-Cre administration

Neurosphere cultures derived from the SVZs of adult mice contain self-renewing and multipotent NSCs (sections 3.3.1 and 3.3.2). To confirm that the intrinsic primary brain tumours generated by i.c.v. Adenovirus-Cre administration were derived from SVZ NSCs we generated neurosphere cultures from the brains of $Rb^{Lox/Lox}$; $p53^{Lox/Lox}$, $PTEN^{Lox/Lox}$; $p53^{Lox/Lox}$, $Rb^{Lox/Lox}$; $PTEN^{Lox/Lox}$, and $Rb^{Lox/Lox}$; $p53^{Lox/Lox}$; $PTEN^{Lox/Lox}$ mice and induced recombination *in vitro* after 15-30 days (passage 1) by infecting them with Adenovirus-Cre. 100% recombination (measured by β-galactosidase staining) of the NS was achieved across all of the genotypes. These *in vitro* recombined NSCs (growing as neurospheres) demonstrated a genotype-dependent increase in growth rate and self-renewal (sections 3.3.3 and 3.3.4). After an additional 2-4 passages (10-40 days) in culture, these NS were engrafted into the striata of a total of 113 non-recombined LoxP mutant mice of matched genetic backgrounds in 14 separate experiments. The viability of the NS was confirmed by examining their cellular morphology (haematoxylin and eosin staining: data not shown) using the cytoblock procedure for paraffin immunohistochemistry (**Error! Reference source not found.**).

Experiment	Cell Recombination Paradigm	Vol. Injected (ul)	Passage #	Genotype (cells)	# Mice	Age (start)	Age (end)	Incubation time (d)	CoD	Diagnosis
07/05/2009	*In vitro* recombined (Adeno-Cre)	15	5	Rb / PTEN / Rosa	6					
						50	246	**196**	sick	no tumour
						50	246	**196**	sick	no tumour
						75	294	**219**	experiment terminated	no tumour
						75	294	**219**	experiment terminated	no tumour
						75	294	**219**	experiment terminated	no tumour
07/05/2009	*In vitro* recombined (Adeno-Cre) 2d post-passage	10 or 30	6	Rb / p53 / Rosa	4					
						98	349	**251**	f/d	-
						98	352	**254**	experiment terminated	no tumour
						98	352	**254**	experiment terminated	no tumour
						98	352	**254**	experiment terminated	no tumour
07/05/2009	*In vitro* recombined (Adeno-Cre)	15	5	Rb / p53 / Rosa	9					
						62	281	**219**	experiment terminated	no tumour
						62	281	**219**	experiment terminated	no tumour
						62	281	**219**	experiment terminated	no tumour
						62	281	**219**	experiment terminated	-
						62	366	**304**	experiment terminated	no tumour
						62	366	**304**	experiment terminated	no tumour
						62	366	**304**	experiment terminated	no tumour
						62	366	**304**	experiment terminated	no tumour
						62	366	**304**	experiment terminated	no tumour
11/08/2008	*In vitro* recombined (Adeno-Cre) Single NSCs	10	5	Rb / p53 / PTEN / Rosa	12					
						79	80	**1**	f/d	no tumour
						79	81	**2**	f/d	no tumour
						79	82	**3**	f/d	-
						78	135	**57**	sick, 24.4g	Oligoastrocytoma
						78	156	**78**	sick, 16.1g	Oligoastrocytoma
						78	164	**86**	sick, 33g	Oligoastrocytoma
						78	204	**126**	sick, ataxic	PNET
						52	189	**137**	sick	PNET + Glioma
						52	200	**148**	sick, 21.1g	PNET + Glioma (giant cells)
						52	207	**155**	sick, ataxic, brain tumour (snap frozen)	PNET (giant cells)
						79	241	**162**	sick, 24g, thin, 2hrs BrdU	no tumour (epidermoid cyst)
						79	287	**208**	f/d	-
09/05/2008	*In vitro* recombined (Adeno-Cre)	12.5	4	Rb / p53 / Rosa	12					
						67	85	**18**	time-cull	Viable graft with scar
						56	74	**18**	time-cull	Viable graft with scar
						56	231	**175**	18.4g, ataxic	PNET (CB)
						59	283	**224**	f/d	-
						67	321	**254**	16g, ataxic	PNET (CB)
						67	343	**276**	sick, ataxic, 2hrs BrdU	PNET (4th ventricle)
						67	353	**286**	35.6g	o tumour (mature neural tissue protrusion in 3rd ventricl
						59	345	**286**	30.5g	no tumour
						59	345	**286**	32.5g	no tumour
						56	342	**286**	27.3g	no tumour
						54	340	**286**	34.3g	no tumour
						54	340	**286**	35.2g	no tumour

29/04/2008	*In vitro* recombined (Adeno-Cre)	8-25	3	Rb / p53 / PTEN / Rosa	6					
						48	99d	**51**	sick, thin, 18.7g	Glioma
						48	99d	**51**	sick, thin, 17.3g	PNET + Glioma
						48	100d	**52**	sick, thin, 18.3g	PNET + Glioma
						48	126d	**78**	-	-
						48	157d	**109**	sick, dome-shaped head, brain tumour, bit snapped froz	Oligodendroglioma
						48	167d	**119**	time-culled for MRI	PNET + Glioma
18/12/2007	*In vitro* recombined (Adeno-Cre)	5-10	3	PTEN / p53 / Rosa	6					
						88	221d	**133**	Sick, brain tumour, bit snap frozen	(Oligo)astrocytoma
						88	240d	**152**	Sick, hydrocephalus	(Oligo)astrocytoma
						88	250d	**162**	Sick	(Oligo)astrocytoma
						88	267d	**179**	Sick, brain tumour, bit snap frozen	(Oligo)astrocytoma
						88	284d	**196**	Sick	(Oligo)astrocytoma
						88	421d	**333**	Sick, tumour snap frozen, sample taken for NS culture,	(Oligo)astrocytoma
29/10/2007	*In vitro* recombined (Adeno-Cre)	5	4	Rb / PTEN / Rosa	15					
						88d	96d	**8**	time-cull, 29.6g	high mitotic activity of graft, activated SVZ
						39d	47d	**8**	time-cull, 19.4g	intraventricular graft
						39d	89d	**50**	sick, massive brain tumour, bit snap frozen, 16.2g	undifferentiated GBM (giant cells)
						39d	-	<75	missing 14.1.08, no sample	-
						39d	114d	**75**	sick, dome shaped head, hydrocephalus, 15.3g	GBM
						88d	165d	**77**	sick, brain tumour, bit snap frozen, 28.8g	GBM (palisading necrosis + vascular proliferation) photo
						88d	174d	**86**	sick, brain tumour, bit snap frozen, 19.3g	GBM (palisading necrosis + vascular proliferation) photo
						88d	180d	**92**	sick, brain tumour, bit snap frozen, 23g	Glioma
						88d	180d	**92**	sick, brain tumour, bit snap frozen, 30g	Glioma
						39d	134d	**95**	sick, brain tumour, culled by Francis, 15g	GBM (giant cells + palisading necrosis)
						39d	155d	**116**	sick, brain tumour, bit snap frozen, 16.4g	GBM + Oligoastrocytoma (photo)
						88d	226d	**138**	sick, hydrocephalus, 18.2g	GBM (giant cells)
						88d	242d	**154**	sick, brain tumour, photo taken, bit snap frozen, 16.8g	GBM (giant cells)
						88d	268d	**180**	sick, brain tumour, bit snap frozen, 15.2g	GBM (palisading necrosis)
						88d	329d	**241**	19.9g, brain tumour bit snap frozen	GBM (palisading necrosis + vascular proliferation) photo
04/05/2007	*In vitro* recombined (Adeno-Cre)	5 (2x10)	4	Rb / p53 / Rosa	10					
						32d	283d	**251**	time-cull, 21.9g	4x levels, no tumour
						37d	381d	**344**	culled, 25.3g, circling	no tumour
						37d	381d	**344**	culled, 29.5g	no tumour
						37d	381d	**344**	culled, 33g	no tumour
						37d	381d	**344**	culled, 36.4g	no tumour
						37d	381d	**344**	culled, 32.6g	no tumour
						32d	381d	**344**	culled, 28.1g	no tumour
						32d	381d	**344**	culled, 24.3g	no tumour
						32d	381d	**344**	culled, 23.8g	no tumour
						32d	381d	**344**	culled, 26.7g	no tumour
18/04/2007	*In vitro* recombined (Adeno-Cre)	5	2	Rb / p53 / Rosa	10					
						73d	289d	**216**	sick, culled by Francis, spleen-, brain tumour!	PNET + Glioma
						35d	302d	**267**	time-cull, 39.2g	no tumour, injection side
						73d	433d	**360**	culled, 39.2g	no tumour
						73d	433d	**360**	culled, 42.6g	no tumour
						73d	433d	**360**	culled, 35.6g	no tumour
						73d	433d	**360**	culled, 48.7g	no tumour
						62d	422d	**360**	culled, 34g	no tumour
						73d	433d	**360**	culled, 42.8g	no tumour
						73d	433d	**360**	culled, 33.3g	no tumour
						73d	433d	**360**	culled, 38.5g	no tumour

03/08/2006	*In vitro* recombined (Adeno-Cre)	10 (2x5)	3	PTEN / p53 / Rosa	13						
#						62d	122d	**60**	f/d, no sample taken	-
						77d	158d	**81**	f/d	small cluster in ventricle
						62d	190d	**128**	sick, brain tumour, 30g	Glioma
						62d	197d	**135**	sick, brain tumour, 23g	PNET
						62d	197d	**135**	sick, brain tumour, 26g, photo taken	Glioma
						62d	197d	**135**	sick, brain tumour, 22g, photo taken	Glioma
						62d	197d	**135**	sick, brain tumour, photo taken	Glioma
						77d	219d	**142**	f/d, no sample taken	-
						62d	222d	**160**	sick, brain tumour, 31g	Glioma
						62d	295d	**233**	sick, culled by animal technicians, 33g	no tumour
						77d	358d	**281**	sick, culled by animal technicians, 24.9g	no tumour
						62d	371d	**309**	culled, 36.4g	no tumour
						62d	371d	**309**	culled, 37.1g	no tumour
25/03/2006	*In vitro* recombined (Adeno-Cre)	5	3	PTEN / p53 / Rosa	13						
#						61d	98d	**37**	time cull	no tumour
						58d	146d	**88**	time cull	graft
						58d	146d	**88**	time cull	no tumour
						61d	149d	**88**	time cull	graft
						58d	146d	**88**	time cull	graft
						58d	146d	**88**	time cull	Glioma
						58d	146d	**88**	time cull	graft
						58d	146d	**88**	time cull	Glioma
						61d	149d	**88**	time cull	no tumour
						61d	149d	**88**	time cull	graft
						61d	149d	**88**	time cull	Glioma
						61d	149d	**88**	time cull	no tumour
						61d	149d	**88**	time cull	no tumour
17/03/2006	*In vitro* recombined (Adeno-Cre)	5	3	Rb / p53 / PTEN / Rosa	12						
#						44d	89d	**45**	time cull	PNET + Glioma
						44d	92d	**48**	sick, no obvious tumour	PNET
						44d	110d	**66**	sick, brain tumour, bit snap frozen, 21g	PNET (giant cells)
						44d	110d	**66**	sick, brain tumour, bit snap frozen, 21.9g	PNET + Glioma
						44d	117d	**73**	sick, brain tumour	PNET + Glioma
						44d	119d	**75**	sick	PNET + Glioma
						44d	130d	**86**	sick, brain tumour, 21g	PNET + Glioma
						44d	130d	**86**	sick, brain tumour, 17.8g	PNET
						44d	132d	**88**	sick, brain tumour, bit snap frozen, 20g	PNET
						44d	132d	**88**	sick, brain tumour, bit snap frozen, 22g	PNET + Glioma
						44d	132d	**88**	sick, brain tumour, bit snap frozen, 30g	PNET + Glioma
						44d	136d	**92**	sick, brain tumour, died during BrdU incubation, 30.8g	PNET + Glioma
24/02/2006	*In vitro* recombined (Adeno-Cre)	10	3	Rb / p53 / Rosa	13						
#						100d	146d	**46**	culled	no tumour
						100d	203d	**103**	culled	no tumour
						86d	200d	**114**	f/d, no sample taken	-
						104d	268d	**164**	sick, slimy tumour grew in front, on top of brain, 32g	PNET
						97d	316d	**219**	culled sick, no obvious tumour, big spleen, 29g	no tumour
						104d	391d	**287**	culled	no tumour
						104d	391d	**287**	culled	no tumour
						104d	391d	**287**	culled	no tumour
						97d	384d	**287**	culled	no tumour
						97d	384d	**287**	culled	no tumour
						97d	384d	**287**	culled	no tumour
						86d	373d	**287**	culled	no tumour
						86d	373d	**287**	culled	no tumour

Figure 37: Summary table of the experimental details of all the mice that received intracerebral injections of *in vitro* recombined NS (#: experiment analysed, but not performed, by the reporter).

9.6% of *in vitro* recombined $Rb^{-/-}$; $p53^{-/-}$ NS (n=52; 4x PNET, 1x PNET + glioma), 79.0% of $PTEN^{-/-}$; $p53^{-/-}$ NS (n=19; 8x glioma, 6x oligoastrocytoma, 1xPNET), 70.6% of $Rb^{-/-}$; $PTEN^{-/-}$ NS (n=17; 11x glioblastoma, 1x glioblastoma + oligoastrocytoma), and 96.0% of $Rb^{-/-}$; $p53^{-/-}$; $PTEN^{-/-}$ NS (n=25; 13x PNET + glioma, 6x PNET, 3x oligoastrocytoma, 1x glioma, 1x oligodendroglioma) generated intrinsic brain tumours following intracerebral engraftment (Figure 38).

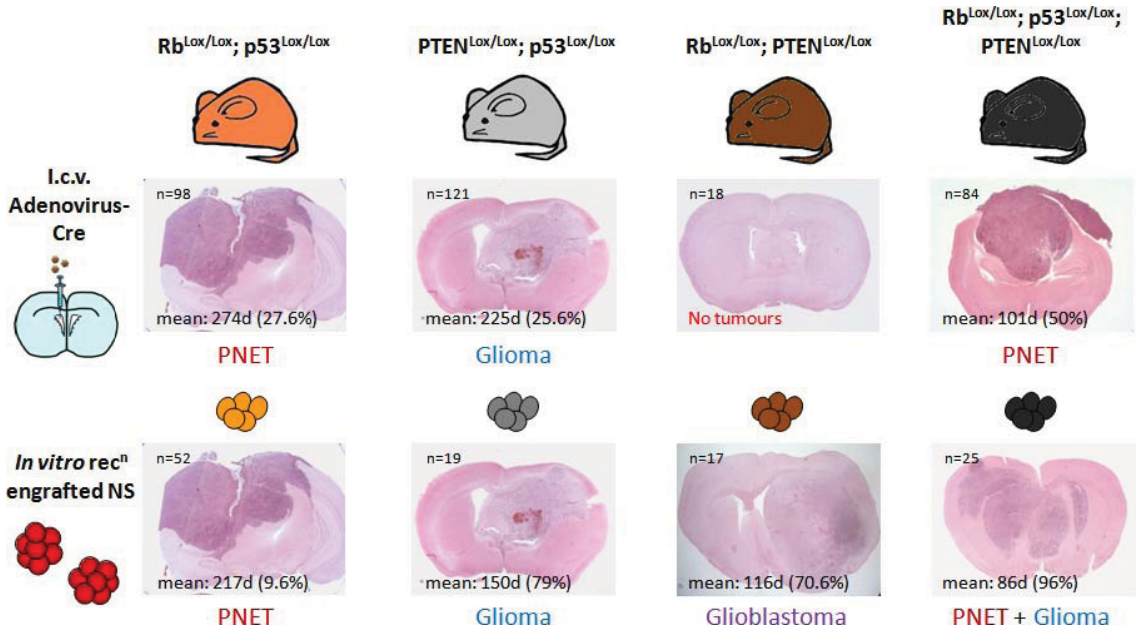

Figure 38: Summary of the experimental results (including 'n' number, mean tumour latency, hit rate, and predominant tumour phenotype) from the i.c.v. administration of Adenovirus-Cre in $Rb^{Lox/Lox}$; $p53^{Lox/Lox}$, $PTEN^{Lox/Lox}$; $p53^{Lox/Lox}$, $Rb^{Lox/Lox}$; $PTEN^{Lox/Lox}$, and $Rb^{Lox/Lox}$; $p53^{Lox/Lox}$; $PTEN^{Lox/Lox}$ mice and the intracerebral engraftment of *in vitro* recombined NS derived from the same mice.

The tumour latencies following *in vitro* recombined NS engraftment were shorter than the respective i.c.v. Adenovirus-Cre-induced tumour latencies across all of the genotypes. The *in vitro* recombined NS spend 10-40 days in culture before being engrafted, this time may therefore account for the observed reduction in latency. This suggests that the *in vivo* tumourigenic process that takes place prior to clinical tumour manifestation (e.g. acquisition of further mutations) is not delayed by *in vitro* culturing. The tumour latency of the $PTEN^{-/-}$; $p53^{-/-}$, $Rb^{-/-}$; $PTEN^{-/-}$, and $Rb^{-/-}$; $p53^{-/-}$; $PTEN^{-/-}$ NS were significantly shorter than the $Rb^{-/-}$; $p53^{-/-}$ NS. As with the i.c.v. Adenovirus-Cre-induced tumours, the $Rb^{-/-}$; $p53^{-/-}$; $PTEN^{-/-}$ genotype generated tumours in the shortest

time, which was also significantly less than that of the PTEN$^{-/-}$; p53$^{-/-}$ NS-induced tumour latency (Figure 39).

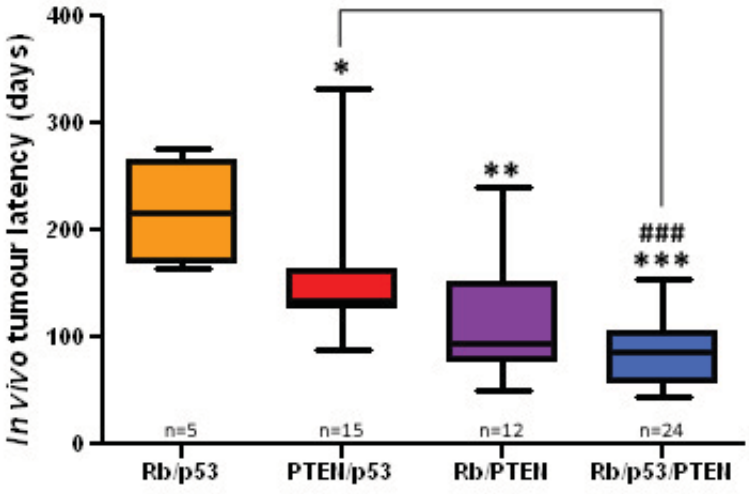

Figure 39: The genotype of the *in vitro* recombined NS determines the latency of tumour formation. Box and whiskers plot showing the mean tumour formation latency +/- 95% confidence intervals with min and max data points. *: P<0.05 vs. Rb$^{-/-}$; p53$^{-/-}$ NS, **: P<0.005 vs. Rb$^{-/-}$; p53$^{-/-}$ NS, ***: P<0.001 vs. Rb$^{-/-}$; p53$^{-/-}$ NS, ###: P<0.001 vs. illustrated comparison (one-way ANOVA with Bonferroni's multiple comparison correction).

As demonstrated by Figure 38, the tumours generated from the engraftment of *in vitro* recombined NS generally appeared to be phenocopies of those tumours generated by i.c.v. Adenovirus-Cre administration (Figure 40).

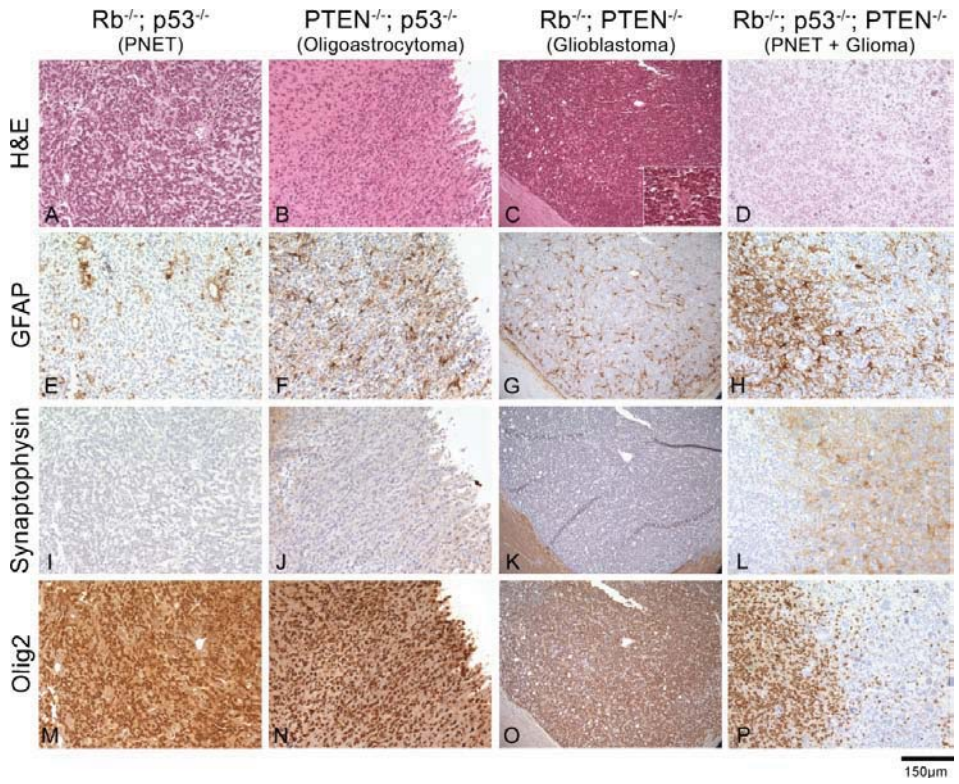

Figure 40: The phenotype of intrinsic brain tumours generated following intracerebral engraftment of *in vitro* recombined neurospheres is dependent on the combination of TSGs inactivated. Representative images taken from tumours generated following intracerebral (in the striatum) engraftment of *in vitro* recombined $Rb^{-/-}$; $p53^{-/-}$ (A,E,I,M), $PTEN^{-/-}$; $p53^{-/-}$ (B,F,J,N), $Rb^{-/-}$; $PTEN^{-/-}$ (C,G,K,O), and $Rb^{-/-}$; $p53^{-/-}$; $PTEN^{-/-}$ (D,H,L,P) NS. The tumours were stained for haematoxylin and eosin (A-D), GFAP (E-H), synaptophysin (I-L), and Olig2 (M-P) to assist in the classification of their phenotype. In the case of the $Rb^{-/-}$; $p53^{-/-}$ NS tumour (A,E,I,M), the well-demarcated morphological appearance of the tumour was suggestive of PNET but the expression profile was counter-intuitively found to be GFAP-negative (E), synaptophysin-negative (I), and Olig2-positive (M). The $Rb^{-/-}$; $PTEN^{-/-}$ NS-induced glioblastoma (C,G,K,O) was identified by palisading necrosis and vascular profileration (C, inset). Images were taken using a ColorView III digital camera mounted on a Zeiss Axioskop 2 MOT microscope with a 10x magnification (40x for inset) and using the AnalySIS software package.

The $Rb^{-/-}$; $p53^{-/-}$ NS generated tumours that morphologically resembled human PNETs due to being well-demarcated and containing closely packed, undifferentiated cells that often appeared in rosette formations (Figure 40: A). However, these 'PNETs' were GFAP-negative, synaptophysin-negative, and Olig2-positive (Figure 40: E,I,M). PNETs are usually classified by their GFAP-negative, synaptophysin-positive, and Olig2-negative profile as observed with the PNET component of the $Rb^{-/-}$; $p53^{-/-}$; $PTEN^{-/-}$ NS-induced tumour (Figure 40: H,L,P). Notably, three of the four PNETs generated by the $Rb^{-/-}$; $p53^{-/-}$ NS (of which the representative image is one) grew around the 4^{th} ventricle in the cerebellum. It may therefore be the case that the $Rb^{-/-}$; $p53^{-/-}$ NS were mistakenly delivered to the cerebellum where they were influenced by extrinsic factors to develop into medulloblastoma-like tumours (Hambardzumyan et al., 2008). Although the $PTEN^{-/-}$; $p53^{-/-}$ NS generated more gliomas than oligoastrocytomas, the proportion of oligoastrocytomas had risen from those observed following i.c.v. Adenovirus-Cre administration. These oligoastrocytomas were identified by their monomorphic and diffuse appearance in addition to their GFAP-positivity, synaptophysin-negativity, and their high level of Olig2-positivity (Figure 40: F,J,N) (Ligon et al., 2004). The absence of vascular proliferation and necrosis was indicative of a lower-grade oligoastrocytoma, but their high cellularity suggests that they are anaplastic (Figure 40: B) (Louis et al., 2007). The $Rb^{-/-}$; $PTEN^{-/-}$ NS generated tumours that resembled human glioblastoma, identified by their infiltrative nature and the presence of vascular proliferation (Figure 40: C, inset), giant cells, palisading necrosis, and high cellularity (Louis et al., 2007). In addition, they were found to weakly express both GFAP (Figure 40: G) (Wilhelmsson et al., 0 AD) and Olig2 (Figure 40: O) (Mokhtari et al., 2005), as well as being synaptophysin-negative (Figure 40: K). The predominant phenotype of the tumours resulting from i.c.v. Adenovirus-Cre administration in $Rb^{Lox/Lox}$; $p53^{Lox/Lox}$; $PTEN^{Lox/Lox}$ mice shifted from PNET (39 out of 42) to a PNET + glioma biphasic phenotype (13 out of 24) following engraftment of $Rb^{-/-}$; $p53^{-/-}$; $PTEN^{-/-}$ NS (Figure 40: D). The PNET component of this tumour was identified as previously described and the glioma component was identified by their infiltrative appearance, the patterning of small dense nuclei (Figure 40: D), and their GFAP-positive (Figure 40: H), synaptophysin-negative (Figure 40: L) and Olig2-positive (Figure 40: P) expression profile (Louis et al., 2007). The shift to a bi-phasic tumour phenotype with an increased glial presence suggests that a wider variety of BTIC populations are present in the *in vitro* environment than *in vivo*. However, the general phenocopy trend observed between the *in vitro* recombined and engrafted NS tumours and the i.c.v. Adenovirus-Cre-induced tumours supports the

hypothesis that intrinsic brain tumours are derived from cells of the SVZ stem / progenitor cell compartment (Rietze and Reynolds, 2006) and also suggests that the act of deriving NSCs *in vitro* does not significantly alter their phenotype. Despite this, differences were observed in the $Rb^{-/-}$; $p53^{-/-}$ and $Rb^{-/-}$; $PTEN^{-/-}$ NSC genotypes.

Interestingly, *in vivo* i.c.v. Adenovirus-Cre recombination in $Rb^{Lox/Lox}$; $p53^{Lox/Lox}$ mice resulted in the development of brain tumours in 27.6% of mice, whereas *in vitro* recombined and engrafted $Rb^{-/-}$; $p53^{-/-}$ NSCs generated tumours with a vastly decreased hit rate of 9.6%. This suggests that either a) *in vivo* Adenovirus-Cre could be targeting a cell population that is not present *in vitro*, or that b) the act of deriving *in vivo* NSCs and putting them in culture alters the phenotype of the cells. We hypothesise that the inactivation of Rb and p53 in an SVZ NSC can result in the tumourigenic transformation of the cell, but that this transformation is facilitated by the *in vivo* SVZ microenvironment of the cell. Conversely, whereas i.c.v. administration of Adenovirus-Cre in $Rb^{Lox/Lox}$; $PTEN^{Lox/Lox}$ mice did not result in the development of any intrinsic brain tumours, *in vitro* recombined and engrafted $Rb^{-/-}$; $PTEN^{-/-}$ NS generated tumours with a hit rate of 70.6%. This suggests that only the *in vitro* neurosphere culture environment is permissive to tumourigenesis following inactivation of the TSGs Rb and PTEN.

4.3.3 Tumourspheres derived from brain tumour biopsies recapitulate the original phenotype over serially engraftments

Tumourspheres (TS) were derived from a glioma that was clinically presenting 333 days post-engraftment of *in vitro* recombined $PTEN^{-/-}$; $p53^{-/-}$ NS. The TS were expanded *in vitro* for 10 passages and re-grafted back into the brains of 9 recipient mice (Figure 41).

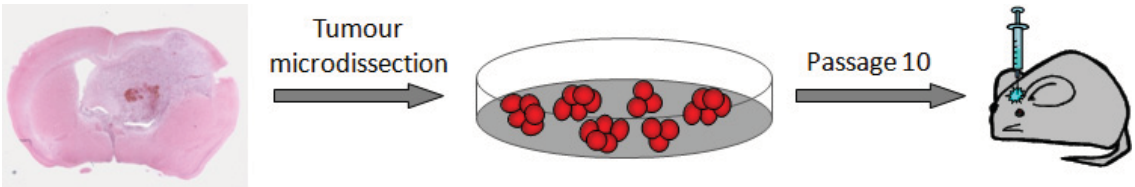

Figure 41: Overview of the experimental procedure used to serially derive and engraft tumourspheres (TS).

The engrafted PTEN$^{-/-}$; p53$^{-/-}$ TS generated intrinsic brain tumours with a 100% hit rate and a mean latency of 91.6 days +/- 5.25; an increase from a hit rate of 79.0% and a significant reduction ($P<0.005$; two-tailed unpaired Student's t-Test) from a mean latency of 149.8 days +/- 15.4 (Figure 42).

Experiment	Cell Recombination Paradigm	Vol. Injected (ul)	Passage #	Genotype (cells)	# Mice	Age (start)	Age (end)	Incubation time (d)	CoD	Diagnosis
24/02/2009	Tumourspheres	10	10	PTEN / p53 / Rosa	9					
	(*in vitro* recombined and engrafted NS)					66	137	**71**	Culled sick , 27.9g, brain tumour snap froze, 2hrs BrdU	Glioma
						66	145	**79**	f/d	Glioma
						66	146	**80**	Found dead after injection with BrdU, brain and gut collected by WFS staff.	Glioma
						66	148	**82**	Culled sick by WFS staff, 2hrs BrdU	Glioma (photo)
						55	144	**89**	culled sick, abdominal lump, brain and gut collected by WFS staff, 3hrs BrdU	Glioma (cystic + necrotic)
						55	148	**93**	Sick, lump on brain, brain and gut collected by WFS staff, 2hrs BrdU	Glioma
						66	166	**100**	Culled sick, 30.3g, hunched, head lump, 2hrs BrdU, brain with tumour sent for	Glioma
						55	170	**115**	Culled sick, 31g, lump on head, brain tumour snap frozen	Glioma
						55	170	**115**	Culled sick, 32g, lump on head, 1hr BrdU	Glioma

Figure 42: Summary table of the experimental details of all the mice that received intracerebral injections of TS derived from a glioma generated by *in vitro* recombined and engrafted PTEN$^{-/-}$; p53$^{-/-}$ NS.

The increased hit rate and reduced latency suggests that the tumour bulk contains a purified, or increased, number of BTICs. In addition, the original glioma phenotype was recapitulated in all 9 of the recipient mice (Figure 43).

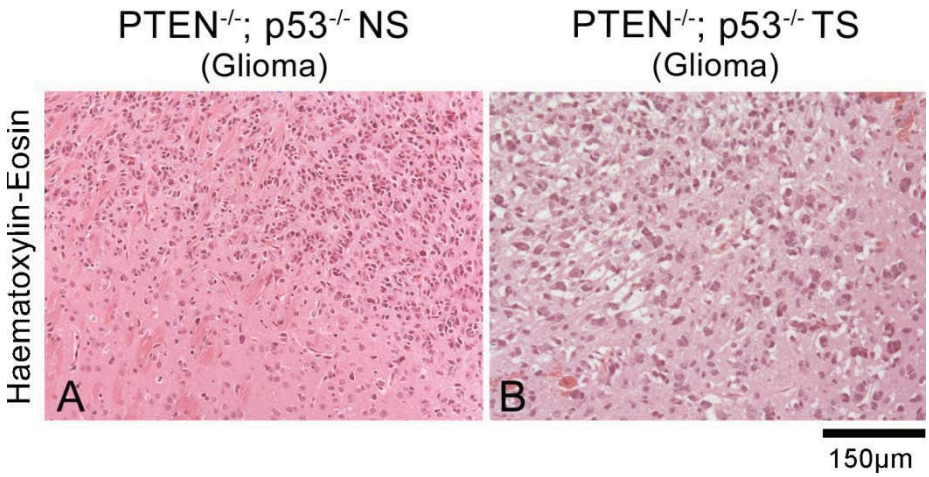

Figure 43: TS derived from a PTEN$^{-/-}$; p53$^{-/-}$ NS-induced glioma recapitulate the phenotype when re-grafted into the brains of recipient mice. Representative images taken from tumours identified as diffusely infiltrating gliomas generated following intracerebral engraftment of *in vitro* recombined PTEN$^{-/-}$; p53$^{-/-}$ NS (A) and PTEN$^{-/-}$; p53$^{-/-}$ TS (B) derived from a PTEN$^{-/-}$; p53$^{-/-}$ NS-induced glioma. Images were taken using a ColorView III digital camera mounted on a Zeiss Axioskop 2 MOT microscope with a 10x magnification and using the AnalySIS software package.

These high-grade gliomas were identified by their diffusely infiltrating cells with a biphasic pattern of small dense and larger vesicular nuclei, and by the presence of micro-vascular proliferation (Louis et al., 2007). These findings suggest that NSC-like TS-forming cells reside within the tumour bulk and are a class of BTIC that it is maintained in a tumourigenic state and committed to the glial phenotypic lineage.

4.3.4 The GFAP-expressing type B astrocytes of the subventricular zone are a class of brain tumour initiating cell

We have previously shown (Chapter One) that i.c.v Adenovirus-CMV-Cre-mediated recombination of the TSGs Rb, p53, and PTEN in cells of the SVZ NSC compartment result in the genotype-dependent development of brain tumours. To assess the relative tumourigenic contribution of the GFAP-expressing type B astrocytes (Doetsch et al., 1999) we delivered i.c.v. Adenovirus-GFAP-Cre (Adenovirus-Cre under the control of

the GFAP promoter) into a total of 91 mice, of all the double and triple TSG LoxP genotypes, in 11 separate experiments (Figure 44).

Experiment	Cell Recombination Paradigm	Vol. Injected (ul)	Genotype (mice)	# Mice	Age (start)	Age (end)	Incubation time (d)	CoD	Diagnosis
03/04/2009	I.c.v. Adenovirus-GFAP-Cre	5	Rb/p53/PTEN/Rosa	11					
					64	96	**32**	Culled too small, lost weight, 9g, 2hrs BrdU	PL
					98	177	**79**	culled sick, 37g, abscess	no tumour
					64	144	**80**	culled sick, ataxic, 17.8g	no tumour (hydrocephalus)
					87	196	**109**	large lump on shoulder	PL
					87	205	**118**	25g, ataxic with hunched posture	Oligoastrocytoma
					98	248	**150**	lump on head, 26.3g, snap frozen brain tumour, collected skull.	Oligoastrocytoma
					64	214	**150**	hunched, 30.6g, snap frozen brain tumour.	PNET
					64	246	**182**	head lump, large liver, skull fragment with brain	PL
					60	250	**190**	hunched, small head lump	-
29/02/2008	I.c.v. Adenovirus-GFAP-Cre	5	PTEN/p53/Rosa	8					
					67d	188d	**120**	32.5g, sick, hydrocephalus	no tumour
					67d	216d	**148**	24g, sick, thin	PL
					67d	256d	**178**	22.2g, sick, thin	PL
					67d	246d	**178**	28.4g, sick	PL
					53d	250d	**168**	24.3g, sick, hydrocephalus	no tumour
					53d	250d	**168**	25.3g, sick, dome-shaped head, possible meningioma, possible gliom	Glioma
					67d	267d	**199**	sick	Glioma
					67d	278d	**210**	sick, 26.4g	no tumour, hydrocephalus
18/12/2007	I.c.v. Adenovirus-GFAP-Cre	5	Rb/p53/Rosa	4					
					59d	417d	**358**	experiment terminated	no tumour
					59d	417d	**358**	experiment terminated	no tumour
					44d	402d	**358**	experiment terminated	no tumour, hydrocephalus
					44d	402d	**358**	experiment terminated	no tumour
18/12/2007	I.c.v. Adenovirus-GFAP-Cre	5	PTEN/p53/Rosa	6					
					101d	102d	**1**	f/d	-
					101d	187d	**86**	sick, hydrocephalus, 32.4g	no tumour, hydrocephalus
					109d	298d	**189**	hydrocephalus, 35.5g	no tumour, hydrocephalus
					101d	307d	**206**	sick, lying on its side, keeps head tilted, 35g	Glioma
					101d	315d	**214**	sick, no obvious tumour, 25g	Glioma
					109d	326d	**217**	sick, hydrocephalus, 35g	Glioma
18/12/2007	I.c.v. Adenovirus-GFAP-Cre	5	Rb/p53/PTEN/Rosa	10					
					94d	95d	**1**	f/d	-
					94d	95d	**1**	f/d	-
					57d	155d	**98**	sick, swollen head, culled by Francis, brain tumour?, 19.6g	PNET + glioma
					94d	200d	**106**	sick (problems moving around, slight swelling on head), 22.8g	Glioma
					94d	225d	**131**	sick, difficulties to move, small tumour in front!, 23.2g	PNET
					94d	225d	**131**	sick, difficulties to move, hydrocephalus, 18.6g	maybe some tumour cells / PL
					63d	202d	**139**	sick, brain tumour, bit snap frozen, 19.2g	PNET
					94d	234d	**140**	sick, small brain tumour, bit snap frozen, 24.3g	PNET
					57d	204d	**147**	sick, 29.4g, small liver, bloated intestines	PNET
					94d	253d	**159**	sick, 29.4g	PL
01/08/2007	I.c.v. Adenovirus-GFAP-Cre	5	Rb/p53/Rosa	12					
					102d	392d	**290**	sick, 25.5g	PNET
					47d	424d	**377**	f/d	-
					113d	610d	**495**	experiment terminated	PL
					113d	610d	**495**	experiment terminated	no tumour
					113d	610d	**495**	experiment terminated	no tumour
					113d	610d	**495**	experiment terminated	no tumour, some infiltrating cells
					113d	610d	**495**	experiment terminated	no tumour
					102d	597d	**495**	experiment terminated	no tumour
					47d	542d	**495**	experiment terminated	no tumour
					47d	542d	**495**	experiment terminated	no tumour
					47d	542d	**495**	experiment terminated	no tumour
					47d	542d	**495**	experiment terminated	no tumour

01/08/2007	I.c.v. Adenovirus-GFAP-Cre	5	Rb/PTEN/Rosa	8					
					57d	187d	**130**	culled sick, Ataxic, no tumour but hydrocephalus, appendecitis, 20.6g	no tumour
					57d	359d	**302**	f/d	-
					57d	367d	**310**	sick, 23.6g, not moving around, no obvious brain tumour, hydrocephal	no tumour
					57d	417d	**360**	sick, lump in throat, 34.6g	PL
					57d	504d	**447**	29.6g, 2hr BrdU, exp terminated	no tumour
					57d	504d	**447**	36.9g, 2hr BrdU, exp terminated	no tumour
					57d	504d	**447**	27.4g, 2hr BrdU, exp terminated	no tumour
					57d	504d	**447**	29.8g, 2hr BrdU, exp terminated	no tumour
18/04/2007	I.c.v. Adenovirus-GFAP-Cre	5	PTEN/p53/Rosa	11					
					63d	99d	**36**	culled sick (no obvious brain tumour)	no tumour
					58d	215d	**157**	sick (doomed head), 32.2g	Glioma
					63d	374d	**311**	time-cull, 49.6g	PL
					63d	374d	**311**	time-cull, 45.2g	PL
					63d	381d	**318**	sick (breathing problems), 21.3g, pale brain, small liver	Glioma
					63d	400d	**337**	sick, calcified brain tumour in front, 27.9g	Osteosarcoma
					58d	415d	**357**	sick, calcified brain tumour, 29.8g	Glioma + osteosarcoma
					63d	423d	**360**	culled, 54.8g	PL
					58d	418d	**360**	culled, 54.6g	no tumour
					58d	418d	**360**	culled, 58.9g	PL
					58d	418d	**360**	culled, 65g	PL
21/02/2007	I.c.v. Adenovirus-GFAP-Cre	5	Rb/PTEN/Rosa	7					
					28d	352d	**324**	time-cull, 42.3g	no tumour
					51d	419d	**368**	time-cull, 39.6g	no tumour
					51d	419d	**368**	time-cull, 33.4g	no tumour
					51d	467d	**416**	culled, 23.5g	no tumour
					51d	467d	**416**	culled, 46g	no tumour
					28d	444d	**416**	culled, 39.6g	no tumour
					28d	444d	**416**	culled,52.3g	no tumour
15/11/2006	I.c.v. Adenovirus-GFAP-Cre	5	Rb/p53/PTEN/Rosa	11					
					56d	221d	**165**	sick, Ataxic, tumour close to cerebellum, 38g	Choroid plexus tumour
					62d	243d	**181**	sick, culled by animal technicians, 25.8g, brain tumuor!	Glioma
					62d	243d	**181**	sick, culled by animal technicians, 27.8g, brain tumuor!	PNET + Glioma
					58d	239d	**207**	sick, tumour in cerebellum, bit snap frozen, photo taken, 16g	Osteosarcoma
					58d	281d	**223**	sick, brain tumour?, liver tumour (1596-07), 21.4g	Glioma
					71d	312d	**241**	sick, unable to move, 35.5g, calcified tumour in cerebellum	neoplastic cells in ventricle / PL
					56d	311d	**255**	sick by animal technician, liver tumour	no tumour
					56d	335d	**279**	sick (bloated), massive liver tumour, 49.7g	PL
					56d	360d	**304**	sick, bloated, massive liver tumour, 37g	infiltrative PL
					71d	446d	**375**	sick (sore eye / ear), culled by Claire	no tumour
					62d	442d	**380**	culled, 32.2g	no tumour
15/11/2006	I.c.v. Adenovirus-GFAP-Cre	5	Rb/p53/Rosa	11					
					81d	337d	**256**	time cull, 39.7g	no tumour
					52d	365d	**313**	f/d	no tumour
					52d	389d	**337**	sick, brain tumour, bit snap frozen, 18.1g	Choroid plexus tumour
					81d	461d	**380**	culled, 45.4g	PL
					81d	461d	**380**	culled, 39.7g	no tumour
					81d	461d	**380**	culled, 34g	PL
					81d	461d	**380**	culled, 30.1g	no tumour
					52d	432d	**380**	culled, 36.7g	PL
					52d	432d	**380**	culled, 38.1g	no tumour
					52d	432d	**380**	culled, 55g	Choroid Plexus inflammation / PL
					52d	432d	**380**	culled, 43.8g	no tumour
15/11/2006 #	I.c.v. Adenovirus-GFAP-GFP	5	Rb/p53/Rosa	4					
					81d	241d	**160**	culled prolapse	no tumour
					81d	461d	**380**	culled, 50g	no tumour
					81d	461d	**380**	culled, 39.7g	no tumour
					81d	461d	**380**	culled, 45.1g	no tumour
15/11/2006 #	I.c.v. Adenovirus-GFAP-GFP	5	Rb/p53/PTEN/Rosa	2					
					91d	451d	**360**	sick, breathing problems, 25.5g	no tumour
					91d	471d	**380**	culled, 28.1g	no tumour

Figure 44: Summary table of the experimental details of all the LoxP mutant mice that received i.c.v. Adenovirus-GFAP-Cre (#: experiment analysed, but not performed, by the reporter).

I.c.v. administration of Adenovirus-GFAP-Cre resulted in the development of tumours with comparable genotype-dependent phenotypic profiles, tumour hit rates, and tumour latencies to i.c.v. Adenovirus-CMV-Cre administration (Figure **45**).

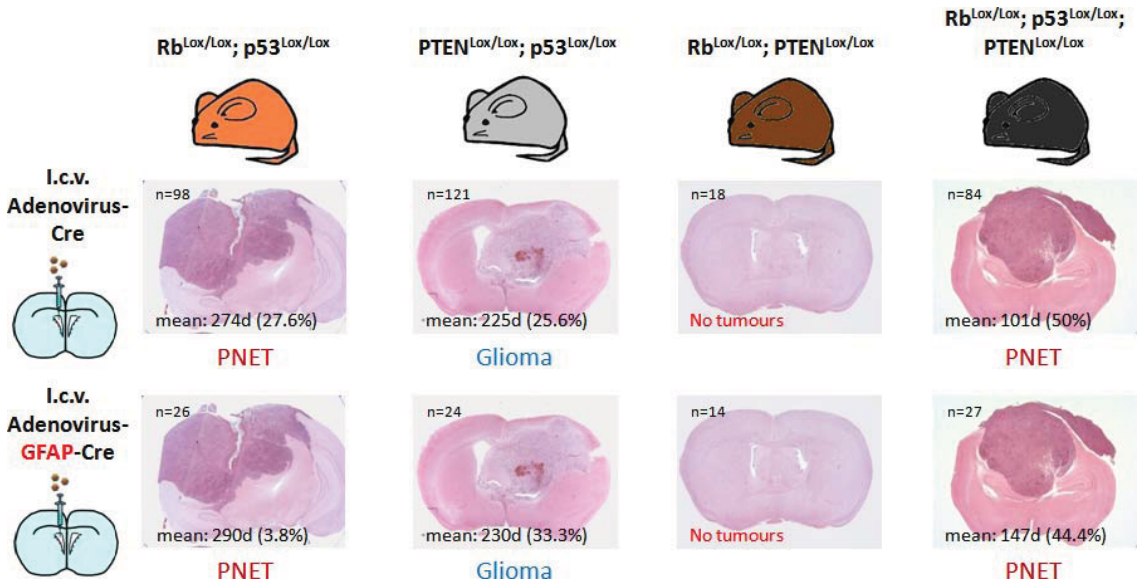

Figure 45: Summary of the experimental results (including 'n' number, mean tumour latency, hit rate, and predominant tumour phenotype) from the i.c.v. administration of Adenovirus-CMV-Cre and Adenovirus-GFAP-Cre in $Rb^{Lox/Lox}$; $p53^{Lox/Lox}$, $PTEN^{Lox/Lox}$; $p53^{Lox/Lox}$, $Rb^{Lox/Lox}$; $PTEN^{Lox/Lox}$, and $Rb^{Lox/Lox}$; $p53^{Lox/Lox}$; $PTEN^{Lox/Lox}$ mice.

I.c.v. Adenovirus-CMV-Cre administration resulted in the development of intrinsic brain tumours in: 27.6% (mean latency: 274 days) of $Rb^{Lox/Lox}$; $p53^{Lox/Lox}$ mice (n=98; 22x PNET, 4x glioma, 1x PNET + glioma), 25.6% (mean latency: 225 days) of $PTEN^{Lox/Lox}$; $p53^{Lox/Lox}$ mice (n=121; 28x glioma, 3x oligoastrocytoma), 0% of $Rb^{Lox/Lox}$; $PTEN^{Lox/Lox}$ mice (n=18), and 50.0% (mean latency: 101 days) of $Rb^{Lox/Lox}$; $p53^{Lox/Lox}$; $PTEN^{Lox/Lox}$ mice (n=84; 39x PNET, 2x glioma, 1x PNET + glioma) (Figure 45). In comparison, i.c.v. Adenovirus-GFAP-Cre administration resulted in the development of intrinsic brain tumours in: 3.8% (mean latency: 290 days) of $Rb^{Lox/Lox}$; $p53^{Lox/Lox}$ mice (n=26; 1x PNET), 33.3% (mean latency: 230 days) of $PTEN^{Lox/Lox}$; $p53^{Lox/Lox}$ mice (n=24; 8x glioma), 0% of $Rb^{Lox/Lox}$; $PTEN^{Lox/Lox}$ mice (n=14), and 44.4% (mean latency: 147 days) of $Rb^{Lox/Lox}$; $p53^{Lox/Lox}$; $PTEN^{Lox/Lox}$ mice (n=27; 5x PNET, 3x glioma, 2x PNET + glioma) (Figure 45). The similar tumour profiles observed following Adenovirus-GFAP-Cre and Adenovirus-CMV-Cre recombination suggests that the GFAP-expressing type B astrocytes of the SVZ are an influential class

of brain tumour initiating cell (BTIC). However, the $Rb^{Lox/Lox}$; $p53^{Lox/Lox}$ mice demonstrated a reduced tumour hit rate when administered with Adenovirus-GFAP-Cre compared against Adenovirus-CMV-Cre. This suggests that either a) in the case of PNETs there are other SVZ cells that contribute towards tumourigenesis, hence a reduction in hit rate when only the type B astrocytes are targeted, and/or b) inactivation of the TSGs Rb and p53 in GFAP-expressing type B astrocytes shifts their cellular signature to a state in which they are less tumourigenic. In addition, $Rb^{Lox/Lox}$; $p53^{Lox/Lox}$; $PTEN^{Lox/Lox}$ mice administered with Adenovirus-GFAP-Cre exhibited a significantly longer mean tumour latency ($P<0.05$; two-tailed unpaired Student's t-Test) and a reduced number of PNETs, suggesting that the PNET BTIC may have been depleted by inactivation of Rb and p53 and that additional PTEN inactivation meant that more gliomas (with longer latencies) were allowed to develop.

4.3.5 Subventricular zone neural stem cells targeted for recombination *in vivo* exhibit the same *in vitro* growth rate, but reduced *in vitro* self-renewal, when compared against their *in vitro* recombined counterparts

It is our hypothesis that NSCs exist in different states, with different functional properties, relative to their environment (*in vitro* versus *in vivo*). We hypothesise that these different states may be the cause of the discrepancy observed between the hit rates of tumours generated from i.c.v. Adenovirus-Cre administration in $Rb^{Lox/Lox}$; $p53^{Lox/Lox}$ mice (24.8%) versus *in vitro* recombined and engrafted $Rb^{-/-}$; $p53^{-/-}$ NS (9.6%), when all the other *in vitro* recombined NS genotypes exhibited increase tumour hit rates (section 4.3.2). To this end, we expanded our model system to allow the characterisation of NSCs in these different *in vitro* and *in vivo* states.

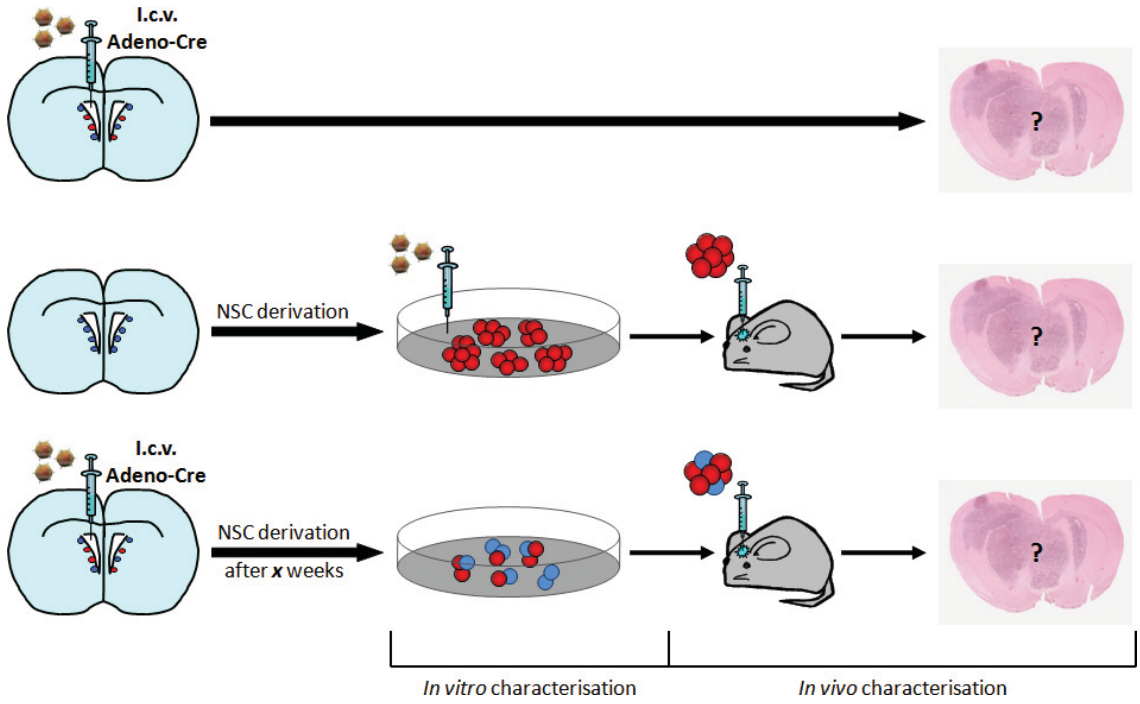

Figure 46: Schematic overview of the model systems used to characterise NSCs targeted for tumourigenic recombination in their *in vitro* (middle schematic) and *in vivo* (bottom schematic) states.

To define the functional properties of the NSCs in their hypothetically different states we used the WST-1 proliferation assay to measure the cumulative mitochondrial activity (as a surrogate marker of *in vitro* growth rate) of passage three $Rb^{-/-}$; $p53^{-/-}$ NSCs at 0, 4, 6, and 8 hours after a 3 day incubation period (Figure 47). The assay was used to compare the growth rates of *in vitro* recombined $Rb^{-/-}$; $p53^{-/-}$ NSCs and *in vivo* recombined $Rb^{Lox/Lox}$; $p53^{Lox/Lox}$ NSCs derived and grown *in vitro* at 2 weeks, 2 months and 4.5 months post-i.c.v. Adenovirus-Cre administration. All of the *in vivo* recombined NS cultures were observed to be 100% β-galactosidase-positive (recombined) by passage two, therefore accounting for any non-recombined NSC interference.

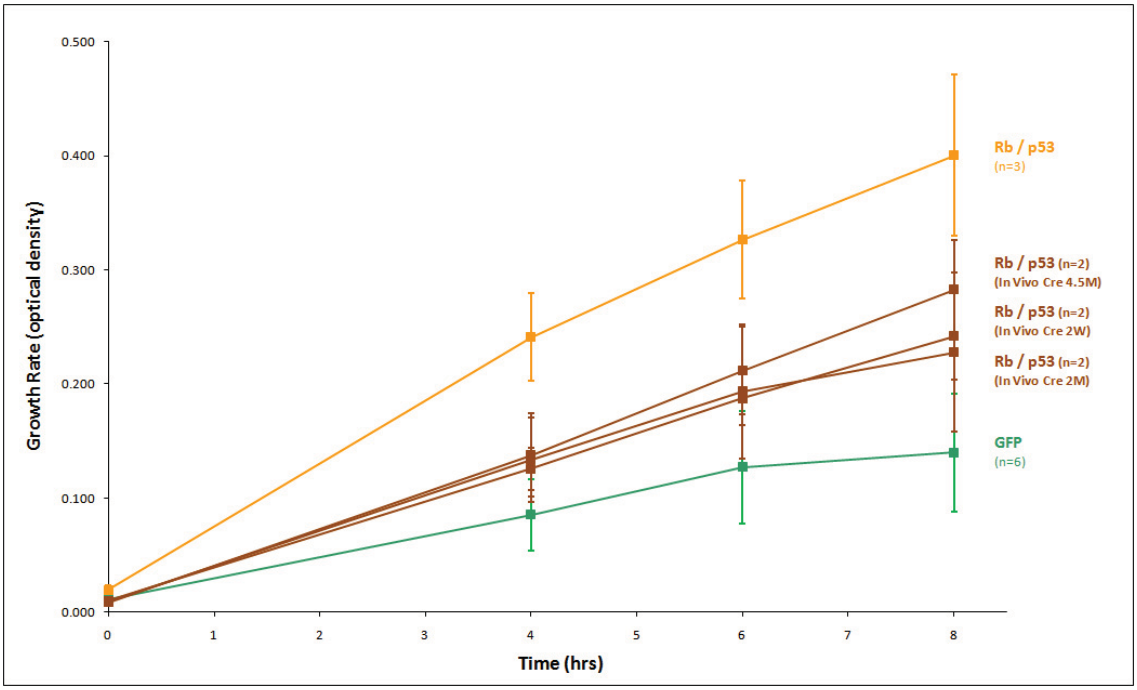

Figure 47: The growth rates of passage three *in vitro* recombined $Rb^{-/-}$; $p53^{-/-}$ NS, *in vivo* recombined $Rb^{Lox/Lox}$; $p53^{Lox/Lox}$ NSCs derived and grown as NS *in vitro* at 2 weeks, 2 months and 4.5 months post-i.c.v. Adenovirus-Cre administration, and non-recombined Adenovirus-GFP-infected are all statistically the same. Using the WST-1 assay the growth rate (y-axis) of NSCs (growing as NS) was measured at 0, 2, 4, and 8hrs (x-axis) after a 3 day incubation period. Growth rate of *in vitro* recombined $Rb^{-/-}$; $p53^{-/-}$ (orange: n=3) vs. *in vivo* recombined $Rb^{Lox/Lox}$; $p53^{Lox/Lox}$ NSCs derived and grown as NS *in vitro* at 2 weeks, 2 months and 4.5 months post-i.c.v. Adenovirus-Cre administration (brown: n=2 each) vs. non-recombined Adenovirus-GFP-infected (green: n=6) NS. Error bars: standard errors. No statistical difference observed between any of the NS growth rates at 8hrs (one-way ANOVA with Bonferroni's multiple comparison correction).

No statistical difference was observed between any of the $Rb^{-/-}$; $p53^{-/-}$ NS, regardless of the cellular environment at the time of recombination (*in vitro* versus *in vivo*) and the length of *in vivo* Adenovirus-Cre incubation (Figure 47). Also, no statistical difference was observed between any of the $Rb^{-/-}$; $p53^{-/-}$ NS and the non-recombined Adenovirus-GFP-infected control NS. The *in vivo* recombined and derived *in vitro* NS appeared to possess a slower growth rate than the *in vitro* recombined NS, but this could be due to variability in the health of the cells prior to the assay. These data suggest that the cellular environment of NSCs at the time of recombination is not correlated to a change in growth rate. Therefore, despite identifying the *in vitro* growth rate of *in vitro* recombined NSCs as a positive predictive indicator of *in vivo* tumour hit rate (section 3.3.5), this concept cannot be applied to the environment-driven NSC state hypothesis.

We also performed a monoclonal self-renewal assay in the aim of elucidating a functional difference between the NSCs of different environmental origins. The non-recombined Adenovirus-GFP-infected NSC control and *in vitro* Adenovirus-Cre-recombined $Rb^{-/-}$; $p53^{-/-}$ NSCs, as analysed in section 3.3.4, are supplied for baseline comparison purposes. Against these we compared the primary and secondary self-renewal abilities of *in vivo* Adenovirus-Cre-recombined and derived *in vitro* (after 3 days) $Rb^{-/-}$; $p53^{-/-}$ NSCs, *in vitro* Adenovirus-GFAP-Cre-recombined $Rb^{-/-}$; $p53^{-/-}$ NSCs, and *in vivo* Adenovirus-GFAP-Cre-recombined and derived *in vitro* (after 3 days) $Rb^{-/-}$; $p53^{-/-}$ NSCs (Figure 48).

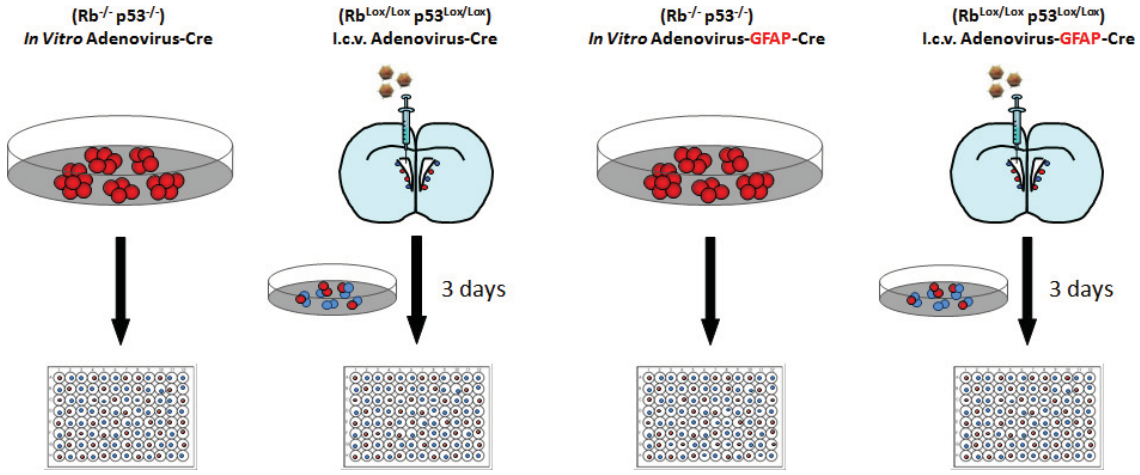

Figure 48: Illustration of the experimental paradigm used to evaluate the self-renewal ability of *in vitro* recombined $Rb^{-/-}$; $p53^{-/-}$ NSCs vs. *in vivo* Adenovirus-Cre-recombined and derived *in vitro* (after 3 days) $Rb^{-/-}$; $p53^{-/-}$ NSCs vs. *in vitro* Adenovirus-GFAP-Cre-recombined $Rb^{-/-}$; $p53^{-/-}$ NSCs vs. *in vivo* Adenovirus-GFAP-Cre-recombined and derived *in vitro* (after 3 days) $Rb^{-/-}$; $p53^{-/-}$ NSCs.

NS at passage two were dissociated into single cells (passage three), FACS-seeded into 96-well plates, and incubated for nine days before the number of NS that formed were counted to assess the primary self-renewal ability. NS were then randomly selected, individually dissociated into single cells, and re-FACS-seeded into 96-well plates and left to assess the secondary self-renewal ability. The efficiency of the MoFlox XDP FACS machine at seeding single cells into single 96-well plate wells was verified at >99% and therefore no correction was applied to the self-renewal data.

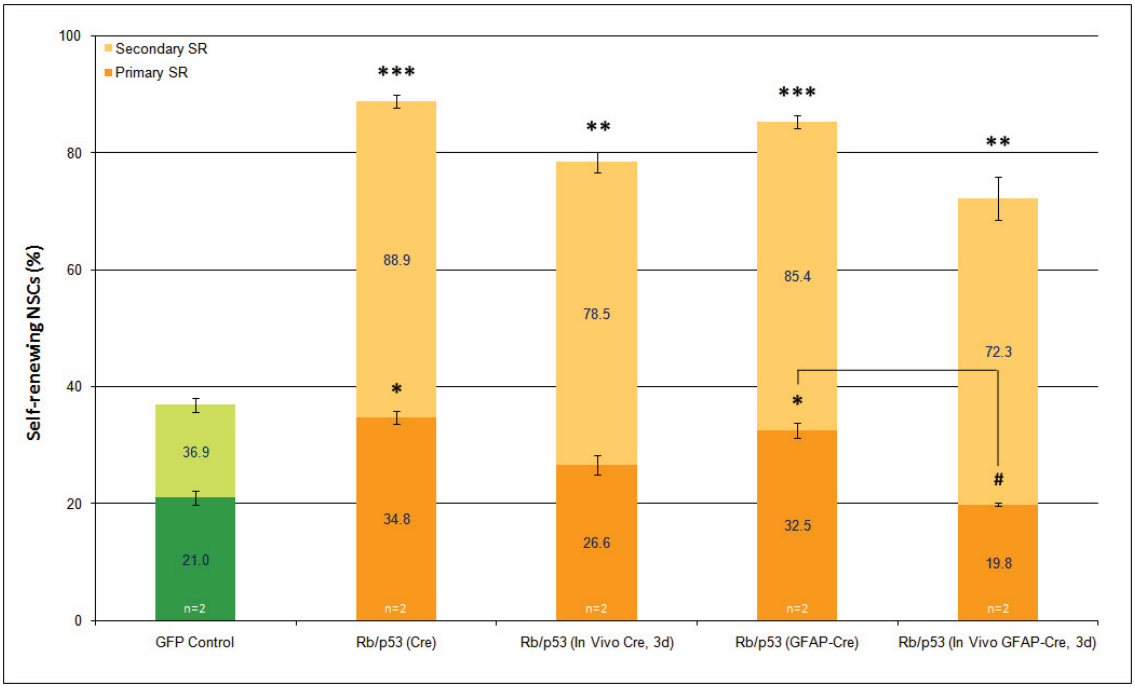

Figure 49: Only the *in vitro* recombined Rb$^{-/-}$; p53$^{-/-}$ NSCs, regardless of the cell targeted, demonstrated a significantly increased primary self-renewal ability over the Adenovirus-GFP-infected control NSCs with significance achieved by all of the NSC groups at the secondary self-renewal phase. NS at passage 2 were dissociated into single NSCs and individually seeded, using a MoFlo XDP FACS machine, into single wells of a 96-well plate containing 200µl NS medium and left to grow for nine days before the number of NS formed was counted and interpreted as the primary self-renewal ability. The process was then repeated for a selection of these monoclonal NS, chosen at random, to assess the secondary self-renewal ability. Primary/secondary self-renewal of non-recombined Adenovirus-GFP-infected (green: n=2) vs. *in vitro* Adenovirus-Cre-recombined Rb$^{-/-}$; p53$^{-/-}$ (orange: n=2) vs. *in vivo* Adenovirus-Cre-recombined and derived *in vitro* (after 3 days) Rb$^{-/-}$; p53$^{-/-}$ NSCs (orange: n=2), *in vitro* Adenovirus-GFAP-Cre-recombined Rb$^{-/-}$; p53$^{-/-}$ NSCs (orange: n=2), and *in vivo* Adenovirus-GFAP-Cre-recombined and derived *in vitro* (after 3 days) Rb$^{-/-}$; p53$^{-/-}$ NSCs (orange: n=2). Primary self-renewal is shown as the solid bars and secondary self-renewal is shown as the paler-coloured bars on top of the primary self-renewal bars. Error bars: standard errors. *: P<0.05 vs. GFP control, **: P<0.01 vs. GFP control, ***: P<0.001 vs. GFP control, #: P<0.05 between highlighted groups (one-way repeated measures ANOVA with Bonferroni's multiple comparison correction).

For primary self-renewal, only the number of *in vitro* Adenovirus-Cre-recombined Rb$^{-/-}$; p53$^{-/-}$ NSCs (34.8% +/- 1.0) and *in vitro* Adenovirus-GFAP-Cre-recombined Rb$^{-/-}$; p53$^{-/-}$ NSCs (32.5% +/- 1.3) were observed to be significantly different from the Adenovirus-GFP-infected control (21.0% +/- 1.2) (Figure 49). At the secondary self-renewal stage, significance against the Adenovirus-GFP-infected control was achieved by all of the Rb$^{-/-}$; p53$^{-/-}$ NSC groups. Fewer *in vivo* recombined and derived primary NSCs appeared to self-renew when compared against their corresponding *in vitro* recombined NSCs, and a

significant reduction was observed with the *in vivo* Adenovirus-GFAP-Cre-recombined and derived *in vitro* (after 3 days) $Rb^{-/-}$; $p53^{-/-}$ NSCs (19.8% +/- 0.3). This suggests that, despite not demonstrating a difference in their *in vitro* growth rate, $Rb^{-/-}$; $p53^{-/-}$ NSCs in their SVZ *in vivo* environment are functionally different from their *in vitro* recombined counterparts in that they possess a reduced self-renewal ability. No correlation was observed between the self-renewal ability of *in vitro* recombined NSCs and their *in vivo* tumour hit rate following engraftment (section 3.3.5), so a reduction in the self-renewal ability of *in vivo* recombined and derived *in vitro* NSCs should not be considered a potential predictive indicator of reduced *in vivo* tumour hit. Instead, the reduction in self-renewal could be interpreted as an indication that NSCs exist in different states dependent on their environment, and that these different states can be discriminated by their functional profiles.

4.3.6 The environment of subventricular zone neural stem cells at the time of recombination influences *in vivo* tumour hit rate and latency but with little effect on phenotype

To examine the *in vivo* tumour hit rate of NSCs recombined *in vivo* and derived *in vitro* we i.c.v. injected multiple mouse cohorts with Adenovirus-Cre before deriving NS at early (2 weeks), intermediate (2 months), or late (>3.5 months) time points. These NS were expanded *in vitro* for 2-8 passages and intracerebrally engrafted into the striata of a total of 86 non-recombined mice of the same genetic background in 10 separate experiments. Mice were left for up to 449 days post-engraftment before the experiment was terminated (Figure 50).

Experiment	Cell Recombination Paradigm	Vol. Injected (ul)	Passage #	Genotype (cells)	# Mice	Age (start)	Age (end)	Incubation time (d)	CoD	Diagnosis
24/04/2009	*In vivo* recombined (Adeno-Cre)	15	4	Rb / PTEN / Rosa	11					
	Late: 6M					77	338	**261**	experiment terminated	no tumour
						77	338	**261**	experiment terminated	no tumour
						77	338	**261**	experiment terminated	no tumour
						77	338	**261**	experiment terminated	no tumour
						77	338	**261**	experiment terminated	no tumour
						77	338	**261**	experiment terminated	no tumour
						77	376	**299**	experiment terminated	no tumour
						77	376	**299**	experiment terminated	no tumour
						77	376	**299**	experiment terminated	no tumour
						77	376	**299**	experiment terminated	no tumour
						77	376	**299**	experiment terminated	no tumour
19/01/2009	*In vivo* recombined (Adeno-Cre)	12.5	6	Rb / p53 / Rosa	11					
	Late: 4.5M					88	88	**0**	f/d	-
						71	72	**1**	f/d	-
						88	338	**250**	experiment terminated	no tumour
						88	338	**250**	experiment terminated	no tumour
						71	321	**250**	experiment terminated	no tumour
						71	321	**250**	experiment terminated	no tumour
						88	338	**250**	experiment terminated	no tumour
						88	338	**250**	experiment terminated	no tumour
						88	338	**250**	experiment terminated	no tumour
						71	321	**250**	experiment terminated	no tumour
						71	321	**250**	experiment terminated	no tumour
30/10/2008	*In vivo* recombined (Adeno-Cre)	15	6	Rb / p53 / Rosa	9					
	Middle: 2M					54	61	**7**	f/d	-
						52	209	**157**	27.3g, sick, ataxic, brain tumour snap frozen	PNET/Glioma
						52	209	**157**	28.1g, sick, ataxic, lump on head, brain tumour snap froze	PNET/Glioma
						59	217	**158**	35g, sick, ataxic, dome skull	PNET/Glioma
						59	246	**187**	f/d	-
						59	380	**321**	exp.terminated	no tumour
						54	375	**321**	exp.terminated	no tumour
						54	375	**321**	exp.terminated	PNET/Glioma
						54	375	**321**	exp.terminated	no tumour
26/09/2008	*In vivo* recombined (Adeno-Cre)	15	8	Rb / p53 / Rosa	10					
	Early: 2W					65	118	**53**	sick, dome skull, tumour snap frozen, 20.2g	PNET/Glioma
						61	126	**65**	sick, dome skull, 23.9g	PNET/Glioma
						61	128	**67**	sick, ataxic, 23.8g	PNET/Glioma
						65	147	**82**	sick, ataxic, lump, 20.1g	PNET/Glioma
						61	156	**95**	sick, dome skull	PNET/Glioma (elevated apoptosis)
						61	162	**101**	sick, ataxic, dome skull, 23.1g, brain tumour snap frozen	PNET/Glioma (necrosis
						61	178	**117**	Sick, 31g, abnormal gait, large brain, 2hrs BrdU	PNET/Glioma
						61	283	**222**	culled sick, dome skull, 28.2g	-
						65	359	**294**	experiment terminated	no tumour
						65	359	**294**	experiment terminated	no tumour

02/09/2008	*In vivo* recombined (Adeno-Cre)	15	4	Rb / p53 / Rosa	9					
	Early: 2W					73	74	**1**	f/d	-
						73	74	**1**	f/d	-
						73	207	**134**	sick, 17.6g, dome skull, brain tumour snap frozen, 2hrs B	PNET/Glioma
						73	218	**145**	sick, only whole brain collected, 2hrs BrdU	Oligoastrocytoma
						73	387	**314**	Experiment terminated	no tumour
						73	387	**314**	Experiment terminated	no tumour
						73	387	**314**	Experiment terminated	no tumour
						73	387	**314**	Experiment terminated	no tumour
						73	387	**314**	Experiment terminated	no tumour
30/05/2007	*In vivo* recombined (Adeno-Cre)	5	4	Rb / p53 / PTEN / Rosa	10					
	Early: 2W					43d	268d	**225**	time-cull, 33.6g	no tumour
						43d	361d	**318**	culled, 52g	no tumour
						43d	361d	**318**	culled, 31g, circling	no tumour
						43d	361d	**318**	culled, 45.5g	no tumour
						43d	361d	**318**	culled, 57g	no tumour
						43d	361d	**318**	culled, 52.7g	no tumour
						43d	361d	**318**	culled, 57g	no tumour
						43d	361d	**318**	culled, 55g	no tumour
						43d	361d	**318**	culled, 51g	no tumour
						43d	361d	**318**	culled, 38g	no tumour
30/05/2007	*In vivo* recombined (Adeno-Cre)	5	4	PTEN / p53 / Rosa	10					
	Early: 2W					43d	263d	**220**	f/d	-
						43d	268d	**225**	time-cull, 36.6g	Oligoastrocytoma
						43d	315d	**272**	f/d, brain tumour	Oligoastrocytoma
						43d	339d	**296**	sick, brain tumour, culled by Francis, 20.6g	GBM
						43d	444d	**401**	experiment terminated	no tumour
						43d	444d	**401**	experiment terminated	no tumour
						43d	444d	**401**	experiment terminated	no tumour
						43d	444d	**401**	experiment terminated	no tumour
						43d	444d	**401**	experiment terminated	no tumour
						43d	444d	**401**	experiment terminated	no tumour
19/09/2006	Non-recombined (Adeno-GFP)	10	2	Rb / p53 / PTEN / Rosa	1					
	Late: 4M					66d	373d	**307**	culled, 39.9g	culled, 39.9g
19/09/2006	*In vivo* recombined (Adeno-Cre)	5	2	Rb / p53 / PTEN / Rosa	11					
	Late: 4M					81d	86d	**5**	f/d no sample taken	-
						81d	184d	**103**	f/d no sample taken	-
						81d	184d	**103**	f/d no sample taken	-
						81d	197d	**109**	sick brain tumour, bit snap frozen, photo taken, 19.3g	PNET + Glioma
						81d	211d	**130**	sick brain tumour, bit snap frozen, 21.5g	PNET + Glioma
						81d	213d	**132**	sick, brain tumour, bit snap frozen, photo taken, 23.8g	PNET
						66d	229d	**163**	sick, brain tumour, photo taken, bit snap frozen, 28.8g	PNET
						66d	305d	**239**	sick, culled by animal technicians, 28g, brain tumour	PNET
						66d	310d	**244**	sick, brain tumour, photo taken, bit snap frozen, 29.7g	PNET
						66d	373d	**307**	culled, 46g	no tumour
						66d	373d	**307**	culled, 42g	no tumour

24/05/2005	*In vivo* recombined (Adeno-Cre)	10	-	Rb / p53 / Rosa flox het	1					
#	Late: 3.5M					105d	451d	346	culled	no tumour
24/05/2005	*In vivo* recombined (Adeno-Cre)	10	-	Rb / p53 / Rosa	11					
#	Late: 3.5M					105d	179d	74	culled sick, brain tumour on left front	PNET
						100d	230d	130	culled sick, brain tumour, grew on top of brain, very "slimy	Glioma
						105d	241d	136	sick, brain tumour, bit frozen, bit for tissue culture	Glioma
						100d	295d	195	f/d, brain fixed but very decayed	PNET
						100d	325d	225	sick, no obvious tumour, but brain / liver / spleen very pale	no tumour
						105d	345d	240	f/d tumour grew on top of skull (280-06)	Glioma
						100d	348d	248	sick, agitated, but no obvious tumour	Glioma
						105d	364d	259	f/d, no sample taken	-
						105d	451d	346	sick, brain tumour, bit frozen	PNET/Glioma
						105d	505d	400	culled	PNET/Glioma
						105d	505d	400	culled, brain tumour	-
05/04/2005	*In vivo* recombined (Adeno-Cre)	10 (2x6)	-	Rb / p53 / Rosa flox het	9					
#	Late: 3.5M					90d	106d	16	culled	no tumour
						90d	131d	41	culled	no tumour
						90d	131d	41	culled	no tumour
						90d	539d	449	culled	no tumour
						90d	539d	449	culled	no tumour
						90d	539d	449	culled	no tumour
						90d	539d	449	culled	no tumour
						90d	539d	449	culled	no tumour
						94d	526d	449	culled	no tumour
05/04/2005	*In vivo* recombined (Adeno-Cre)	10	-	Rb / p53 / Rosa	10					
#	Late: 3.5M					77d	93d	16	culled	graft
						85d	126d	41	culled	small graft
						85d	126d	41	culled	no tumour
						94d	390d	296	culled	no tumour
						94d	390d	296	culled sick, swollen stomach	no tumour
						77d	409d	332	sick, "slimy" brain tumour	PNET
						77d	526d	449	culled	no tumour
						77d	526d	449	culled	no tumour
						94d	526d	449	culled	no tumour
						94d	526d	449	culled	no tumour

Figure 50: Summary table of the experimental details of all the mice that received intracerebral injections of *in vivo* recombined and derived *in vitro* NS (#: experiment analysed, but not performed, by the reporter).

These data were combined with the *in vitro* recombined and engrafted NS data to generate a tumour incident plot comparing the trends between cell genotype, cell recombination environment, tumour latency, and tumour phenotype (Figure 51).

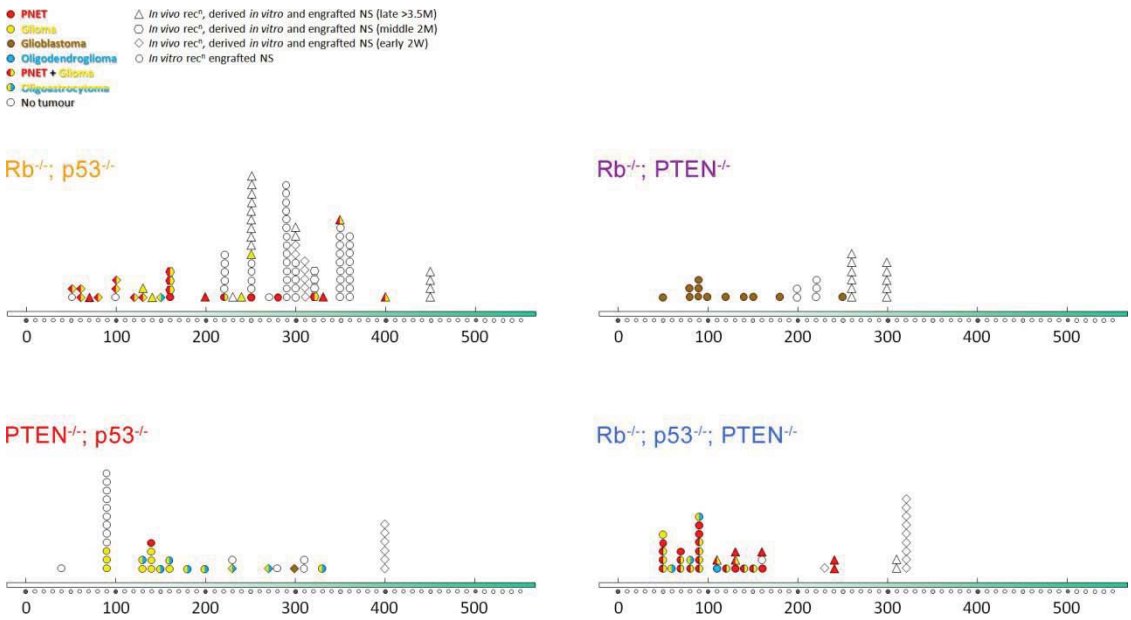

Figure 51: Incidence plot of the tumours generated from the intracerebral engraftment of Rb$^{-/-}$; p53$^{-/-}$, Rb$^{-/-}$; PTEN$^{-/-}$, PTEN$^{-/-}$; p53$^{-/-}$ and Rb$^{-/-}$; p53$^{-/-}$; PTEN$^{-/-}$ NS recombined *in vitro* (circles) or *in vivo* and derived after 2 weeks (diamonds), 2 months (hexagons), and 4.5 months (triangles). Axis: tumour latency (days).

The incident plot highlights the differences between the hit rates, latencies, and phenotypes of the tumours generated by the different engrafted NS genotypes. Interestingly, it also highlights a clear difference within the different NS genotypes based on the environment of the NSCs at the time of recombination (Figure 52).

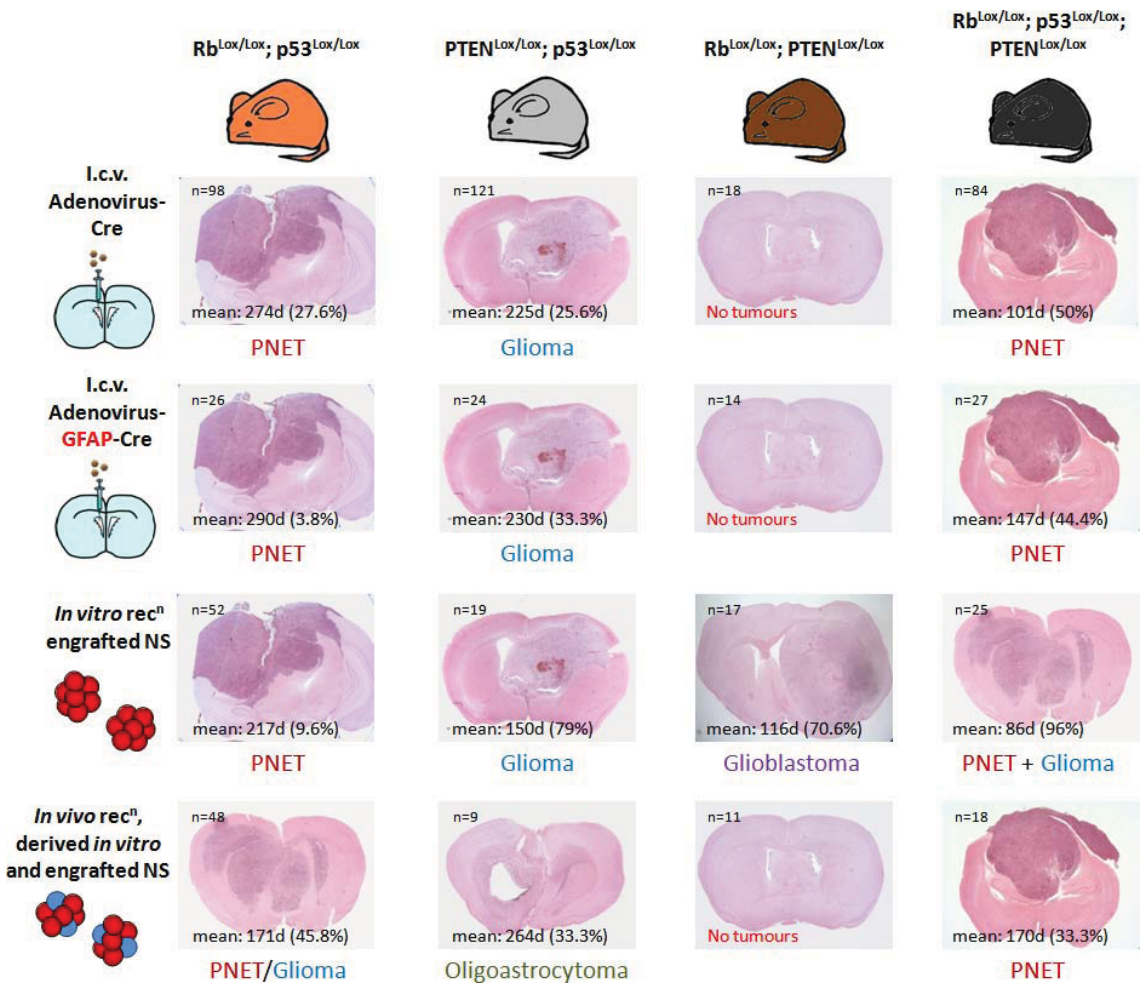

Figure 52: Summary of the experimental results (including 'n' number, mean tumour latency, hit rate, and predominant tumour phenotype) from the i.c.v. administration of Adenovirus-CMV-Cre and Adenovirus-GFAP-Cre in $Rb^{Lox/Lox}$; $p53^{Lox/Lox}$, $PTEN^{Lox/Lox}$; $p53^{Lox/Lox}$, $Rb^{Lox/Lox}$; $PTEN^{Lox/Lox}$, and $Rb^{Lox/Lox}$; $p53^{Lox/Lox}$; $PTEN^{Lox/Lox}$ mice in addition to the results from the intracerebral engraftment of *in vitro* recombined NS and *in vivo* recombined and derived *in vitro* NS derived from the same mice.

Intracerebral engraftment of *in vivo* recombined and derived *in vitro* NS (regardless of time prior to *in vitro* derivation) resulted in an intrinsic tumour hit rate of 45.8% for $Rb^{-/-}$; $p53^{-/-}$ NS (n=48; 14x PNET/glioma, 4x glioma, 3x PNET, 1x oligoastrocytoma), 33.3% for $PTEN^{-/-}$; $p53^{-/-}$ NS (n=9; 2x oligoastrocytoma, 1x glioma), 0% of $Rb^{-/-}$; $PTEN^{-/-}$ NS (n=11), and 33.3% of $Rb^{-/-}$; $p53^{-/-}$; $PTEN^{-/-}$ NS (n=18; 4x PNET, 2x PNET + glioma) (Figure 52). Notably, the tumour hit rates and latencies following engraftment of the *in vivo* recombined and derived *in vitro* NS appeared to more closely resemble those following i.c.v. Adenovirus-Cre administration rather than engraftment of *in vitro* recombined NS. For example, *in vitro* recombined and engrafted $Rb^{-/-}$; $PTEN^{-/-}$ NS generated tumours with a 70.6% hit rate and 116 day latency whereas both i.c.v.

Adenovirus-Cre administration in $Rb^{Lox/Lox}$; $PTEN^{Lox/Lox}$ mice and *in vivo* recombined, derived *in vitro* and engrafted $Rb^{-/-}$; $PTEN^{-/-}$ NS failed to generate a single brain tumour (Figure 52). A similar trend was observed with the *in vivo* recombined, derived *in vitro* and engrafted $PTEN^{-/-}$; $p53^{-/-}$ and $Rb^{-/-}$; $p53^{-/-}$; $PTEN^{-/-}$ NS, which demonstrated hit rates (both 33.3%) that more closely resembled the 25.6-33.3% and 44.4-50% respectively achieved with i.c.v. Adenovirus-Cre. In addition, the tumour latencies of the same *in vivo* recombined, derived *in vitro* and engrafted NS were significantly longer ($P<0.05$ and $P<0.001$ respectively; two-tailed unpaired Student's t-Test) than following engraftment of their *in vitro* recombined counterparts. However, despite these differences in tumour hit rate and latency, the tumour phenotypes remained comparable. This suggests that the environment of the NSC at the time of recombination influences the *in vivo* tumour hit rate of the NSCs but has no effect on the phenotype. In the case of the $PTEN^{-/-}$; $p53^{-/-}$, $Rb^{-/-}$; $PTEN^{-/-}$, and $Rb^{-/-}$; $p53^{-/-}$; $PTEN^{-/-}$ genotypes, NSCs recombined in an *in vitro* environment possess the greatest tumourigenicity (highest hit rate and shortest latency). We propose that this is either because a) the number of BTICs is at its greatest in the *in vitro* environment, or b) the NSCs exist in an altered and more tumourigenically susceptible state *in vitro*.

The one exception to this rule is the $Rb^{-/-}$; $p53^{-/-}$ NS genotype, for which NSCs recombined in the *in vitro* environment were less tumourigenic (albeit non-significantly for tumour latency: $P>0.05$; two-tailed unpaired Student's t-Test) than their *in vivo* recombined, derived *in vitro* and engrafted NS (Figure 52). However, when the tumour latencies of the *in vivo* recombined, derived *in vitro* and engrafted NS are broken down based on the length of time prior to derivation (2 weeks vs. 2 months vs. >3.5 months) a significant difference was observed between the 2 week and the >3.5 months groups (Figure 53).

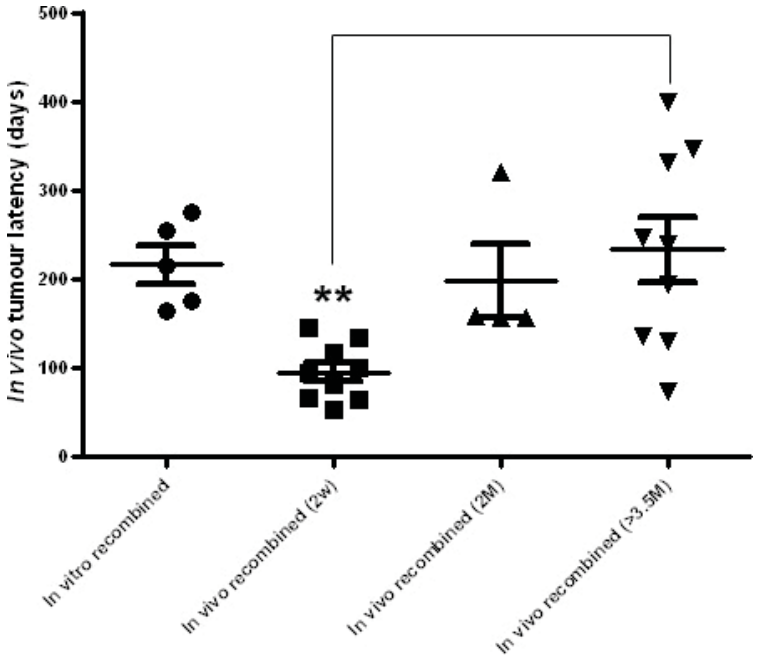

Figure 53: *In vivo* recombined and derived *in vitro* after 2 weeks $Rb^{-/-}$; $p53^{-/-}$ NS generate brain tumours with a significantly shorter latency following engraftment than when derived after >3.5 months. Mean and standard error plot with all the data points showing the *in vivo* tumour latency. **: P<0.001 vs. illustrated comparison (one-way ANOVA with Bonferroni's multiple comparison correction).

The tumour latencies of the *in vivo* recombined NS derived after 2 weeks were not significantly different from those of the *in vitro* recombined NS but a trend could be observed between increased tumour latency and an increase in the length of time before *in vitro* derivation. The tumour hit rates of the *in vivo* recombined NS derived after 2 weeks, 2 months, and >3.5 months were 56.3%, 75.0%, and 36.0% respectively. No statistically significant correlation, exclusive or inclusive of the *in vitro* recombined and engrafted NS data set, was observed between the length of time before derivation and tumour hit rate (P>0.05; two-tailed Pearson test). We propose that the observed increase in tumour latency with increased time between *in vivo* recombination and *in vitro* derivation may be as a result of micro-dissecting different populations of transformed SVZ cells. In addition, the fact that an elevated hit rate (36.0-75.0% versus 27.6% with i.c.v. Adenovirus-Cre) was observed with *in vivo* recombined $Rb^{-/-}$; $p53^{-/-}$ NSCs that were derived *in vitro* and engrafted back into the brains of mice suggests that the hypothetical *in vivo* state of $Rb^{-/-}$; $p53^{-/-}$ NSCs is maintained in transition from *in vivo* to the *in vitro* environment. In section 4.3.1 we identified that after 2 months (60 days) the SVZ cells targeted for recombination had proliferated and begun to migrate away from the SVZ. It is possible that the SVZ micro-dissections performed at the 2 week time

points captures the greatest number of recombined tumourigenic SVZ NSCs before this proliferation and migration occurs. And that after 3.5 months, the majority of the tumourigenic SVZ cells had migrated away from the SVZ leaving a depleted pool available for capture by micro-dissection. This hypothesis implies that tumour latency is dependent on tumourigenic cell load. In turn, this would suggest that leaving *in vivo* recombined and derived *in vitro* NS in culture for longer would result in a greater number of tumourigenic NSCs as they out-compete the other cells. This was the case with NSCs derived after 2 weeks that had tumour hit rates of 28.6% and 77.8% after 4 and 8 passages in culture respectively (Figure 50). However, both cultures were 100% β-galactosidase-positive prior to engraftment, which suggests that either β-galactosidase staining is not sensitive enough in determining the proportion of recombined cells or that recombined SVZ cells can exist with different grades of tumourigenicity.

4.3.7 *In vivo* recombined, derived *in vitro* and engrafted $Rb^{-/-}$; $p53^{-/-}$ neurospheres reproducibly generate a novel tumour resembling a small cell glioblastoma highlighting a potential influence of neural stem cell environment on lineage specificity

In vivo recombined and derived *in vitro* $Rb^{-/-}$; $p53^{-/-}$ NS were engrafted into the brains of recipient mice as described in section 4.3.6. Whereas the predominant tumour phenotype generated by tumourigenic NSCs of the $PTEN^{-/-}$; $p53^{-/-}$, $Rb^{-/-}$; $PTEN^{-/-}$, and $Rb^{-/-}$; $p53^{-/-}$; $PTEN^{-/-}$ genotypes remained relatively constant, regardless of recombination environment, *in vivo* recombined and derived *in vitro* $Rb^{-/-}$; $p53^{-/-}$ NSCs reproducibly gave rise to a novel tumour phenotype following engraftment. I.c.v. Adenovirus-Cre administration in $Rb^{Lox/Lox}$; $p53^{Lox/Lox}$ mice had a 27.6% tumour hit rate of which 81.5% were PNETs. I.c.v. Adenovirus-GFAP-Cre administration in $Rb^{Lox/Lox}$; $p53^{Lox/Lox}$ mice had a 3.8% tumour hit rate of which 100% were PNETs. *In vitro* recombined and engrafted $Rb^{-/-}$; $p53^{-/-}$ NS had a tumour hit rate of 9.6% of which 80% were PNETs. However, *in vivo* recombined, derived *in vitro* and engrafted $Rb^{-/-}$; $p53^{-/-}$ NS had a hit rate of 45.8% of which only 13.6% were PNETs but 63.6% were a novel glioma-like tumour with some PNET characteristics (Figure 54).

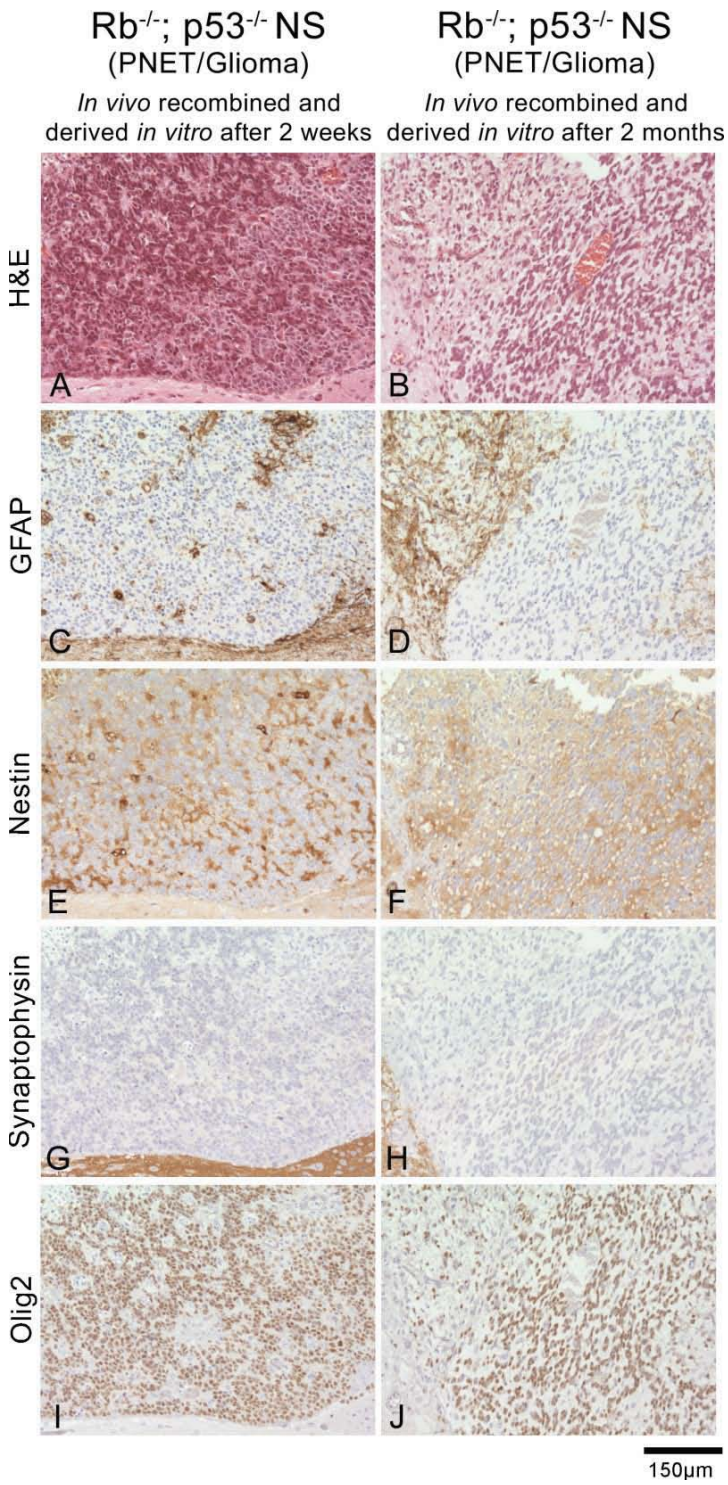

Figure 54: *In vivo* recombined, derived *in vitro* and engrafted $Rb^{-/-}$; $p53^{-/-}$ NS reproducibly generate a novel glioblastoma-like tumour with some undifferentiated neuronal characteristics, regardless of the time between *in vivo* recombination and derivation *in vitro*. Representative images taken from tumours generated following intracerebral (in the striatum) engraftment of *in vivo* recombined and derived *in vitro* after 2 weeks (A,C,E,G,I) or 2 months (B,D,F,H,J) $Rb^{-/-}$; $p53^{-/-}$ NS. The tumours were stained for haematoxylin and eosin (A,B), GFAP (C,D), nestin (E,F), synaptophysin (G,H), and Olig2 (I,J) to assist in the classification of their phenotype. The tumours were often bi-phasic with some areas morphologically resembling a PNET (A, left side of image) but that were always synaptophysin-negative (G). Areas of GFAP-positivity (D, left side of image) were suggestive of a glial or astro/oligodendroglial

phenotype but counter-intuitively those areas were Olig2-negative (J, left side of image). The nestin-positivity of all the tumours (E,F) confirmed their undifferentiated state. Images were taken using a ColorView III digital camera mounted on a Zeiss Axioskop 2 MOT microscope with a 10x magnification and using the AnalySIS software package.

Typically, PNETs appear well-demarcated with closely packed and undifferentiated cells positive for synaptophysin, and often appearing in rosette formations (Louis et al., 2007). These particular tumours contained foci that matched this description (Figure 54: A, left half of image), but were always synaptophysin-negative (Figure 54: G,H). These undifferentiated cells also contained elongated nuclei, little cytoplasm (Figure 54: B, right side of image), and were GFAP-negative (Figure 54: D, right side of image). Rhythmic monomorphic astroglial-like patterning was also observed in some foci (Figure 54: A, right side of image), but these were also GFAP-negative (Figure 54: C). In addition, all of the tumours were Olig2-positive (Figure 54: I,J) except in areas of highly infiltrative GFAP-positive cells (Figure 54: J, left side of image); suggestive of a glioblastoma-like phenotype (Louis et al., 2007). Taken together, unlike the typical pleomorphic appearance of conventional glioblastomas, these particular tumours contained undifferentiated neuronal-like foci that were more indicative of a small cell astrocytoma / glioblastoma phenotype (Perry et al., 2004; Pina-Oviedo et al., 2006). This phenotype, novel to our model and unique to the $Rb^{-/-}$; $p53^{-/-}$ genotype, highlights a potential effect of the NSC recombination environment on tumourigenic lineage-specificity.

4.4 Conclusion

In this chapter we demonstrated that brain tumourigenesis is initiated and driven by SVZ NSCs by showing that a) i.c.v. Adenovirus-Cre recombination of TSGs in the SVZ causes cells to proliferate and migrate into the brain parenchyma where they generate tumours, and b) NSCs derived from the SVZ of adult mice and grown / recombined *in vitro* generate tumours that recapitulate the i.c.v. Adenovirus-Cre-induced phenotypes following intracerebral engraftment. Neurosphere-forming stem-like cells were observed to exist in the brain tumour bulk, as brain tumour initiating cells (BTICs), and were found to remain committed to a specific phenotype / lineage over serial engraftments. We hypothesise that these committed BTICs are the progeny of the SVZ NSCs targeted for recombination. To trace the origins of these committed BTICs we

used i.c.v. Adenovirus-GFAP-Cre to target only the GFAP-expressing type B astrocytes of the SVZ for recombination in the aim of examining their relative contribution to tumourigenesis. Using this approach we identified that targeting only the type B astrocytes of the SVZ for recombination induced the same patterns of tumour hit rate, latency, and phenotype as seen following non-specific targeting of all SVZ cells. This suggests that the type B astrocytes represent an SVZ class of BTIC. Interestingly, we revealed that the environment of SVZ NSCs (*in vivo* versus *in vivo*) at the time of recombination influences *in vivo* tumour hit rate and latency, but with little effect on phenotype. In addition, SVZ NSCs targeted for recombination *in vivo* were found to possess the same *in vitro* growth rate as their *in vitro* recombined counterparts, but exhibited reduced self-renewal. We therefore propose that the cellular environment of NSCs influences the states and ratios of different NSC sub-populations, and that these states determine their tumourigenic profile. This cell phenotype-based model of identifying BTICs complements the work of Clement et al, who have also pursued marker-independent identification of BTICs (Clement et al., 2010).

Despite this, the majority of research has focussed on identifying BTICs based on their marker expression profile. To this end, CD133 was identified (Singh et al., 2003; Singh et al., 2004) and has been widely studied / disputed for its potential as a marker of BTICs (Bao et al., 2006; Clement et al., 2009; Facchino et al., 2010; Nishide et al., 2009). In the next chapter we aim to examine the roll of CD133 expression and its potential as a marker of BTICs in our model of tumourigenesis.

4.5 Future Work

Expansion of the sample numbers across all of the *in vivo* experiments would allow for a more robust analysis of tumour hit rate, latency, and phenotype correlates. BTICs from the bulk of a tumour were serially engrafted through only one passage but were found to generated tumours with an increased hit rate and significantly reduced latency. By serially engrafting these BTICs through further passages we could derive a purified and highly tumourigenic primary cell line, which we could use to conduct a comprehensive functional characterisation in addition to identifying markers of BTICs. Ideally, this would be done for all the cell genotypes and all the different tumour phenotypes that they can induce. The concept of environment influencing NSC state

was devised by primarily using $Rb^{-/-}$; $p53^{-/-}$ NSCs. Repeating the experiment for all of the genotypes would provide additional insight into this concept.

5 Investigating CD133 (Prominin-1) as a Marker of Brain Tumour Initiating Cells

5.1 Introduction

The cancer stem cell hypothesis states that only a small sub-population of cells within a tumour is tumourigenic. There is a large body of literature implicating the cell surface protein CD133 (Prominin-1) as both a marker of organ-specific adult stem cells and cancer stem cells. This association was first comprehensively characterised in colon cancer stem cells (Ricci-Vitiani et al., 2007; O'Brien et al., 2007; Singh et al., 2003) but continues to be debated (Shmelkov et al., 2008; Clement et al., 2009). The study of CD133 as a marker of cancer stem cells has expanded across a range of cancers including haematopoietic (Vercauteren and Sutherland, 2001), kidney (Florek et al., 2005), ovarian (Ferrandina et al., 2008), prostate (Vander Griend et al., 2008), lung (Eramo et al., 2008), and brain (Singh et al., 2003; Singh et al., 2004). The study of CD133 as a marker of brain cancer stem cells, or brain tumour initiating cells (BTICs), is the most widely studied field in which CD133-positive cells represent a radio-resistant and aberrantly proliferating population of glioma BTICs (Bao et al., 2006). However, subsequent contradictory studies in which CD133-negative glioma cells have been found to form tumours (Wang et al., 2008) have precluded definitive verfication of CD133 as a marker of BTICs. Little is known about the functional properties of murine CD133-positive cells both *in vitro* and *in vivo*, and using our model system we aim to address this knowledge gap.

In this chapter we use a combination of magnetic-activated cell sorting (MACS) and fluorescence-activated cell sorting (FACS) to sort NSCs into their respective CD133-negative (CD133-) and CD133-positive (CD133+) populations. Using these methods we aim to characterise the influence of CD133 expression on the *in vitro* functional properties and *in vivo* tumour hit rates, latencies, and phenotype propensities of NSCs.

Aims

1. Verify that SVZ NSCs express CD133 both *in vivo* and *in vitro*.
2. Characterise the CD133 expression pattern in wild-type and recombined tumourigenic NSCs.

3. Characterise the functional differences of tumourigenic CD133+ and CD133- NSCs *in vitro*.
4. Characterise the *in vivo* tumour hit rates, latencies, and phenotype propensities of tumourigenic CD133+ and CD133- NSCs and assess whether CD133 expression can be used as a predictive indicator.
5. Identify novel markers of BTICs.

5.2 Materials and Methods

Refer to the main materials and methods (Chapter Two).

5.3 Results

5.3.1 CD133 is expressed by subventricular zone neural stem cells targeted by intracerebroventricular Adenovirus-GFP administration *in vivo* and by neurospheres *in vitro*

Adenovirus-GFP was administered i.c.v. into the brains of five wild-type $Rosa^{Lox/Lox}$ mice, which were left for five days before being culled and their brains taken for immunohistochemistry. 50μm thick vibratome sections of the SVZ were stained for CD133, GFAP, and GFP to observe whether CD133 is expressed by GFAP-positive SVZ NSCs *in vivo*, and whether Adenovirus-GFP administration targets these CD133-expressing cells.

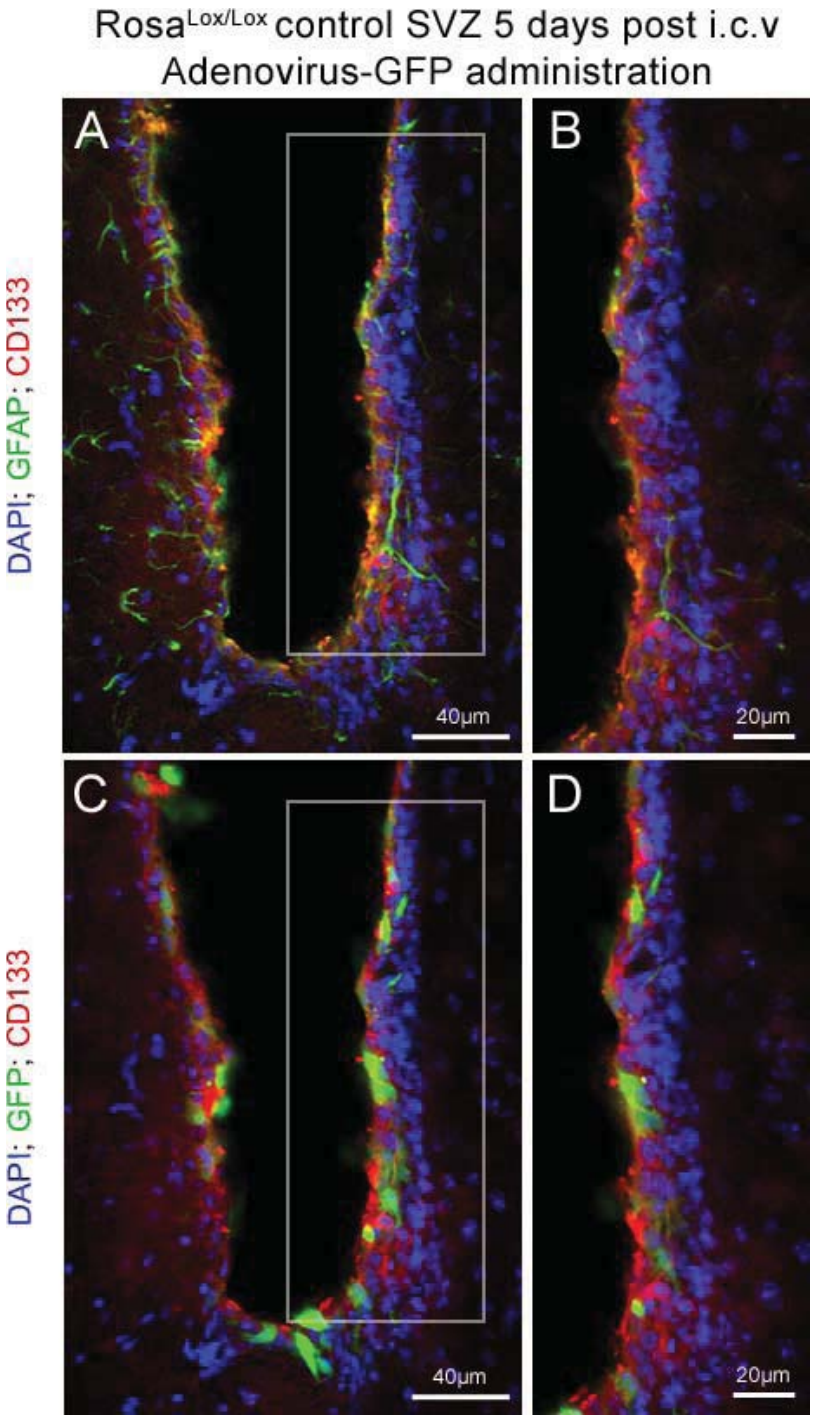

Figure 55: CD133 is expressed by SVZ cells, including GFAP-positive type B NSCs, and also by cells targeted for Adenovirus-GFP-infection. Representative images of the Rosa$^{Lox/Lox}$ wild-type SVZ 5 days post-i.c.v. Adenovirus-GFP administration immunofluorescently stained for GFAP and CD133 (A,B), or GFP and CD133 (C,D) with a Hoechst 33342 (DAPI) counterstain. Blue: excitation at 405nm, green: excitation at 488nm, red: excitation at 546nm. Images were taken using a 20x objective on a Zeiss LSM510 META confocal laser scanning microscope with the LSM software.

The SVZ of Rosa$^{Lox/Lox}$ mice was found to contain some GFAP-positive NSCs that co-expressed CD133 (Figure 55: A,B). This suggests that CD133 can also be expressed by

the GFAP-positive type B astrocytes of the SVZ (Doetsch et al., 1997). In addition, CD133 expression was observed by some ependymal cells and some GFAP-negative cells residing within the SVZ NSC niche, possibly including the transiently amplifying type C progenitor cells (Doetsch et al., 1999). Adenovirus-GFP-infected cells could be seen throughout the SVZ at five days post-i.c.v. administration, some of which were also CD133-positive (Figure 55: C,D). This confirms that i.c.v. Adenovirus administration targets CD133-expressing cells of the SVZ. An E14.5 mouse embryo was used as the positive control for this CD133 antibody (data not shown) on the basis that cells within both the developing brain and the kidneys are known expressors of CD133 (Miraglia et al., 1997; Corbeil et al., 1998). In addition, non-neurogenic brain parenchyma was used as the negative control.

To observe whether these CD133-positive SVZ cells survive SVZ micro-dissection and maintain their expression *in vitro*, we immunofluorescently stained free-floating NS (passage 3) generated from $Rosa^{Lox/Lox}$ control mice for CD133 and compared their expression against *in vitro* recombined $Rb^{-/-}$; $p53^{-/-}$; $PTEN^{-/-}$ NS (passage 4).

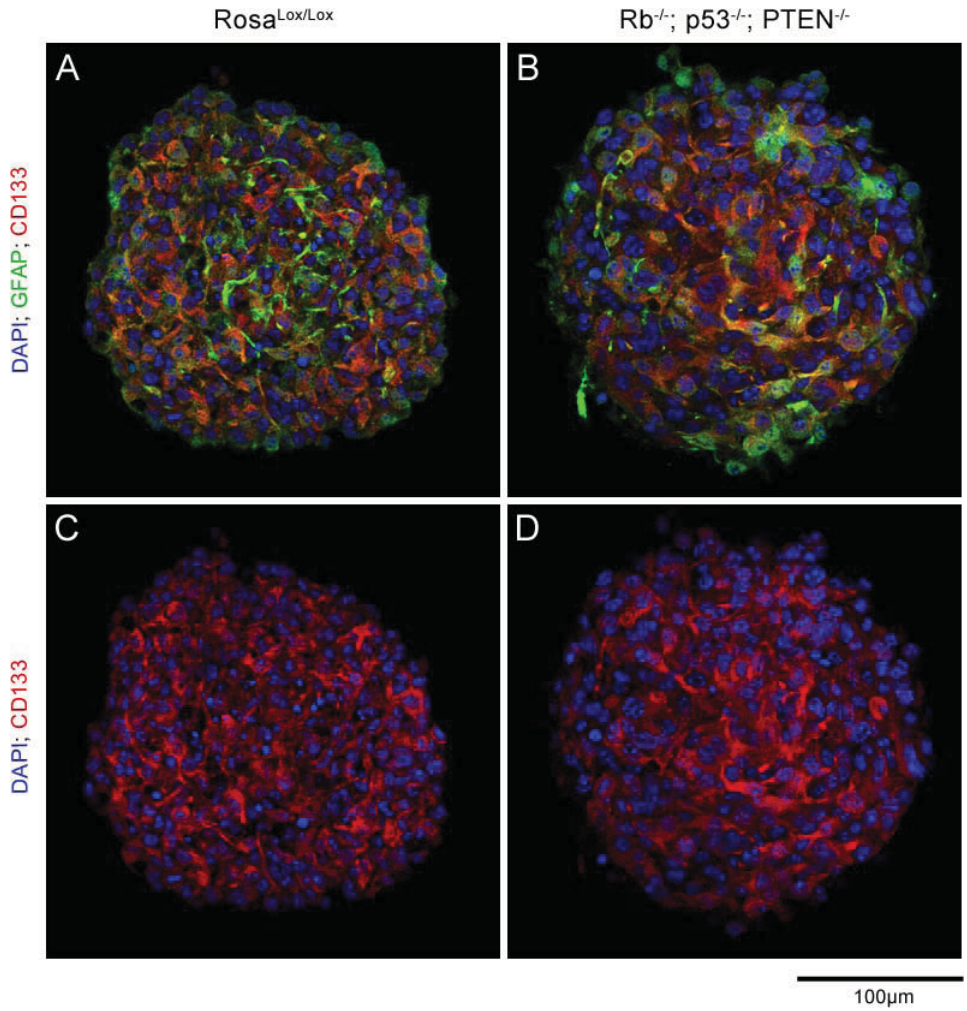

Figure 56: CD133 is expressed by both GFAP-positive/negative NS cells *in vitro*, with little immunofluorescent difference discernable between non-recombined Rosa$^{Lox/Lox}$ and *in vitro* recombined Rb$^{-/-}$; p53$^{-/-}$; PTEN$^{-/-}$ NS. (A,C) Representative images of Rosa$^{Lox/Lox}$ wild-type NS (passage 3) derived 5 days post-i.c.v. Adenovirus-GFP administration immunofluorescently stained for GFAP and CD133. (B,D) Representative images of *in vitro* recombined Rb$^{-/-}$; p53$^{-/-}$; PTEN$^{-/-}$ NS (passage 4) immunofluorescently stained for GFAP and CD133. All images include a Hoechst 33342 (DAPI) counterstain. Blue: excitation at 405nm, green: excitation at 488nm, red: excitation at 546nm. Images were taken using a 40x objective under oil immersion on a Zeiss LSM510 META confocal laser scanning microscope with the LSM software.

The Rosa$^{Lox/Lox}$ NS contained CD133-positive cells that were both GFAP-positive and negative, suggesting that the CD133-positive SVZ NSCs observed *in vivo* are included in *ex vivo* microdissection and maintain their expression *in vitro* (Figure 56: A,C). It has been proposed that CD133 is a marker of brain tumour initiating cells (Singh et al., 2004; Singh et al., 2003), however, no real difference in the level or pattern of CD133 expression was observed between the tumourigenic *in vitro* recombined Rb$^{-/-}$; p53$^{-/-}$; PTEN$^{-/-}$ NS (Figure 56: B,D) and the non-tumourigenic Rosa$^{Lox/Lox}$ NS. The proportion

of CD133-positive NS cells *in vitro* was large in comparison to the proportion observed *in vivo* and suggests that the *in vitro* microenvironment may preserve NSCs in an undifferentiated CD133-positive state. However, it is more likely to be indicative of non-specific staining caused by antibody trapping. Therefore, to accurately measure the proportion of CD133-positive cells we used single cell magnetic/fluorescence-activated cell sorting (MACS / FACS) and FACS analysis.

5.3.2 Wild-type neural stem cells equilibrate CD133 expression *in vitro*

Before studying the expression levels of CD133 in tumourigenic NSCs it is we verified the baseline pattern of CD133 expression in non-recombined NSCs. Non-recombined PTEN$^{Lox/Lox}$; p53$^{Lox/Lox}$ NSCs (passage four) were used as wild-type NSCs and were MACSorted into CD133- and CD133+ populations (Figure 57).

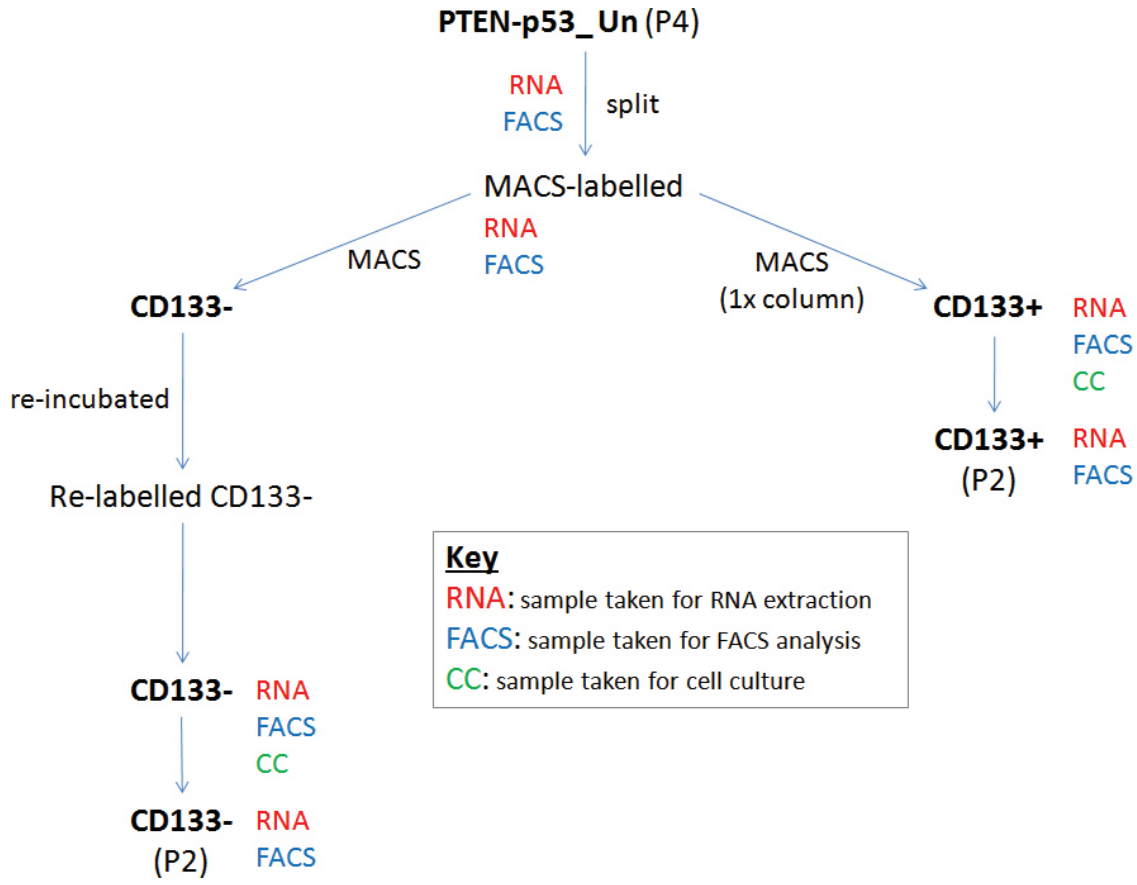

Figure 57: Schematic of the paradigm used for the MACSorting of non-recombined wild-type PTEN$^{Lox/Lox}$; p53$^{Lox/Lox}$ NSCs into CD133- and CD133 + populations *in vitro*. PTEN$^{Lox/Lox}$; p53$^{Lox/Lox}$ NS were split into single cells and labelled with mouse anti-CD133 magnetic MicroBeads and mouse anti-Prominin-1-PE-conjugated antibody for MACSeparation and downstream FACS analysis respectively. The NSCs were run through a MACS column and the CD133-/+ fractions were eluted into

two separate containers. The CD133+ fraction was sampled or added to NS medium and left for two passages. The CD133- fraction was re-labelled with anti-CD133 MicroBeads and run through a second MACS column for further purification before being sampled or added to NS medium and left for two passages.

A sample of unlabelled and unsorted NSCs was FACS-analysed in order to set the side scatter vs. forward scatter gate to only permit detection of viable and non-aggregated NSCs (Figure 58: A). The same population of cells was also used to set the M1 fluorescence threshold for positivity to include a false-positive detection of 2.8%, which was then corrected to a 0% baseline (Figure 58: B). The CD133-labelled NSCs were observed to contain 2.5% CD133+ve cells prior to being sorted (Figure 58: C). Immediately after MACSorting, the CD133- and CD133+ populations were found to contain 2.2% (Figure 58: D) and 47.9% (Figure 58: E) CD133+ cells respectively, and altered levels of 8.28% (Figure 58: F) and 6.92% (Figure 58: G) CD133+ cells after two passages. However, it should be noted that only side-scatter versus forward-scatter, and propidium iodide (data not shown), gating measures were taken to correct against non-specific staining of the CD133 antibody (as a result of cellular debris / aggregates and apoptotic cells). Therefore, without the inclusion of an isotype control it is possible that: a) non-specific binding of the CD133 antibody to cellular proteins, lipids, surface antigens (e.g. Fc receptors), and b) cellular autofluorescence, could have contributed to the observed fluorescence. For this reason, the results described here should be interpreted with caution.

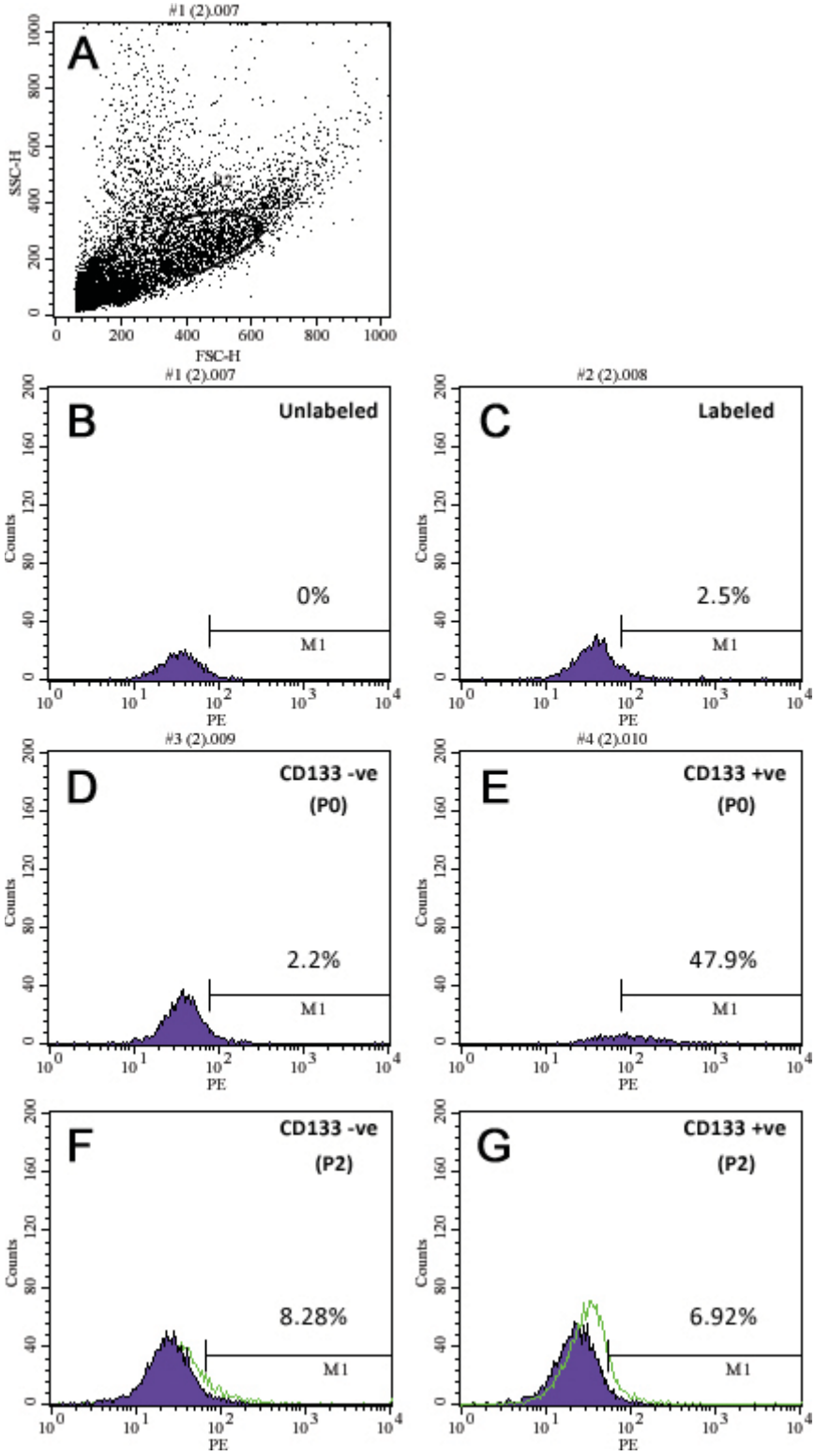

Figure 58: The level of CD133 expressed by MACSorted wild-type PTEN$^{Lox/Lox}$; p53$^{Lox/Lox}$ NSCs returns to equilibrium after two passages *in vitro*. (A) The FACS side scatter vs. forward scatter gate of detection was set to detect viable non-aggregated NSCs. An unlabelled and unsorted population of NSCs was used as the baseline control (B) against which the (C) labelled but unsorted, (D) MACSorted CD133- passage 0, (E) MACSorted CD133+ passage 0, (F) MACSorted CD133- passage 2 (G) MACSorted CD133+ passage 2 NSC populations were shown to contain 2.5%, 2.2%, 47.9%, 8.28%, and

6.92% CD133+ cells respectively. Purple curve: unlabelled control, green curve: overlay of labelled fraction.

The setting of a false-positive detection rate of 2.8% represents a technical limitation of FACS analysis as it is arbitrarily set. If inaccurate we could not be certain that a hypothetically 100% pure population of CD133- cells was in fact 100% pure. This could compromise the *in vivo* grafting experiments in which 100% purity of CD133-/+ cells is desired. In addition, the low shift in fluorescence intensity (Figure 58: C,E; ~0.5 log units) of CD133-positive cells is suggestive of weak expression, and makes accurate separation difficult. However, this could be addressed by using the more precise method of FACSorting. An additional source of error is highlighted by in Figure 58: E which shows the lack of a peak in the CD133+ population. This might suggest that the range of CD133 expression is particularly large but the lack of a peak is more indicative of the fact that we could only analyse a low number of 65,000 cells due to receiving a very small yield. This low yield of 131,000 CD133+ cells in total makes downstream analysis difficult. Despite this, the 21-fold difference in the proportion of CD133+ cells obtained in the CD133- and CD133+ fractions mean that a viable comparison of their functional properties is possible.

Interestingly, after being cultured for two passages post-sorting, the CD133 expression profile of the negative and positive populations had both altered. The number of CD133 expressing cells in the CD133- population increased from 2.2% to 8.28%, and conversely, the number of CD133+ cells in the CD133+ population reduced from 47.9% to 6.92%. This implies that wild-type NSCs equilibrate CD133 expression *in vitro* and that this change can take as little as two passages (~20 days). We hypothesise that the CD133-/+ NSCs may reach the original level of 2.5% CD133+ cells if left for additional passages. Interestingly, the elevation in the number of CD133+ NSCs observed in the CD133- fraction after two passages is suggestive of expression overcompensation. Alternatively, it may be possible that the MACSorting event altered the behavioural of the NSCs by placing a slight selection pressure on them, resulting in a distorted (>2.5%) CD133 expression equilibrium. This would suggest that CD133+ cells are more capable of surviving this selection pressure, much in the same way that they have also been shown to be more capable of surviving radiation (Bao et al., 2006).

To validate the CD133 expression overcompensation of the CD133- NSCs after two passages the level of CD133 RNA expression level was measured in parallel by reverse transcriptase PCR (rt-PCR).

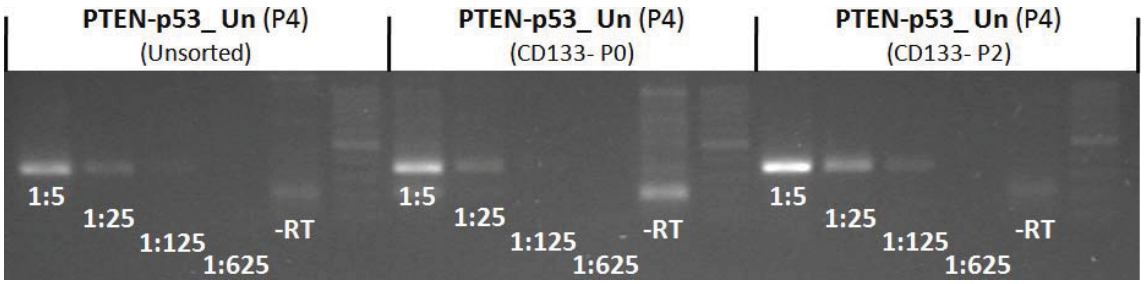

Figure 59: The expression level of CD133 RNA by MACSorted CD133- NSCs is seen to increase after 2 passages *in vitro*. Reverse transcriptase-PCR of CD133 RNA expression in unsorted vs. CD133-ve (P0) vs. CD133-ve (P2) neurospheres. The unsorted control cells and the P0 MACSorted CD133- cells exhibited similar titration patterns and 1:25 dilution band visibility, thus mirroring the FACS analysis finding (2.5% unsorted vs. 2.2% P0). After two passages *in vitro* this level of CD133 RNA expression was seen to increase, as shown by the RNA band visibility in the 1:125 dilution, once again mirroring the FACS analysis finding of increased CD133 protein expression (8.28%).

The FACS analysis showed that the CD133- (P0) population contained 2.2% CD133+ cells (Figure 58: D), similar to the 2.5% observed in the original unsorted population (Figure 58: C). This finding was mirrored at the RNA expression level as shown by the rt-PCR in which no difference could be observed between the same two populations (Figure 59: Unsorted vs. CD133- P0). The slight band seen in the 1:125 dilution of the unsorted cells but not the CD133- (P0) population may represent the 0.31% difference in CD133 expression observed in the FACS analysis. Interestingly, the correlation between the patterns of CD133 expression at the protein (FACS) and RNA (rt-PCR) levels suggests that they possess a 1:1 ratio. After two passages the CD133- population exhibited an increased level of CD133 as illustrated by the strong bands in the 1:5, 1:25, and 1:125 dilution lanes (Figure 59). This finding correlates with the FACS data that showed the expression of CD133 to rise from 2.2% (P0) to 8.28% (P2) (Figure 58: D,F).

This experiment was repeated using *in vitro* recombined NSCs to characterise the effect of tumourigenic transformation on CD133 expression.

5.3.3 Tumourigenic transformation of NSCs alters the pattern of CD133 expression *in vitro*

As the the genotype that produced tumours with the shortest latency, $Rb^{-/-}$; $p53^{-/-}$; $PTEN^{-/-}$ NSCs were chosen as the tumourigenic NSCs. *In vitro* recombined $Rb^{-/-}$; $p53^{-/-}$; $PTEN^{-/-}$ NSCs were taken at passage seven and MACSorted into CD133- and CD133+ populations (Figure 60).

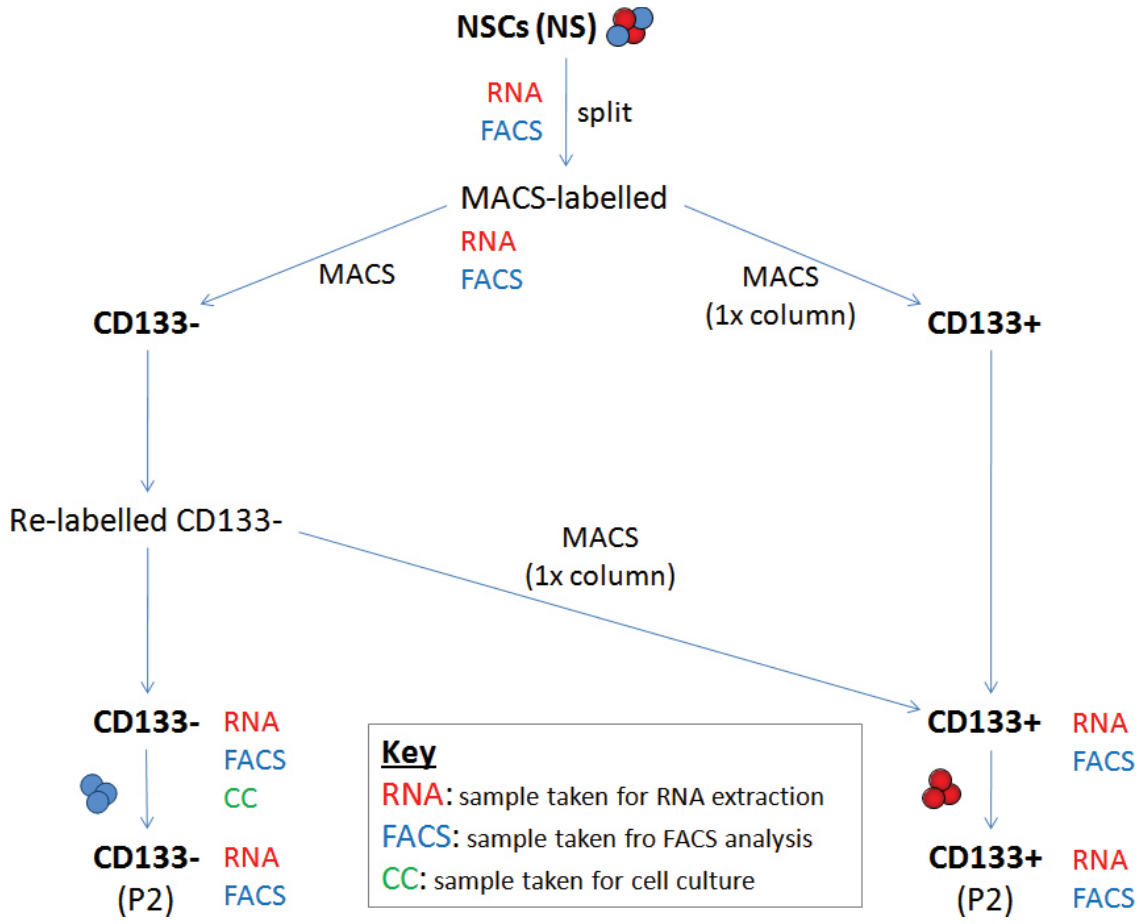

Figure 60: Schematic of the paradigm used for the MACSorting of tumourigenically transformed $Rb^{-/-}$; $p53^{-/-}$; $PTEN^{-/-}$ NSCs into CD133- and CD133 + populations *in vitro*. $Rb^{-/-}$; $p53^{-/-}$; $PTEN^{-/-}$ NS were split into single cells and labelled with mouse anti-CD133 magnetic MicroBeads and mouse anti-Prominin-1-PE-conjugated antibody for MACSeparation and downstream FACS analysis respectively. The NSCs were run through a MACS column and the CD133-/+ fractions were eluted into two separate containers. The CD133+ fraction was sampled or added to NS medium and left for two passages. The CD133- fraction was re-labelled with anti-CD133 MicroBeads and run through a second MACS column for further purification, after which the secondary yield of CD133+ NSCs were added to the primary yield, before being sampled or added to NS medium and left for two passages.

A false-positive detection of 3.0% was set as the baseline. Prior to sorting, the tumourigenic NSCs were found to contain 12% CD133+ cells (Figure 61: A), a notable increase over the 2.5% observed in the wild-type NSCs (Figure 58: C). Over serial passages both populations of the CD133- and CD133+ NSCs were once again observed to reach an equilibrium, but at a vastly different rate to the non-tumourigenic NSCs.

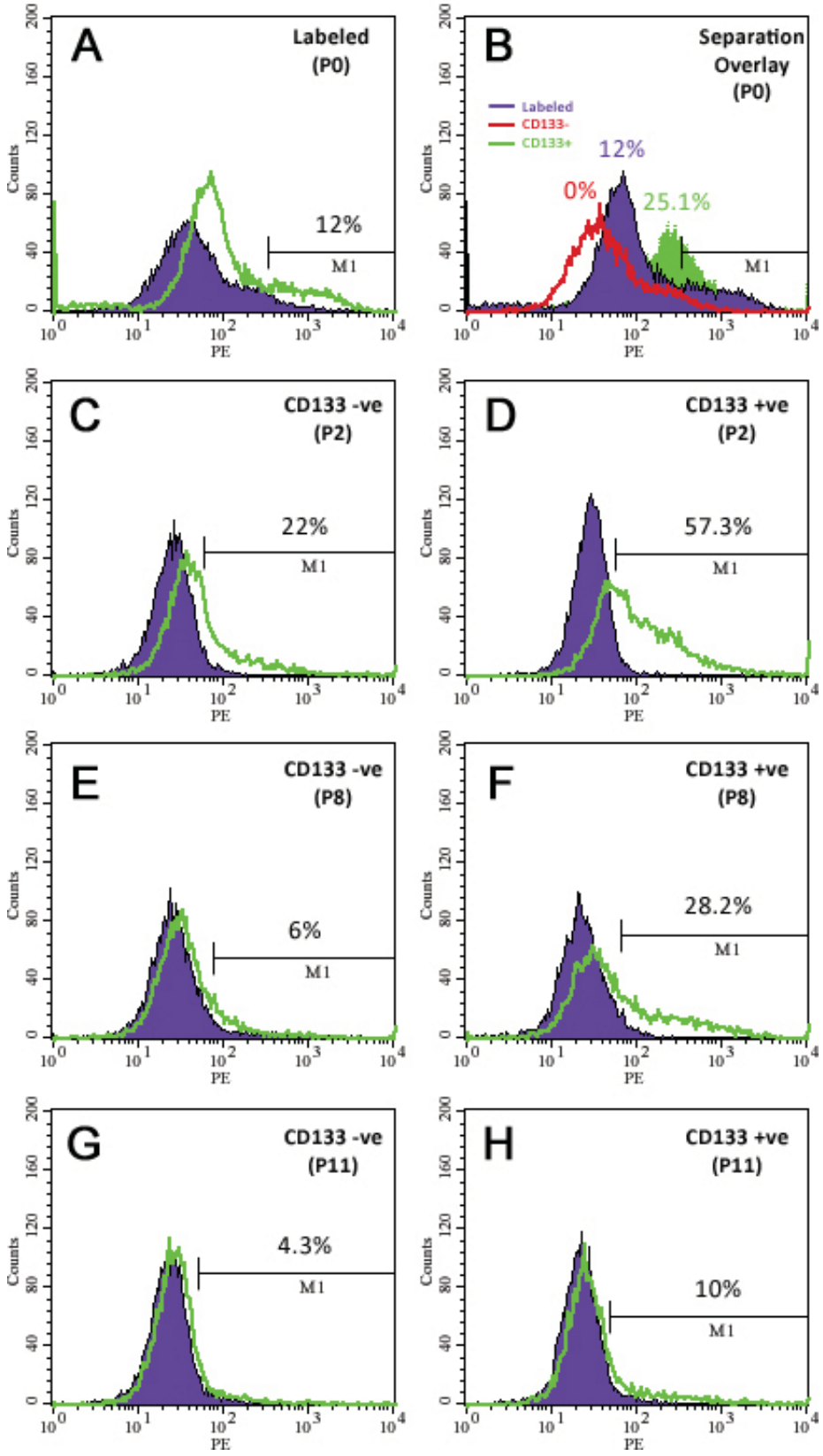

Figure 61: *In vitro* recombined and tumourigenic Rb$^{-/-}$; p53$^{-/-}$; PTEN$^{-/-}$ NSCs have an increased level of CD133 expression vs. wild-type NSCs which takes longer to equilibrate following MACSorting into CD133-/+ populations. FACS analysis showing the level of CD133 expression in Rb$^{-/-}$; p53$^{-/-}$; PTEN$^{-/-}$ NSCs prior to, and at zero, two, eight, and 11 passages after MACSorting. (A) The endogenous expression of CD133 in Rb$^{-/-}$; p53$^{-/-}$; PTEN$^{-/-}$ NSCs is 12%. Rb$^{-/-}$; p53$^{-/-}$; PTEN$^{-/-}$ NSCs were MACSorted

into CD133- and CD133+ populations that respectively contained 0% and 25.1% at passage 0 (B) to 22% (C) and 57.3% (D) after two passages, 6% (E) and 28.2% (F) after eight passages, and 4.3% (G) and 10% (H) after 11 passages. (A,C-H) Purple curve: unlabelled control, green curve: overlay of labelled fraction. (B) Red curve: MACSorted CD133- P0 fraction, purple curve: underlay of labelled but unsorted fraction, green curve: underlay of MACSorted CD133+ P0 fraction.

The number of CD133 expressing cells for the CD133- and CD133+ MACSorted populations respectively changed from 0% and 25.1% (Figure 61: B) at passage 0 (immediately after sorting) to 22% (Figure 61: C) and 57.3% (Figure 61: D) after two passages, 6% (Figure 61: E) and 28.2% (Figure 61: F) after eight passages, and 4.3% (Figure 61: G) and 10% (Figure 61: H) after 11 passages. This suggests that tumourigenic NSCs possess an altered rate of CD133 expression equilibration, potentially because of CD133 expression-associated functional differences. To validate this finding protein samples were extracted from NS at post-MACSorting passages one and seven. Passage one and seven NS were chosen, rather than passage two and eight NS, because the passage one and seven NS were dissociated into single NSCs which were then immediately FACS-analysed to give the results given as P2 and P8 (Figure 61: C-F). We hypothesised that the number of CD133-expressing cells could change by the time 12 day old NS at passage two and eight were ready to be sampled, and concluded that the 12 day old passage one and seven NS were more representative of the single passage two and eight NSCs that were FACS-analysed. For comparison purposes, a protein sample was also taken from single NSCs at passage eight to examine the effect of NS dissociation on detection of the surface antigen CD133. Such surface antigens are exposed to the action of the protease-based dissociation chemical.

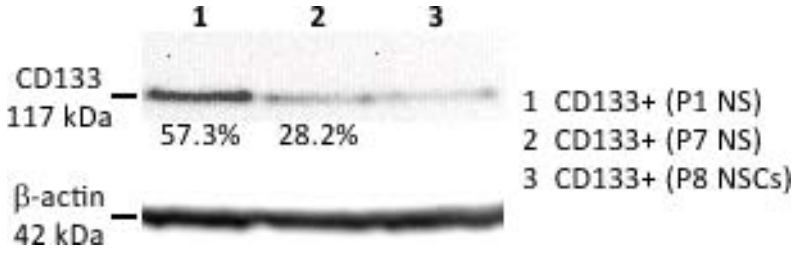

Figure 62: The reduction of CD133 intensity observed from the CD133+ (P1 NS) band to the CD133+ (P7 NS) band mirrors the reduction in CD133 expression observed from the FACS-analysis shown in Figure 61 (percentage CD133+ expression given). Western blot for CD133 expression in the MACSorted CD133+ $Rb^{-/-}$; $p53^{-/-}$; $PTEN^{-/-}$ NSCs at one, seven, and eight passages post-sort. The CD133+ (P8 NSCs) band appears less intense than that of the P7 NS, from which they were

derived, suggesting that NS-NSC dissociation reduces CD133 expression. The percentages associated with bands 1 and 2 are the respective proportions of CD133+ cells as measured in parallel by FACS .

FACS analysis of the CD133+ $Rb^{-/-}$; $p53^{-/-}$; $PTEN^{-/-}$ NSCs at passages two and eight post-MACSorting showed that the number of CD133+ cells had reduced from 57.3% to 28.2% (Figure 61). This reduction was validated by Western blot which showed a similar reduction in expression (Figure 62). Interestingly, the CD133+ (P8 NSCs), which were derived from the P7 NS, appear to exhibit an even lower level of CD133 expression. Using the KODAK 1D Image Analysis Software we have been able to quantify these changes.

Band	Recombination Paradigm	Genotype (cells)	Net CD133 Intensity	Net β-actin Intensity	Corrected CD133 Intensity
1	*In vitro* recombined (Adeno-Cre) MACSorted CD133 +ve (P1 NS)	Rb/p53/PTEN_Cre	8422	90333	93.23
2	*In vitro* recombined (Adeno-Cre) MACSorted CD133 +ve (P7 NS)	Rb/p53/PTEN_Cre	3999	82830	48.28
3	*In vitro* recombined (Adeno-Cre) MACSorted CD133 +ve (P8 NSCs)	Rb/p53/PTEN_Cre	2337	88416	26.43

Figure 63: Table of the corrected CD133 expression intensities for each of the Western blot MACSorted CD133+ fraction bands in Figure 62. The corrected CD133 band intensities support and confirm the reduction in CD133 expression observed in the CD133+ population over serial passages, as originally shown in Figure 61 by FACS analysis. The net intensity was calculated as the sum of the background-subtracted pixel intensity values within the band area defined. The corrected intensity was calculated as (Net CD133 Intensity / Net β-actin Intensity)*1000.

The semi-quantitative analysis of these bands confirms that we can indeed see a reduction in the CD133 expression of MACSorted CD133+ cells between the P1 NS and the P7 NS. In addition, the 48.2% reduction in CD133 expression obtained from the Western blot (Figure 63: Band 1 vs. band 2) matches the 50.8% reduction obtained from the FACS analysis (Figure 61). Interestingly, the act of dissociating NS into single NSCs caused a reduction in CD133 expression of 45.3% (a reduction in corrected intensity from 48.28 to 26.43) (Figure 63). This suggests that a ~45% overestimation in CD133 protein expression is observed by Western blot if representative NS are used instead of the single NSCs used for FACS-analysis. In addition, it appears that CD133 expression increases temporally over the ~12 days of a passage, otherwise a 45% dissociation-based reduction in CD133 expression would translate into the observed 10% equilibrium having been achieved at passage five instead of passage 11.

The CD133+ NSCs isolated from the MACSort were only 25.1% pure when compared to the 47.9% purity achieved with the wild-type NSCs, despite an elevated baseline endogenous expression of 12%. This level of 25.1% CD133 expression in the CD133+ population was generated from a larger yield of cells with a better defined fluorescence peak. However, the unsorted but labelled NSCs exhibited an extended skew of fluorescence covering an entire log unit on the upper boundary of their FACS plot (Figure 64: B). This will have resulted in the setting of an artificially high M1 fluorescence threshold and a subsequent underestimation of the level of CD133 expression. Therefore, the 25.1% proportion of CD133+ cells may have been closer to the 57.3% observed after two passages (Figure 61: D). This may explain the presence of an overcompensation of the number of CD133+ cells after two passages by a population whose expression of CD133 was expected to decrease. However, from the side scatter vs. forward scatter plot (Figure 64: A) for the unsorted NSCs it can be seen that the cells lacked distinct populations and that the cellular debris (SSC-H <300, FSC-H<300) merged into the gated viable population. This may explain the skewed fluorescence of the NSCs as some auto-fluorescent debris will have been included in the viable cell gate and whose could have intensified the output of the fluorescent Phycoerythrin (PE) dye.

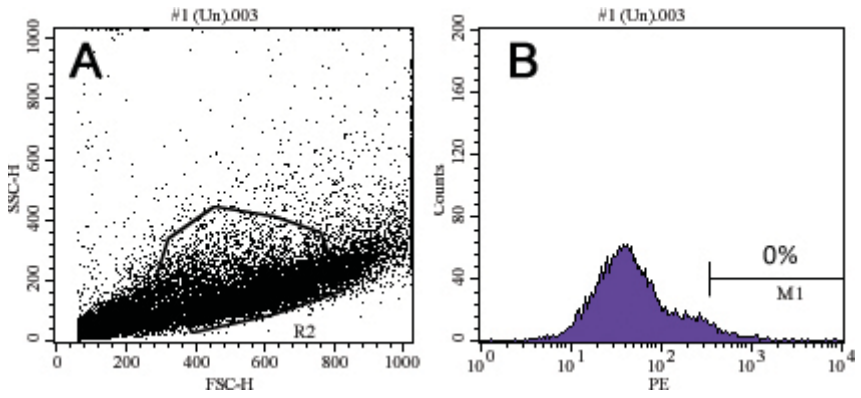

Figure 64: An excess of cellular debris and a lack of distinct populations interferes with selecting a viable population gate and results in a skewed fluorescence plot. FACS plots illustrating the gate of detection set for MACSorting the $Rb^{-/-}$; $p53^{-/-}$; $PTEN^{-/-}$ NSCs. (A) The side-scatter (SSC-H) vs. forward-scatter (FSC-H) FACS plot highlights the lack of distinct populations of cells within the sample being analysed, hence the difficult setting of a gate of detection which is likely to have included cellular debris. (B) This inclusion of this debris may adversely interact with the viable NSCs and/or the antibody to cause the fluorescence skew observed in the unsorted population.

Previously we showed that it took two passages for wild-type MACSorted CD133-/+ NSCs to reach a CD133 expression equilibrium of ~7.5% (Figure 58). In contrast, the $Rb^{-/-}$; $p53^{-/-}$; $PTEN^{-/-}$ CD133- NSCs took eight passages to return to an equilibrium of 6% and the CD133+ NSCs were still only approaching a hypothesised equilibrium of 10% after 11 passages (Figure 65).

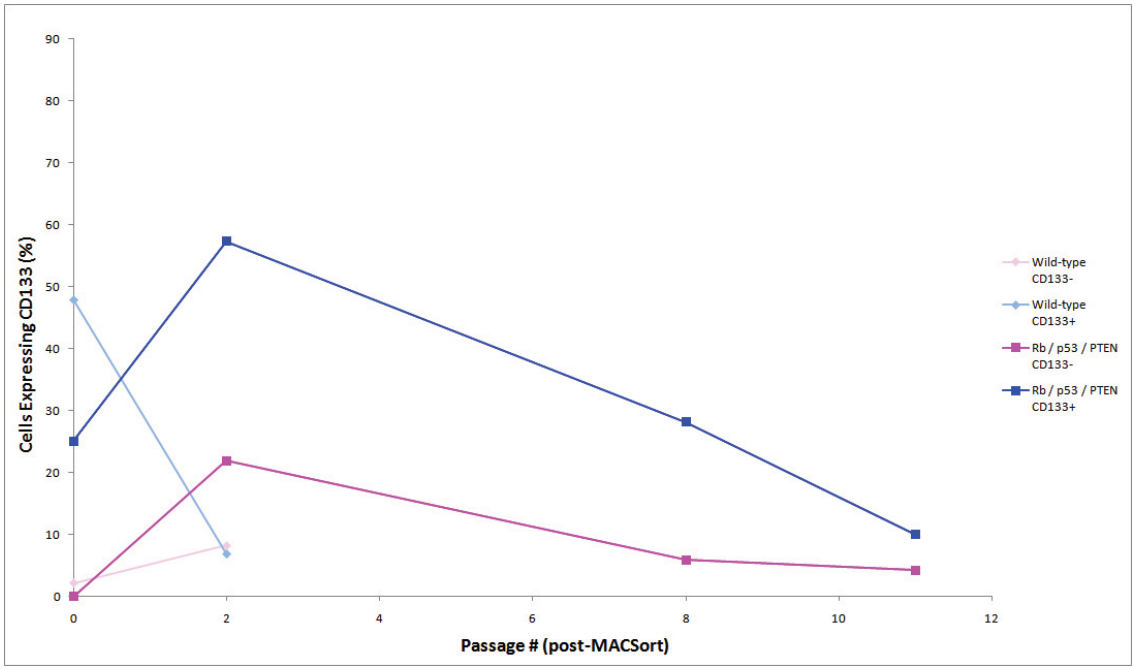

Figure 65: FACS analysis of CD133 expression in NSCs over serial passages following MACSorting for CD133-/+ shows that both populations of wild-type NSCs return to a CD133 expression equilibrium after two passages whereas *in vitro* recombined and tumourigenic $Rb^{-/-}$; $p53^{-/-}$; $PTEN^{-/-}$ NSCs take up to 11 passages. A line plot of the percentage of NSCs expressing CD133 post-MACSorting (y-axis) over serial passages (x-axis).

The $Rb^{-/-}$; $p53^{-/-}$; $PTEN^{-/-}$ CD133- and CD133+ NSC population equilibrations have trend line slopes of -2.1 and -5.2 respectively (ignoring the overcompensation observed between passages zero and two). The increased negative slope (faster rate of equilibration) of the CD133+ population may be caused by a functional quality, or alternatively the mechanism of equilibration could be entirely expression-dependent with the increased CD133+ equilibration a consequence of higher initial expression. The latter is difficult to explain as the wild-type CD133+ NSCs had the highest rate of equilibration (Figure 65: Pale blue line, slope: -20.5). We therefore hypothesise that the different equilibration rates are determined by functional differences. This study was repeated using a second population of $Rb^{-/-}$; $p53^{-/-}$; $PTEN^{-/-}$ NSCs from which only the

CD133+ population was isolated. This repeat population of the tumourigenic NSCs were found to contain 13.8% CD133+ cells (data not shown), therefore validating the previously acquired figure of 12%.

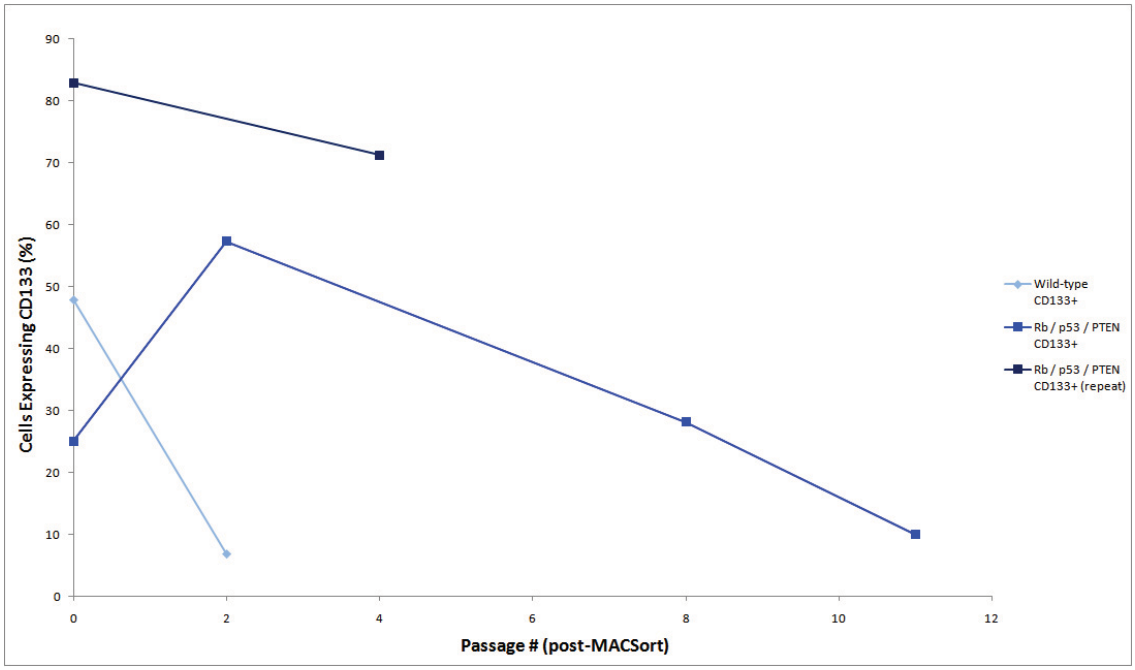

Figure 66: FACS analysis of CD133 expression in a repeat population of MACSorted CD133+ $Rb^{-/-}$; $p53^{-/-}$; $PTEN^{-/-}$ NSCs shows that the observed CD133 expression equilibration is a reproducible effect (up to passage 4). A line plot of the percentage of NSCs expressing CD133 post-MACSorting (y-axis) over serial passages (x-axis).

The repeat $Rb^{-/-}$; $p53^{-/-}$; $PTEN^{-/-}$ CD133+ NSCs exhibited an equilibration slope of -2.93 (Figure 66), which is different from the previously observed slope of -5.2 and is in fact more similar to the CD133- NSC equilibration slope of -2.1. This suggests that variation in the health of the cells influences the equilibration rate. No CD133 expression overcompensation was observed in the repeat CD133+ NSCs, which began with a remarkably high purity of 82.9% (Figure 66). This highlights that a) the MACSorting technique has an inherent variability most likely based on NSC health state, and b) the observed overcompensation of CD133 expression in the $Rb^{-/-}$; $p53^{-/-}$; $PTEN^{-/-}$ CD133+ NSCs (Figure 61: B,D) was indeed an anomalous finding caused by an underestimation of the initial level of CD133 expression.

Interestingly, as seen with the wild-type NSCs, the expression of CD133 by the CD133- $Rb^{-/-}$; $p53^{-/-}$; $PTEN^{-/-}$ NSCs was observed to overcompensate from 0% CD133+ cells at

passage 0 to 22% after two passages (Figure 61: C). It is possible that the lower starting CD133 expression level of 0% drove an exacerbated overcompensation. The CD133 expression equilibria attained by the $Rb^{-/-}$; $p53^{-/-}$; $PTEN^{-/-}$ CD133-/+ (4.3%/10%) NSCs after 11 passages are lower than the starting level of expression (12%), with the converse being true for the wild-type NSCs. This reinforces our earlier suggestion that the level of CD133 expression in the CD133-/+ wild-type NSCs would have reduced further over additional passages. For this reason, it is difficult to state that the CD133 expression equilibrium to which NSCs reset themselves following MACSorting is different from the resting equilibrium observed in unsorted control NSCs. We do, however, propose that *in vitro* recombined $Rb^{-/-}$; $p53^{-/-}$; $PTEN^{-/-}$ NSCs possess an elevated basal level of CD133 expression as well as an altered pattern of CD133 expression when compared to wild-type controls, most likely as a result of functional changes brought about by tumourigenic transformation. In addition, the presence of an equilibrium implies that CD133 expression is regulated by the NSC microenvironment.

To test the hypothesis that CD133-/+ $Rb^{-/-}$; $p53^{-/-}$; $PTEN^{-/-}$ NSCs possess different functional characteristics we examined their growth rate and NS-forming ability *in vitro*.

5.3.4 CD133 expression influences growth rate but not the NS-forming ability of tumourigenic NSCs *in vitro*

Our findings suggest that *in vitro* recombination of Rb, p53, and PTEN alters CD133 expression as $Rb^{-/-}$; $p53^{-/-}$; $PTEN^{-/-}$ NS possessed a higher proportion of CD133+ NSCs (12%) than wild-type NSCs (2.5%). Also, more passages were needed by $Rb^{-/-}$; $p53^{-/-}$; $PTEN^{-/-}$ NS to reach an equilibrium of ~7.5% CD133+ cells. We hypothesise that these alterations in CD133 expression are as a result of acquired / induced functional property changes in the NSCs. In an attempt to elucidate these behavioural differences *in vitro* we assayed MACSorted CD133-/+ $Rb^{-/-}$; $p53^{-/-}$; $PTEN^{-/-}$ NSCs for their growth rate (WST-1 assay) and NS-forming ability (NS size and NS-forming clonogenicity assay). Using the WST-1 assay we measured the mitochondrial activity (as a surrogate marker of growth rate) of NSCs at 0, 2, 4, and 8 hours after a 3 day incubation period.

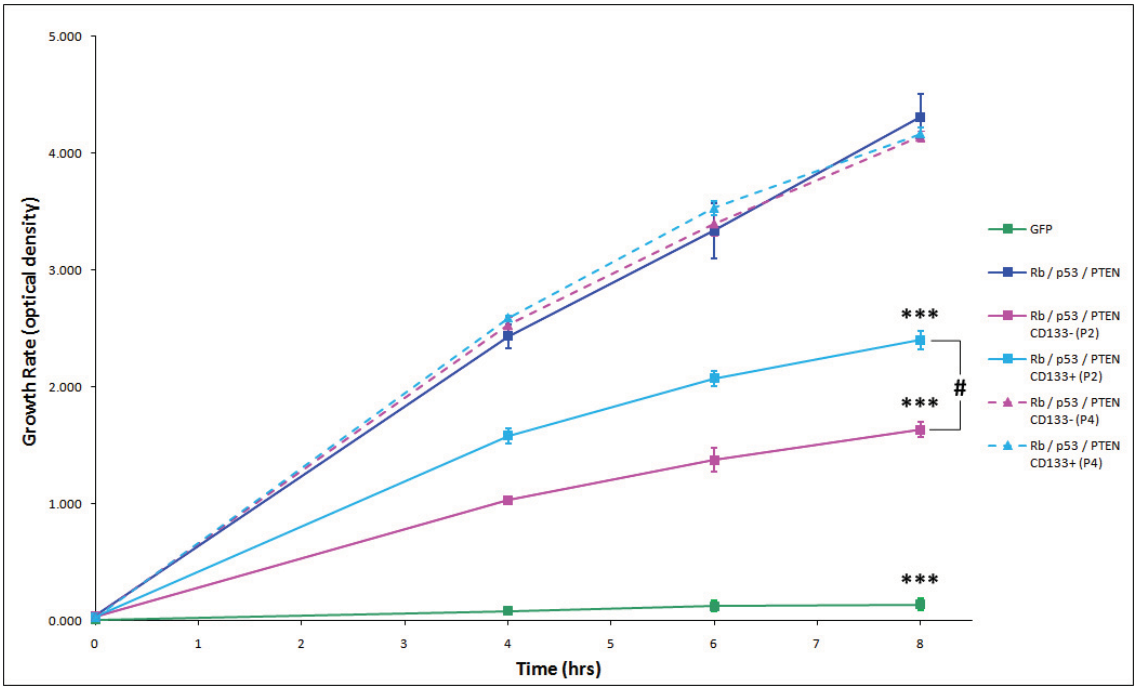

Figure 67: CD133-/+ NSCs appear to have a reduced growth rate at 2 passages post-MACSorting which corrects back to the level exhibited by the unsorted controls after 4 passages. The difference observed between the CD133- and CD133+ NSC populations after 2 passages also disappears after 4 passages, suggesting a normalisation or equilibration. Using the WST-1 assay the growth rate (y-axis) of NSCs (growing as NS) was measured at 0, 2, 4, and 8hrs (x-axis) after a 3 day incubation period. Growth rate of *in vitro* recombined $Rb^{-/-}$; $p53^{-/-}$; $PTEN^{-/-}$ NSCs at 2 (block lines) and 4 (dotted lines) passages post-MACSorting for CD133- (pink: n=2) / CD133+ (blue: n=2) vs. unsorted controls (dark blue: n=3) vs. non-recombined Adenovirus-GFP-infected controls (green: n=6). Error bars: standard errors. ***: $P<0.001$ vs. $Rb^{-/-}$; $p53^{-/-}$; $PTEN^{-/-}$ NSCs at 8hrs, #: $P<0.05$ (one-way ANOVA with Bonferroni's multiple comparison correction).

After two passages, the unsorted control $Rb^{-/-}$; $p53^{-/-}$; $PTEN^{-/-}$ NSCs grew significantly faster than the MACSorted CD133+ cells, which also grew significantly faster than their CD133- counterparts (Figure 67). All of these cells grew significantly faster than the non-tumourigenic Adenovirus-GFP-infected control NSCs. After four passages the growth rate of both the MACSorted CD133-/+ cells had increased to a statistically similar rate as the unsorted controls, and the difference between the CD133+ and CD133- had disappeared. We have already shown that CD133+ $Rb^{-/-}$; $p53^{-/-}$; $PTEN^{-/-}$ NSCs have a faster equilibration rate than their CD133- counterparts, and attributed this difference to a hypothesised functional difference. That difference is illustrated by these findings from passage two in which the CD133+ NSCs are observed to have a faster growth rate than the CD133- NSCs. Interestingly, this difference had disappeared as the growth rates of both the CD133-/+ NSCs had returned to normal levels after four

passages, a passage number at which the equilibration of CD133 expression was still in progress (Figure 65).

As an indicator of NS-forming ability we measured the size of the NS formed by the NSCs when left in culture for eight days.

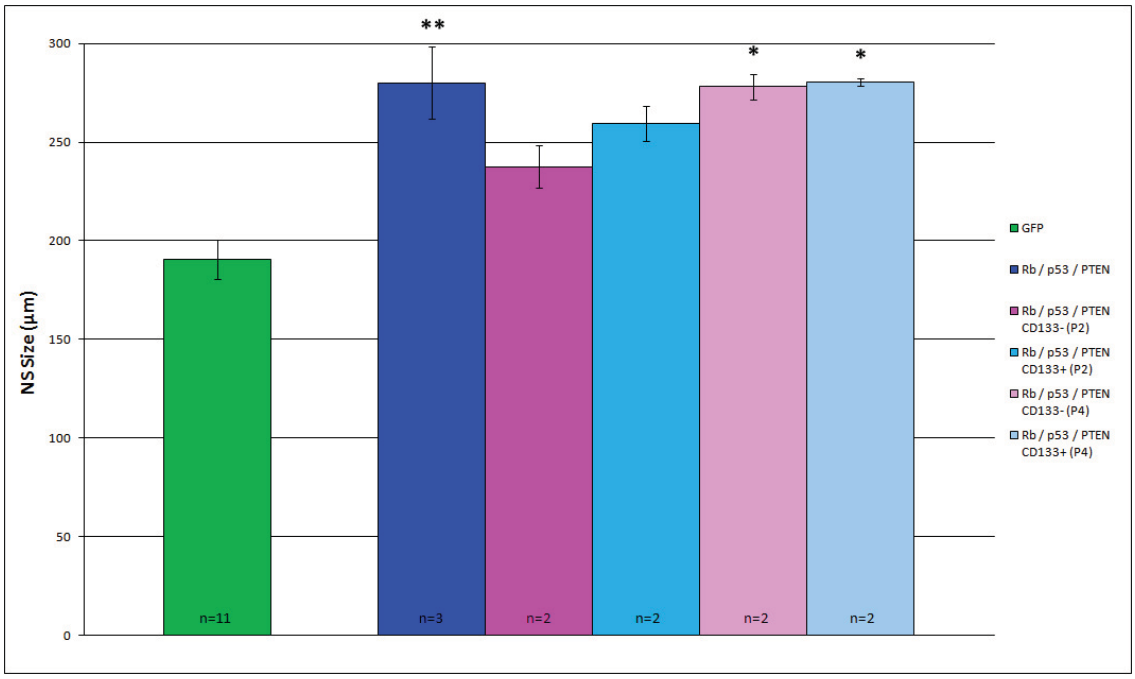

Figure 68: MACSorted Rb$^{-/-}$; p53$^{-/-}$; PTEN$^{-/-}$ CD133-/+ NSCs appear to form smaller NS than their unsorted counterparts after 2 passages, but NS of the same size after 4 passages. The difference observed between the CD133- and CD133+ NSC populations after 2 passages also disappears after 4 passages, suggesting a normalisation or equilibration. NSCs were seeded into NS medium and left to grow as NS for eight days before their diameters were measured using an Axiovert 135 microscope (Zeiss) and the Openlab 5 software package. NS size of non-recombined Adenovirus-GFP-infected controls (green: n=11) vs. *in vitro* recombined unsorted Rb$^{-/-}$; p53$^{-/-}$; PTEN$^{-/-}$ NSC controls (dark blue: n=3) vs. Rb$^{-/-}$; p53$^{-/-}$; PTEN$^{-/-}$ NSCs MACSorted for CD133- (pink: n=2) and CD133+ (blue: n=2) cells at passage 2 vs. Rb$^{-/-}$; p53$^{-/-}$; PTEN$^{-/-}$ NSCs MACSorted for CD133- (pale pink: n=2) and CD133+ (pale blue: n=2) cells at passage 4. Error bars: standard errors. *: P<0.05 vs. GFP control, **: P<0.01 vs. GFP control (one-way ANOVA with Bonferroni's multiple comparison correction).

The NS size assay confirmed the growth-difference observed in the WST-1 assay, but was less marked. In this assay the unsorted control Rb$^{-/-}$; p53$^{-/-}$; PTEN$^{-/-}$ NSCs formed the significantly largest NS (Figure 68). And although the MACSorted CD133+/- NSCs at passage two appeared to form smaller NS than the Rb$^{-/-}$; p53$^{-/-}$; PTEN$^{-/-}$ NSCs, this difference was in fact non-significant. In addition, no significant difference was

observed between the size of the CD133+ and CD133- NS at passage two. However, the passage four CD133+/- NS were significantly larger than the controls. This suggests that there is also a CD133 expression-related equilibration in NS-forming ability. The reductions in growth rate and NS-forming ability of the CD133- and CD133+ NSCs at passage (from the unsorted $Rb^{-/-}$; $p53^{-/-}$; $PTEN^{-/-}$ NSCs) were less significant in the case of the NS size assay than the WST-1 assay (~15% and ~7% vs. ~60% and 40% respectively). However, both assays confirm the functional differences of the unsorted, CD133+ and CD133- NSCs.

In addition, an NS-forming clonogenicity assay was used to measure the NS-forming ability of the same CD133-/+ $Rb^{-/-}$; $p53^{-/-}$; $PTEN^{-/-}$ NSCs.

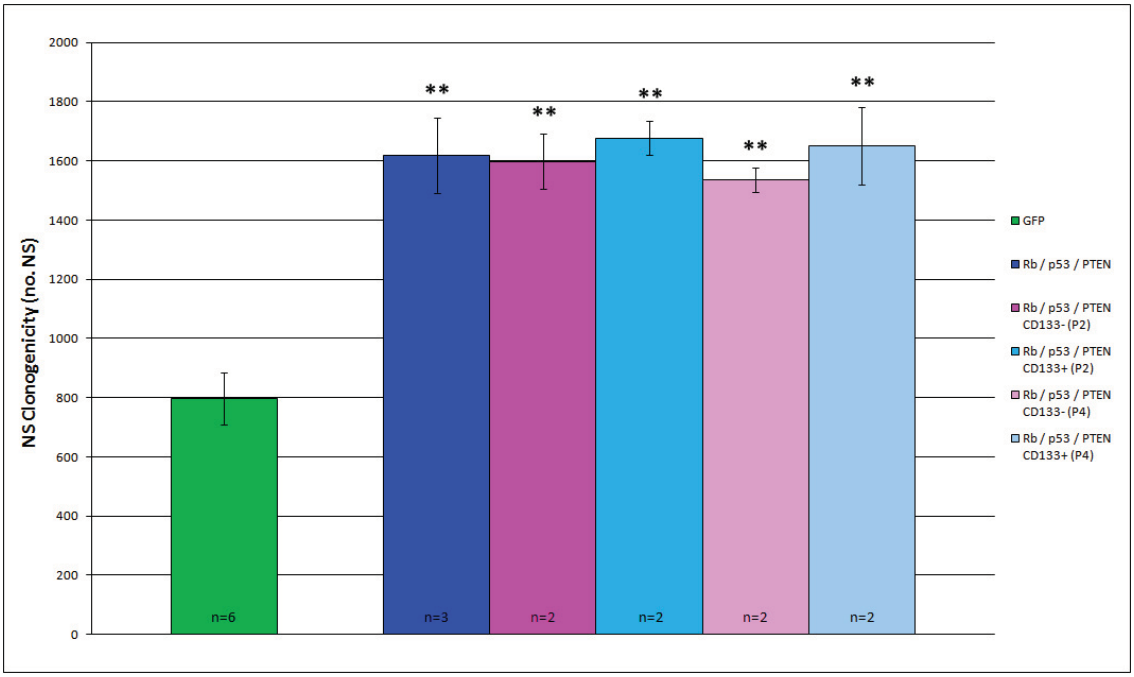

Figure 69: MACSorting for CD133-/+ NSCs has no effect on the NS-forming ability of the cells as no significant difference can be observed between any of the CD133-/+ populations and the unsorted control. NSCs were seeded in medium and left to grow for eight days before the number of NS formed was counted. NS-forming ability of non-recombined Adenovirus-GFP-infected controls (green: n=6) vs. *in vitro* recombined unsorted $Rb^{-/-}$; $p53^{-/-}$; $PTEN^{-/-}$ NSC controls (dark blue: n=3) vs. $Rb^{-/-}$; $p53^{-/-}$; $PTEN^{-/-}$ NSCs MACSorted for CD133- (pink: n=2) and CD133+ (blue: n=2) cells at passage 2 vs. $Rb^{-/-}$; $p53^{-/-}$; $PTEN^{-/-}$ NSCs MACSorted for CD133- (pale pink: n=2) and CD133+ (pale blue: n=2) cells at passage 4. Error bars: standard errors. **: $P<0.01$ vs. GFP control (one-way ANOVA with Bonferroni's multiple comparison correction).

The unsorted $Rb^{-/-}$; $p53^{-/-}$; $PTEN^{-/-}$ NSCs and MACSorted CD133+/- NSCs at passage two and four all had significantly increased NS-forming abilities when compared against the Adenovirus-GFP-infected control NSCs (Figure 69). Despite previously showing an interaction between CD133 expression and growth rate, no statistical difference was observed between the CD133 expression profile and NS-forming ability of the unsorted versus CD133+/- $Rb^{-/-}$; $p53^{-/-}$; $PTEN^{-/-}$ NSCs. Previous studies support this lack of functional difference between CD133+ and CD133- NSCs (Clement et al., 2009).

Previously we disregarded that the equilibration rate is CD133 expression-dependent as the wild-type CD133+ NSCs, despite having a comparable level of CD133 expression (post-MACSorting) to their tumourigenic counterparts, exhibited the fastest equilibration rate of all. However, we hypothesise that MACSorting for CD133 expression may select for a specific sub-population of NSCs. There are at least three sub-populations of NSCs in the SVZ, each with different functional properties (Doetsch et al., 1997). If we assume that NSCs exist as a heterogeneous population *in vitro*, MACSorting for CD133-/+ NSCs may essentially be purifying for specific NSC sub-populations, which could be delineated by their functional properties *in vitro*. Alternatively, others have shown that CD133 is downregulated by HIF1α in response to hypoxic conditions (Matsumoto et al., 2009), indicating that CD133 expression may be a reflection of NSCs environmental conditions and provide no insight into NSC sub-type classification. This latter suggestion would mean that the increased CD133 expression and reduced rate of CD133 equilibration observed following tumourigenic transformation was a manifestation of tumourigenic NSCs being more resistant to *in vitro* hypoxia, and therefore exhibiting less response in the form of downregulated CD133 expression. Or that CD133 expression correlates with hypoxia resistance and that tumourigenic $Rb^{-/-}$; $p53^{-/-}$; $PTEN^{-/-}$ NSCs therefore have a higher endogenous level of CD133 expression when compared to wild-type NSCs. This hypothesis would mean that only the survival rates of CD133-/+ NSCs in hypoxic conditions should be different and that the *in vivo* tumourigenic capacity of isolated CD133- and CD133+ $Rb^{-/-}$; $p53^{-/-}$; $PTEN^{-/-}$ NSCs should be the same. To test this hypothesis we examined the *in vivo* tumour hit rates, latencies, and phenotype propensities of intracerebrally engrafted CD133- and CD133+ $Rb^{-/-}$; $p53^{-/-}$; $PTEN^{-/-}$ NSCs.

5.3.5 *In vivo* engraftment of CD133+ versus both CD133- and unsorted Rb$^{-/-}$; p53$^{-/-}$; PTEN$^{-/-}$ NSCs results in the preferential development of gliomas

Both MACS and FACS methods were used to isolate Rb$^{-/-}$; p53$^{-/-}$; PTEN$^{-/-}$ CD133- and CD133+ NSCs. It was previously mentioned (section 5.3.2) that MACSorting may not be sensitive enough for the purpose of *in vivo* cell grafting experiments as the purity of the CD133-/+ populations cannot be guaranteed. For the purposes of distinguishing the different *in vivo* properties of CD133- and CD133+ NSCs *in vivo* it could be argued that 100% purities are required for both populations to be grafted. The two methods of separation were compared to test this hypothesis.

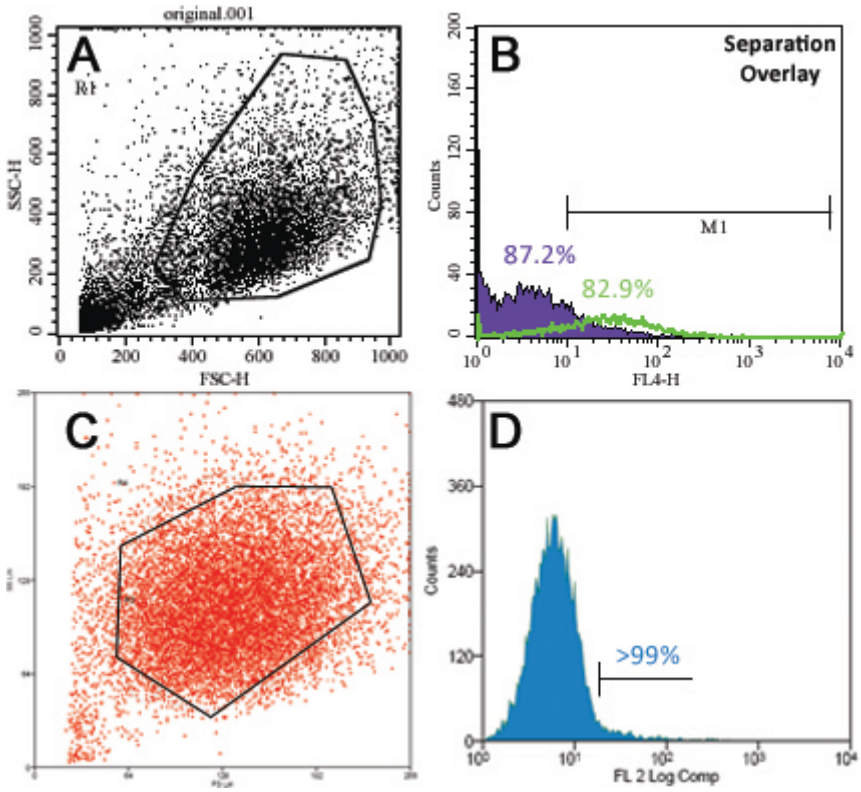

Figure 70: FACSorting NSCs for CD133 achieves greater CD133-/+ isolate purities than MACSorting. FACS plots showing the CD133-/+ NSC purities achieved using MACSorting (A,B) and FACSorting (C,D). Side-scatter vs. forward-scatter FACS plot of the MACSorted (A) and FACSorted (C) NSCs showing the gated regions of detection. Fluorescence FACS plots of the CD133- (purple) and CD133+ (green) NSCs showing that the purities of the MACSorted (B) isolates are 87.2% and 82.9% respectively, whereas those of the FACSorted (D) are both >99%.

The purities of the MACSorted CD133- and CD133+ isolates were 87.2% and 82.9% respectively (data not shown). In comparison, FACSorting $Rb^{-/-}$; $p53^{-/-}$; $PTEN^{-/-}$ NSCs for CD133- /+ populations achieved an impressive >99% purity in both cases (Figure 70). The first MACSorting experiment used two pooled cohorts of mice (n=16) separately grafted with unsorted $Rb^{-/-}$; $p53^{-/-}$; $PTEN^{-/-}$ NS as the controls. The second FACSorting experiment used the same controls but with an additional cohort of mice (n=8) grafted with dissociated but unsorted $Rb^{-/-}$; $p53^{-/-}$; $PTEN^{-/-}$ single NSCs.

Experiment	Cell Recombination Paradigm	Vol. Injected (ul)	Passage #	Genotype (cells)	# Mice	Age (start)	Age (end)	Incubation (d)	Cause of Death	Diagnosis
11/08/2008	*In vitro* recombined (Adeno-Cre)	7	5	Rb / p53 / PTEN / Rosa	2					
	FACSorted CD133 +ve	~35,700 cells				89	216	**127**	sick, lump on head (tumour)	Glioma (extracranial with fibroblastic infiltration) #
						89	343	**254**	sick, abnormal breathing, hunched, ataxic	no tumour
11/08/2008	*In vitro* recombined (Adeno-Cre)	10 - 15	5	Rb / p53 / PTEN / Rosa	6					
	FACSorted CD133 -ve	~460,714 cells (10ul)				103	164	**61**	sick	Oligoastrocytoma #
						103	275	**172**	sick, 28.7g, lump on head (tumour), 2hrs BrdU	no tumour (head tumour of unknown status)
						71	279	**208**	time-cull, 41.6g, 2hrs BrdU	no tumour
						71	279	**208**	time-cull, 53g, 2hrs BrdU	no tumour
						71	335	**264**	experiment terminated, 50g, 2hrs BrdU	no tumour
						71	335	**264**	experiment terminated, 51g, 2hrs BrdU	no tumour
11/08/2008	*In vitro* recombined (Adeno-Cre)	10	5	Rb / p53 / PTEN / Rosa	8					
	Unsorted single NSCs	~217,600 cells				78	135	**57**	sick, 24.4g	Oligoastrocytoma
						78	156	**78**	sick, 16.1g	Oligoastrocytoma
						78	164	**86**	sick, 33g	Oligoastrocytoma
						78	204	**126**	sick, ataxic	PNET
						52	189	**137**	sick	PNET + Glioma #
						52	200	**148**	sick, 21.1g	PNET + Glioma (giant cells)
						52	207	**155**	sick, ataxic, brain tumour (snap frozen)	PNET (giant cells) #
						79	241	**162**	sick, 24g, thin, 2hrs BrdU	no tumour (epidermoid cyst)
29/04/2008	*In vitro* recombined (Adeno-Cre)	8 - 25	3	Rb / p53 / PTEN / Rosa	4					
		1202 NS (10ul)				48	99	**51**	sick, thin, 18.7g	Glioma #
		~1.38x10^6 cells (10ul)				48	99	**51**	sick, thin, 17.3g	PNET + Glioma
						48	100	**52**	sick, thin, 18.3g	PNET + Glioma
						48	157	**109**	sick, dome-shaped head, brain tumour, bit snapped froz	Oligodendroglioma #
16/10/2007	*In vitro* recombined (Adeno-Cre)	8 - 10	4	Rb / p53 / PTEN / Rosa	4					
	MACSorted CD133 +ve	~50,000 (8ul)				117	317	**200**	culled, 34.8g, brain tumour	Glioma #
						117	317	**200**	culled, 34.5g	no tumour
						117	317	**200**	culled, 37.3g	no tumour
						117	317	**200**	culled, 35g	no tumour
16/10/2007	*In vitro* recombined (Adeno-Cre)	5	4	Rb / p53 / PTEN / Rosa	10					
	MACSorted CD133 -ve	~1.8x10^6 cells				75	82	**7**	timecull, 21.8g	intraventricular NS + scar
						75	82	**7**	timecull, 22.9g	intraventricular NS + scar with gliosis + inflammation #
						75	89	**14**	timecull, 23g	intraventricular NS
						75	89	**14**	timecull, 25.4g	intraventricular NS
						117	178	**61**	sick, swollen head, no tumour, but hydrocephalus	Oligoastrocytoma
						117	184	**67**	sick, culled by Francis	no tumour (small lesion beneath cerebellum)
						117	201	**84**	sick, brain tumour, bit snap frozen, 18.4g	PNET + Glioma #
						117	212	**95**	sick, died during BrdU injection, 24.9g	PNET (some glial infiltration) #
						117	213	**96**	sick, culled by Francis, 17.5g	PNET + Glioma
						117	312	**195**	sick, 31g	no tumour
17/03/2006	*In vitro* recombined (Adeno-Cre)	5	3	Rb / p53 / PTEN / Rosa	12					
		601 NS				44	89	**45**	time cull	PNET + Glioma
		(~690,000 cells)				44	92	**48**	sick, no obvious tumour	PNET
						44	110	**66**	sick, brain tumour, bit snap frozen, 21g	PNET (giant cells)
						44	110	**66**	sick, brain tumour, bit snap frozen, 21.9g	PNET + Glioma
						44	117	**73**	sick, brain tumour	PNET + Glioma
						44	119	**75**	sick	PNET + Glioma
						44	130	**86**	sick, brain tumour, 21g	PNET + Glioma
						44	130	**86**	sick, brain tumour, 17.8g	PNET
						44	132	**88**	sick, brain tumour, bit snap frozen, 20g	PNET
						44	132	**88**	sick, brain tumour, bit snap frozen, 22g	PNET + Glioma
						44	132	**88**	sick, brain tumour, bit snap frozen, 30g	PNET + Glioma #
						44	136	**92**	sick, brain tumour, died during BrdU incubation, 30.8g	PNET + Glioma

Figure 71: Summary table of all the *in vivo* intracerebral grafting experiments performed with *in vitro* recombined $Rb^{-/-}$; $p53^{-/-}$; $PTEN^{-/-}$ NS/NSCs (controls) and MACS/FACSorted $Rb^{-/-}$; $p53^{-/-}$; $PTEN^{-/-}$ CD133- and CD133+ NSCs (#: micrograph taken of this tumour for the histology panel).

No real difference was observed in the phenotype of intracerebral tumours generated from engrafted $Rb^{-/-}$; $p53^{-/-}$; $PTEN^{-/-}$ single NSCs or NS (Figure 71). The only difference between these two control sets was that the single NSCs appeared to have longer tumour latencies. However, we propose that this is due to lower numbers of cells being injected (~217,600) than with the NS controls (~690,000 and ~$1.38x10^6$). For the purpose of the analysis, both of these control sets were pooled to create a single cohort of 24 controls. Interestingly, there appeared to be minimal difference between the results of the MACS and FACSorted CD133-/+ cells in terms of both tumour phenotype and latency. Both sets of MACS and FACSorted CD133+ NSCs gave rise to only pure gliomas after 200 and 127 days respectively (Figure 71). And the CD133- cells even gave rise to identical oligoastrocytomas at the same 61 day latency with both sorting methods. The only difference was that MACSorted CD133- NSCs appeared to have a higher tumour hit rate with the additional tumours coming after longer incubations and with a tendency to the PNET or PNET + glioma phenotypes (a similar effect as observed with the controls). It could be that the ratio of CD133+ to CD133- NSCs in the MACSorted CD133- (87.2% pure) population more closely resembled that of the controls than that of the FACSorted CD133- (>99% pure) population. Or that more cells (~$1.8x10^6$) were injected following MACSorting than FACSorting (~460,714). In light of only minor differences, both sets of MACS and FACSorted NSCs have been pooled for the analysis into a single cohort for the mice injected with CD133- NSCs (n=12, excludes 4x time-culls) and another for those injected with CD133+ NSCs (n=6). The trends between cell profile, tumour latency period, and tumour phenotype are illustrated in an incidence plot (Figure 72).

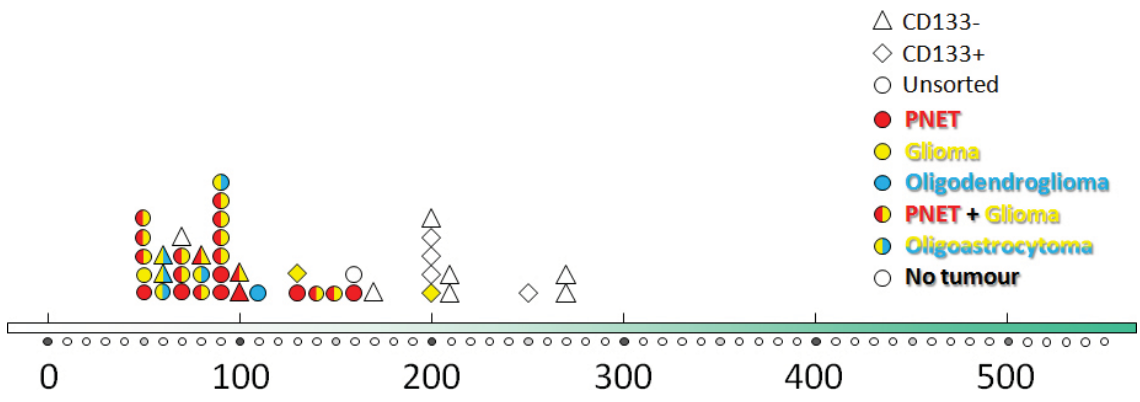

Figure 72: Incidence plot of the tumours generated from the intracerebral engraftment of $Rb^{-/-}$; $p53^{-/-}$; $PTEN^{-/-}$ NS/NSCs vs. MACS/FACSorted CD133-/+ $Rb^{-/-}$; $p53^{-/-}$; $PTEN^{-/-}$ NSCs. Axis: tumour latency (days).

The grafted $Rb^{-/-}$; $p53^{-/-}$; $PTEN^{-/-}$ NSC/NS controls had a tumour hit rate of 95.8% with 23 out of the 24 mice exhibiting an intrinsic brain tumour after a mean latency of 85 days (Figure 71 and Figure 72). Of these 23 tumours, the most predominant phenotype was PNET + glioma (n=12: mean latency = 83 days), followed by PNET (n=6: mean latency = 95 days), oligoastrocytoma (n=3: mean latency = 74 days), oligodendroglioma (n=1: mean latency = 109 days), and glioma (n=1: mean latency = 51 days). Interestingly, many of the tumours presented features of both PNETs and gliomas after the same latency. This goes against our previous finding that gliomas appear to develop after a much longer latency than PNETs. One possible explanation is that the *in vitro* generated $Rb^{-/-}$; $p53^{-/-}$; $PTEN^{-/-}$ NSC populations contain multiple lineage populations of tumourigenic BTICs, and that mice carrying purely glioma BTICs survive considerably longer as the progression of the glioma is slower. The grafted CD133- NSCs had an intrinsic brain tumour hit rate of 41.7% (5 out of 12) with a mean latency of 79 days and a phenotypic profile of oligoastrocytoma (n=2: mean latency = 61 days), PNET + glioma (n=2: mean latency = 90 days), and PNET (n=1: mean latency = 95 days). In comparison, the grafted CD133+ NSCs had an intrinsic brain tumour hit rate of 33.3% with a much increased mean latency of 164 days and a phenotypic profile of solely glioma (n=2: mean latency = 164 days). These findings suggest that a) MACS/FACSorted CD133- and CD133+ $Rb^{-/-}$; $p53^{-/-}$; $PTEN^{-/-}$ NSCs have a reduced tumourigenic capacity when compared to the unsorted controls (or that the MACS/FACSorting procedure reduces the viability of the cells prior to grafting), b) obtaining 100% purity of CD133-/+ NSCs prior to grafting may not be strictly necessary to achieving meaningful results, c) increased expression of CD133 may be associated with an increased presence of a glioma-specific BTIC population (in $Rb^{-/-}$; $p53^{-/-}$; $PTEN^{-/-}$ NSCs), d) CD133- NSCs can in fact be tumourigenic *in vivo*, and share a similar tumour phenotype profile to the unsorted controls.

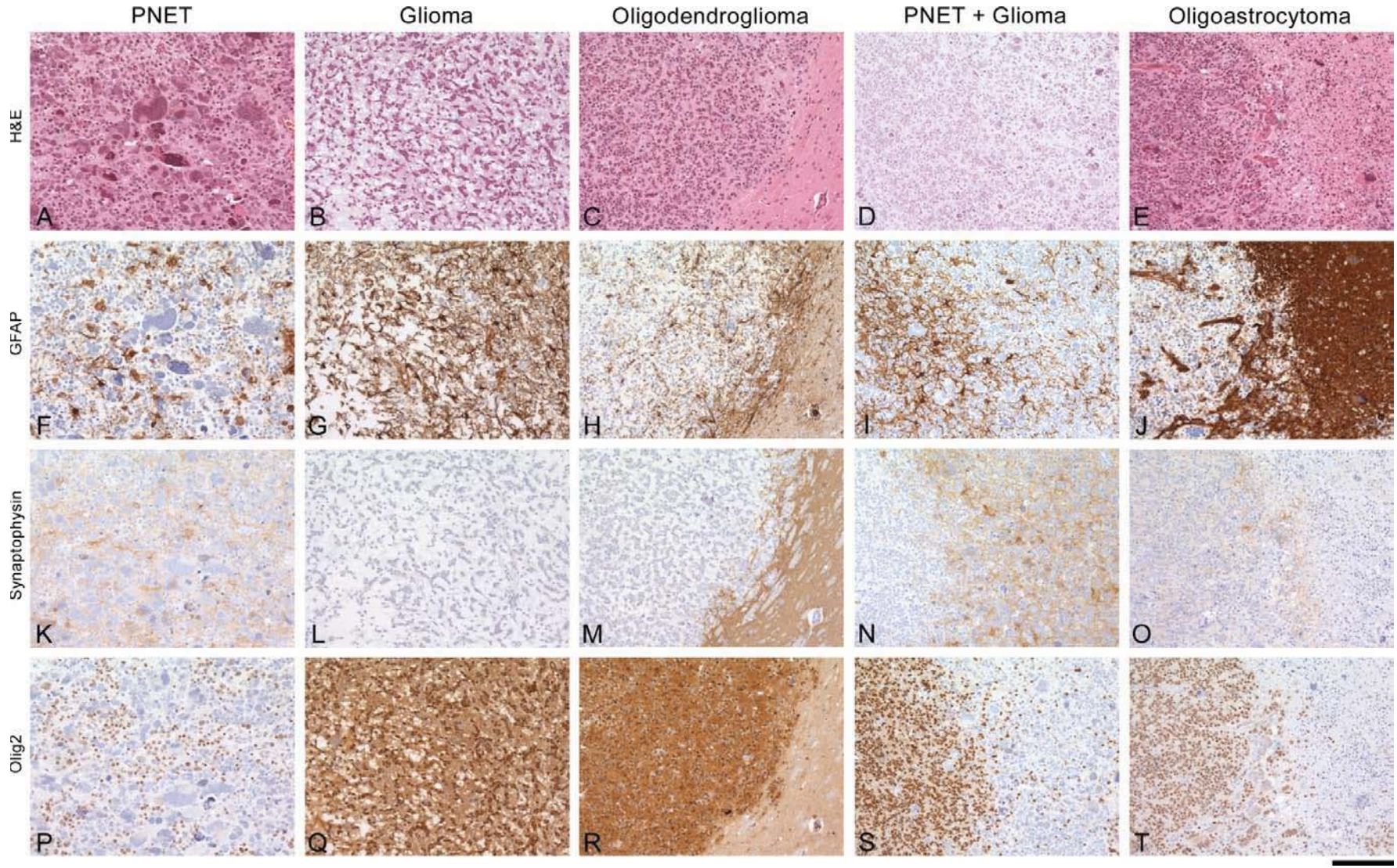
PNET
Glioma
Oligodendroglioma
PNET + Glioma
Oligoastrocytoma
H&E
GFAP
Synaptophysin
Olig2
A
B
C
D
E
F
G
H
I
J
K
L
M
N
O
P
Q
R
S
T

Figure 73: Intracerebral engraftment of unsorted control $Rb^{-/-}$; $p53^{-/-}$; $PTEN^{-/-}$ NSCs/NS results in the development of a wide range of tumour phenotypes (predominantly PNET + Glioma) with a high hit rate of 95.8% and a mean latency of 85 days. Immunohistochemical analysis of the intrinsic brain tumour profile following the intracerebral grafting of unsorted control $Rb^{-/-}$; $p53^{-/-}$; $PTEN^{-/-}$ NSCs/NS. Representative tumours were taken from the each of the PNET, Glioma, Oligodendroglioma, PNET + Glioma, and Oligoastrocytoma phenotypes observed and stained for H&E (A-E), GFAP (F-J), synaptophysin (K-O), and olig2 (P-T). Images were taken using a ColorView III digital camera mounted on a Zeiss Axioskop 2 MOT microscope with a 10x objective and using the AnalySIS software package. Scale bar: 150μm.

Tumours were classified as PNETs following the identification of a GFAP- / synaptophysin+ / olig2-/+ expression profile often associated with the presence of giant cells and a well-demarcated but disorganised and dense cell arrangement (Figure 73: A,F,K,P). Conversely, gliomas possess a GFAP+ / synaptophysin- / olig2+ profile and are more diffusely distributed in addition to being highly infiltrative (Figure 73: B,G,L,Q). The PNET + glioma tumours contained aspects of both phenotypes, often next to one another in a tumour mass (Figure 73: D,I,N,S). The single oligodendroglioma was so classified in accordance with the presence of its “fried egg” cellular appearance and a GFAP-/+ / synaptophysin - / olig2+ expression profile (Figure 73: C,H,M,R). And finally, the oligoastrocytomas appear very similar to the gliomas but with a reduced expression of GFAP (Figure 73: E,J,O,T).

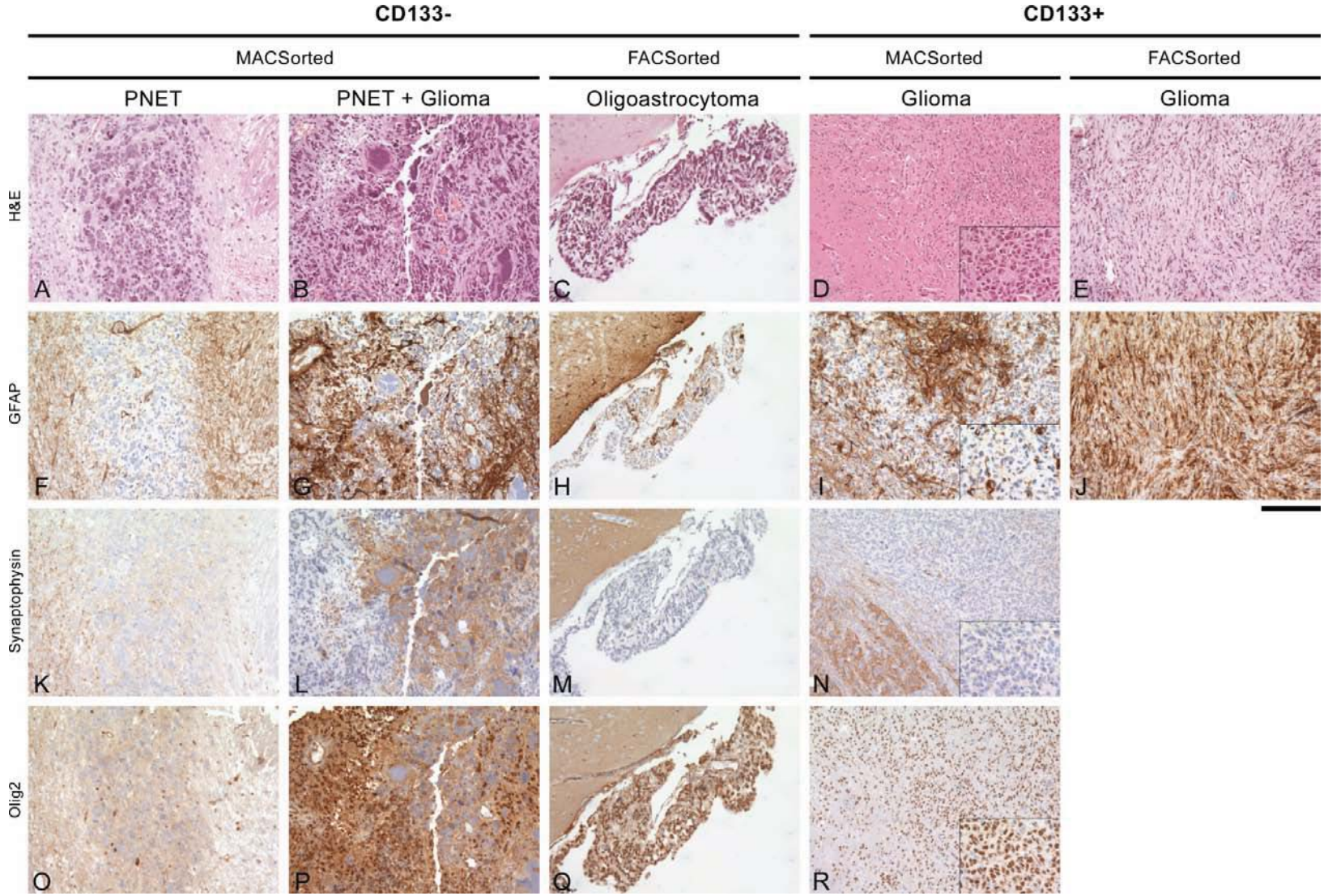
CD133-
CD133+
MACSorted
FACSorted
MACSorted
FACSorted
PNET
PNET + Glioma
Oligoastrocytoma
Glioma
Glioma
H&E
GFAP
Synaptophysin
Olig2
A
B
C
D
E
F
G
H
I
J
K
L
M
N
O
P
Q
R

Figure 74: Intracerebral engraftment of MACSorted CD133- Rb$^{-/-}$; p53$^{-/-}$; PTEN$^{-/-}$ NSCs results in the development of a variety of tumours (predominantly PNET + Glioma) with a mean latency of 79 days, both similar to that of the unsorted controls, but with a lower hit rate of 41.7%. Intracerebral engraftment of MACSorted CD133+ Rb$^{-/-}$; p53$^{-/-}$; PTEN$^{-/-}$ NSCs results in the development of solely gliomas with a vastly increased mean latency of 164 days and an equally low hit rate of 33.3%. Immunohistochemical analysis of the brain tumour profile resulting from the intracerebral grafting of MACS/FACSorted CD133-/+ Rb$^{-/-}$; p53$^{-/-}$; PTEN$^{-/-}$ NSCs. Representative tumours were taken from the each of the PNET, PNET + Glioma, and Oligoastrocytoma phenotypes observed with the CD133- grafted NSCs, in addition to the Glioma phenotype observed with the CD133+ grafted NSCs, and stained for H&E (A-E), GFAP (F-J), synaptophysin (K-N), and olig2 (O-R). Images were taken using a ColorView III digital camera mounted on a Zeiss Axioskop 2 MOT microscope with a 10x or 20x (insets) objective and using the AnalySIS software package. Scale bar: 150μm for main images and 10 μm for insets.

The tumour phenotypes were classified as above, but interestingly, fewer phenotypes were observed following the engraftment of MACS/FACSorted CD133-/+ NSCs. In particular, the CD133+ NSCs were observed to only generate gliomas irrespective of the sorting method. The MACSorted CD133+ NSCs gave rise to a classical glioma with highly mitotic and infiltrative cells (Figure 74: D) possessing a GFAP+ / synaptophysin- / olig2+ profile. On the other hand, the FACSorted CD133+ NSCs also gave rise to a glioma, but one that grew extracranially and with an infiltrative fibroblastic component (Figure 74: J). The CD133- grafted cells generated tumours and did so with a phenotypic profile similar to that of the unsorted controls. These findings suggest that an alteration of the CD133 expression away from its equilibrium to either a purely CD133- or CD133+ status reduces *in vivo* tumour hit rate by up to ~60%. However, this may be due to the MACS / FACSorting process altering the viability of NSCs prior to engraftment. Interestingly, CD133+ Rb$^{-/-}$; p53$^{-/-}$; PTEN$^{-/-}$ NSCs appear to have a propensity towards generating gliomas. To validate this finding we performed a Western blot for CD133 in order to correlate its expression against the *in vivo* tumour hit rates, latencies, and phenotype propensities of the four double and triple knock-out NSC genotypes (PTEN$^{-/-}$; p53$^{-/-}$, Rb$^{-/-}$; p53$^{-/-}$, Rb$^{-/-}$; PTEN$^{-/-}$, and Rb$^{-/-}$; p53$^{-/-}$; PTEN$^{-/-}$).

5.3.6 *In vitro* CD133 expression by tumourigenic NS does not correlate with either *in vivo* tumour hit rate or latency

Protein samples were collected from each of the four different *in vitro* recombined NSC genotypes ($PTEN^{-/-}$; $p53^{-/-}$, $Rb^{-/-}$; $p53^{-/-}$, $Rb^{-/-}$; $PTEN^{-/-}$, $Rb^{-/-}$; $p53^{-/-}$; $PTEN^{-/-}$) and a CD133 western blot was performed (Figure 75) to compare their relative expression levels (n=3 for each). The NSC passage number of the samples varied between three and five (and 10 in the case of the NS derived from a $PTEN^{-/-}$; $p53^{-/-}$ tumoursphere-induced glioma sample).

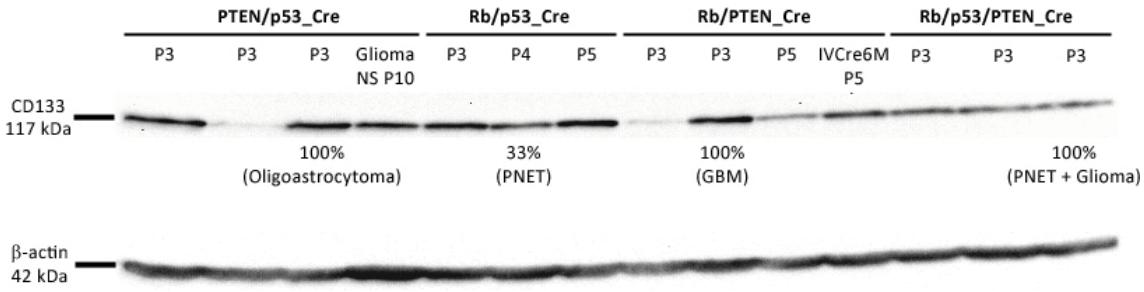

Figure 75: *In vitro* CD133 protein expression of tumourigenic NS varies both within and between genotypes. Western blot of CD133 (117kDa) and β-actin (42kDa) expression in $PTEN^{-/-}$; $p53^{-/-}$ vs. $Rb^{-/-}$; $p53^{-/-}$ vs. $Rb^{-/-}$; $PTEN^{-/-}$ vs.$Rb^{-/-}$; $p53^{-/-}$; $PTEN^{-/-}$ NS (n=3 for each genotype), with associated passage numbers and the results of any corresponding *in vivo* engraftment studies. Two additional samples (NS grown from a $PTEN^{-/-}$; $p53^{-/-}$ NS-induced glioma and NS derived from the brains of a cohort of $Rb^{Lox/Lox}$; $PTEN^{Lox/Lox}$ mice six months after having had received an intracerebroventricular injection of Adeno-Cre) were included on the blot for preliminary comparison purposes.

The net (relative) intensities of the CD133 bands were semi-quantitatively measured using the respective β-actin bands as baseline controls. Corrected CD133 intensities were then generated for comparative analysis purposes (Figure 76). No correlation between passage number and CD133 expression was observed.

Band	Recombination Paradigm	Genotype (cells)	Grafted	Tumour Hit Rate (%)	Average Latency (d)	Predominant Phenotype	Net CD133 Intensity	Net β-actin Intensity	Corrected CD133 Intensity	Average	SE
1	*In vitro* recombined (Adeno-Cre)	PTEN/p53_Cre (P3)	-	-	-	-	18667	22485	830.17		
2	*In vitro* recombined (Adeno-Cre)	PTEN/p53_Cre (P3)	-	-	-	-	2037	18284	111.38	643.24	269.81
3	*In vitro* recombined (Adeno-Cre)	PTEN/p53_Cre (P3)	18/12/2007	100	192.5	Oligoastrocytoma	19380	19612	988.17		
4	*Glioma Tumourspheres*	PTEN/p53_NS tum (P10)	24/02/2009	100	91.6	Glioma	16377	30393	538.84	538.84	-
5	*In vitro* recombined (Adeno-Cre)	Rb/p53_Cre (P3)	-	-	-	-	17866	22983	777.36		
6	*In vitro* recombined (Adeno-Cre)	Rb/p53_Cre (P4)	09/05/2008	33	235.0	PNET	11499	22128	519.64	791.26	160.99
7	*In vitro* recombined (Adeno-Cre)	Rb/p53_Cre (P5)	07/05/2009	-	-	-	21147	19639	1076.79		
8	*In vitro* recombined (Adeno-Cre)	Rb/PTEN_Cre (P3)	-	-	-	-	1833	15841	115.71		
9	*In vitro* recombined (Adeno-Cre)	Rb/PTEN_Cre (P3)	29/10/2007	100	116.3	GBM	18560	21795	851.58	469.21	212.92
10	*In vitro* recombined (Adeno-Cre)	Rb/PTEN_Cre (P5)	07/05/2009	-	-	-	7755	17612	440.32		
11	*In vivo* recombined (Adeno-Cre)	Rb/PTEN_IVCre6M (P5)	24/04/2009	-	-	-	13111	20019	654.92	654.92	-
12	*In vitro* recombined (Adeno-Cre)	Rb/p53/PTEN_Cre (P3)	-	-	-	-	10392	19223	540.60		
13	*In vitro* recombined (Adeno-Cre)	Rb/p53/PTEN_Cre (P3)	-	-	-	-	8363	20487	408.21	495.06	43.44
14	*In vitro* recombined (Adeno-Cre)	Rb/p53/PTEN_Cre (P3)	29/04/2008	100	76.0	PNET + Glioma	9113	16990	536.37		

Figure 76: Summary table of all the samples used to generate the western blot (Figure 75) along with their genotype, *in vivo* grafting data (if applicable), raw CD133 and β-actin intensities, corrected CD133 intensities, and genotype group averages with standard errors.

The corrected CD133 intensities were grouped by genotype (the two additional non-basic genotype samples were omitted from this grouping) to examine the intra- and inter-genotype expression profile of tumourigenic NSCs (Figure 77).

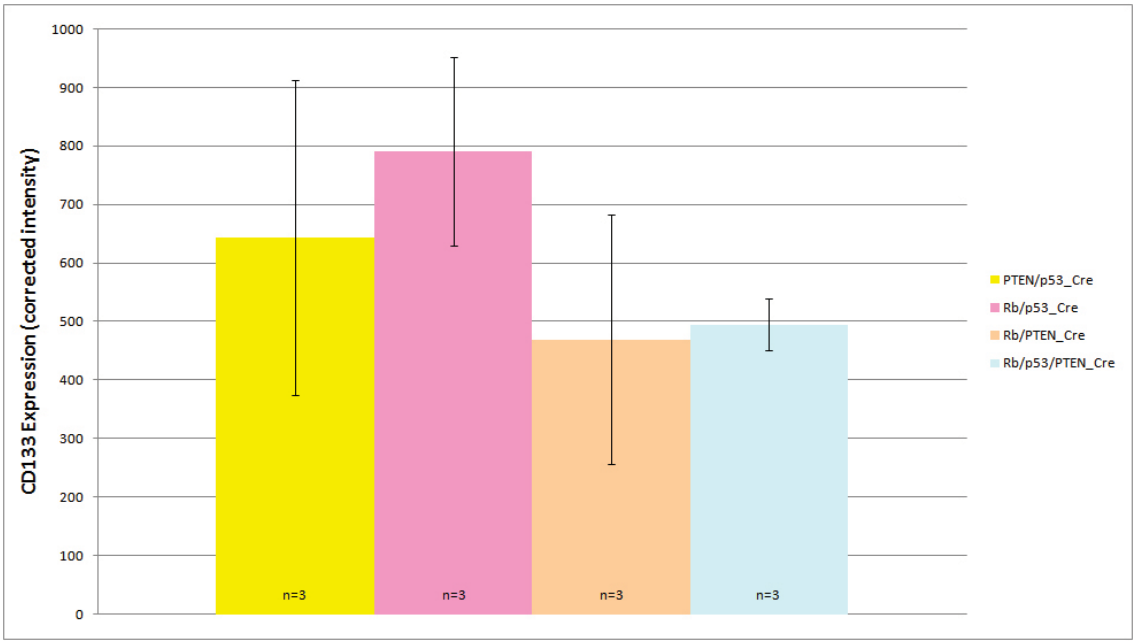

Figure 77: There are no statistically significant differences in the levels of CD133 expressed by PTEN$^{-/-}$; p53$^{-/-}$ vs. Rb$^{-/-}$; p53$^{-/-}$ vs. Rb$^{-/-}$; PTEN$^{-/-}$ vs. Rb$^{-/-}$; p53$^{-/-}$; PTEN$^{-/-}$ NS *in vitro*. A bar chart comparing the grouped corrected CD133 expression intensities (net CD133 intensity / net β-actin intensity, *1000) expressed (y-axis) by each of the four genotypes of tumourigenic NS *in* vitro (x-axis). Error bars: standard errors. No significance difference observed between any of the groups (one-way ANOVA with Bonferroni's multiple comparison correction).

No statistical differences were observed between any of the genotypes, with the exception of the Rb$^{-/-}$; p53$^{-/-}$; PTEN$^{-/-}$ genotype, and large variations in CD133 expression levels were observed within each of the genotypes (Figure 77). It is possible that a significant difference between two of the groups may be achieved with a sample number greater than three, and the inclusion of an internal control would allow for an absolute comparison. However, the size of the intra-genotype variability (PTEN$^{-/-}$; p53$^{-/-}$: 111.38, band 2 vs. 988.17, band 3) suggests that either a) CD133 protein expression *in vitro* is influenced more strongly by environmental conditions (e.g. culture conditions, general cellular health) than by the tumourigenic profile of the cells (combination of TSGs lost), and/or b) the cellular composition of NS is highly heterogeneous and CD133 expression may not need to be 100% representative of all the NSCs within the

NS in order to see a CD133-correlated effect on tumour hit rate, latency, and phenotype. The latter suggestion is difficult to address as it assumes that there are subclasses of CD133+ NSCs.

To address whether *in vitro* CD133 expression correlates with *in vivo* tumour hit rate, latency, and phenotype we compared the CD133 expression data of the Western blot samples with their respective *in vivo* grafting data and visualised the correlation on a bubble plot of mean *in vivo* tumour latency (y-axis) vs. CD133 expression (x-axis) vs. *in vivo* tumour hit rate (z-axis: bubble size). It should be noted that limited *in vivo* grafting data was available from the samples selected for the western blot (n=1 per genotype).

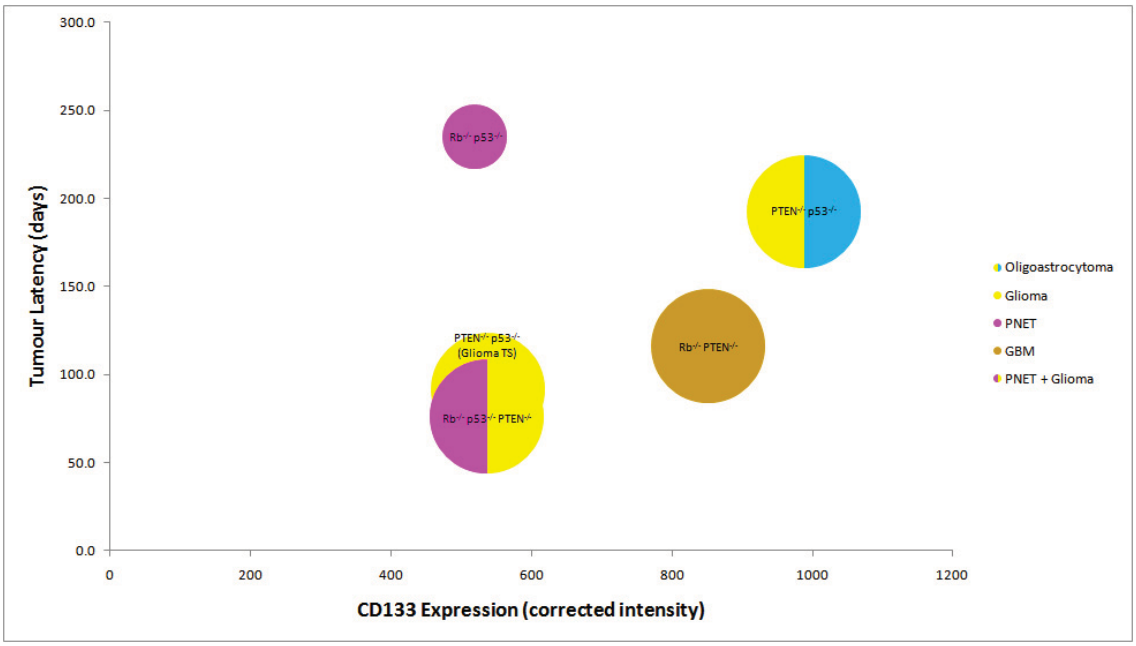

Figure 78: There appears to be a correlation between increased *in vitro* CD133 expression of NS and a propensity towards generating glial tumours *in vivo*, but no correlation between CD133 expression and tumour hit rate or latency. Each bubble represents a single *in vivo* grafting experiment encompassing a cohort of 6-13 mice with the phenotype given being the predominant tumour phenotype generated and plotted according to *in vivo* tumour latency (y-axis) vs. CD133 expression (x-axis) vs. *in vivo* tumour hit rate (z-axis: bubble size).

These data show that the tumour phenotypes found at the high CD133-expression (right) side of the plot are glial tumours and suggests that there may be some correlation between *in vitro* CD133 expression and a propensity towards generating a glial tumour *in vivo* (Figure 78), as previously suggested. The $Rb^{-/-}$; $p53^{-/-}$ PNET tumour phenotype illustrated (in full pink) was actually not the predominant phenotype expressed with 'no

tumour' being found in 66% of the mice injected with cells. Additional sample numbers would be required to conduct a robust correlation analysis between CD133 expression and *in vivo* tumour hit rate as all four of the other plotted *in vivo* graft experiment tumour phenotypes possessed a 100% tumour hit rate. To address this, in section 5.3.8 we repeat the Western blot experiment using only samples for which there was associated *in vivo* grafting data and incorporating an internal control (non-recombined NS).

5.3.7 *In vitro* HIF1α expression by tumourigenic NS appears to inversely correlate with CD133 expression but does not correlate with either *in vivo* tumour hit rate or latency

As described in section 5.3.4 HIF1α expression levels have been shown to inversely correlate with those of CD133 by downregulating it in response to hypoxic conditions (Matsumoto et al., 2009). This suggests that tumourigenic NS expressing high levels of CD133 may be more resistant to hypoxia and possess increased *in vivo* survival and tumour hit rate. Here we used the same samples as for the CD133 Western blot in section 5.3.6 to perform a parallel Western blot for HIF1α (Figure 79).

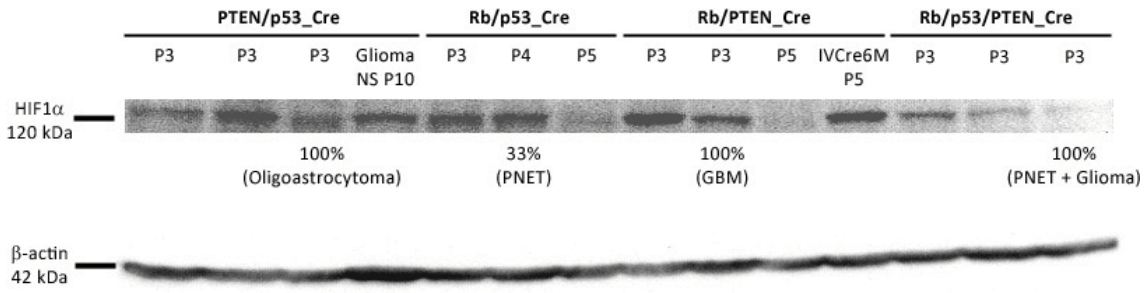

Figure 79: *In vitro* HIF1α protein expression of tumourigenic NS varies both within and between genotypes. Western blot of HIF1α (120kDa) and β-actin (42kDa) expression in $PTEN^{-/-}$; $p53^{-/-}$ vs. $Rb^{-/-}$; $p53^{-/-}$ vs. $Rb^{-/-}$; $PTEN^{-/-\ vs.}$ $Rb^{-/-}$; $p53^{-/-}$; $PTEN^{-/-}$ NS (n=3 for each genotype), with associated passage numbers and the results of any corresponding *in vivo* engraftment studies. Two additional samples (NS grown from a $PTEN^{-/-}$; $p53^{-/-}$ NS-induced glioma and NS derived from the brains of a cohort of $Rb^{Lox/Lox}$; $PTEN^{Lox/Lox}$ mice six months after having had received an intracerebroventricular injection of Adeno-Cre) were included on the blot for preliminary comparison purposes.

The net (relative) intensities of the HIF1α bands were semi-quantitatively measured using the respective β-actin bands as baseline controls. Corrected HIF1α intensities

were then generated for comparative analysis purposes (Figure 80). No correlation between passage number and HIF1α expression was observed.

Band	Recombination Paradigm	Genotype (cells)	Grafted	Tumour Hit Rate (%)	Average Latency (d)	Predominant Phenotype	Net HIF1α Intensity	Net β-actin Intensity	Corrected HIF1α Intensity	Average	SE
1	*In vitro* recombined (Adeno-Cre)	PTEN/p53_Cre (P3)	-	-	-	-	1240	22485	55.14		
2	*In vitro* recombined (Adeno-Cre)	PTEN/p53_Cre (P3)	-	-	-	-	3629	18284	198.50	101.24	48.65
3	*In vitro* recombined (Adeno-Cre)	PTEN/p53_Cre (P3)	18/12/2007	100	192.5	Oligoastrocytoma	982	19612	50.09		
4	*Glioma Tumourspheres*	PTEN/p53_NS tum (P10)	24/02/2009	100	91.6	Glioma	3034	30393	99.84	99.84	-
5	*In vitro* recombined (Adeno-Cre)	Rb/p53_Cre (P3)	-	-	-	-	3336	22983	145.15		
6	*In vitro* recombined (Adeno-Cre)	Rb/p53_Cre (P4)	09/05/2008	33	235.0	PNET	2394	22128	108.18	107.34	22.08
7	*In vitro* recombined (Adeno-Cre)	Rb/p53_Cre (P5)	07/05/2009	-	-	-	1349	19639	68.69		
8	*In vitro* recombined (Adeno-Cre)	Rb/PTEN_Cre (P3)	-	-	-	-	5150	15841	325.09		
9	*In vitro* recombined (Adeno-Cre)	Rb/PTEN_Cre (P3)	29/10/2007	100	116.3	GBM	3341	21795	153.28	205.41	60.01
10	*In vitro* recombined (Adeno-Cre)	Rb/PTEN_Cre (P5)	07/05/2009	-	-	-	2428	17612	137.86		
11	*In vitro* recombined (Adeno-Cre)	Rb/PTEN_IVCre6M (P5)	24/04/2009	-	-	-	5991	20019	299.28	299.28	-
12	*In vitro* recombined (Adeno-Cre)	Rb/p53/PTEN_Cre (P3)	-	-	-	-	3655	19223	190.12		
13	*In vitro* recombined (Adeno-Cre)	Rb/p53/PTEN_Cre (P3)	-	-	-	-	2803	20487	136.81	115.03	50.82
14	*In vitro* recombined (Adeno-Cre)	Rb/p53/PTEN_Cre (P3)	29/04/2008	100	76.0	PNET + Glioma	309	16990	18.18		

Figure 80: Summary table of all the samples used to generate the western blot given in Figure 79 along with their genotype, *in vivo* grafting data (if applicable), raw HIF1α and β-actin intensities, corrected HIF1α intensities, and genotype group averages with standard errors.

The corrected HIF1α intensities were grouped by genotype (the two additional non-basic genotype samples were omitted from this grouping) to examine the intra- and inter-genotype expression profile of tumourigenic NSCs (Figure 81).

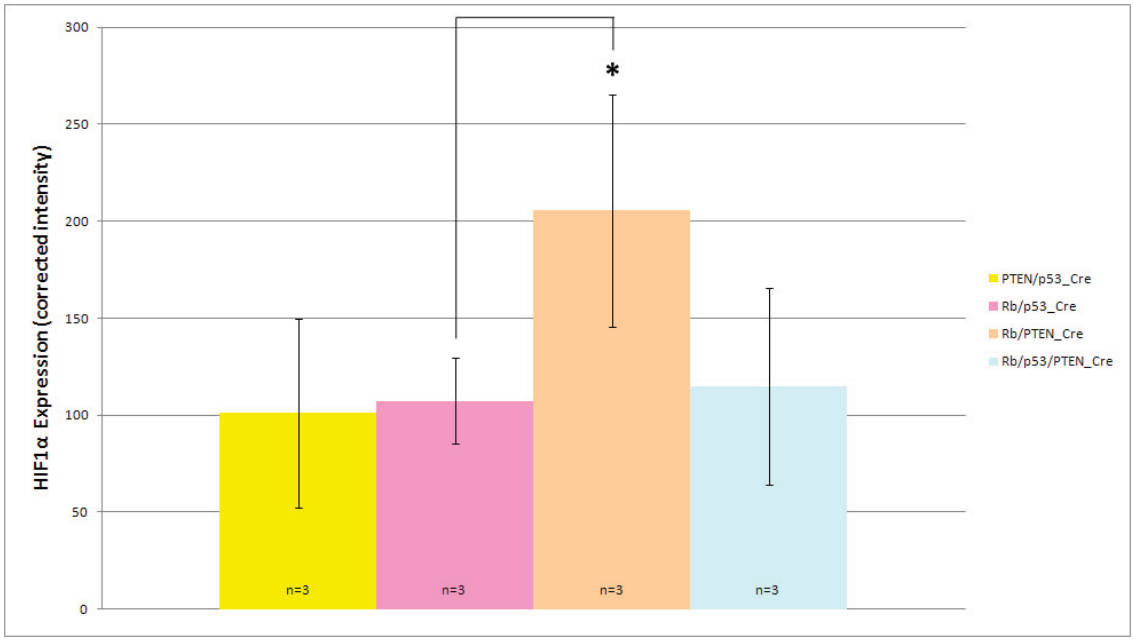

Figure 81: Only Rb$^{-/-}$; PTEN$^{-/-}$ vs. Rb$^{-/-}$; p53$^{-/-}$ NS *in vitro* have a statistically significant difference in the level of HIF1α expressed. A bar chart comparing the grouped corrected HIF1α expression intensities (net HIF1α intensity / net β-actin intensity, *1000) expressed (y-axis) by each of the four genotypes of tumourigenic NS (n=3 for each) *in vitro* (x-axis). Error bars: standard errors. *: P<0.05 (one-tailed paired Student's t-Test). No significance difference observed between any of the groups using a one-way ANOVA with Bonferroni's multiple comparison correction).

As seen with the CD133 expression data, each of the genotypes possessed a large amount of internal variation in the level of HIF1α expression, further validating the need for a sample size greater than three. However, whereas no statistically significant differences in CD133 expression were observed between any of the genotypes, a statistically significant (P=0.04) difference was observed between the HIF1α expression of Rb$^{-/-}$; PTEN$^{-/-}$ and Rb$^{-/-}$; p53$^{-/-}$ NS *in vitro* (Figure 81). Interestingly, the same two genotypes were the closest to exhibiting a statistically significant difference (p=0.071) in CD133 expression. The correlation between the expression levels of the CD133 and HIF1α was examined by plotting them against one another (Figure 82).

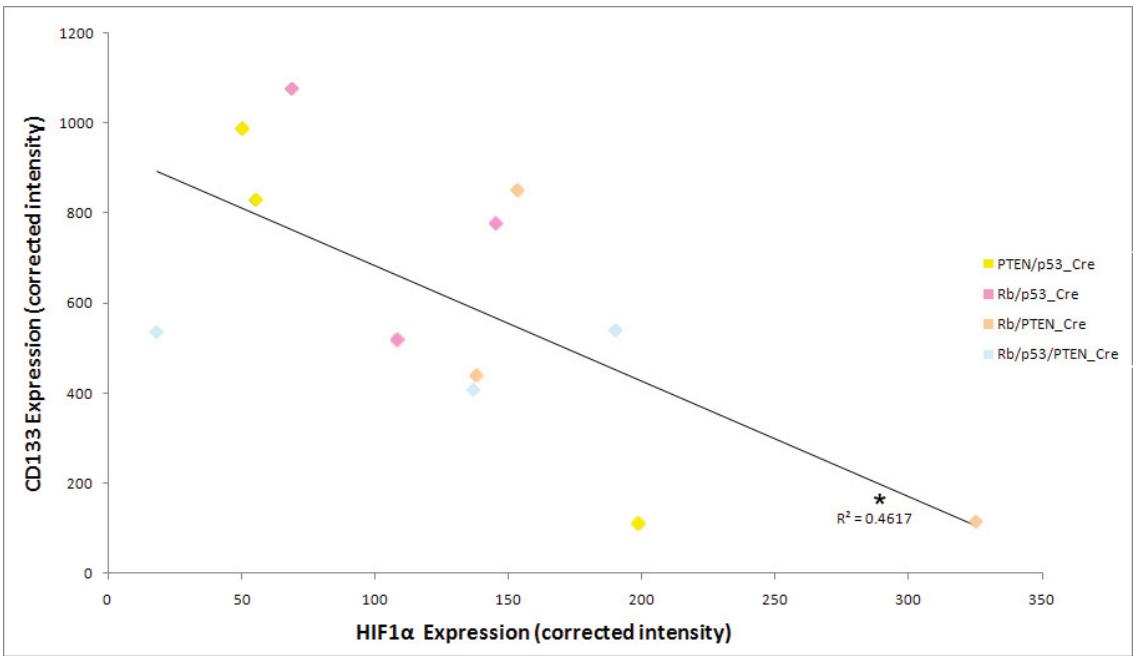

Figure 82: Expression of CD133 by *in vitro* recombined $Rb^{-/-}$; $p53^{-/-}$; $PTEN^{-/-}$ tumourigenic NS inversely correlates with HIF1α expression. A scatter plot of CD133 expression (y-axis) against HIF1α expression (x-axis), for each of the four genotypes of tumourigenic NS (n=3 for each), in the form of corrected intensities as measured semi-quantitatively from Western blots run using the same samples in parallel. The data points from the different genotypes are colour coded in accordance with the key. The correlation coefficient of the two data sets ($R^2 = 0.4617$) was significant ($P<0.05$). Linear regression was used to determine the goodness of the fit (R^2), and a two-tailed Pearson test was used to measure the level of correlation (*: $P<0.05$).

CD133 was found to be significantly inversely correlated to HIF1α expression (Figure 81). This finding validates the use of HIF1α as a surrogate marker of CD133. On this basis, we compared the HIF1α expression data of the Western blot samples with the same *in vivo* grafting data used for CD133 in order to elucidate any potential correlations between *in vitro* HIF1α expression and *in vivo* tumour hit rate, latency, and phenotype. The results were once again visualised on a bubble plot of mean *in vivo* tumour latency (y-axis) vs. HIF1α expression (x-axis) vs. *in vivo* tumour hit rate (z-axis: bubble size).

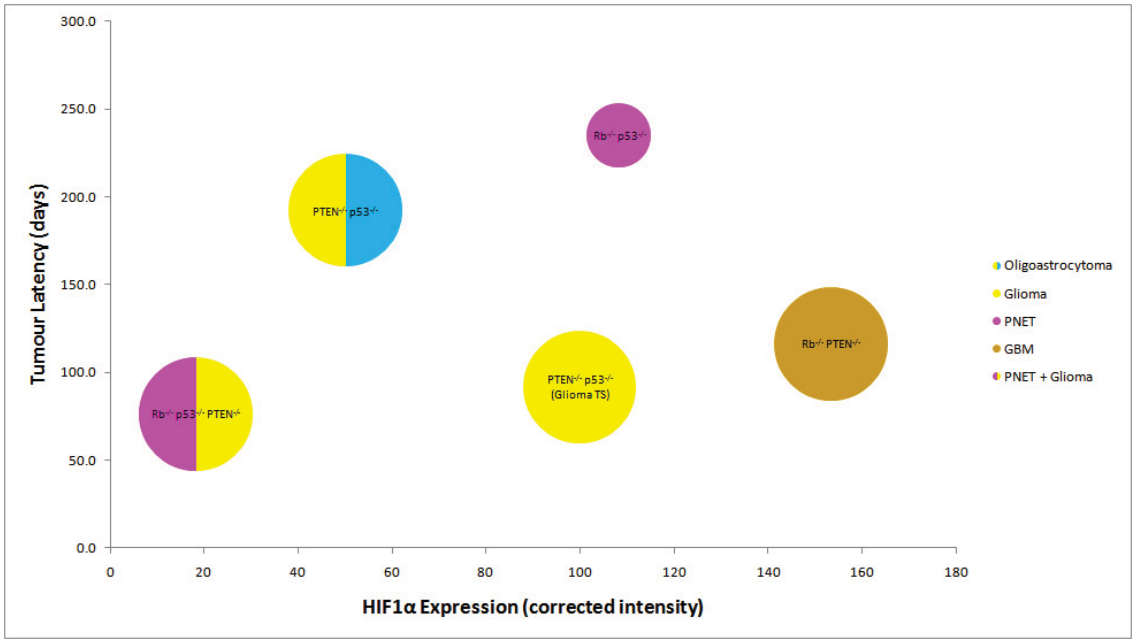

Figure 83: No correlations were observed between *in vitro* HIF1α expression of NS and *in vivo* tumourigenicity (hit rate), *in vivo* tumour latency, or *in vivo* tumour phenotype. Each bubble represents a single *in vivo* grafting experiment encompassing a cohort of 6-13 mice with the phenotype given being the predominant tumour phenotype generated and plotted according to *in vivo* tumour latency (y-axis) vs. HIF1α expression (x-axis) vs. *in vivo* tumour hit rate (z-axis: bubble size).

No correlations were observed between the *in vitro* expression of HIF1α and *in vivo* tumour hit rate, latency, or phenotype (Figure 83). Only the PTEN$^{-/-}$; p53$^{-/-}$ NS, which predominantly generated oligodendrogliomas, were observed to express the expected inversely correlated (low) level of HIF1α (Figure 83). Furthermore, the level of HIF1α expressed by the Rb$^{-/-}$; PTEN$^{-/-}$ NS was equally high as it was for CD133, suggesting that glioblastoma-generating NS may have aberrantly functioning hypoxia-response mechanisms whereby the normal interaction of CD133 and HIF1α does not apply and both proteins remain highly expressed. Taken together our data suggests a more complex relationship, than a simple inverse correlation, exists between HIF1α and CD133 expression. In addition, although our data did not identify any correlation between the expression of either CD133 or HIF1α and *in vivo* tumour hit rate, CD133 remains a potential marker of hypoxia resistance.

Although much focus has been directed towards CD133 as a marker, and potential target, of glioblastoma-initiating cells (GICs) it has been shown that shRNA knock down of HIF-1α in these cells significantly impairs their migration and self-renewal *in vitro* and their invasion *in vivo* (Mendez et al., 2010). This suggests that HIF-1α may represent a more promising therapeutic target in the treatment of glioblastoma.

5.3.8 Glioblastoma-initiating cells appear to exhibit increased CD133 expression *in vitro*

Protein samples were collected from five different NSC genotypes (controls vs. PTEN$^{-/-}$; p53$^{-/-}$, Rb$^{-/-}$; p53$^{-/-}$, Rb$^{-/-}$; PTEN$^{-/-}$, Rb$^{-/-}$; p53$^{-/-}$; PTEN$^{-/-}$) and a CD133 western blot was performed to compare their relative expression levels (n=2 for each) (Figure 84). The NSC passage number of the samples varied between two and five and no correlation was observed with CD133 expression.

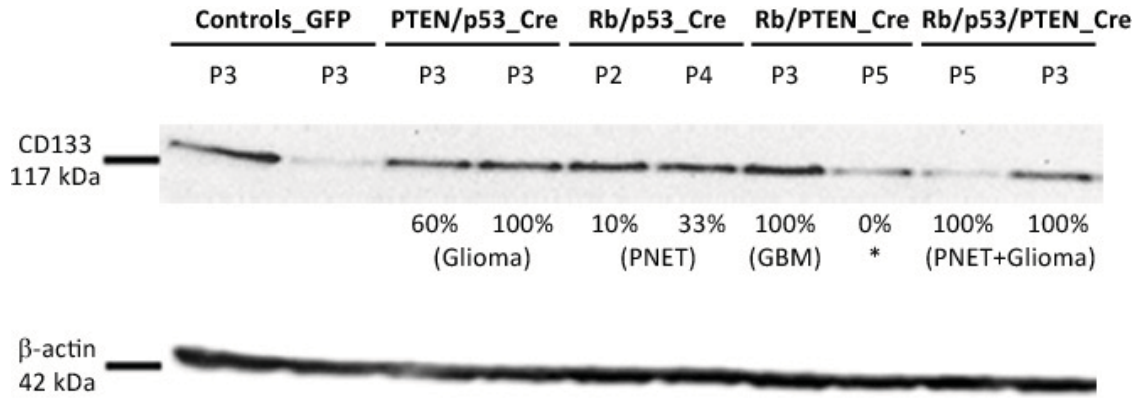

Figure 84: *In vitro* CD133 protein expression of tumourigenic NS has a high degree of genotype-independent variability but appears to be a predictor of glioblastoma development. Western blot of CD133 (117kDa) and β-actin (42kDa) expression in non-recombined Adenovirus-GFP-infected control vs. PTEN$^{-/-}$; p53$^{-/-}$ vs. Rb$^{-/-}$; p53$^{-/-}$ vs. Rb$^{-/-}$; PTEN$^{-/-}$ vs. Rb$^{-/-}$; p53$^{-/-}$; PTEN$^{-/-}$ NS (n=2 for each genotype), with associated passage numbers and the results (hit rate and predominant tumour phenotype) of corresponding *in vivo* engraftment studies.

The net (relative) intensities of the CD133 bands were semi-quantitatively measured using the respective β-actin bands as baseline controls. Corrected CD133 intensities were then generated for comparative analysis purposes (Figure 85).

Band	Recombination Paradigm	Genotype (cells)	Grafted	Tumour Hit Rate (%)	Average Latency (d)	Predominant Phenotype	Net CD133 Intensity	Net β-actin Intensity	Corrected CD133 Intensity	Average	SE
1	Non-recombined (Adeno-GFP)	PTEN/p53_GFP (P3)	-	-	-	-	7555	105250	71.78	40.39	31.39
2	Non-recombined (Adeno-GFP)	Rb/p53_GFP (P3)	-	-	-	-	760	84455	9.00		
3	*In vitro* recombined (Adeno-Cre)	PTEN/p53_Cre (P3)	03/08/06	60	138.0	Glioma	5611	79526	70.56	68.79	1.77
4	*In vitro* recombined (Adeno-Cre)	PTEN/p53_Cre (P3)	18/12/07	100	192.5	(Oligo)astrocytoma	5971	89077	67.03		
5	*In vitro* recombined (Adeno-Cre)	Rb/p53_Cre (P2)	18/04/07	10	216.0	PNET + Glioma	7811	100629	77.62	76.46	1.16
6	*In vitro* recombined (Adeno-Cre)	Rb/p53_Cre (P4)	09/05/08	33	235.0	PNET	7377	97970	75.30		
7	*In vitro* recombined (Adeno-Cre)	Rb/PTEN_Cre (P3)	29/10/07	100	116.3	GBM	8434	103683	81.35	57.68	23.67
8	*In vitro* recombined (Adeno-Cre)	Rb/PTEN_Cre (P5)	07/05/09	-	-	-	3007	88409	34.01		
9	*In vitro* recombined (Adeno-Cre)	Rb/p53/PTEN_Cre (P5)	17/03/06	100	75.1	PNET + Glioma	1268	93055	13.62	40.51	26.89
10	*In vitro* recombined (Adeno-Cre)	Rb/p53/PTEN_Cre (P3)	29/04/08	100	76.0	PNET + Glioma	6224	92331	67.41		

Figure 85: Summary table of all the samples used to generate the western blot (Figure 84) along with their genotype, *in vivo* grafting data (if applicable), raw CD133 and β-actin intensities, corrected CD133 intensities, and genotype group averages with standard errors.

The corrected CD133 intensities were grouped by genotype to examine the intra- and inter-genotype expression profile of tumourigenic NSCs. As we have previously demonstrated, the tumourigenic NS samples reproducibly gave rise to the same predominant tumour phenotype within each genotype. The one exception being the $Rb^{-/-}$; $PTEN^{-/-}$ genotype for which only one of the *in vivo* grafting experiments gave rise to the development of tumours (glioblastoma).

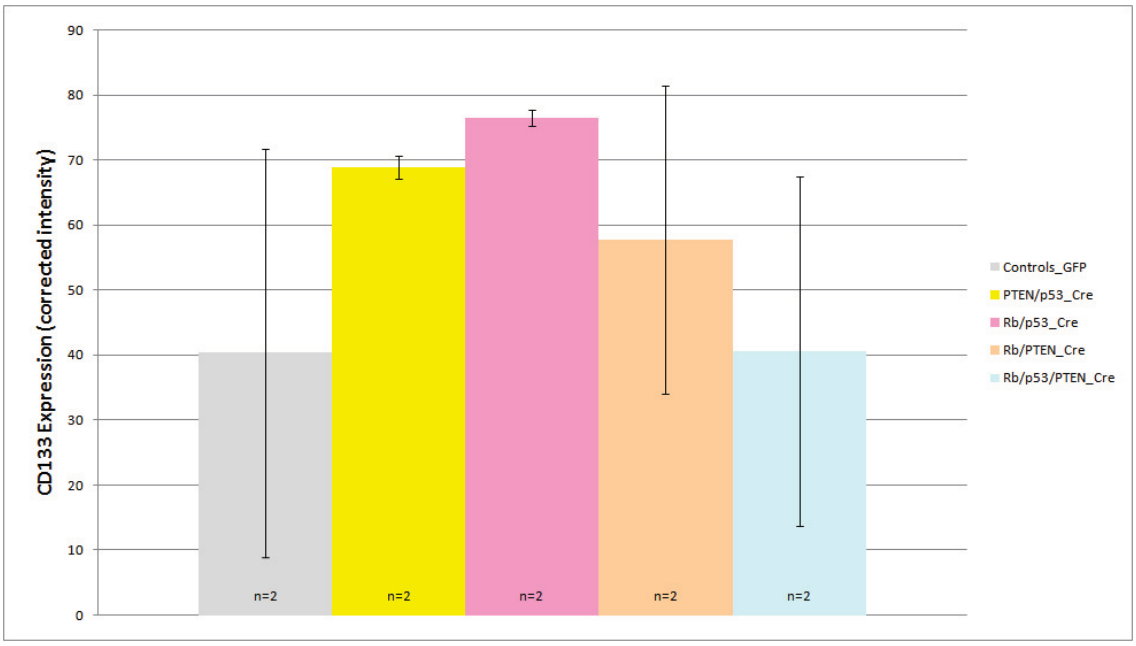

Figure 86: There are no statistically significant differences in the levels of CD133 expressed by non-recombined Adenovirus-GFP-infected controls vs. $PTEN^{-/-}$; $p53^{-/-}$ vs. $Rb^{-/-}$; $p53^{-/-}$ vs. $Rb^{-/-}$; $PTEN^{-/-}$ vs. $Rb^{-/-}$; $p53^{-/-}$; $PTEN^{-/-}$ NS *in vitro* (n=2 for each genotype). A bar chart comparing the grouped corrected CD133 expression intensities (net CD133 intensity / net β-actin intensity, *1000) expressed (y-axis) by each of the five genotypes of tumourigenic NS *in vitro* (x-axis). Error bars: standard errors. No significance difference observed between any of the groups (one-way ANOVA with Bonferroni's multiple comparison correction).

No statistically significant differences were observed in the level of CD133 expression between any of the *in vitro* NS genotypes being examined (including non-recombined Adenovirus-GFP-infected controls) (Figure 86). The genotype sample sizes were limited to two by the restriction of only using samples for which there was associated *in vivo* grafting data. In the case of the $PTEN^{-/-}$; $p53^{-/-}$ and $Rb^{-/-}$; $p53^{-/-}$ NS genotypes the internal variation in CD133 expression was minimal, whereas it was too large for a comparative analysis in the control, $Rb^{-/-}$; $PTEN^{-/-}$ and $Rb^{-/-}$; $p53^{-/-}$; $PTEN^{-/-}$ genotypes.

The variation in the $Rb^{-/-}$; $PTEN^{-/-}$ genotype is because only one of the two NS samples gave rise to tumours following intracerebral engraftment. Interestingly, these *in vivo* tumourigenic $Rb^{-/-}$; $PTEN^{-/-}$ NS generated glioblastomas with a 100% hit rate. Their level of CD133 expression was measured at a corrected intensity of 81.35 (the highest recorded across all the samples) versus the 34.01 (second lowest across all the experimental samples) measured from the $Rb^{-/-}$; $PTEN^{-/-}$ NS that generated no tumours (Figure 85). This validates the similar finding from sections 5.3.5 and 5.3.6 that *in vitro* CD133 expression may be a marker of glioma initiating cells.

The large variation observed within the control group raises the question of sample validity. The Western blot bands (Figure 84) themselves are valid, but the variation from a CD133 expression corrected intensity of 71.78 (control sample 1: Band #1) to 9.00 (control sample 2: Band #2) suggests that either a) Band #1 was caused by a sample or technical anomaly, or as previously proposed (section 5.3.6) b) CD133 protein expression *in vitro* is influenced more strongly by environmental conditions (e.g. culture conditions, general cellular health) than by the tumourigenic profile of the cells (combination of TSGs lost). The findings from sections 5.3.2 and 5.3.3 showed that *in vitro* recombined and tumourigenic NS were found to contain 12% CD133+ cells versus 2.5% in non-recombined controls. Ignoring control sample 1 (Band #1), this expected ~5-fold increase in CD133 expression from the controls to the $Rb^{-/-}$; $p53^{-/-}$; $PTEN^{-/-}$ NS was observed.

These findings suggest that *in vitro* CD133 expression is strongly influenced by environmental conditions which must be carefully controlled for if CD133 its potential as a marker of glioblastoma initiating cells is to be examined.

In an attempt to draw out any further correlations between *in vitro* CD133 expression and *in vivo* tumour hit rate, latency, and phenotype we once again plotted the Western blot data on a bubble plot of mean *in vivo* tumour latency (y-axis) vs. CD133 expression (x-axis) vs. *in vivo* tumour hit rate (z-axis: bubble size).

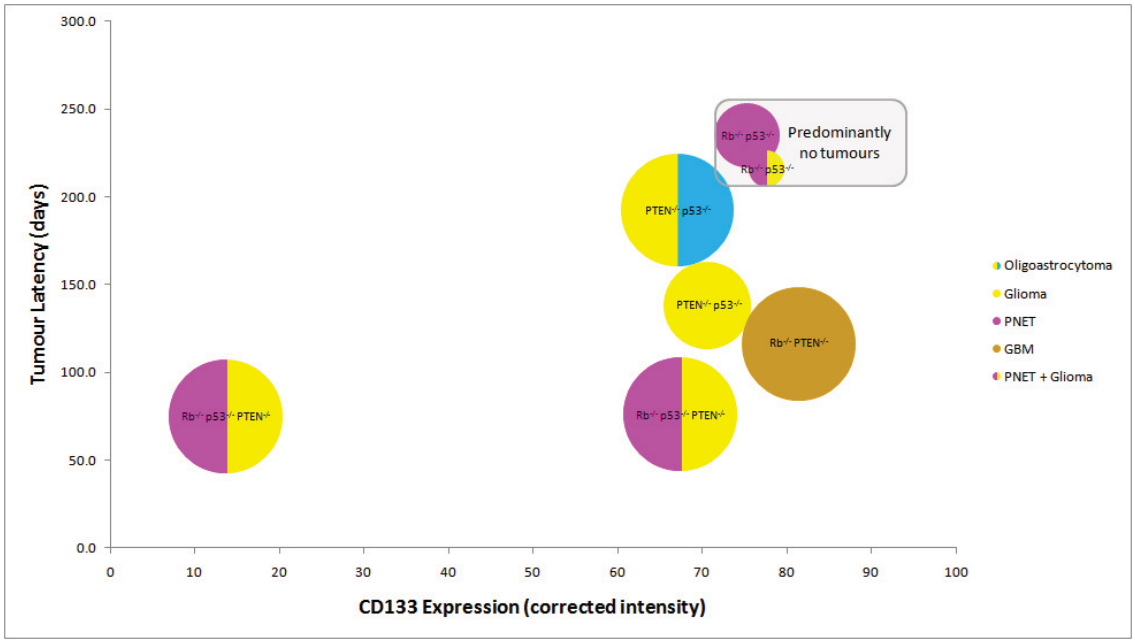

Figure 87: CD133 is most strongly expressed *in vitro* by NS that generate glioblastoma (glioblastoma) tumours following intracerebral engraftment, but no correlation was observed between CD133 expression and tumour hit rate or latency. Each bubble represents a single *in vivo* grafting experiment encompassing a cohort of 6-13 mice with the phenotype given being the predominant tumour phenotype generated and plotted according to *in vivo* tumour latency (y-axis) vs. CD133 expression (x-axis) vs. *in vivo* tumour hit rate (z-axis: bubble size). The *in vivo* engraftment data for the $Rb^{-/-}$; $p53^{-/-}$ NS is included for comparison purposes despite predominantly generating no tumours.

Despite generating few tumours *in vivo*, the $Rb^{-/-}$; $p53^{-/-}$ NS possessed a high relative expression of CD133 *in vitro* (Figure 87). This finding confirms the lack of a correlation between *in vitro* CD133 expression and tumour hit rate. Also, no correlation was observed between CD133 expression and tumour latency, as shown by the two $Rb^{-/-}$; $p53^{-/-}$; $PTEN^{-/-}$ NS grafting cohorts which expressed vastly different levels of CD133 *in vitro* despite having indistinguishable tumour profiles (Figure 87). The only finding validated by this visualisation was the trend between a high relative expression of CD133 *in vitro* and a propensity towards generating a glioblastoma tumour *in vivo*.

5.4 Conclusion

In this chapter we demonstrated that CD133 is expressed *in vivo* by the same SVZ NSCs that generate tumours following i.c.v. Adenovirus-Cre-mediated recombination of TSGs. In addition, this *in vivo* expression of CD133 was maintained by the SVZ NSCs when grown as NS *in vitro*. Interestingly, we identified that only 2.5% of wild-type

NSCs express CD133, a similar proportion to that seen with colon cancer cells (Ricci-Vitiani et al., 2007), but that this proportion rose to 12% following tumourigenic transformation (to $Rb^{-/-}$; $p53^{-/-}$; $PTEN^{-/-}$ NSCs). This is the first model system to suggest a causative link between elevated CD133 expression and early neoplastic transformation (pre-tumour development). Additionally, it is also the first model to identify that CD133 possesses a dynamic expression equilibrium *in vitro*, seemingly governed by an interaction between the functional properties of the NSCs and their health state / microenvironment. Both wild-type and tumourigenic NSCs were found to possess a similar CD133 expression equilibrium of ~7.5%, but the rate of equilibration for the tumourigenic NSCs was notably slower (11 passages) than for the wild-type NSCs (2 passages). It was thought that this could have been as a result of a functional differences between wild-type and tumourigenic and/or CD133+ and CD133- NSCs, and indeed we found that CD133 expression positively correlates with the *in vitro* growth rate (but not the NS-forming ability) of tumourigenic NSCs. However, the variability in the equilibration rates observed versus the highly reproducible *in vitro* growth rates suggests that the CD133 expression equilibrium is influenced most strongly by NSC health state and culture conditions. The contribution of such variable influencers to CD133 expression may account for the ambiguity surrounding the status of CD133 as a marker of BTICs, as seen in the literature (Bao et al., 2006; Shmelkov et al., 2008; Griguer et al., 2008). Nevertheless we are able to report that *in vitro* recombined $Rb^{-/-}$; $p53^{-/-}$; $PTEN^{-/-}$ NSCs possess an elevated basal level of CD133 expression and an altered pattern of CD133 expression when compared to wild-type controls, and that further work is required to deduce the functional characteristics governing the level of CD133 expression and its rate of equilibration. In contrast to reports in the literature that CD133- cells do not represent the BTIC (Bao et al., 2006) we found that CD133- NSCs generated tumours following intracerebral engraftment, and did so with a tumour profile (hit rate, latency, phenotype) that was similar to non-sorted tumourigenic NSCs. Although no correlation was observed between NSC CD133 expression and *in vivo* tumour hit rate or latency, a potential correlation was identified between elevated expression and a propensity towards generating glial, or more specifically glioblastoma, tumours. This finding supports the widespread documentation of CD133 as a marker of the glioblastoma cancer stem cell (Singh et al., 2003; Murat et al., 2008). In addition, we originally proposed that a part of the functional difference between CD133- and CD133+ NSCs may be hypoxia-related and that CD133+ NSCs may be more resistant to the *in vivo* environment and subsequently possess an increased tumour hit rate.

However, we in fact saw that CD133-/+ NSCs possessed comparable tumour hit rates (41.7% and 33.3%) following *in vivo* engraftment. To this end, we validated the status of HIF1α as a surrogate marker of CD133 but deduced that the relationship is not a basic inverse correlation as high levels of both proteins were observed in glioblastoma-generating NS, suggestive of aberrantly functioning hypoxia-response mechanisms.

The majority of research has focussed on the origins of BTICs as neural stem or progenitor cells (Zaidi et al., 2009), however, in the next chapter we address whether terminally differentiated astrocytes can contribute to the development of brain tumours.

5.5 Future Work

The methodological rigour of the MACS / FACS studies should be strengthened through the inclusion of isotype controls into the experimental design. Only $Rb^{-/-}$; $p53^{-/-}$; $PTEN^{-/-}$ NSCs were FACS analysed for their level of CD133 expression. By repeating this analysis, along with an equilibration rate analysis, for all the other NSC genotypes it would allow us to assess the effect of TSG loss on CD133 expression in addition to allowing a more robust comparison between CD133 expression and *in vivo* tumour phenotype. A full *in vitro* functional characterisation of these additional genotypes would also allow us to examine whether the functional effects of CD133 expression are genotype-dependent. NSC self-renewal and multipotency assays should be included in the *in vitro* functional assay portfolio to examine the effect of CD133 expression of the two defining qualities of NSCs. Finally, the correlations analysis between CD133 expression and *in vivo* tumour hit rate and latency were based on a maximum sample number of n=2. The intrinsic variability of both CD133 and HIF1α expression meant that any statistical analyses were underpowered. It is therefore necessary to significantly increase those sample numbers to allow for a more robust and viable analysis.

6 The Relative Contribution of Terminally Differentiated Astrocytes to the Development of Brain Tumours

6.1 Introduction

The majority of research has focussed on the role of neural stem, neural progenitor, and stem-like cells (Zaidi et al., 2009) and less is understood about the relative contribution of mature cell types to the development of intrinsic brain tumours. Knocking-out the cell cycle regulator genes Ink4a-Arf and constitutively activating the EGF receptor in mature murine glial cells causes them to develop into high-grade gliomas (Bachoo et al., 2002). It is also possible that other differentiated cell types such as oligodendrocytes and neurons could possess the same ability. These models have extrinsically induced neoplastic transformation by the loss-of-function of TSGs and the incorporation of oncogenic factors. It is believed that this approach drives astrocytes to de-differentiate towards a stem-like tumourigenic cell type. It is therefore extremely difficult to attribute any *in vivo* tumourigenesis observed specifically to a terminally differentiated whose cellular signature will no longer be recognisable when compared to its original form. In section 1.8 we laid out the aim of addressing whether brain tumour initiating cells (BTICs) could originate from terminally differentiated cells such as astrocytes, however, such a process should be thought of as two-step considering that mature astrocytes may be able to de-differentiate into stem-like / progenitor cells, but it is only these stem-like / progenitor cells (regardless of origin) that have the ability to develop into BTICs.

Using our model system we set out to confirm whether terminally differentiated astrocytes are targeted for recombination by intracerebral Adenovirus-Cre administration, and to test the hypothesis of whether these mature astrocytes can undergo neoplastic transformation and contribute to tumourigenesis.

Aims

1. Verify whether i.c.v. Adenovirus-Cre administration targets terminally differentiated astrocytes, outside of the SVZ, for TSG recombination.
2. Assess whether TSG loss in terminally differentiated astrocytes induces a transformation in function and/or differentiation state of the cells.

3. Examine whether these hypothetically transformed astrocytes can generate tumours *in vivo*.

6.2 Materials and Methods

Refer to the main materials and methods (Chapter Two).

6.3 Results

6.3.1 Intracerebroventricular Adenovirus-Cre administration targets terminally differentiated astrocytes for recombination

In verify whether terminally differentiated astrocytes are susceptible to Adenovirus-mediated infection we injected Adenovirus-GFP into the cortices of wild-type C57/Bl6 mice and culled them after 7 days. The sub-cortical region, into which the Adenovirus-GFP was delivered, was found to have a high number of GFAP-positive mature astrocytes, a large proportion of which were also positive for GFP (Figure 88).

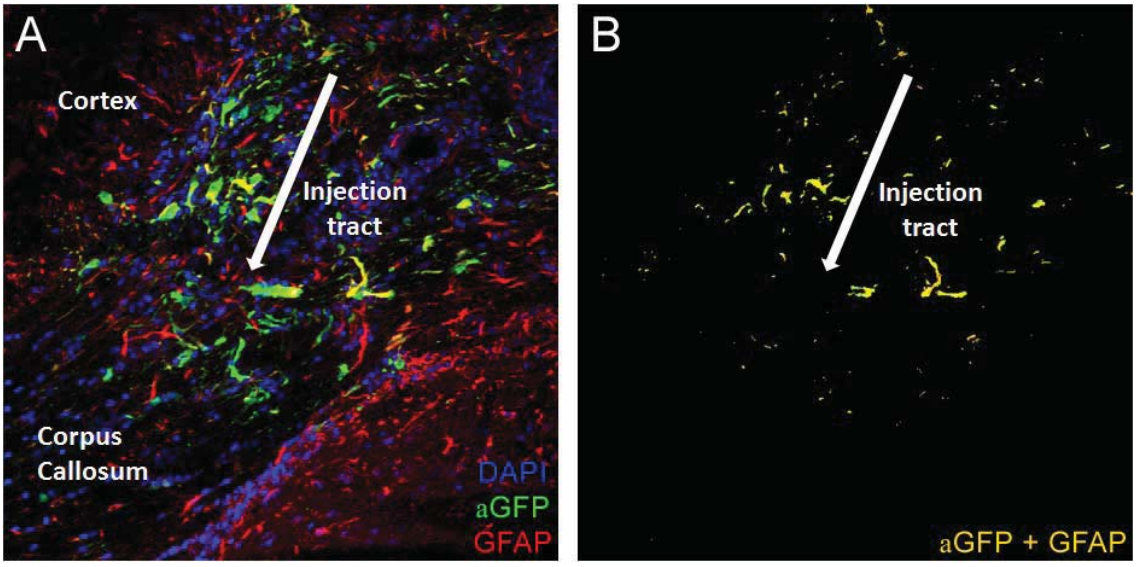

Figure 88: Mature astrocytes are targeted for infection by intracerebral Adenovirus-GFP administration. (A) Representative image showing the presence of both mature astrocytes (red) and Adenovirus-GFP infected cells (green). (B) Mature astrocytes can be targeted for Adenovirus-mediated recombination, as shown here by the colocalisation of the mature astrocytic marker GFAP with GFP at 7 days following intracerebral Adenovirus-GFP administration. DAPI: Hoechst nuclear staining, aGFP: GFP protein detected using an anti-GFP antibody, GFAP: glial fibrilliary acidic protein for the detection

of mature astrocytes, aGFP + GFAP: colocalisation of aGFP + GFAP). Blue: excitation at 405nm, green: excitation at 488nm, red: excitation at 546nm. Images were taken using a 20x objective on a Zeiss Axioplan 2 microscope and captured using a mounted AxioCam MRm camera and the Axiovision software.

The colocalisation of GFAP and GFP staining highlights that GFAP-positive mature astrocytes were targeted for infection by Adenovirus-GFP (Figure 88). This suggests that if Adenovirus-Cre were to diffuse into the brain parenchyma following i.c.v. administration it would target mature astrocytes for TSG recombination.

To validate this suggestion we retrospectively analysed the brains of 12 $Rb^{Lox/Lox}$; $p53^{Lox/Lox}$, 7 $Rb^{Lox/Lox}$; $p53^{Lox/Lox}$; $PTEN^{Lox/Lox}$, and 5 $PTEN^{Lox/Lox}$; $p53^{Lox/Lox}$ mice that received i.c.v. Adenovirus-Cre injections but that had survived more than twice the length of the expected tumour latency. Only mice with no SVZ β-galactosidase immunoreactivity were used for the analysis, as this would suggest that the Adenovirus-Cre injection had missed the lateral ventricles and targeted an ectopic (striatum, cortex, corpus callosum, hippocampus) region of the brain. These ectopic regions were then examined to see whether recombination had occurred in terminally differentiated cell types.

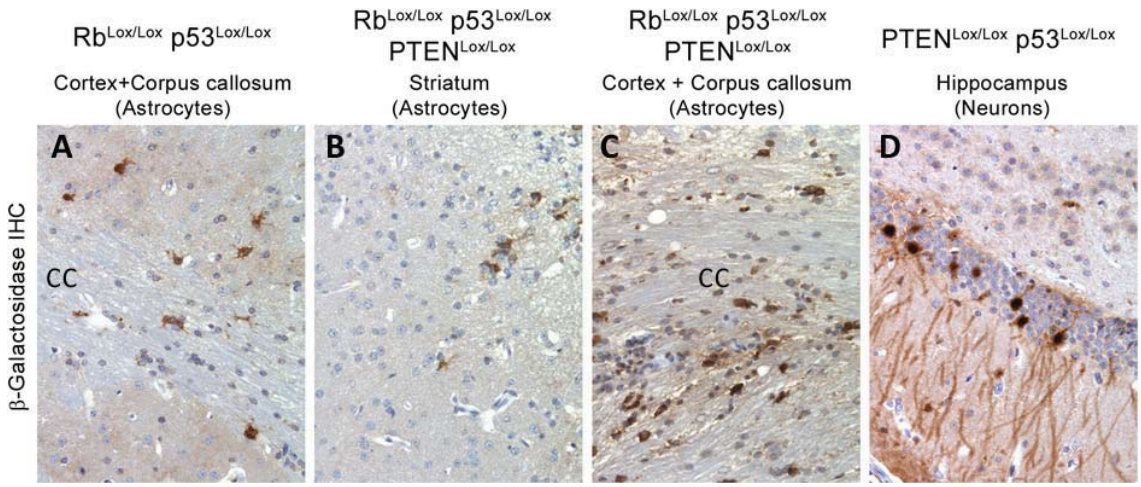

Figure 89: Ectopic injection of Adenovirus-Cre recombines grey and white matter astrocytes and hippocampal neurons *in vivo*. Representative images of recombined β-galactosidase-positive astrocytes (A-C) and neurons (D) in the cortex + corpus callosum (A,C), striatum (B), and hippocampus (D) of $Rb^{Lox/Lox}$; $p53^{Lox/Lox}$ (A), $Rb^{Lox/Lox}$; $p53^{Lox/Lox}$; $PTEN^{Lox/Lox}$ (B,C), and $PTEN^{Lox/Lox}$; $p53^{Lox/Lox}$ mice. CC: corpus callosum. Images were taken using a ColorView III digital camera mounted on a Zeiss Axioskop 2 MOT microscope with a 20x objective and using the AnalySIS software package.

β-galactosidase-positive recombination was found in both grey (cortex and striatum) and white (corpus callosum) matter astrocytes in the brains of $Rb^{Lox/Lox}$; $p53^{Lox/Lox}$ and $Rb^{Lox/Lox}$; $p53^{Lox/Lox}$; $PTEN^{Lox/Lox}$ mice (Figure 89: A-C). In addition, mature neurons of the hippocampus were observed to have been targeted for recombination in $PTEN^{Lox/Lox}$; $p53^{Lox/Lox}$ mice (Figure 89: D). Despite this, none of the brains examined exhibited any sign of neoplasms. This suggests that mature astrocytes and neurons, outside of the SVZ, may not contribute towards tumourigenesis. However, unless we analyse the ectopic expression of β-galactosidase in all the brains of mice which did develop tumours, then we cannot be sure that mature astrocytes do not contribute towards tumourigenesis as the occurrence may be extremely low.

6.3.2 *In vitro* recombination of Rb, p53, and PTEN in terminally differentiated astrocytes induces a functional transformation

As it is difficult to trace the origin of a neural progenitor / stem-like cell back to a terminally differentiated astrocyte *in vivo*, we devised an *in vitro* model system that allowed us to functionally characterise the effects of Rb, p53, and PTEN loss in fully differentiated astrocytes. To this end, astrocytes were derived from post-natal day 2-5 mice carrying the same LoxP genotypes as previously used. Rb, p53, and PTEN were then conditionally knocked-out in these astrocytes by *in vitro* recombination with Adenovirus-Cre. We propose the following four hallmark features the astrocytes must exhibit for them to be considered 'neoplastically transformed':

1. Increased growth rate and/or a loss of senescence;
2. Loss of contact inhibition (i.e. the ability of cells to grow over the top of one another in a disorganised fashion *in vitro*);
3. Loss of adhesion dependence (i.e. the ability of cells to grow as free-floating aggregates *in vitro*, or metastisise *in vivo*);
4. Capable of *in vivo* tumourigenesis.

In order to address point one we characterised the effect inactivation of the TSGs Rb, p53, and PTEN had on the *in vitro* growth rate of astrocytes by using the WST-1 proliferation assay to measure their cumulative mitochondrial activity (as a surrogate marker of growth rate) at 0, 4, 6, and 8 hours after a 2 day incubation period.

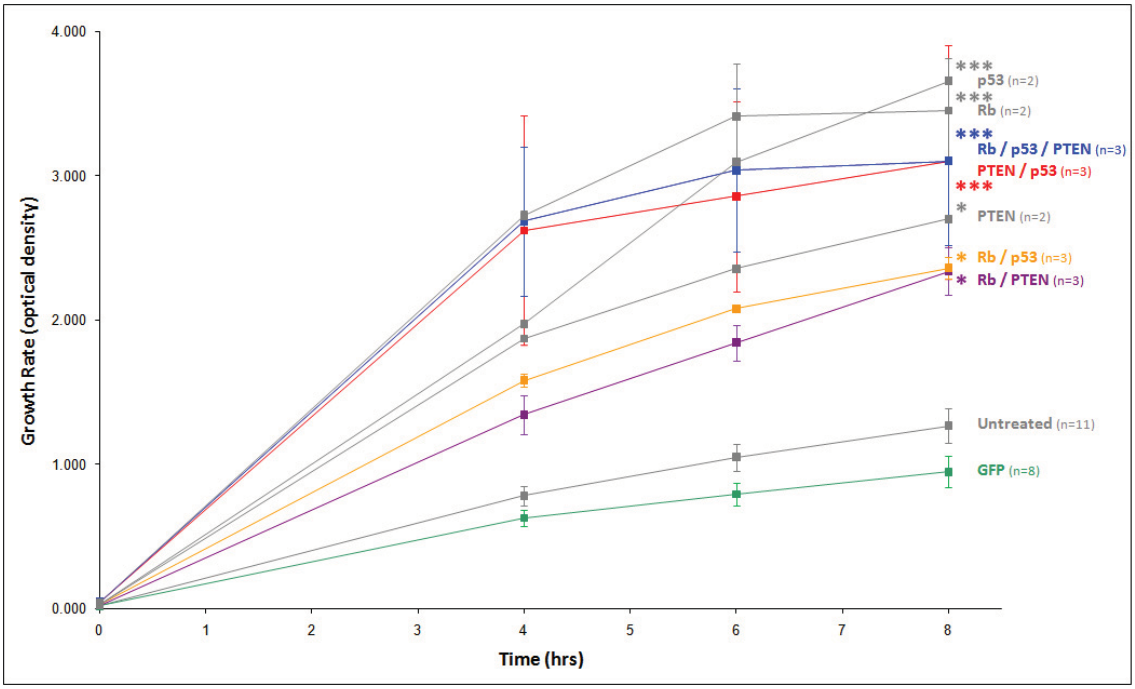

Figure 90: The growth rates of *in vitro* recombined Rb$^{-/-}$; p53$^{-/-}$; PTEN$^{-/-}$, PTEN$^{-/-}$; p53$^{-/-}$, Rb$^{-/-}$, and p53$^{-/-}$ astrocytes at passage 3 are significantly higher than that of non-recombined Adenovirus-GFP-infected control astrocytes. The Rb$^{-/-}$; p53$^{-/-}$, Rb$^{-/-}$; PTEN$^{-/-}$, and PTEN$^{-/-}$ astrocytes also grew significantly faster than the Adenovirus-GFP-infected control astrocytes but to a lower degree than the other genotypes. There was no significant difference in growth between any of the experimental genotypes. Using the WST-1 assay the growth rate (y-axis) of astrocytes at passage 3 was measured at 0, 2, 4, and 8hrs (x-axis) after a 2 day incubation period. Growth rate of *in vitro* recombined Rb$^{-/-}$; p53$^{-/-}$; PTEN$^{-/-}$ (blue: n=3) vs. PTEN$^{-/-}$; p53$^{-/-}$ (red: n=3) vs. Rb$^{-/-}$; p53$^{-/-}$ (orange: n=3) vs. Rb$^{-/-}$; PTEN$^{-/-}$ (purple: n=3) vs. Rb$^{-/-}$ (grey: n=2) vs. p53$^{-/-}$ (grey: n=2) vs. PTEN$^{-/-}$ (grey: n=2) vs. non-recombined untreated (grey: n=11) vs. non-recombined Adenovirus-GFP-infected (green: n=8) astrocytes. Error bars: standard errors. *: P<0.05 vs. GFP control at 8hrs, ***: P<0.001 vs. GFP control at 8hrs (one-way ANOVA with Bonferroni's multiple comparison correction).

As with the NSC WST-1 assay, a decreased growth rate the non-recombined Adenovirus-GFP-infected astrocytes (Figure 90: green data set) was observed when compared against the non-recombined untreated NSCs (Figure 90: grey data set), and highlighted a potential Adenovirus-mediated reduction on growth. However, this difference was not significant (as with the NSC WST-1 assay) and the Adenovirus-GFP-infected astrocytes were used as the control group for the purpose of statistical analysis. All of the experimental genotypes, regardless of the number of TSGs lost, exhibited a significantly increased growth rate over the controls. The Rb$^{-/-}$; p53$^{-/-}$; PTEN$^{-/-}$ (3.10 +/- 0.59; 8hrs), PTEN$^{-/-}$; p53$^{-/-}$ (3.10 +/- 0.81; 8hrs), Rb$^{-/-}$ (3.45 +/- 0.26;

8hrs) and $p53^{-/-}$ (3.66 +/- 0.36; 8hrs) astrocytes demonstrated the most significant ($P<0.001$) increase in growth rate over the Adenovirus-GFP-infected controls (0.95 +/- 0.11) (Figure 90). And the $Rb^{-/-}$; $p53^{-/-}$ (2.36 +/- 0.08; 8hrs), $Rb^{-/-}$; $PTEN^{-/-}$ (2.34 +/- 0.17; 8hrs) and $PTEN^{-/-}$ (2.70 +/- 0.01; 8hrs) astrocytes also demonstrated a significant increase in growth rate ($P<0.05$) over the controls, but to a lesser extent than the other experimental genotypes. Despite this, no significant difference was observed between any of the experimental genotypes. Overall, the *in vitro* recombined astrocytes possessed a similar genotype-dependent growth rate profiles as the NSCs (section 3.3.3), but with two notable exceptions. Firstly, the single knock-out astrocyte genotypes all exhibited increased growth rates over the controls, and in the case of $Rb^{-/-}$ and $p53^{-/-}$ even greater than the double knock-out $Rb^{-/-}$; $p53^{-/-}$ and $Rb^{-/-}$; $PTEN^{-/-}$ genotypes. This contradicts the previously proposed additive effect of additional TSG loss on *in vitro* growth rate. However, after passage one in culture (prior to the WST-1 assay), immediately following *in vitro* recombination, the single knock-out astrocytes were observed to grow even slower than the controls. As a result, the single knock-out astrocytes had to be kept in culture for a significantly extended period of up to four months rather than the typical two weeks for them to reach the passage requirement for the WST-1 assay. After passage two the single knock-out astrocytes began to grow more quickly and we propose that this was as a result of acquiring additional mutations in genes / pathways outside of those targeted for recombination. This acquired growth advantage is therefore not directly representative of the TSGs targeted for recombination. The second difference observed between the growth rate profiles of the astrocytes and the NSC was that the $Rb^{-/-}$; $p53^{-/-}$ astrocytes exhibited a significant increase over the controls, suggesting that the mechanisms governing growth rate may be different between astrocytes and NSCs. However, the increase in $Rb^{-/-}$; $p53^{-/-}$ astrocyte growth rate was only double that of the control; the same relative increase as observed with the $Rb^{-/-}$; $p53^{-/-}$ NSCs.

Taken together, these findings verify that inactivation of the TSGs Rb, p53, and PTEN in astrocytes confers an increased growth rate. To confirm that these astrocytes were also immortalised, we kept $Rb^{-/-}$; $p53^{-/-}$ astrocytes in culture for 75 passages without observing any signs of senescence.

Point two was addressed by observing *in vitro* recombined astrocytes in their normal culture conditions. And point three was addressed by plating *in vitro* recombined

astrocytes into pro-mitogenic NSC medium to observe whether they could grow in a similar manner to neurospheres.

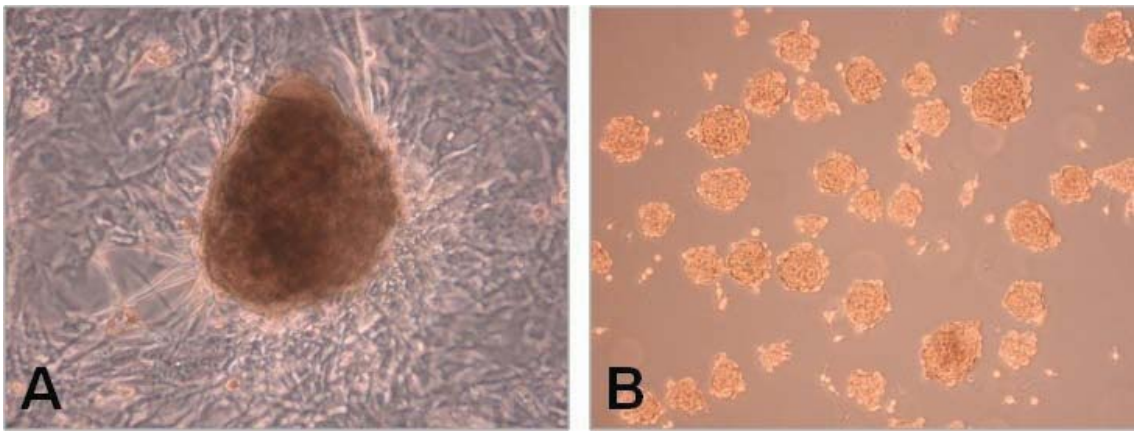

Figure 91: *In vitro* recombined $Rb^{-/-}$; $p53^{-/-}$; $PTEN^{-/-}$ astrocytes appear to transform as shown by their loss of contact inhibition as they are observed to grow over the top of one another (A), and loss of adhesion dependence as they are observed to grow as free-floating NS-like aggregates when plated as a single cells (B).

Recombined $Rb^{-/-}$; $p53^{-/-}$; $PTEN^{-/-}$ astrocytes were observed to grow in a disorganised non-uniform manner *in vitro* (Figure 91: A). Rather than growing as an adherent monolayer that arrests upon confluence the astrocytes had lost their contact inhibition and grew over the top of one another and even formed aggregated buds in areas of high density. In some cases these buds were observed to detach from the plates and grow as free-floating aggregates. In addition, astrocytes plated in NSC medium were observed to grow non-adherently as free-floating NS-like aggregates termed "astrospheres" (Figure 91: B). These astrospheres could be serially passaged (an indirect measure of self-renewal), suggesting that they could represent de-differentiated astrocytes with stem-like properties.

6.3.3 *In vitro* recombination of Rb, p53, and PTEN appears to shift mature astrocytes towards a de-differentiated phenotype

In sections 6.3.1 and 6.3.2 we suggested that terminally differentiated astrocytes could become tumourigenic by first de-differentiating into neural progenitor / stem-like cells, as originally proposed by Laywell et al in 2000 (Laywell et al., 2000). We

immunofluorescently stained astrocytes (passage three) grown on glass coverslips for GFAP and nestin to examine the effect of TSG loss on their expression profile.

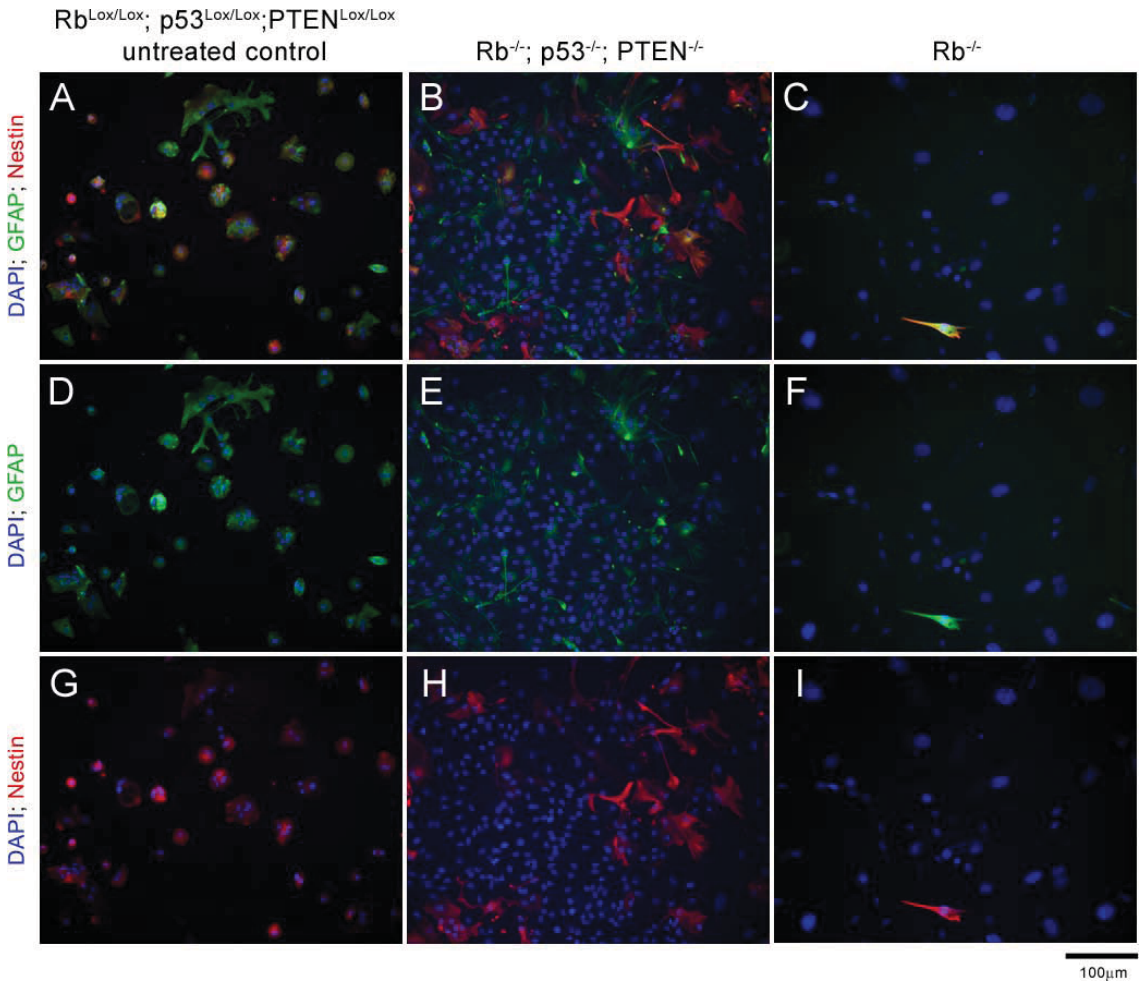

Figure 92: The number of astrocytes expressing the differentiation biomarkers GFAP and nestin appears to reduce after *in vitro* recombination of the TSGs Rb, p53, and PTEN; suggestive of an altered phenotype. Representative images of $Rb^{Lox/Lox}$; $p53^{Lox/Lox}$; $PTEN^{Lox/Lox}$ non-recombined untreated control (A,D,G) vs. $Rb^{-/-}$; $p53^{-/-}$; $PTEN^{-/-}$ (B,E,H) vs. $Rb^{-/-}$ (C,F,I) astrocytes at passage three that were left to grow on laminin-coated glass coverslips for 5 days before being fixed and immunofluorescently dual-stained for GFAP and nestin (A-C) with the individual GFAP (D-F) and nestin (G-I) stains also given. All cells were counterstained with Hoechst 33342 (DAPI). Blue: excitation at 405nm, green: excitation at 488nm, red: excitation at 546nm. Images were taken Zeiss AxioCam MRm camera mounted on a Zeiss Axioplan 2 microscope using a 20x objective and the Axiovision software.

The majority of non-recombined untreated $Rb^{Lox/Lox}$; $p53^{Lox/Lox}$; $PTEN^{Lox/Lox}$ astrocytes at passage three expressed GFAP and/or nestin (Figure 92: A,D,G), with co-expression also observed in the majority of the cells. However, fewer *in vitro* recombined $Rb^{-/-}$; $p53^{-/-}$; $PTEN^{-/-}$ astrocytes expressed GFAP and/or nestin, and co-expression was also

seen in less cells (Figure 92: B,E,H). This suggests that *in vitro* recombination of Rb, p53, and PTEN alters the expression profile of astrocytes. It is difficult to verify whether this altered expression profile corresponds to an altered de-differentiated phenotype, as the decreased number of GFAP-expressing cells suggests de-differentiation away from the astrocytic lineage but the reduced number of nestin-expressing cells suggests a progression towards a more differentiated cell phenotype (Vescovi et al., 1993). For this reason, additional markers of differentiation are required to verify this hypothetical de-differentiation. To illustrate the reduced growth crate of single knock-out astrocytes immediately following *in vitro* recombination, we included $Rb^{-/-}$ astrocytes in the analysis. Firstly, the overall number of viable cells observed at five days post-plating was less than both the control and $Rb^{-/-}$; $p53^{-/-}$; $PTEN^{-/-}$ astrocytes. And secondly, the number of cells expressing GFAP and/or nestin had almost disappeared (Figure 92: C,F,I).

To verify whether the $Rb^{-/-}$; $p53^{-/-}$; $PTEN^{-/-}$ astrocytes were driven to a de-differentiated state we trypsinised confluent passage three astrocytes from *in vitro* culture and studied the expression of a range of different biomarkers using the cytoblock paraffin immunohistochemistry format.

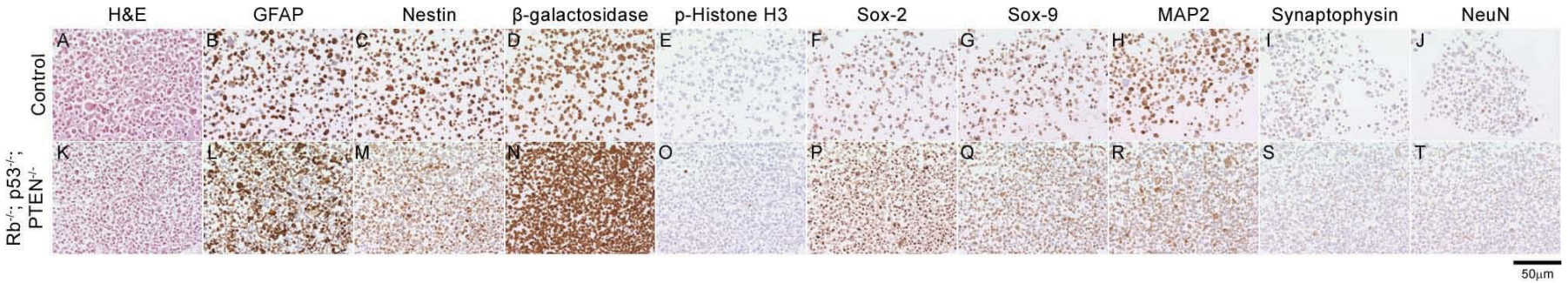

Figure 93: *In vitro* recombined $Rb^{-/-}$; $p53^{-/-}$; $PTEN^{-/-}$ astrocytes appear to an increased expression of Sox-2, and in a greater number of cells, but a reduced expression of nestin and MAP2; suggestive of a de-differentiated phenotype. Representative images taken from cytoblocks of non-recombined untreated $Rb^{Lox/Lox}$; $p53^{Lox/Lox}$; $PTEN^{Lox/Lox}$ (A-J) vs. $Rb^{-/-}$; $p53^{-/-}$; $PTEN^{-/-}$ (K-T) astrocytes stained for haematoxylin-eosin (A,K), GFAP (B,L), nestin (C,M), β-galactosidase (D,N), phospho-Histone H3 (E,O), Sox-2 (F,P), Sox-9 (G,Q), MAP2 (H,R), synaptophysin (I,S), and NeuN (J,T). Images were taken using a ColorView III digital camera mounted on a Zeiss Axioskop 2 MOT microscope with a 10x magnification and using the AnalySIS software package.

The $Rb^{-/-}$; $p53^{-/-}$; $PTEN^{-/-}$ astrocytes appeared to possess an atypical morphology when compared to the non-recombined untreated controls, as shown by their shrunken and more spherical cellular appearance (Figure 93: K vs. A). As expected the $Rb^{-/-}$; $p53^{-/-}$; $PTEN^{-/-}$ astrocytes were β-galactosidase-positive (Figure 93: N vs. D) and exhibited increased proliferation as demonstrated by their phospho-Histone H3 immunoreactivity (Figure 93: O vs. E). As a verification of the earlier immunofluorescence finding, *in vitro* recombination of Rb, p53, and PTEN appeared to cause a reduction in the number of nestin-expressing cells with a reduction also observed in the strength of its expression (Figure 93: M vs. C). However, despite previously suggesting that the number of GFAP-expressing cells was lower in the $Rb^{-/-}$; $p53^{-/-}$; $PTEN^{-/-}$ astrocytes (as measured by immunofluorescence), here we observed a comparative pattern and level of GFAP to the control (Figure 93: L vs. B). Comparable levels of expression were also observed with the putative stem cell marker Sox-9 (Figure 93: Q vs. G) and the differentiated neuronal markers synaptophysin (Figure 93: S vs. I) and NeuN (Figure 93: T vs. J). However, a notable increase was observed in the level and number of cells expressing the stem cell marker Sox-2 (Figure 93: P vs. F) with an associated reduction in the level of MAP2 expression (Figure 93: R vs. H). Nestin is not an undisputable marker of de-differentiated cells as a reduction in its expression may be due to TSG loss rather than de-differentiation, and chromosomal loss of the nestin locus is possible.

Taking all of these findings into account, it appears that *in vitro* recombination of the TSGs Rb, p53, and PTEN shifts mature astrocytes towards a high Sox-2 and low nestin/MAP2-expressing de-differentiated phenotype.

6.3.4 *In vitro* recombined and engrafted astrocytes do not give rise to tumours and degenerate by four weeks

To address the fourth criterion of neoplastic transformation we grafted *in vitro* recombined astrocytes into the striata of non-recombined mice of the same genetic background. Engraftment of at least 10^5 *in vitro* recombined astrocytes into 48 immune-competent mice (11 received $Rb^{-/-}$; $PTEN^{-/-}$ astrocytes, 9 received $Rb^{-/-}$; $p53^{-/-}$ astrocytes, 14 received $Rb^{-/-}$; $p53^{-/-}$; $PTEN^{-/-}$ astrocytes, 6 received $p53^{-/-}$ astrocytes, and 8 received $Rb^{-/-}$ astrocytes) of the same genetic background did not result in a single viable tumour when the mice were left for up to 307 days post-engraftment (Figure 94).

Experiment	Adenovirus	Vol. Injected (ul)	Passage #	Genotype (cells)	# Mice	Age (start)	Age (end)	Incubation (d)	Cause of Death	QN	Diagnosis
24/06/2008	cre	8ul	5	Rb / Rosa	8						
						63d	77d	14	time-cull, 21.5g	1771-08	no tumour
						63d	77d	14	time-cull, 22g	1772-08	no tumour
						63d	77d	14	time-cull, 21g	1773-08	no tumour
						63d	77d	14	time-cull, 21.5g	1774-08	no tumour
						44d	283d	239	experiment terminated, 33g	1098-09	no tumour
						44d	283d	239	experiment terminated, 38g	1099-09	no tumour
						44d	283d	239	experiment terminated, 34g	1100-09	no tumour
						44d	283d	239	experiment terminated, 30g	1101-09	no tumour
25/04/2008	cre	12.5ul	12	Rb / p53 / Rosa (astrospheres)	5						
						69d	70d	1	f/d the next day	-	-
						69d	70d	1	f/d the next day	-	-
						61d	72d	11	time-cull, 21g	1120-08	viable graft
						69d	134d	65	25.7g	1765-08	no tumour (L2 for photo)
						69d	134d	65	24.4g	1766-08	no tumour (scar)
17/04/2008	cre	12.5ul	3	p53 / Rosa	6						
						74d	74d	0	didn't recover from anaesthesia	-	-
						74d	102d	28	time-cull (1 month)	1386-08	no tumour
						80d	108d	28	time-cull (1 month)	1387-08	no tumour
						52d	190d	138	sick	2373/74-08	no tumour
						74d	236d	162	f/d	-	-
						80d	268d	168	sick	2869-08	no tumour
04/04/2008	cre	12.5ul	4	Rb / p53 / PTEN / Rosa	11 nude mice						
						44d	58d	14	time-cull, 25.9g, skull with lump	1024/25-08	no tumour
						44d	58d	14	time-cull, 19.7g	1026-08	no tumour
						44d	58d	14	time-cull, 25.2g, skin + lump	1027-08	no tumour
						44d	76d	32	time-cull, 27g, growth on skull	1112-08	no tumour
						44d	76d	32	time-cull, 24g, growth on skull	1113-08	no tumour
						44d	76d	32	time-cull, 25.5g, growth on skull	1114-08	no tumour
						44d	79d	35	sick, big growth on skull, 25.1g	1128/29-08	no tumour
						44d	79d	35	sick, growth on skull, 26.4g	1130/31-08	no tumour
						44d	79d	35	sick, growth on skull, 27.6g	1132/33-08	no tumour
						44d	79d	35	sick, growth on skull, 24.4g	1134/35-08	no tumour
						44d	79d	35	sick, growth on skull, 23.9g	1136/37-08	no tumour
04/04/2008	cre	12.5ul	10	Rb / p53 / Rosa	11 nude mice						
						44d	44d	0	f/d, didn't recover from anaesthesia	-	-
						44d	58d	14	time-cull, 24.1g	1028-08	no tumour, photo
						44d	58d	14	time-cull, 26.2g	1029-08	no tumour
						44d	76d	32	time-cull, 25g	1115-08	no tumour
						44d	76d	32	time-cull, 27g	1116-08	no tumour
						44d	76d	32	time-cull, 25.3g	1117-08	no tumour
						44d	76d	97	time-cull, 29.2g	2062-08	no tumour
						44d	76d	97	time-cull, 28g	2063-08	no tumour
						44d	76d	97	time-cull, 28g	2064-08	no tumour
						44d	76d	97	time-cull, 26g	2065-08	no tumour
						44d	76d	97	time-cull, 30g	2066-08	no tumour

03/07/2007	cre	12.5ul	4	Rb / p53 / PTEN / Rosa	14							
						76d	83d	7	time cull, 19g, dome shaped head	1720-07	no tumour	
						76d	83d	7	time cull, 22g	1721-07	no tumour	
						76d	83d	7	time cull, 29.9g	1722-07	no tumour	
						76d	84d	8	culled sick, 18g	1723-07	no tumour	
						35d	43d	8	culled sick, 14g	1724-07	no tumour	
						35d	49d	14	time-cull, 19.3g	1922-07	no tumour	
						35d	49d	14	time-cull, 20.1g	1923-07	no tumour	
						35d	49d	14	time-cull, 21.4g	1924-07	no tumour	
						76d	104d	28	time cull, 30.5g	2097-07	no tumour	
						76d	104d	28	time cull, 32.8g	2098-07	no tumour	
						76d	104d	28	time cull, 39g	2099-07	no tumour	
						76d	120d	44	time cull, 34g	2198-07	no tumour	
						76d	120d	44	time cull, 30.8g	2199-07	no tumour	
						35d	79d	44	time cull, 23.1g	2200-07	no tumour	
18/04/2007	cre	5ul	3	Rb / p53 / Rosa	9							
						62d	82d	20	time-cull	1026-07	no tumour	
						35d	174d	139	culled, 34g	2425-07	no tumour	
						35d	174d	139	culled, 34.1g	2426-07	no tumour	
						35d	174d	139	culled, 33g	2427-07	no tumour	
						62d	201d	139	culled, 33.3g	2428-07	no tumour	
						62d	201d	139	culled, 36.1g	2429-07	no tumour	
						35d	174d	139	culled, 26.1g	2430-07	no tumour	
						35d	174d	139	culled, 33.6g	2431-07	no tumour	
						35d	174d	139	culled, 28.4g	2432-07	no tumour	
15/11/2006	cre	5ul	5	Rb / PTEN / Rosa	11							
						36d	328d	292	culled, 31.6g	2414-07	no tumour	
						36d	328d	292	culled, 36.1g	2415-07	no tumour	
						36d	328d	292	culled, 24.5g	2416-07	no tumour	
						36d	328d	292	culled, 36.2g	2417-07	no tumour	
						36d	328d	292	culled, 30.3g	2418-07	no tumour	
						36d	328d	292	culled, 45.6g	2419-07	no tumour	
						36d	328d	292	culled, 37g	2420-07	no tumour	
						36d	328d	292	culled, 48.6g	2421-07	no tumour	
						59d	351d	292	culled, 28.4g	2422-07	no tumour	
						59d	351d	292	culled, 24.4g	2423-07	no tumour	
						59d	351d	292	culled, 29.2g	2424-07	no tumour	

Figure 94: Table outlining the parameters and results for all the *in vitro* recombined astrocytes engrafted into the brains of recipient mice.

This long-term finding led us to design and conduct a short-term study in the aim of tracking the short-term fate of engrafted astrocytes. $Rb^{-/-}$; $p53^{-/-}$; $PTEN^{-/-}$ astrocytes were used for this purpose as, like the NSCs, they possessed the highest *in vitro* growth rate. $1x10^6$ *in vitro* recombined $Rb^{-/-}$; $p53^{-/-}$; $PTEN^{-/-}$ astrocytes were grafted into the striata of 14 immune-competent mice of the same genetic background with time-culls (n=3 for each) performed at one, two, four, and six weeks post-engraftment, and the remaining mice (n=2) being left for long-term analysis (Figure 95).

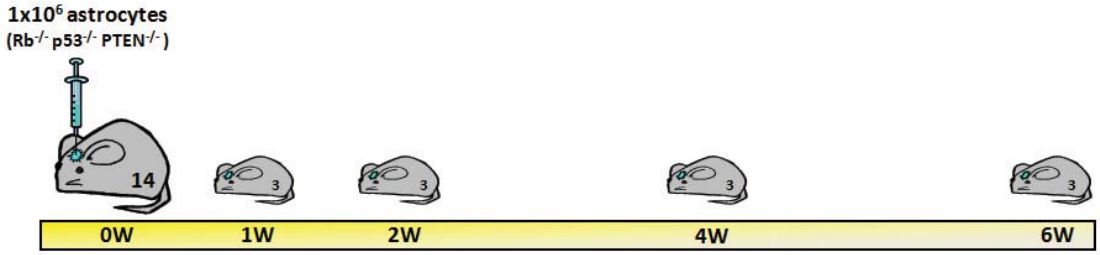

Figure 95: Schematic of the short-term astrocyte engraftment experiment indicating the number of $Rb^{-/-}$; $p53^{-/-}$; $PTEN^{-/-}$ astrocytes engrafted into the striata of 14 mice and the planned time culls (n=3 for each) at 1, 2, 4, and 6 weeks post-engraftment (the 2 remaining mice were left for a long-term assessment).

Two mice were culled after 8 days due to the onset of clinical symptoms. These mice were found to be suffering from hydrocephalus, presumably caused by some of the cells being deposited in the lateral ventricles and causing a blockage to the circulation of cerebral spinal fluid. Grafted astrocytes were detectable, as localized foci proximal to the graft site, up to two weeks post-engraftment (Figure 96: A,B). Their viability was demonstrated by their positive staining for BrdU (Figure 96: D, E), a synthetic nucleoside that is incorporated into the newly synthesized DNA of actively replicating/proliferating cells. However, by two weeks there was a decrease in the number of viable astrocytes associated with the graft site as shown by the reduced BrdU (Figure 96: D, E) and β-galactosidase (Figure 96: G, H) positivity. By four weeks the area that was previously occupied by the grafted astrocytes had been completely replaced by fibrous connective tissue (Figure 96: C). The complete degeneration and clearance of these proliferating astrocytes was validated by the negative BrdU (Figure 96: F) and β-galactosidase (Figure 96: I) stains of the graft site.

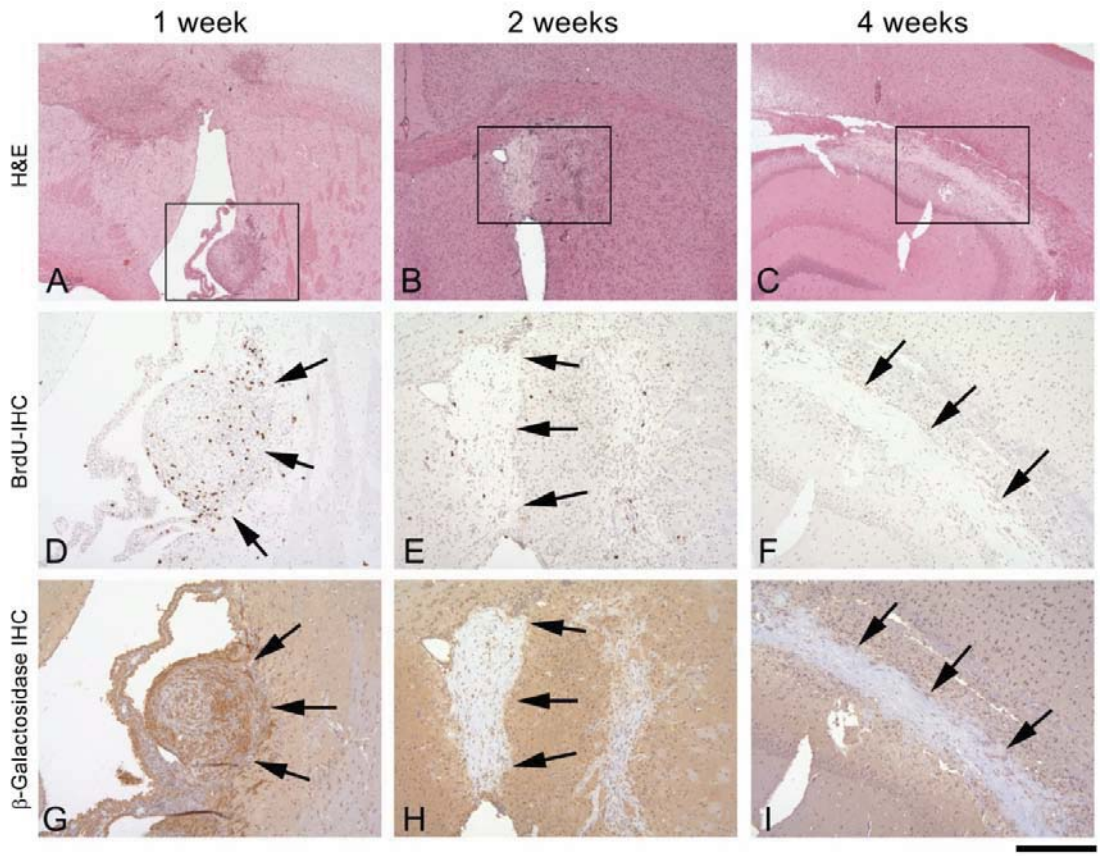

Figure 96: *In vitro* recombined and engrafted $Rb^{-/-}$; $p53^{-/-}$; $PTEN^{-/-}$ astrocytes do not give rise to tumours and degenerate by 4 weeks. Representative images taken from each time point showing that grafted astrocytes were detectable up to two weeks post-engraftment (A,B). After 1 week the grafted astrocytes were highly positive for BrdU (D) and β-galactosidase (G). However, by 2 weeks there was a decrease in the number of proliferating grafted astrocytes as shown by the combined reduced number of BrdU (E) and β-galactosidase (H) positive cells. By four weeks the grafted astrocytes had been completely cleared from the area (C, F, I). Images were taken using a ColorView III digital camera mounted on a Zeiss Axioskop 2 MOT microscope with a 2.5x magnification (A-C) or a 6.3x magnification (D-I) and using the AnalySIS software package. Scale bar: A-C, 700μm and D-I, 275μm.

These findings suggest that, despite their functional transformation *in vitro*, terminally differentiated astrocytes do not contribute to *in vivo* tumourigenesis in our model. Previous studies by other groups in which astrocytes were found to be capable of tumourigenesis all used immune-compromised mice (Bachoo et al., 2002; Lee et al., 2008b). It is therefore possible that by engrafting these cells into the brains of immune-competent mice we were less likely to observe astrocytic tumourigenesis due to an immune-mediated response against the cells. For this reason, repeated the experiment but engrafted the $Rb^{-/-}$; $p53^{-/-}$; $PTEN^{-/-}$ astrocytes into the striata of immune-deficient nude mice.

6.3.5 *In vitro* recombined astrocytes engrafted into immune-deficient nude mice do not give rise to tumours but persist as non-proliferating cells within the graft site for over 5 weeks

$5x10^5$ *in vitro* recombined $Rb^{-/-}$; $p53^{-/-}$; $PTEN^{-/-}$ astrocytes were grafted into the striata of 11 immune-deficient nude mice with time-culls (n=3 for each) performed at two and four weeks, and with the remaining mice being left for the long-term (n=5) to see if any tumours would develop (Figure 97).

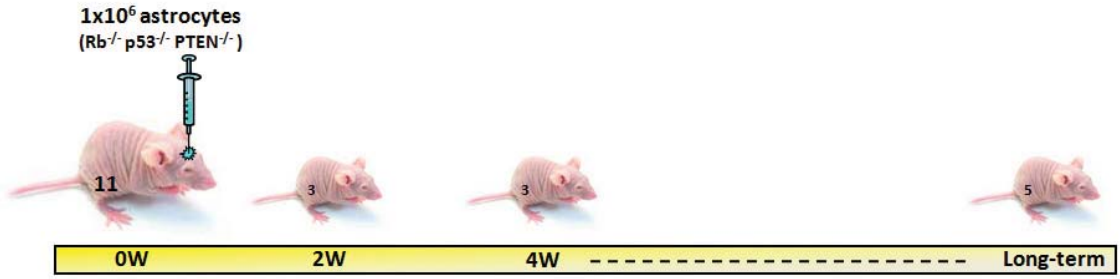

Figure 97: Schematic of the astrocyte engraftment experiment indicating number of $Rb^{-/-}$; $p53^{-/-}$; $PTEN^{-/-}$ astrocytes engrafted into the striata of 11 nude mice and the planned time culls at 2 (n=3) and 4 weeks (n=3) post-engraftment, with the remaining 5 mice left for long-term assessment.

The experiment was terminated after five weeks due to the remaining five long-term mice exhibiting clinical symptoms of behavioural incapacitation and extrinsic tumours of the skull. Grafted astrocytes were detectable, as localized foci proximal to the graft site, up to five weeks post-engraftment (Figure 98: A-C). Their viability and identity was confirmed up to two weeks by their positive staining for BrdU (Figure 98: D) and β-galactosidase (Figure 98: G). However, by four and five weeks there was a decrease in the number of proliferating grafted astrocytes associated as shown by the reduced number of BrdU-positive cells in the graft site (Figure 98: E, F). Despite no longer proliferating, the grafted astrocytes were observed to persist within the graft site after five weeks as verified by their positivity for β-galactosidase (Figure 98: I).

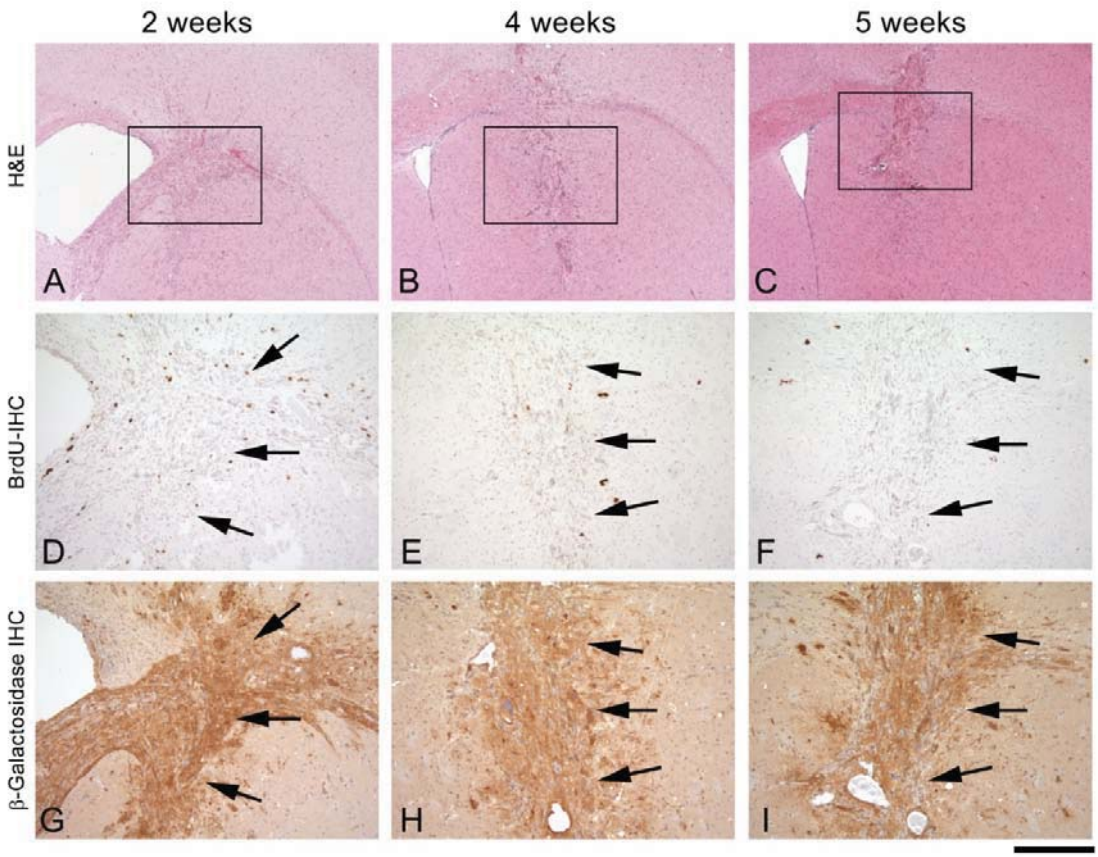

Figure 98: *In vitro* recombined $Rb^{-/-}$; $p53^{-/-}$; $PTEN^{-/-}$ astrocytes engrafted into the striata of nude mice do not give rise to tumours but are observed to persist as non-proliferating cells after 5 weeks. Representative images taken from each time point showing that grafted astrocytes were detectable up to five weeks post-engraftment (A-C). After 2 weeks the grafted astrocytes were positive for BrdU (D) and β-galactosidase (G). By 4 and 5 weeks there was a decrease in the number of proliferating transplanted astrocytes as shown by the reduced number of BrdU-positive cells (E,F). These grafted astrocytes, although not proliferating, had not been cleared and were observed to remain as β-galactosidase-positive cells (I). Images were taken using a ColorView III digital camera mounted on a Zeiss Axioskop 2 MOT microscope with a 2.5x magnification (A-C) or a 6.3x magnification (D-I) and using the AnalySIS software package. Scale bar: A-C, 700μm and D-I, 275μm.

Astrocytes were cleared from the graft site by four weeks in immune-competent mice, whereas they persisted in immune-deficient nude mice. This finding supports the hypothesis of an immune-mediated degeneration and clearance of the astrocytes in immune-competent mice. Despite this, this additional experiment provided no evidence to suggest that terminally differentiated astrocytes could be contribute to tumourigenesis. However, as previously stated, a number of mice exhibited large tumours of the skull over the course of the experiment. All five of the long-term mice,

and one of the two week time-cull mice, had to be culled due to the development of these tumours.

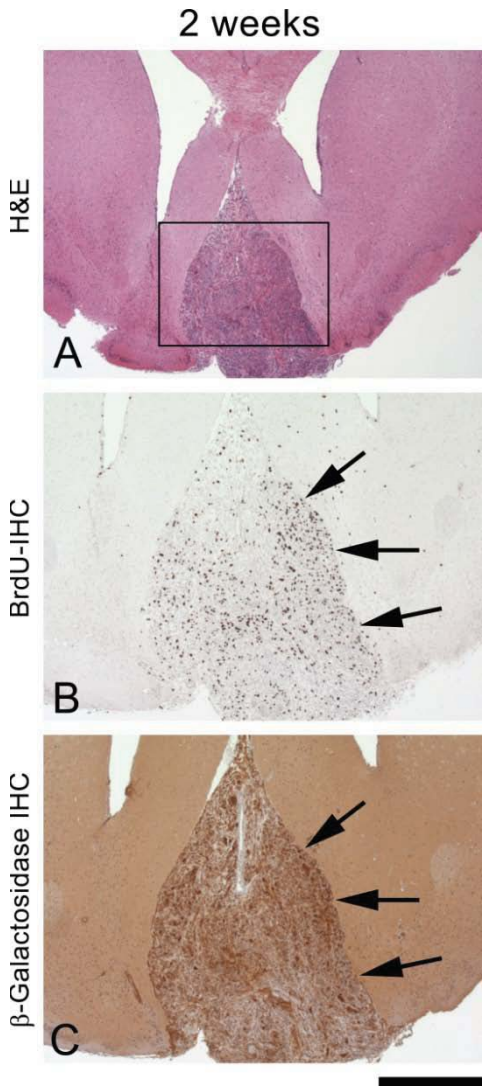

Figure 99: *In vitro* recombined Rb-/-; p53-/-; PTEN-/- astrocytes engrafted into nude mice can give rise to extrinsic tumours of the skull after 2 weeks. β-galactosidase-positive grafted astrocytes (C) were observed to generate a highly proliferating (B) extrinsic tumour mass (A). Images were taken using a ColorView III digital camera mounted on a Zeiss Axioskop 2 MOT microscope with a 1.6x magnification (A) or a 2.5x magnification (B,C) and using the AnalySIS software package. Scale bar: A, 700μm and B-C, 450μm.

In the two week time-cull mouse a large well-demarcated tumour cell mass was found to be mechanically infiltrating into the brain (Figure 99: A). The cells were identified as grafted astrocytes by the fact that they were highly proliferative (Figure 99: B) and positive for β-galactosidase (Figure 99: C). The pathology of the tumour was identified

as a large spindle cell tumour from an H&E stain of a skull fragment viewed under high power magnification in which the infiltration zone could be observed (Figure 100).

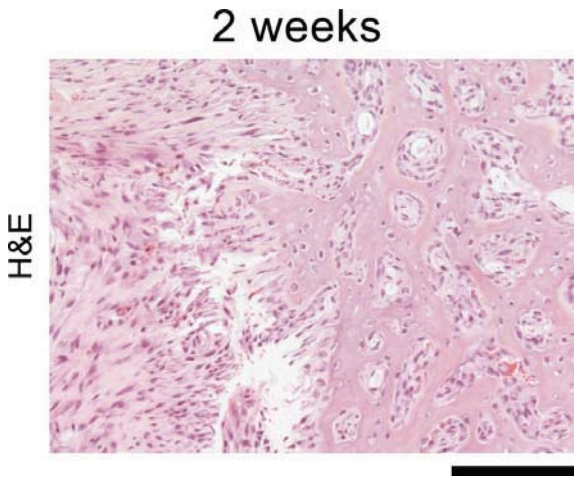

Figure 100: *In vitro* recombined Rb$^{-/-}$; p53$^{-/-}$; PTEN$^{-/-}$ astrocytes engrafted into the brains of nude mice can give rise to large spindle cell tumours within the skull after 2 weeks. Images were taken using a ColorView III digital camera mounted on a Zeiss Axioskop 2 MOT microscope with a 10x magnification and using the AnalySIS software package. Scale bar: 175 μm.

However, these tumours cannot be considered as intrinsic brain tumours as they develop extrinsically and intrude into the brain parenchyma.

6.3.6 *In vitro* recombined Rb$^{-/-}$; p53$^{-/-}$ astrocytes grown as NS-like "astrospheres" behaviourally resemble their neural stem cell counterparts but do not give rise to tumours

As previously mentioned, astrocytes are usually cultured adherently in the presence of fetal calf serum. However, astrocytes plated in pro-mitogenic NSC medium were observed to grow non-adherently as free-floating aggregates we termed "astrospheres" (Figure 91). These astrospheres could be serially passaged (an indirect measure of self-renewal), suggesting that they could represent de-differentiated astrocytes with stem-like properties. To characterise the functional changes associated with this transformation we measured the *in vitro* growth rate (WST-1 assay) and aggregate-forming ability (AS size and AS-forming clonogenicity assays) of Rb$^{-/-}$; p53$^{-/-}$ astrospheres. No statistical comparisons could be made between the different cell types in each of these assays as the astrosphere sample size was only one.

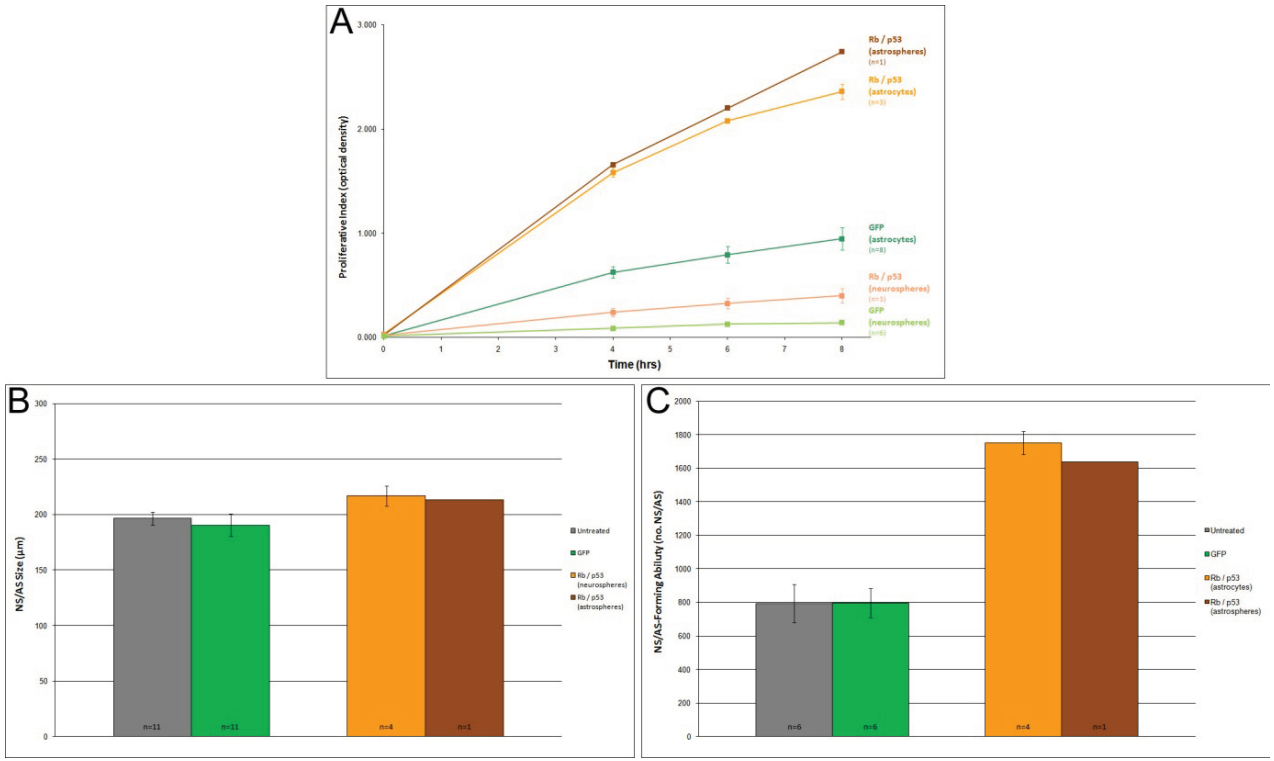

Figure 101: *In vitro* recombined $Rb^{-/-}$; $p53^{-/-}$ astrocytes grown as astrospheres exhibit a growth rate similar to their adherently grown astrocytic counterparts but form astrospheres of a similar size and number to their neurosphere counterparts. (A) WST-1 assay: Astrospheres were dissociated at passage two and the single cells were seeded at $6x10^4$ cells/well into a 96-well plate containing NS medium and the proliferative index (y-axis) was measured at 0, 2, 4, and 8hrs (x-axis) after a 3 day incubation period. (B) NS/astrosphere size assay: Astrospheres were dissociated at passage two and the single cells were seeded at $0.5x10^6$ cells/well into a 6-well plate containing NS medium and left to grow as astrospheres for eight days before their diameters were measured using a Zeiss Axiovert 135 microscope and the Openlab 5 software package. (C) NS/astrosphere-forming clonogenicity assay: Astrospheres were dissociated at passage two and the single cells were seeded at $0.5x10^6$ cells/well into a 6-well plate containing NS medium and left to grow as astrospheres for eight days before the number of astrospheres formed were counted. Cell genotypes and 'n' numbers supplied on graphs. Error bars: standard errors.

In vitro recombined $Rb^{-/-}$; $p53^{-/-}$ astrospheres exhibited a growth rate that was similar to that of the adherently grown $Rb^{-/-}$; $p53^{-/-}$ astrocytes rather than the NSCs, despite being grown in NSC medium (Figure 101: A). This finding suggests that despite being transformed into a stem-like state, the $Rb^{-/-}$; $p53^{-/-}$ astrospheres retain the intrinsic growth properties of their astrocytic origin. Whereas the $Rb^{-/-}$; $p53^{-/-}$ NS displayed a relatively low growth rate with a correlated reduction in tumourigenicity *in vivo*, we propose that the increased growth rate of the $Rb^{-/-}$; $p53^{-/-}$ astrospheres could be an indicator of the ability to form tumours *in vivo*. The $Rb^{-/-}$; $p53^{-/-}$ astrospheres exhibited similar aggregate-forming abilities of $Rb^{-/-}$; $p53^{-/-}$ NSC counterparts as they were observed to develop into spheres of a similar size (Figure 101: B) and with a similar overall number (Figure 101: C).

To test whether these stem-like astrospheres could form tumours *in vivo* we conducted a short-term study whereby we engrafted *in vitro* recombined $Rb^{-/-}$; $p53^{-/-}$ astrospheres into the striata of 5 immune-competent mice with time-culls at 11 days and 2 months (Figure 102).

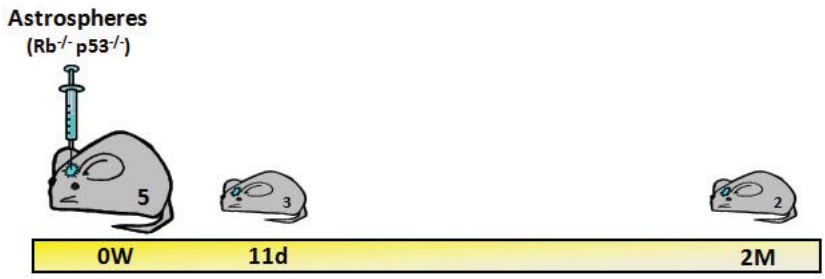

Figure 102: Schematic of the astrosphere engraftment experiment whereby $Rb^{-/-}$; $p53^{-/-}$ astrospheres were engrafted into the striata of 5 immune-competent mice with time-culls planned at 11 days (n=3) and 2 months (n=2) post-engraftment.

Two mice were found dead at day one post-engraftment, caused by acute hydrocephalus as a result of accidentally injecting the astrospheres into the lateral ventricles. For this reason, only a single mouse was time-culled after 11 days.

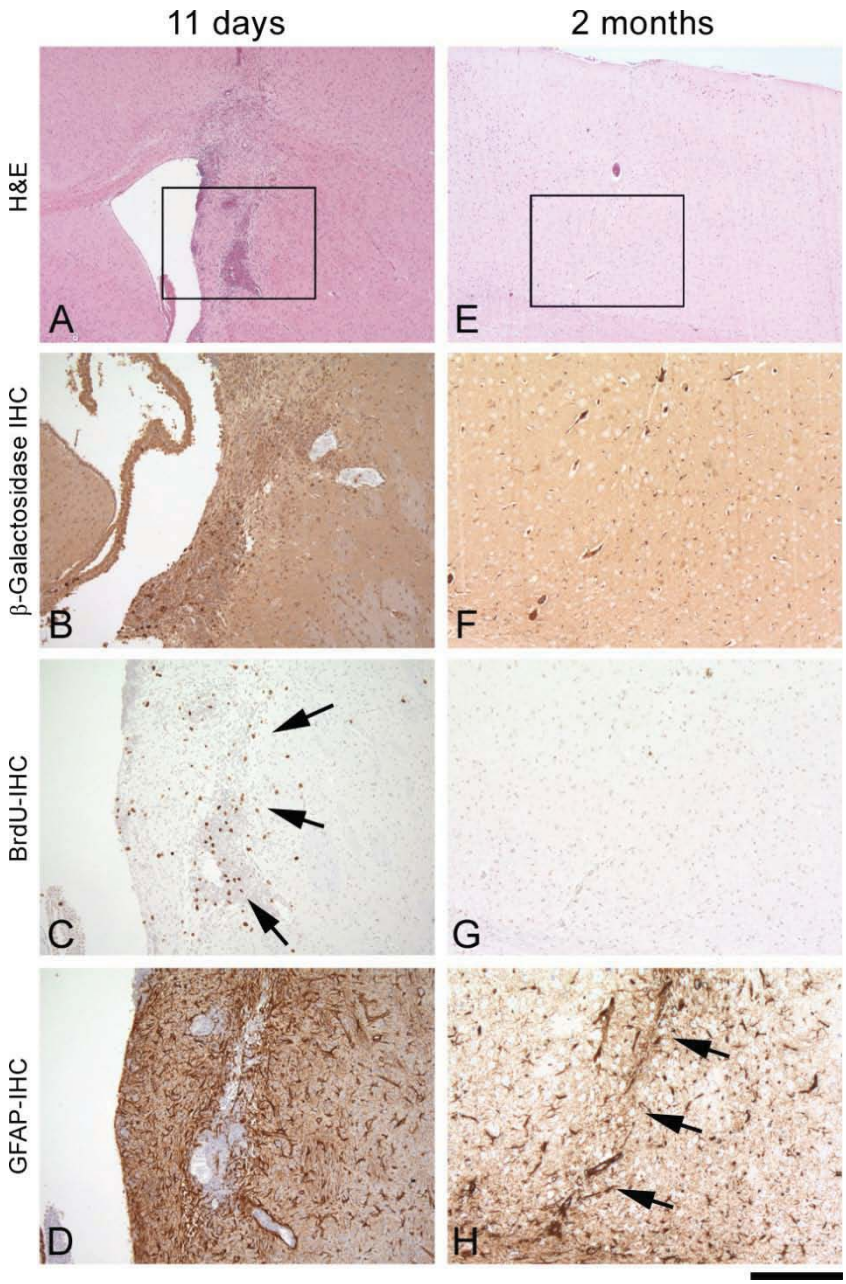

Figure 103: *In vitro* recombined $Rb^{-/-}$; $p53^{-/-}$ astrospheres engrafted into the striata of immune-competent mice do not give rise to tumours and are cleared by 2 months. Representative images taken from each time point showing that grafted astrospheres were detectable up to 11 days post-engraftment (A-D) but had been cleared by 2 months (E-H). After 11 days the β-galactosidase-positive grafted astrospheres (B) were still viable in the graft site (C: black arrows) and were GFAP-negative (D). By 2 months there was no evidence of any viable grafted astrospheres (E-G) despite verification of a successful graft as shown by the reactive astrocytosis circumventing the injection tract (H). Images were taken using a ColorView III digital camera mounted on a Zeiss Axioskop 2 MOT microscope with a 2.5x magnification (A-C) or a 6.3x magnification (D-I) and using the AnalySIS software package. Scale bar: A-C, 700μm and D-I, 275μm.

A cell mass with atypical morphology was identified within the striatum at 11 days post-engraftment (Figure 103: A). These cells were positive for β-galactosidase (Figure 103: B) and BrdU (Figure 103: C), confirming their status as viable proliferating cells derived from the grafted astrospheres. Interestingly, the astrospheres cells within the graft site were observed to be GFAP-negative (Figure 103: D). This mirrored the finding in section 6.3.3 that *in vitro* recombination caused $Rb^{-/-}$; $p53^{-/-}$ astrocytes to de-differentiate to a GFAP-negative/nestin-negative phenotype and suggests that this hypothetical de-differentiation is maintained *in vivo*. By two months post-engraftment there was little evidence of any surviving $Rb^{-/-}$; $p53^{-/-}$ astrospheres, despite a successful engraftment as verified by the high level of reactive astrocytosis observed along the injection tract (Figure 103: H). No atypical (Figure 103: E) or BrdU-positive proliferating cells (Figure 103: G), and only a few β-galactosidase-positive cells (Figure 103: F) were identified along the injection tract. This suggests that by two months the astrospheres had been completely broken down into single cells and cleared from the brain leaving a glial scar (Figure 103: H). It should be noted, however, that $Rb^{-/-}$; $p53^{-/-}$ NSCs also failed (in the majority of cases) to generate tumours *in vivo*. For this reason, repeats of this experiment with other genotypes (e.g. $Rb^{-/-}$; $p53^{-/-}$; $PTEN^{-/-}$) may provide a more rigorous model system.

Taken together, the results of the various *in vivo* engraftment studies suggest that terminally differentiated astrocytes, regardless of the combination of TSGs lost and of their differentiation state, do not contribute to *in vivo* tumour development.

6.4 Conclusion

In this chapter we demonstrated that i.c.v. Adenovirus-Cre administration targets terminally differentiated astrocytes, outside of the SVZ, for recombination. Such recombination and loss of the TSGs Rb, p53, and PTEN in these mature astrocytes was shown to induce a) a functional transformation to cells with an increased *in vitro* growth rate, a loss of contact inhibition, and a loss of adhesion dependence, and b) a phenotypic transformation to a de-differentiated stem-like state. Despite these transformations, we showed that terminally differentiated astrocytes, regardless of the combination of TSGs lost, did not contribute to *in vivo* tumour development in our model system. This immune-competency of the mice receiving the intracerebral astrocytes engraftments had

no effect on this result, despite the identification of an immune-mediated degeneration and clearance of engrafted astrocytes in immune-competent mice.

6.5 Future Work

The sample numbers for the astrocyte grafting experiments were 14 and 11 for the immune-competent and immune-deficient mice respectively. These sample numbers should be expanded to rule out the possibility that astrocytic *in vivo* tumourigenesis has a <4% rate of occurrence. In addition, the *in vivo* grafting experiments should be repeated for all of the experimental genotypes to assess whether there is a genotype-dependent influence. $Rb^{-/-}$; $p53^{-/-}$ astrocytes were used to generate astrospheres to test their *in vivo* tumourigenicity despite $Rb^{-/-}$; $p53^{-/-}$ NSCs possessing a low tumour hit rate of 9.6%. This low tumour hit rate of the $Rb^{-/-}$; $p53^{-/-}$ may have impeded the chance of observing *in vivo* tumour formation with engrafted $Rb^{-/-}$; $p53^{-/-}$ astrospheres. For this reason, the astrosphere grafting experiment should be repeated with either all the genotypes or the at least the genotypes that carried the highest *in vivo* tumour hit rate for the NS grafting experiments (e.g. $Rb^{-/-}$; $p53^{-/-}$; $PTEN^{-/-}$: 96%). Also, additional repeats of the astrosphere *in vitro* functional characterisation experiments would allow for statistical analysis (the sample number used was n=1). It would also be interesting to see if the RNA and protein expression profiles of the transformed stem-like astrocytes more closely resembles that of NSCs or the original terminally differentiated astrocytes. To this end, the pattern of CD133 expression (as examine in Chapter Five) in transformed astrocytes could be examined.

7 Summary and Conclusion

Brain tumours represent one of the most devastating pathologies of the central nervous system. Their diagnosis, especially in the case of WHO grade IV glioblastoma, often carries a poor prognosis. In order to develop effective therapeutic treatment regimens it is essential to identify the cell type from which brain tumours arise, and to define the cellular and molecular events that occur during tumourigenesis. A variety of human tumours, such as those of the haematopoietic system, have well defined cells of origin. However, the BTIC is less well defined, and little is known about how the genetic changes observed in established tumours influence their functional and phenotypic profiles. In addition, relatively few markers of the BTIC cell have been identified, and all are still debated. Brain tumours commonly exhibit cellular characteristics typical of highly undifferentiated cells, a quality that first led to the implication of NSCs in tumour formation. There is growing evidence that BTICs are derived from cells of the neural stem cell compartment. Despite this, the relative contribution of terminally differentiated cell types (e.g. astrocytes and oligodendrocytes) to the formation of brain tumours has been widely studied (Holland et al., 1998b; Bachoo et al., 2002). The aim of our work was to a) characterise the *in vitro* functional profiles of tumourigenic neural stem cells (based on the combination of tumour suppressor genes inactivated), b) refine the origin and characterise the profile of the brain tumour initiating cell, c) identify and/or validate markers of brain tumour initiating cells, and d) assess the relative contribution of terminally differentiated astrocytes to the development of brain tumours. These aims were designed to achieve a better understanding of both the genetic and cellular processes driving brain tumour initiation.

7.1 Brain tumours originate from adult neural stem/progenitor cells of the subventricular zone and their genotype influences tumour hit rate, latency, and phenotype

We have shown that intrinsic brain tumours can arise from cells of the subventricular zone (SVZ) neural stem cell compartment in mice (Figure 11, Figure 13, Figure 14). By conditionally inactivating tumour suppressor genes in this compartment we induced neoplastic transformation and formation of tumours. The tumours generated in our model correlated with the combination of genetic mutations (Figure 12). Specifically, inactivating Rb and p53 led to the development of well demarcated primitive embryonal

tumours with evidence of neuronal differentiation, similar to human primitive neuroectodermal tumours (PNETs). The additional loss of PTEN did not alter the differentiation of the tumours, but it was associated with a significantly reduced latency and change in the tumour architecture in terms of increased cellular migration. In contrast, deletion of PTEN and p53 resulted in the development of diffusely infiltrative glial tumours, similar to high grade human gliomas and best corresponding to anaplastic oligoastrocytomas. Instead, combined inactivation of Rb and PTEN in the SVZ did not result in the development of any tumours. We hypothesise that the events which succeed the initial genetic lesion may play a role in determining the tumour phenotype, and may account for the variability observed in the tumour genotype-phenotype correlation. In epithelial tumours, there are well-described morphologically recognisable precursor lesions that correlate with specific early genetic abnormalities (Miller et al., 2005). In contrast, no such abnormalities have yet been identified in the CNS. In our model, tumours develop after a reproducible latency dependent on genotype. Mice in which all three TSGs Rb, p53, and PTEN are conditionally knocked out exhibit a reduced tumour latency (Figure 12: S), because it will take less time for them to accrue additional mutations to reach the tumourigenic threshold. This paradigm provides an excellent model to identify precursor lesions of the SVZ (Figure 12: A,B,C + Figure 13) and the sequence of pathways that may be mutated during oncogenesis. Despite major advances in identifying mutations, chromosomal abnormalities and activated pathways for many of the human brain tumours, the known genetic abnormalities only account for a minority of the tumours analysed and would therefore provide a highly subjective form of analysis (Collins, 2002; Louis et al., 2007). Whilst there are superficial differences between the murine tumours generated in our model and their proposed human equivalents, pathways relevant for human brain tumours were also dysregulated in the corresponding murine tumours. For example, while in our model of glioma formation Rb loss was not the primary genetic lesion, alteration of the Ink4a/Arf pathway may have lead to an inactivation of Rb function. Interestingly, our data indicates a novel role for Rb (loss) in driving tumour development towards the PNET phenotype. However, Rb (or more specifically its inhibition) may play a role in glioma progression as CDK4, a kinase that phosphorylates and inactivates Rb, is upregulated in glioma (Wiedemeyer et al., 2010). However, discrepancies remain between the genotype-phenotype mechanisms proposed in our model when compared to those of others. For example, in a glioma model Wang et al demonstrated a loss of p16/Ink4a in GFAP-expressing precursor cells as a result of p53 mutation (Wang et al, 2009), whereas we found a

significant upregulation of Cdkn2a (refer to section 3.3.8) following the same genetic insult. However, it is possible that deletion of p53 (prior to the development of glioma in our model) results in the upregulation of p19/Arf and subsequent inhibition of Mdm2, in an effort to stabilize and re-activate p53 (Tao and Levine, 1999). The involvement of the Rb pathway at a later stage in our glioma model underlines the importance of the sequence of mutations in determining the tumour phenotype. Our results suggest that CNS tumourigenesis is a process where genetic mutations and activation of particular pathways determine the phenotype of the tumour.

7.2 The *in vitro* functional profile of neural stem cells is influenced by genotype and can be used as a predictive indicator of *in vivo* tumour hit rate and latency

We have shown that i.c.v. administration of Adenovirus-Cre targets self-renewing and multipotent cells in the SVZ niche. The combination and number of TSGs lost in these NSCs determines their *in vitro* growth rates, with a growth rate that is proportional to the number of tumour suppressor genes inactivated. Tumourigenic NSCs show increased self-renewal, in a genotype-dependent manner, as well as altered expression levels of GFAP, Sox-2, and nestin. The *in vitro* growth rate, but not the *in vitro* self-renewal ability, of NSCs corresponds to *in vivo* tumour hit rate (initiation) and an inversely correlates to *in vivo* tumour latency.

We hypothesise that the different NSC genotypes show functional differences *in vitro* because they are composed of NSC sub-populations with different functional profiles. It is known that cancer stem cells are dependent on their microenvironment (Calabrese et al., 2007), and we therefore hypothesise that the *in vitro* or *in vivo* microenvironment of NSCs influences their functional profile and ability to initiate tumour development.

7.3 The cellular environment of neural stem cells at the time of tumour suppressor gene inactivation influences their *in vivo* tumourigenic profile

We demonstrated that brain tumourigenesis is initiated and driven by SVZ NSCs: a) i.c.v. Adenovirus-Cre-mediated recombination of TSGs in the SVZ causes cells to proliferate and migrate into the brain parenchyma where they generate tumours, and b)

NSCs derived from the SVZ of adult mice, expanded and recombined *in vitro* generate tumours following intracerebral engraftment that recapitulate the i.c.v. Adenovirus-Cre-induced phenotypes. Cells with the ability to self-renew were observed in the brain tumour bulk and probably represent BTICs. These cells were found to remain committed to a specific phenotype / lineage over serial engraftments. We hypothesise that these committed BTICs are the progeny of genetically targeted cells in the SVZ. To trace the origins of these committed BTICs we used i.c.v. Adenovirus-GFAP-Cre to target only the GFAP-expressing type B astrocytes of the SVZ for recombination in order to examine if they produce a similar or identical tumour phenotype. Using this approach we identified that targeting only the type B astrocytes of the SVZ for recombination induced similar tumour incidences, latencies, and histological phenotypes as seen following CMV-driven expression of Cre in SVZ cells. This suggests that the GFAP-expressing type B astrocytes of the SVZ are key contributors to the formation of brain tumours in our model. However, in the case of PNETs it was found that there was a reduction in incidence when only the type B astrocytes were targeted; suggesting that other SVZ cells (e.g. transient-amplifying progenitor cells) can contribute towards tumourigenesis. In addition, $Rb^{Lox/Lox}$; $p53^{Lox/Lox}$; $PTEN^{Lox/Lox}$ mice injected with Adenovirus-GFAP-Cre exhibited a significantly longer mean tumour latency and a reduced number of PNETs, suggesting that targeting the GFAP-expressing type B cells induces a differentiaiotn toward glial lieages.

Interestingly, we observed that the environment of SVZ NSCs (*in vivo* versus *in vivo*) at the time of recombination influences *in vivo* tumour hit rate and latency, but has limited effect on the phenotype. *In vivo* i.c.v. Adenovirus-Cre-mediated recombination in $Rb^{Lox/Lox}$; $p53^{Lox/Lox}$ mice resulted in the development of brain tumours in 27.6% of mice, whereas *in vitro* recombined and engrafted $Rb^{-/-}$; $p53^{-/-}$ NSCs generated tumours with a reduced incidence of 9.6%. This suggests that *in vivo* Adenovirus-Cre targets a cell type that is not present *in vitro*, and that $Rb^{-/-}$; $p53^{-/-}$ NSCs preferentially transform into a tumourigenic state in the *in vivo* SVZ microenvironment. Conversely, whereas i.c.v. administration of Adenovirus-Cre in $Rb^{Lox/Lox}$; $PTEN^{Lox/Lox}$ mice did not result in the development of intrinsic brain tumours, *in vitro* recombined and engrafted $Rb^{-/-}$; $PTEN^{-/-}$ NS generated tumours with a hit rate of 70.6%. This suggests that, following inactivation of the TSGs Rb and PTEN, the transformed and tumourigenic cells only exist in the *in vitro* neurosphere culture environment. In addition, SVZ NSCs targeted for recombination *in vivo* had the same *in vitro* growth rate as their *in vitro* recombined

counterparts, but reduced self-renewal. We also found that tumour latency is dependent on the number of cells injected and that increased passage number results in an increased tumour incidence of grafts.

NSCs and their progeny alter their function to match that of the local microenvironment, for example, NSCs that are introduced into the mammary epithelium niche adopt the function of intrinsic mammary epithelial cells (Booth et al., 2008). We propose that a similar mechanism of environmental influence affects the function and properties of NSCs, and that these properties subsequently determine their ability to initiate tumour development.

7.4 Increased CD133 expression by tumourigenic neural stem cells appears to correlate with a propensity towards generating glioblastoma, but not the *in vivo* tumour hit rate or latency

We demonstrated that CD133 is expressed by the same SVZ NSCs (e.g. GFAP-positive type B astrocytes of the SVZ) that generate tumours following recombination of TSGs by i.c.v. Adenovirus-Cre administration. Only 2.5% of wild-type NSCs were found to express CD133, and they possessed a CD133 expression equilibrium of 6.92-8.28% to which they return after only two passages following purification to either CD133- or CD133+ isolates. In comparison, 12% of tumourigenic NSCs expressed CD133, and although these tumourigenic NSCs possessed a similar CD133 expression equilibrium (4.3-10%) their rate of equilibration was reduced from two passages to 11 passages. At a functional level, CD133 expression positively correlates with the *in vitro* growth rate of tumourigenic NSCs but not their NS-forming ability. In contrast to some reports in the literature that CD133- cells do not represent the BTIC (Bao et al., 2006) we found that CD133- NSCs also generated tumours following intracerebral engraftment, and did so with a tumour profile (hit rate, latency, phenotype) that was similar to non-sorted tumourigenic NSCs. Also, contrary to suggestions in the literature, sorted CD133-/+ NSC isolate purities as low as 82.9% were adequate for observing a difference in their *in vivo* tumourigenic profiles. Although no correlation was observed between NSC CD133 expression and *in vivo* tumour hit rate or latency, a potential correlation was identified between elevated expression and a propensity towards generating glioblastoma. In addition, we verified HIF1α as a surrogate marker of CD133 but found that their relationship is not the basic inverse correlation as previously thought. High

levels of both proteins were observed in glioblastoma-generating NS, hypothetically as a result of aberrantly functioning hypoxia-response mechanisms. For example, others have shown that CD133 is downregulated by HIF1α in response to hypoxic conditions (Matsumoto et al., 2009), indicating that CD133 expression may be a reflection of NSC environmental conditions / hypoxia resistance and provide no insight into NSC sub-type classification. It therefore appears that a) CD133 protein expression *in vitro* is influenced more strongly by environmental conditions (e.g. culture conditions, general cellular health) than by the tumourigenic profile of the cells (combination of TSGs lost), and b) the cellular composition of NS is highly heterogeneous and CD133 expression may not need to be 100% representative of all the NSCs within the NS in order to see a CD133-correlated effect on tumour hit rate, latency, and phenotype.

7.5 Terminally differentiated astrocytes do not contribute to brain tumour formation

Brain tumours are classified according to morphological and/or immunophenotypic resemblance of the tumour cells to terminally differentiated cells of the brain, e.g. astrocytomas or oligodendrogliomas are characterised by expression profiles similar to those of astrocytes or oligodendrocytes (Louis et al., 2007). This classification was based on the original thinking that brain tumours arose from these mature cell types. However, since the discovery of neural stem cells, the focus of research into the BTIC has shifted onto neural stem, neural progenitor, and stem-like cells (Zaidi et al., 2009; Kondo, 2006). Despite this, several studies have shown that terminally differentiated astrocytes can be (extrinsically) transformed into a de-differentiated and tumourigenic stem-like state. This has been achieved using a variety of methods including: a) ectopic overexpression of the (proto)oncogenes H-Ras^{V12} and K-Ras (Lee et al., 2008b; Ding et al., 2001; Uhrbom et al., 2005), SV40 T/t-Ag (Rich et al., 2001; Blouw et al., 2003), human telomerase catalytic subunit (hTERT) (Sonoda et al., 2001), and epidermal growth factor receptor (EGFR) (Bachoo et al., 2002); b) deletion of the Ink4-Arf tumour suppressor gene (Uhrbom et al., 2005; Holland et al., 1998b; Bachoo et al., 2002); or c) deletion of the hypoxia-responsive transcription factor HIF-1α or its target gene, the angiogenic vascular endothelial growth factor (VEGF) (Blouw et al., 2003).

However, it should be noted that such model systems are different to our paradigm in that they all include ectopic overexpression of oncogenes. We believe that these model

systems do not accurately replicate tumourigenesis as the ectopic overexpression of H-Ras^{V12}, SV40 T/t-Ag, and hTERT can convert almost any normal cell into a tumour-initiating cancer cells (MacKenzie et al., 2002). For example, H-Ras^{V12} p53$^{-/-}$ astrocytes exhibit increased proliferation and are tumourigenic *in vivo* (Lee et al., 2008b). Ras is a G-protein that is activated by guanine exchange factors (GEFs) and is responsible for the coupling of growth factor receptors to downstream mitogenic activators involved in cell proliferation, differentiation, and survival. Mutations in the Ras family of genes Ras are present in 20-30% of all human cancers, and in many cell types overexpression of H-Ras results in loss of growth control and neoplastic transformation (Omerovic et al., 2007). For this reason, we believe that H-Ras overexpression drives the tumourigenic transformation of mature astrocytes in a way that does not accurately model the true *in vivo* process, hence the vastly reduced tumour latencies observed with such model systems when compared against our own. It may be possible to oncogenically de-differentiate mature astrocytes into stem-like / progenitor cells, but only these stem-like / progenitor cells (regardless of origin) should be thought of as BTICs and not the orginal astrocytes.

It has been suggested that a) *in vitro* and *in vivo* targeting of astrocytes selects for a less mature astrocytic cell with enhanced growth and differential potential, and b) *in vitro* culturing of astrocytes, only possible from neonatal brains, includes astrocytes capable of cell divisions (Stiles and Rowitch, 2008). In our model, we: a) use a model system with no ectopically-induced overexpression of oncogenes, b) derive astrocytes from the brains of post-natal mice, and c) investigate whether ectopic recombination of the TSGs in astrocytes of non-neurogenic brain regions (e.g. cortex, striatum, hippocampus) can result in tumour formation.

To this end, we demonstrated that i.c.v. Adenovirus-Cre administration targets terminally differentiated astrocytes, outside of the SVZ, for recombination. Loss of the TSGs Rb, p53, and PTEN in terminally differentiated astrocytes induced transformation to de-differentiated cells with increased *in vitro* growth rate, loss of contact inhibition, and loss of adhesion dependence. Despite these transformations, we showed that terminally differentiated astrocytes, regardless of the combination of TSGs lost, were unable to form tumours in our model system.

Using a model system that resembles our own, Xiao et al have demonstrated that ectopic inactivation of Rb and PTEN in terminally differentiated astrocytes results in the development of high-grade astrocytomas (Xiao et al., 2002). However, this model

system used truncated, but still oncogenic, SV40 T antigen expressed under the GFAP promoter to inactivate pRb; meaning that the tumourigenic effect was both ectopically induced, and could not be discriminated from a GFAP-expressing type B astrocyte stem cell-mediated effect. Other groups have also used TSG inactivation / loss to study the role of mature astrocytes in tumourigenesis, with most focussing on the INK4a and ARF genes. INK4a and ARF are TSGs whose proteins, $p16^{INK4a}$ and $p14/p19^{ARF}$, are regulators of the Rb and p53 pathways respectively. Homozygous deletion of the INK4a-ARF locus is one of the most frequent mutations in human glioblastoma (Liggett and Sidransky, 1998) and a variety of experiments have shown that INK4a-ARF loss in mature astrocytes transforms them into a tumourigenic state. However, once again these experiments combine INK4a-ARF inactivation with overexpression of oncogenic factors such as EGFR, platelet-derived growth factor (PDGF), Akt, and K-Ras (Bachoo et al., 2002; Tchougounova et al., 2007; Weiss et al., 2003; Holland et al., 1998a; Holland et al., 1998b). Not all experiments have found that (supposedly) mature astrocytes can contribute to tumourigenesis; with the same end result as our model Holland et al found that *in vivo* overexpression of activated Ras and Akt in terminally differentiated astrocytes of non-neurogenic regions does not transform them into tumourigenic cells (Holland et al., 2000).

7.6 A novel model of genotype/microenvironment-dependent tumourigenesis

Our model system suggests that there is a causative link between tumour genotype and fate determination, with the combination of initial genetic mutations (TSG loss) strongly influencing both the hit rate and the phenotype of the resulting brain tumours. Although a variety of mouse models have independently been used to model glioma, PNET, or medulloblastoma tumours in isolation (refer to section 1.6: Table 1), we show here that cells of the same compartment are capable of forming all these tumour types, depending on the combination of induced genetic mutations, in a single and intra-comparable model. However, as the SVZ stem cell compartment is known to contain at least three functionally different sub-populations of NSCs (Doetsch et al., 1997), we hypothesise that these may be differentially susceptible to any given combination of oncogenic signals. For example, in our model *in vivo* recombination of Rb and p53 in all cells of the SVZ NSC compartment resulted in the development of PNETs with a 27.6% hit rate, however, the same genetic lesion targeted to only the GFAP-expressing type B

astrocytes of the same compartment resulted in the almost complete abolishment of any tumour development (3.8% hit rate). This hypothesis of a 'NSC subtype functional profile – genetic lesion' inter-dependency as a key determinant of tumour phenotype is supported by the histological reproducibility of the tumours seen in our model across a range of other models. For example, Zheng et al have also shown that GFAP-cre-mediated inactivation of PTEN and p53 in neural progenitor cells results in the development of malignant astrocytomas (Zheng et al, 2008).

In order to explain this proposed relationship between NSC subtype functional profile and genetic mutation combination we believe there are three primary hypotheses requiring consideration:

(i) *The SVZ NSC compartment contains pre-committed glial / neuronal BTIC subtypes that produce the distinct tumour phenotypes regardless of the combination of genetic mutations*. This hypothesis is difficult to disprove from an *in vivo* perspective as controlling against variation in cell-targeting-specificity provides many challenges. However, using our model system we were able to isolate cells from the same *in vivo* locale and create parallel *in vitro* cultures where the only difference between them was combination of induced genetic mutations. Using this approach we were able to delineate *in vitro* functional differences as well as *in vivo* differences in tumour development hit rate, latency, and phenotype propensity as a direct consequence of the combination of genetic mutations.

(ii) *The SVZ NSC compartment contains a single BTIC that is responsible for producing all tumour phenotypes and does so as a direct consequence of the combination of genetic mutations*. However, this hypothesis does not adequately explain the variability of tumour hit rate, latency, and phenotype observed in our mode system unless we attribute all of this to a microenvironment-mediated effect.

(iii) *The SVZ NSC compartment contains multiple functionally different BTIC subtypes (neural stem/progenitor cell subtypes) that are predisposed to particular differentiation lineages when presented with specific oncogenic signals*. Considering that all SVZ NSC subtypes are non-preferentially targeted in our model, this would mean that loss of Rb (in any combination context) would confer a growth advantage to neuronal progenitors (perhaps by ctransforming them into a

neuroblast type A cell phenotype) and drive the tumour down a PNET lineage. Conversely, loss of PTEN and p53 would only take effect on glial-committed progenitors and therefore result in the preferential development of glioma with variable oligodendroglial features. This would also explain why the loss of all three TSGs primarily results in the development of PNETs but with some gliomas after longer latencies and the occasional bi-phasic PNET + glioma phenotype. This is because despite the loss of Rb some glial-committed progenitors would respond to the loss of PTEN and p53 and develop into gliomas in parallel to the PNETs.

Taking all our findings into account (Figure 104), we believe hypothesis (iii) to be the most accurate. However, most hypotheses of tumourigenesis (including this one) describe tumour phenotype as a direct result of tumour cell lineage specificity (Huse and Holland, 2010; Zaidi et al., 2009; Laks et al., 2010; Vescovi et al., 2006; Fomchenko and Holland, 2005; Oliver and Wechsler-Reya, 2004). In light of our novel finding that the environment of SVZ NSCs (*in vivo* versus *in vivo*) at the time of recombination influences their *in vivo* tumour hit rate and latency but with limited effect on the phenotype (Figure 104), we propose that microenvironment should constitute an additional variable to produce the following hypothesis (iv):

(iv) *The SVZ NSC compartment contains multiple BTIC subtypes (neural stem/progenitor cell subtypes) that are predisposed to particular differentiation lineages when presented with specific oncogenic signals, but whose tumourigenic permissiveness and functional profile is influenced by their microenvironment*.

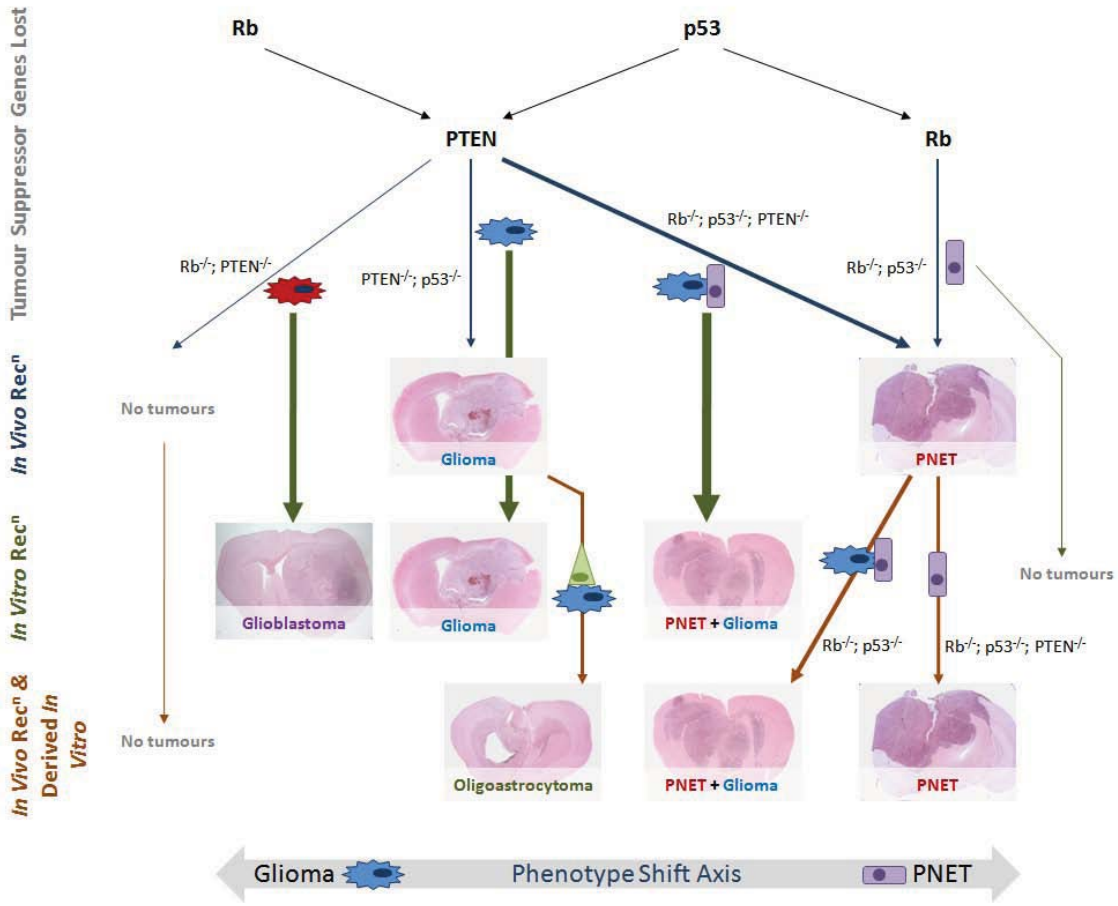

Figure 104: Environment-dependent tumourigenesis. This schematic of the results depicted in Figure 52 illustrates the influence NSC environment at the time of tumour suppressor gene inactivation has on the ability of NSCs to initiate tumour development. Arrow thickness indicates *in vivo* tumour hit rate. Blue arrows: tumour development from i.c.v. Adenovirus-Cre-mediated *in vivo* recombination of the indicated genotype. Green arrows: tumour development from *in vitro* recombined and engrafted NSCs of the indicated genotype. Orange arrows: tumour development from *in vivo* recombined, derived *in vitro* and engrafted NSCs of the indicated genotype.

The three-layered schematic (Figure 104) highlights the *in vivo* tumour hit rate and phenotype observed for each of the NSC genotypes depending on the cellular microenvironment at the time of gene inactivation. For example, *in vitro* recombined Rb$^{-/-}$; PTEN$^{-/-}$ NSCs efficiently generate glioblastomas with a high hit rate, whilst no tumours form after *in vivo* recombination. Our studies suggest that BTICs can possess a varying range of tumour-initiating abilities dependent on genotype and cellular microenvironment.

7.7 Impact of Work on Brain Tumour Diagnosis and Treatment

In order to understand the histogenesis of brain tumour development and develop effective therapeutic treatment regimens it is important to identify the "cell of origin" from which brain tumours arise, and to define the cellular and molecular events that occur during tumourigenesis. A variety of animal models (refer to section 1.6) have been used to further our understanding of the genetic basis of CNS tumourigenesis, however, the cell of origin for most CNS tumours remains only indirectly inferred or unknown. Our research has added significant weight to the argument that neural stem/progenitor cells of the SVZ neurogenic niche can become a class of brain tumour initiating cell (BTIC) capable of generating multiple phenotypes. The similarities between normal adult NSCs and BTICs have been discussed in detail (refer to section 1.3.2 and 1.4.1). We also defined a causative link between the genotype (initial genetic lesion) of BTICs and the phenotype of the tumours they produce. The additional research we have done into this genotype-phenotype relationship has added to our understanding of fate determination during tumourigenesis. As a result, we have identified that fate determination can be a contextually-relevant event whereby NSCs can give rise to an array of BTIC sub-types based on the interaction between their genetic / functional profile and their microenvironment. We used spatial and temporal cell isolation techniques (intrinsic to our model system) and comparative functional profiling to delineate these BTIC sub-types and subsequently deduce that they possess different tumourigenic and phenotypic propensities. We therefore propose that the efficacy of single signalling pathway therapeutics (e.g. gene therapy) as a post-symptomatic treatment option will remain limited and highly variable, and that the focus of treatment research should lie with concomitant therapies (e.g. the incorporation of temozolomide into established chemo/radiotherapy treatment regimes for glioma). The pre-clinical success seen with antiangiogenic therapies (Calabrese et al., 2007) supports this argument and we believe that therapies targeting the tumour microenvironment hold significant potential. In summary, the potential therapeutic implication of defining the BTIC is enormous as: a) treatments that specifically target tumour growth would minimising the cytotoxic side-effects seen with traditional chemo/radiotherapy, and b) defining the aetiology of tumourigenesis would foster a greater understanding of how to prevent tumour formation and recurrence.

Perhaps the greatest potential of our model system is in its potential contribution to the diagnosis and management of brain tumours. The ability of the model to genetically

control the production of a range of different tumours means that we have been able to use comparative expression profiling to identify differentially expressed signalling pathways implicated in tumour fate determination. We aim to continue this research to identify and validate novel diagnostic markers and potential therapeutic targets with known correlates to tumour hit rate, latency, phenotype propensity, and treatment resistance.

7.8 Future Work

Detailed below are several additional experiments that could be carried out to further test the hypotheses generated in the course of this research program.

7.8.1 Investigation of the relative contribution of neural stem cells from other neurogenic niches to tumourigenesis

Our research has focussed on the role that SVZ NSCs play in tumourigenesis of the CNS. It could be examined if stem/progenitor cells from other niches (e.g. NSCs of the subgranular zone within the dentate gyrus of the hippocampus (Seri et al., 2001)) are capable of forming brain tumours.

7.8.2 Specifically target tumour suppressor gene inactivation in other neural stem cell sub-types

We reported results from specifically targeting TSG inactivation in the GFAP-expressing type B astrocytes of the SVZ. By using Adenovirus-Cre expressed under the control of different promoters such as CD133, the orphan nuclear receptor TLX (Shi et al., 2004), or PDGFRα (Jackson et al., 2006) it could be investigated whether cell populations expressing specific markers give rise to distinct brain tumour phenotypes.

7.8.3 Investigate the relative contribution of other cell types to brain tumour formation

We demonstrated that terminally differentiated astrocytes do not contribute to *in vivo* tumour development in our model system. Using the same approach it could be

investigated whether oligodendrocytes, neurons, and ependymal cells could contribute to brain tumour formation.

7.8.4 Analyse tumour samples generated from our mouse model to identify markers that correlate with *in vivo* tumour hit rate, latency, and phenotype

By using a combination of cDNA microarray and laser capture micro-dissection it is possible to analyse brain tumour samples generated from our model for markers of *in vivo* tumour hit rate, latency, and phenotype. Such markers could then be used to assist in the delineation of BTICs and ultimately as targets for the therapeutic treatment of brain tumours (e.g. antibody-assisted chemotherapy).

7.8.5 Compare murine and human brain tumours

By carrying out an *in vitro* functional characterisation, in addition to profiling the *in vivo* tumourigenic properties of human brain tumour samples, as we did for mouse BTICs, it will be possible to identify similarities between the two systems. These correlates could then be used to translate our findings into a human-relevant context as well as identifying which aspects of the mouse model system can be extrapolated to the human condition.

8 Bibliography

Aaberg-Jessen,C., Christensen,K., Offenberg,H., Bartels,A., Dreehsen,T., Hansen,S., Schroder,H.D., Brunner,N., and Kristensen,B.W. (2009). Low expression of tissue inhibitor of metalloproteinases-1 (TIMP-1) in glioblastoma predicts longer patient survival. Journal of Neuro-Oncology *95*, 117-128.

Aaberg-Jessen,C., Christensen,K., Schroder,H.D., Offenberg,H., Brunner,N., and Kristensen,B.W. (2008). Immunohistochemical tissue inhibitor of metalloproteinases-1 (TIMP-1) score is a prognostic marker in glioblastoma. Apmis *116*, 425.

Ahmed,S. (2009). The Culture of Neural Stem Cells. Journal of Cellular Biochemistry *106*, 1-6.

Akagi,K., Sandig,V., Vooijs,M., VanderValk,M., Giovannini,M., Strauss,M., and Berns,A. (1997). Cre-mediated somatic site-specific recombination in mice. Nucleic Acids Research *25*, 1766-1773.

Akiyama,T., Ohuchi,T., Sumida,S., Matsmoto,K., and Toyoshima,K. (1992). Phosphorylation of the retinoblastoma protein by cdk2. PNAS *89*, 7900-7904.

Al Hajj,M., Wicha,M.S., Benito-Hernandez,A., Morrison,S.J., and Clarke,M.F. (2003). Prospective identification of tumorigenic breast cancer cells (vol 100, pg 3983, 2003). Proceedings of the National Academy of Sciences of the United States of America *100*, 6890.

Almqvist,P.M., Mah,R., Lendahl,U., Jacobsson,B., and Hendson,G. (2002). Immunohistochemical Detection of Nestin in Pediatric Brain Tumors. J. Histochem. Cytochem. *50*, 147-158.

Altman,J. (1963). Autoradiographic Investigation of Cell Proliferation in Brains of Rats and Cats. Anatomical Record *145*, 573.

Altman,J. and Das,G.D. (1965). Autoradiographic and Histological Evidence of Postnatal Hippocampal Neurogenesis in Rats. Journal of Comparative Neurology *124*, 319.

Alvarez-Buylla,A., Garcia-Verdugo,J.M., Mateo,A.S., and Merchant-Larios,H. (1998). Primary neural precursors and intermitotic nuclear migration in the ventricular zone of adult canaries. Journal of Neuroscience *18*, 1020-1037.

Alvarez-Buylla,A. and Lim,D.A. (2004). For the long run: Maintaining germinal niches in the adult brain. Neuron *41*, 683-686.

Alvarez-Buylla,A., Seri,B., and Doetsch,F. (2002). Identification of neural stem cells in the adult vertebrate brain. Brain Research Bulletin *57*, 751-758.

Anderson,D.J., Gage,F.H., and Weissman,I.L. (2001). Can stem cells cross lineage boundaries? Nature Medicine *7*, 393-395.

Arvidsson,A., Collin,T., Kirik,D., Kokaia,Z., and Lindvall,O. (2002). Neuronal replacement from endogenous precursors in the adult brain after stroke. Nature Medicine *8*, 963-970.

Asano,T., Ageyama,N., Takeuchi,K., Momoeda,M., Kitano,Y., Sasaki,K., Ueda,Y., Suzuki,Y., Kondo,Y., Torii,R., Hasegawa,M., Ookawara,S., Harii,K., Terao,K., Ozawa,K., and Hanazono,Y. (2003). Engraftment and tumor formation after allogeneic in utero transplantation of primate embryonic stem cells. Transplantation *76*, 1061-1067.

Auguste,K.I. and Gupta,N. (2006). Pediatric intramedullary spinal cord tumors. Neurosurgery Clinics of North America *17*, 51-59.

Bachoo,R.M., Maher,E.A., Ligon,K.L., Sharpless,N.E., Chan,S.S., You,M.J.J., Tang,Y., DeFrances,J., Stover,E., Weissleder,R., Rowitch,D.H., Louis,D.N., and DePinho,R.A. (2002). Epidermal growth factor receptor and Ink4a/Arf: Convergent mechanisms governing terminal differentiation and transformation along the neural stem cell to astrocyte axis. Cancer Cell *1*, 269-277.

Backman,S.A., Stambolic,V., Suzuki,A., Haight,J., Elia,A., Pretorius,J., Tsao,M.S., Shannon,P., Bolon,B., Ivy,G.O., and Mak,T.W. (2001). Deletion of Pten in mouse brain causes seizures, ataxia and defects in soma size resembling Lhermitte-Duclos disease. Nature Genetics *29*, 396-403.

Bao,S.D., Wu,Q.L., McLendon,R.E., Hao,Y.L., Shi,Q., Hjelmeland,A.B., Dewhirst,M.W., Bigner,D.D., and Rich,J.N. (2006). Glioma stem cells promote

radioresistance by preferential activation of the DNA damage response. Nature *444*, 756-760.

Barker,N., Ridgway,R.A., van Es,J.H., van de Wetering,M., Begthel,H., van den Born,M., Danenberg,E., Clarke,A.R., Sansom,O.J., and Clevers,H. (2009). Crypt stem cells as the cells-of-origin of intestinal cancer. Nature *457*, 608.

Barski,J.J., Dethleffsen,K., and Meyer,M. (2000). Cre recombinase expression in cerebellar Purkinje cells. Genesis *28*, 93-98.

Beier,D., Wischhusen,J., Dietmaier,W., Hau,P., Proescholdt,M., Brawanski,A., Bogdahn,U., and Beier,C.P. (2008). CD133 expression and cancer stem cells predict prognosis in high-grade oligodendroglial tumors. Brain Pathology *18*, 370-377.

Betz,U.A.K., Vosshenrich,C.A.J., Rajewsky,K., and Muller,W. (1996). Bypass of lethality with mosaic mice generated by Cre-loxP-mediated recombination. Current Biology *6*, 1307-1316.

Blanco-Aparicio,C., Renner,O., Leal,J.F.M., and Carnero,A. (2007). PTEN, more than the AKT pathway. Carcinogenesis *28*, 1379-1386.

Blouw,B., Song,H.Q., Tihan,T., Bosze,J., Ferrara,N., Gerber,H.P., Johnson,R.S., and Bergers,G. (2003). The hypoxic response of tumors is dependent on their microenvironment. Cancer Cell *4*, 133-146.

Bodmer,S., Strommer,K., Frei,K., Siepl,C., de Tribolet,N., Heid,I., and Fontana,A. (1989). Immunosuppression and transforming growth factor-beta in glioblastoma. Preferential production of transforming growth factor-beta 2. J Immunol *143*, 3222-3229.

Boiani,M. and Scholer,H.R. (2005). Regulatory networks in embryo-derived pluripotent stem cells. Nature Reviews Molecular Cell Biology *6*, 872-884.

Bonnet,D. and Dick,J.E. (1997). Human acute myeloid leukemia is organized as a hierarchy that originates from a primitive hematopoietic cell. Nature Medicine *3*, 730-737.

Booth,B.W., Mack,D.L., Androutsellis-Theotokis,A., Mckay,R.D.G., Boulanger,C.A., and Smith,G.H. (2008). The mammary microenvironment alters the differentiation

repertoire of neural stem cells. Proceedings of the National Academy of Sciences of the United States of America *105*, 14891-14896.

Bourdon,J.C. (2007). p53 and its isoforms in cancer. British Journal of Cancer *97*, 277-282.

Bruce,W.R. and VANDERGA.H (1963). A Quantitative Assay for Number of Murine Lymphoma Cells Capable of Proliferation in Vivo. Nature *199*, 79.

Bruggeman,S,. Hulsman,D., Tanger,E., Buckle,T., Blom,M., Zevenhoven,J., van Tellingen,O. and van Lohuizen,M. (2007) Bmi1 Controls Tumor Development in an Ink4a/Arf-Independent Manner in a Mouse Model for Glioma. Cancer Cell *12*, 328-341.

Brustle,O., Jones,K.N., Learish,R.D., Karram,K., Choudhary,K., Wiestler,O.D., Duncan,I.D., and Mckay,R.D.G. (1999). Embryonic stem cell-derived glial precursors: A source of myelinating transplants. Science *285*, 754-756.

Buckner,J.C., Brown,P.D., O'Neill,B.P., Meyer,F.B., Wetmore,C.J., and Uhm,J.H. (2007). Central Nervous System Tumors. Mayo Clinic Proceedings *82*, 1271-1286.

Burkhart,D.L. and Sage,J. (2008). Cellular mechanisms of tumour suppression by the retinoblastoma gene. Nature Reviews Cancer *8*, 671-682.

Calabrese,C., Poppleton,H., Kocak,M., Hogg,T.L., Fuller,C., Hamner,B., Oh,E.Y., Gaber,M.W., Finklestein,D., Allen,M., Frank,A., Bayazitov,I.T., Zakharenko,S.S., Gajjar,A., Davidoff,A., and Gilbertson,R.J. (2007). A perivascular niche for brain tumor stem cells. Cancer Cell *11*, 69-82.

Central Brain Tumor Registry of the United States. First Annual Report. 1995.

Central Brain Tumor Registry of the United States. Statistical Report, 1998-2002. 2005.

Central Brain Tumor Registry of the United States. http://www.cbtrus.org. 2006.

Chaichana,K., McGirt,M., Frazier,J., Attenello,F., Guerrero-Cazares,H., and Quinones-Hinojosa,A. (2008). Relationship of glioblastoma multiforme to the lateral ventricles predicts survival following tumor resection. Journal of Neuro-Oncology *89*, 219-224.

Clark,G.B., Henry,J.M., and Mckeever,P.E. (1985). Cerebral Pilocytic Astrocytoma. Cancer *56*, 1128-1133.

Clarke,A.R., Maandag,E.R., Vanroon,M., Vanderlugt,N.M.T., VanderValk,M., Hooper,M.L., Berns,A., and Riele,H.T. (1992). Requirement for A Functional Rb-1 Gene in Murine Development. Nature *359*, 328-330.

Clement,V., Dutoit,V., Marino,D., Dietrich,P.Y., and Radovanovic,I. (2009). Limits of CD133 as a marker of glioma self-renewing cells. International Journal of Cancer *125*, 244-248.

Clement,V., Sanchez,P., de Tribolet,N., Radovanovic,I., and Altaba,A.R.I. (2007). HEDGEHOG-GLI1 signaling regulates human glioma growth, cancer stem cell self-renewal, and tumorigenicity. Current Biology *17*, 165-172.

Clement,V., Marino,D., Cudalbu,C., Hamou,M.F., Mlynarik,V., de Tribolet,N., Dietrich,P.Y., Gruetter,R., Hegi,M.E., and Radovanovic,I. (2010). Marker-independent identification of glioma-initiating cells. Nat Meth *7*, 224-228.

Coles-Takabe,B.L.K., Brain,I., Purpura,K.A., Karpowicz,P., Zandstra,P.W., Morshead,C.M., and van der Kooy,D. (2008). Don't Look: Growing Clonal Versus Nonclonal Neural Stem Cell Colonies. Stem Cells *26*, 2938-2944.

Collins,V.P. (2002). Cellular mechanisms targeted during astrocytoma progression. Cancer Letters *188*, 1-7.

Conti,L. and Cattaneo,E. (2010). Neural stem cell systems: physiological players or *in vitro* entities? Nature Reviews Neuroscience *11*, 176-187.

Corbeil,D., Roper,K., Hellwig,A., Tavian,M., Miraglia,S., Watt,S.M., Simmons,P.J., Peault,B., Buck,D.W., and Huttner,W.B. (2000). The human AC133 hematopoietic stem cell antigen is also expressed in epithelial cells and targeted to plasma membrane protrusions. Journal of Biological Chemistry *275*, 5512-5520.

Corbeil,D., Roper,K., Weigmann,A., and Huttner,W.B. (1998). AC133 hematopoietic stem cell antigen: Human homologue of mouse kidney prominin or distinct member of a novel protein family? Blood *91*, 2625-2626.

Dacey,M.L. and Wallace,R.B. (1974). Postnatal Neurogenesis in Feline Cerebellum - Structural Functional Investigation. Acta Neurobiologiae Experimentalis *34*, 253-263.

Dahlstrand,J., Collins,V.P., and Lendahl,U. (1992). Expression of the Class-Vi Intermediate Filament Nestin in Human Central-Nervous-System Tumors. Cancer Research *52*, 5334-5341.

Datta,S.R., Brunet,A., and Greenberg,M.E. (1999). Cellular survival: a play in three Akts. Genes & Development *13*, 2905-2927.

Daumasduport,C., Scheithauer,B., Ofallon,J., and Kelly,P. (1988). Grading of Astrocytomas - A Simple and Reproducible Method. Cancer *62*, 2152-2165.

Deleo,A.B., Jay,G., Appella,E., Dubois,G.C., Law,L.W., and Old,L.J. (1979). Detection of A Transformation-Related Antigen in Chemically-Induced Sarcomas and Other Transformed-Cells of the Mouse. Proceedings of the National Academy of Sciences of the United States of America *76*, 2420-2424.

Denise,A., Garcia,R., Doan,N.B., Imura,T., Bush,T.G., and Sofroniew,M.V. (2004). GFAP-expressing progenitors are the principal source of constitutive neurogenesis in adult mouse forebrain. Nature Neuroscience *7*, 1233-1241.

Di Cristofano,A., Kotsi,P., Peng,Y.F., Cordon-Cardo,C., Elkon,K.B., and Pandolfi,P.P. (1999). Impaired Fas response and autoimmunity in Pten(+/-) mice. Science *285*, 2122-2125.

Di Cristofano,A., Pesce,B., Cordon-Cardo,C., and Pandolfi,P.P. (1998). Pten is essential for embryonic development and tumour suppression. Nature Genetics *19*, 348-355.

Diehn,M., Cho,R.W., Lobo,N.A., Kalisky,T., Dorie,M.J., Kulp,A.N., Qian,D., Lam,J.S., Ailles,L.E., Wong,M., Joshua,B., Kaplan,M.J., Wapnir,I., Dirbas,F., Somlo,G., Garberoglio,C., Paz,B., Shen,J., Lau,S.K., Quake,S.R., Brown,J.M., Weissman,I.L., and Clarke,M.F. (2009). Association of reactive oxygen species levels and radioresistance in cancer stem cells. Nature *458*, 780-783.

Ding,H., Roncari,L., Shannon,P., Wu,X.L., Lau,N., Karaskova,J., Gutmann,D.H., Squire,J.A., Nagy,A., and Guha,A. (2001). Astrocyte-specific expression of activated p21-ras results in malignant astrocytoma formation in a transgenic mouse model of human gliomas. Cancer Research *61*, 3826-3836.

Dirks,P.B. (2008). Brain tumour stem cells: the undercurrents of human brain cancer and their relationship to neural stem cells. Philosophical Transactions of the Royal Society B-Biological Sciences *363*, 139-152.

Doetsch,F. (2003). The glial identity of neural stem cells. Nature Neuroscience *6*, 1127-1134.

Doetsch,F., Caille,I., Lim,D.A., Garcia-Verdugo,J.M., and Alvarez-Buylla,A. (1999). Subventricular zone astrocytes are neural stem cells in the adult mammalian brain. Cell *97*, 703-716.

Doetsch,F., GarciaVerdugo,J.M., and Alvarezbuylla,A. (1997). Cellular composition and three-dimensional organization of the subventricular germinal zone in the adult mammalian brain. Journal of Neuroscience *17*, 5046-5061.

Doetsch,F., Petreanu,L., Caille,I., Garcia-Verdugo,J.M., and Alvarez-Buylla,A. (2002). EGF converts transit-amplifying neurogenic precursors in the adult brain into multipotent stem cells. Neuron *36*, 1021-1034.

Engstrom,C.M., Demers,D., Dooner,M., McAuliffe,C., Benoit,B.O., Stencel,K., Joly,M., Hulspas,R., Reilly,J.L., Savarese,T., Recht,L.D., Ross,A.H., and Quesenberry,P.J. (2002). A method for clonal analysis of epidermal growth factor-responsive neural progenitors. Journal of Neuroscience Methods *117*, 111-121.

Eramo,A., Lotti,F., Sette,G., Pilozzi,E., Biffoni,M., Di Virgilio,A., Conticello,C., Ruco,L., Peschle,C., and De Maria,R. (2008). Identification and expansion of the tumorigenic lung cancer stem cell population. Cell Death and Differentiation *15*, 504-514.

Eriksson,P.S., Perfilieva,E., Bjork-Eriksson,T., Alborn,A.M., Nordborg,C., Peterson,D.A., and Gage,F.H. (1998). Neurogenesis in the adult human hippocampus. Nature Medicine *4*, 1313-1317.

Eschbacher,J.M., Yeh,R.F., Smirnov,I., Feuerstein,B., and Coons,S. (2008). SOX2: A Glioma-Specific Marker and a Potential Target for Therapy. FASEB J. *22*, 706.

Esposito,I., Kleeff,J., Bischoff,S.C., Fischer,L., Collecchi,P., Iorio,M., Bevilacqua,G., Buchler,M.W., and Friess,H. (2002). The stem cell factor-c-kit system and mast cells in human pancreatic cancer. Laboratory Investigation *82*, 1481-1492.

Facchino,S., Abdouh,M., Chatoo,W., and Bernier,G. (2010). BMI1 Confers Radioresistance to Normal and Cancerous Neural Stem Cells through Recruitment of the DNA Damage Response Machinery. Journal of Neuroscience *30*, 10096-10111.

Falk,S., Wurdak,H., Ittner,L.M., Ille,F., Sumara,G., Schmid,M.T., Draganova,K., Lang,K.S., Paratore,C., Leveen,P., Suter,U., Karlsson,S., Born,W., Ricci,R., G÷tz,M., and Sommer,L. (2008). Brain Area-Specific Effect of TGF-[beta] Signaling on Wnt-Dependent Neural Stem Cell Expansion. Cell Stem Cell *2*, 472-483.

Ferrandina,G., Bonanno,G., Pierelli,L., Perillo,A., Procoli,A., Mariotti,A., Corallo,M., Martinelli,E., Rutella,S., Paglia,A., Zannoni,G., Mancuso,S., and Scambia,G. (2008). Expression of CD133-1 and CD133-2 in ovarian cancer. International Journal of Gynecological Cancer *18*, 506-514.

Fine,H.A. (2009). Glioma Stem Cells: Not All Created Equal. Cancer Cell *15*, 247-249.

Florek,M., Haase,M., Marzesco,A.M., Freund,D., Ehninger,G., Huttner,W.B., and Corbeil,D. (2005). Prominin-1/CD133, a neural and hematopoietic stem cell marker, is expressed in adult human differentiated cells and certain types of kidney cancer. Cell and Tissue Research *319*, 15-26.

Fomchenko,E.I. and Holland,E.C. (2005). Stem cells and brain cancer. Experimental Cell Research *306*, 323-329.

Friend,S.H., Bernards,R., Rogelj,S., Weinberg,R.A., Rapaport,J.M., Albert,D.M., and Dryja,T.P. (1986). A Human Dna Segment with Properties of the Gene That Predisposes to Retinoblastoma and Osteosarcoma. Nature *323*, 643-646.

Gage,F.H., Coates,P.W., Palmer,T.D., Kuhn,H.G., Fisher,L.J., Suhonen,J.O., Peterson,D.A., Suhr,S.T., and Ray,J. (1995). Survival and Differentiation of Adult Neuronal Progenitor Cells Transplanted to the Adult Brain. Proceedings of the National Academy of Sciences of the United States of America *92*, 11879-11883.

Galli,R., Binda,E., Orfanelli,U., Cipelletti,B., Gritti,A., De Vitis,S., Fiocco,R., Foroni,C., Dimeco,F., and Vescovi,A. (2004). Isolation and characterization of tumorigenic, stem-like neural precursors from human glioblastoma. Cancer Research *64*, 7011-7021.

Galvin,K.E., Ye,H., and Wetmore,C. (2007). Differential gene induction by genetic and ligand-mediated activation of the Sonic hedgehog pathway in neural stem cells. Developmental Biology *308*, 331-342.

Gangemi,R.M.R., Griffero,F., Marubbi,D., Perera,M., Capra,M.C., Malatesta,P., Ravetti,G.L., Zona,G.L., Daga,A., and Corte,G. (2009). SOX2 Silencing in Glioblastoma Tumor-Initiating Cells Causes Stop of Proliferation and Loss of Tumorigenicity. Stem Cells *27*, 40-48.

Garcia-Verdugo,J., Doetsch,F., Wichterle,H., Lim,D.A., and Alvarez-Buylla,A. (1998). Architecture and cell types of the adult subventricular zone: In search of the stem cells. Journal of Neurobiology *36*, 234-248.

Goodrich,L.V., Milenkovic,L., Higgins,K.M., and Scott,M.P. (1997). Altered neural cell fates and medulloblastoma in mouse patched mutants. Science *277*, 1109-1113.

Gould,E., Tanapat,P., Mcewen,B.S., Flugge,G., and Fuchs,E. (1998). Proliferation of granule cell precursors in the dentate gyrus of adult monkeys is diminished by stress. Proceedings of the National Academy of Sciences of the United States of America *95*, 3168-3171.

Griguer,C.E., Oliva,C.R., Gobin,E., Marcorelles,P., Benos,D.J., Lancaster,J.R., and Gillespie,G.Y. (2008). CD133 Is a Marker of Bioenergetic Stress in Human Glioma. PLoS ONE *3*, e3655.

Gritti,A., Frolichsthal-Schoeller,P., Galli,R., Parati,E.A., Cova,L., Pagano,S.F., Bjornson,C.R., and Vescovi,A.L. (1999). Epidermal and fibroblast growth factors behave as mitogenic regulators for a single multipotent stem cell-like population from the subventricular region of the adult mouse forebrain. Journal of Neuroscience *19*, 3287-3297.

Gritti,A., Parati,E.A., Cova,L., Frolichsthal,P., Galii,R., Wanke,E., Faravelli,L., Morassutti,D.J., Roisen,F., Nickel,D.D., and Vescovi,A.L. (1996). Multipotential stem cells from the adult mouse brain proliferate and self-renew in response to basic fibroblast growth factor. Journal of Neuroscience *16*, 1091-1100.

Groszer,M., Erickson,R., Scripture-Adams,D.D., Dougherty,J.D., Le Belle,J., Zack,J.A., Geschwind,D.H., Liu,X., Kornblum,H.I., and Wu,H. (2006). PTEN negatively regulates

neural stem cell self-renewal by modulating G(0)-G(1) cell cycle entry. Proceedings of the National Academy of Sciences of the United States of America *103*, 111-116.

Groszer,M., Erickson,R., Scripture-Adams,D.D., Lesche,R., Trumpp,A., Zack,J.A., Kornblum,H.I., Liu,X., and Wu,H. (2001). Negative regulation of neural stem/progenitor cell proliferation by the Pten tumor suppressor gene *in vivo*. Science *294*, 2186-2189.

Gu,H., Zou,Y.R., and Rajewsky,K. (1993). Independent Control of Immunoglobulin Switch Recombination at Individual Switch Regions Evidenced Through Cre-Ioxp-Mediated Gene Targeting. Cell *73*, 1155-1164.

Gunther,H.S., Schmidt,N.O., Phillips,H.S., Kemming,D., Kharbanda,S., Soriano,R., Modrusan,Z., Meissner,H., Westphal,M., and Lamszus,K. (2008). Glioblastoma-derived stem cell-enriched cultures form distinct subgroups according to molecular and phenotypic criteria. Oncogene *27*, 2897-2909.

Hambardzumyan,D., Becher,O.J., Rosenblum,M.K., Pandolfi,P.P., Manova-Todorova,K., and Holland,E.C. (2008). PI3K pathway regulates survival of cancer stem cells residing in the perivascular niche following radiation in medulloblastoma *in vivo*. Genes & Development *22*, 436-448.

Hanahan,D. and Weinberg,R.A. (2000). The hallmarks of cancer. Cell *100*, 57-70.

Harris,M.A., Yang,H., Low,B.E., Mukherje,J., Guha,A., Bronson,R.T., Shultz,L.D., Israel,M.A., and Yun,K. (2008). Cancer Stem Cells Are Enriched in the Side Population Cells in a Mouse Model of Glioma. Cancer Research *68*, 10051-10059.

Hemmati,H.D., Nakano,I., Lazareff,J.A., Masterman-Smith,M., Geschwind,D.H., Bronner-Fraser,M., and Kornblum,H.I. (2003). Cancerous stem cells can arise from pediatric brain tumors. Proceedings of the National Academy of Sciences of the United States of America *100*, 15178-15183.

Herrera,D.G., Garcia-Verdugo,J.M., and Alvarez-Buylla,A. (1999). Adult-derived neural precursors transplanted into multiple regions in the adult brain. Annals of Neurology *46*, 867-877.

Hoess,R.H., Ziese,M., and Sternberg,N. (1982). P1 Site-Specific Recombination - Nucleotide-Sequence of the Recombining Sites. Proceedings of the National Academy of Sciences of the United States of America-Biological Sciences *79*, 3398-3402.

Holland,E,C., Li,Y., Celestino,J., Dai,C., Schaefer,L., Sawaya,R,A. et al. (2000) Astrocytes give rise to oligodendrogliomas and astrocytomas after gene transfer of polyoma virus middle T antigen in vivo. American Journal of Pathology *157*, 1031–1037.

Holland,E.C., Celestino,J., Dai,C.K., Schaefer,L., Sawaya,R.E., and Fuller,G.N. (2000). Combined activation of Ras and Akt in neural progenitors induces glioblastoma formation in mice. Nature Genetics *25*, 55-57.

Holland,E.C., Hively,W.P., DePinho,R.A., and Varmus,H.E. (1998a). A constitutively active epidermal growth factor receptor cooperates with disruption of G1 cell-cycle arrest pathways to induce glioma-like lesions in mice. Genes Dev. *12*, 3675-3685.

Holland,E.C., Hively,W.P., DePinho,R.A., and Varmus,H.E. (1998b). A constitutively active epidermal growth factor receptor cooperates with disruption of G1 cell-cycle arrest pathways to induce glioma-like lesions in mice. Genes Dev. *12*, 3675-3685.

Hong,H., Takahashi,K., Ichisaka,T., Aoi,T., Kanagawa,O., Nakagawa,M., Okita,K., and Yamanaka,S. (2009). Suppression of induced pluripotent stem cell generation by the p53-p21 pathway. Nature *460*, 1132.

Hope,K.J., Jin,L.Q., and Dick,J.E. (2004). Acute myeloid leukemia originates from a hierarchy of leukemic stem cell classes that differ in self-renewal capacity. Nature Immunology *5*, 738-743.

Huntly,B.J.P. and Gilliland,D.G. (2005). Leukaemia stem cells and the evolution of cancer-stem-cell research. Nature Reviews Cancer *5*, 311-321.

Huse,J.T. and Holland,E.C. (2010). Targeting brain cancer: advances in the molecular pathology of malignant glioma and medulloblastoma. Nat Rev Cancer *10*, 319-331.

Ignatova,T.N., Kukekov,V.G., Laywell,E.D., Suslov,O.N., Vrionis,F.D., and Steindler,D.A. (2002). Human cortical glial tumors contain neural stem-like cells expressing astroglial and neuronal markers *in vitro*. Glia *39*, 193-206.

Ivanchuk,S.M., Mondal,S., Dirks,P.B., and Rutka,J.T. (2001) The INK4A/ARF locus: role in cell cycle control and apoptosis and implications for glioma growth. J Neurooncol *51*, 219-229.

Jacks,T., Fazeli,A., Schmitt,E.M., Bronson,R.T., Goodell,M.A., and Weinberg,R.A. (1992). Effects of An Rb Mutation in the Mouse. Nature *359*, 295-300.

Jackson,E.L., Garcia-Verdugo,J.M., Gil-Perotin,S., Roy,M., Quinones-Hinojosa,A., VandenBerg,S., and Alvarez-Buylla,A. (2006). PDGFR alpha-positive B cells are neural stem cells in the adult SVZ that form glioma-like growths in response to increased PDGF signaling. Neuron *51*, 187-199.

Jacques,T.S., Swales,A., Brzozowski,M.J., Henriquez,N.V., Linehan,J.M., Mirzadeh,Z., Malley,C.O., Naumann,H., Alvarez-Buylla,A., and Brandner,S. (2010). Combinations of genetic mutations in the adult neural stem cell compartment determine brain tumour phenotypes. Embo Journal *29*, 222-235.

Jemal,A., Siegel,R., Ward,E., Murray,T., Xu,J., and Thun,M.J. (2007). Cancer Statistics, 2007. CA Cancer J Clin *57*, 43-66.

Jeter,C.R., Badeaux,M., Choy,G., Chandra,D., Patrawala,L., Liu,C., Calhoun-Davis,T., Zaehres,H., Daley,G.Q., and Tang,D.G. (2009). Functional Evidence that the Self-Renewal Gene NANOG Regulates Human Tumor Development. Stem Cells *27*, 993-1005.

Ji,J.F., Werbowetski-Ogilvie,T.E., Zhong,B.N., Hong,S.H., and Bhatia,M. (2009). Pluripotent Transcription Factors Possess Distinct Roles in Normal versus Transformed Human Stem Cells. PLoS ONE *4 (11)*, e8065.

Johansson,M., Brañnnstrom,T., Tommy Bergenheim,A., and Henriksson,R. (2002). Spatial Expression of VEGF-A in Human Glioma. Journal of Neuro-Oncology *59*, 1-6.

Kamijo,T., Bodner,S., van de K,E., Randle,D,H. and Sherr,C,J. (1999) Tumor spectrum in ARF-deficient mice. Cancer Researcg 59, 2217–2222.

Kaplan,M.S. and Hinds,J.W. (1977). Neurogenesis in Adult Rat - Electron-Microscopic Analysis of Light Autoradiographs. Science *197*, 1092-1094.

Kastan,M.B., Onyekwere,O., Sidransky,D., Vogelstein,B., and Craig,R.W. (1991). Participation of P53 Protein in the Cellular-Response to Dna Damage. Cancer Research *51*, 6304-6311.

Kawamura,T., Suzuki,J., Wang,Y.V., Menendez,S., Morera,L.B., Raya,A., Wahl,G.M., and Belmonte,J.C.I. (2009). Linking the p53 tumour suppressor pathway to somatic cell reprogramming. Nature *460*, 1140.

Kelly,P.N., Dakic,A., Adams,J.M., Nutt,S.L., and Strasser,A. (2007). Tumor growth need not be driven by rare cancer stem cells. Science *317*, 337.

Kirschenbaum,B., Nedergaard,M., Preuss,A., Barami,K., Fraser,R.A.R., and Goldman,S.A. (1994). In-Vitro Neuronal Production and Differentiation by Precursor Cells Derived from the Adult Human Forebrain. Cerebral Cortex *4*, 576-589.

Kleihues,P., Burger,P.C., and Scheithauer,B.W. (1993). The New Who Classification of Brain-Tumors. Brain Pathology *3*, 255-268.

Kleihues,P. and Sobin,L.H. (2000). World health organization classification of tumors. Cancer *88*, 2887.

Knudson,A.G. (1984). Genetic Predisposition to Cancer. Cancer Detection and Prevention *7*, 1-8.

Kondo,T. (2006). Brain cancer stem-like cells. European Journal of Cancer *42*, 1237-1242.

Kornack,D.R. and Rakic,P. (2001). The generation, migration, and differentiation of olfactory neurons in the adult primate brain. Proceedings of the National Academy of Sciences of the United States of America *98*, 4752-4757.

Krex,D., Klink,B., Hartmann,C., von Deimling,A., Pietsch,T., Simon,M., Sabel,M., Steinbach,J.P., Heese,O., Reifenberger,G., Weller,M., and Schackert,G. (2007). Long-term survival with glioblastoma multiforme. Brain *130*, 2596-2606.

Kukekov,V.G., Laywell,E.D., Suslov,O., Davies,K., Scheffler,B., Thomas,L.B., O'Brien,T.F., Kusakabe,M., and Steindler,D.A. (1999). Multipotent stem/progenitor cells with similar properties arise from two neurogenic regions of adult human brain. Experimental Neurology *156*, 333-344.

Kwon,C,H., Zhao,D., Chen,J., Alcantara,S., Li,Y., Burns,D,K., Mason,R,P., Lee,E., Wu,H. and Parada,L,F. (2008) Pten Haploinsufficiency Accelerates Formation of High-Grade Astrocytomas. Cancer Research *68*, 3286-3294.

Lakka,S.S., Rajan,M., Gondi,C., Yanamandra,N., Chandrasekar,N., Jasti,S.L., Adachi,Y., Siddique,K., Gujrati,M., Olivero,W., Dinh,D.H., Kouraklis,G., Kyritsis,A.P., and Rao,J.S. (2002). Adenovirus-mediated expression of antisense MMP-9 in glioma cells inhibits tumor growth and invasion. Oncogene *21*, 8011-8019.

Laks,D.R., Visnyei,K., and Kornblum,H.I. (2010). Brain Tumor Stem Cells as Therapeutic Targets in Models of Glioma. Yonsei Med J *51*, 633-640.

Lane,D.P. (1992). Cancer - P53, Guardian of the Genome. Nature *358*, 15-16.

Laywell,E.D., Rakic,P., Kukekov,V.G., Holland,E.C., and Steindler,D.A. (2000). Identification of a multipotent astrocytic stem cell in the immature and adult mouse brain. Proceedings of the National Academy of Sciences of the United States of America *97*, 13883-13888.

Lee,A., Kessler,J.D., Read,T.A., Kaiser,C., Corbeil,D., Huttner,W.B., Johnson,J.E., and Wechsler-Reya,R.J. (2005). Isolation of neural stem cells from the postnatal cerebellum. Nature Neuroscience *8*, 723-729.

Lee,E.Y.H.P., Chang,C.Y., Hu,N.P., Wang,Y.C.J., Lai,C.C., Herrup,K., Lee,W.H., and Bradley,A. (1992). Mice Deficient for Rb Are Nonviable and Show Defects in Neurogenesis and Hematopoiesis. Nature *359*, 288-294.

Lee,J., Son,M.J., Woolard,K., Donin,N.M., Li,A., Cheng,C.H., Kotliarova,S., Kotliarov,Y., Walling,J., Ahn,S., Kim,M., Totonchy,M., Cusack,T., Ene,C., Ma,H., Su,Q., Zenklusen,J.C., Zhang,W., Maric,D., and Fine,H.A. (2008a). Epigenetic-mediated dysfunction of the bone morphogenetic protein pathway inhibits differentiation of glioblastoma-initiating cells. Cancer Cell *13*, 69-80.

Lee,J.S., Gil,J.E., Kim,J.H., Kim,T.K., Jin,X., Oh,S.Y., Sohn,Y.W., Jeon,H.M., Park,H.J., Park,J.W., Shin,Y.J., Chung,Y.G., Lee,J.B., You,S., and Kim,H. (2008b). Brain cancer stem-like cell genesis from p53-deficient mouse astrocytes by oncogenic Ras. Biochemical and Biophysical Research Communications *365*, 496-502.

Lee,S.H., Lumelsky,N., Studer,L., Auerbach,J.M., and Mckay,R.D. (2000). Efficient generation of midbrain and hindbrain neurons from mouse embryonic stem cells. Nature Biotechnology *18*, 675-679.

Li,J., Yen,C., Liaw,D., Podsypanina,K., Bose,S., Wang,S.I., Puc,J., Miliaresis,C., Rodgers,L., McCombie,R., Bigner,S.H., Giovanella,B.C., Ittmann,M., Tycko,B., Hibshoosh,H., Wigler,M.H., and Parsons,R. (1997). PTEN, a putative protein tyrosine phosphatase gene mutated in human brain, breast, and prostate cancer. Science *275*, 1943-1947.

Li,L., Liu,F.H., and Ross,A.H. (2003). PTEN regulation of neural development and CNS stem cells. Journal of Cellular Biochemistry *88*, 24-28.

Liaw,D., Marsh,D.J., Li,J., Dahia,P.L.M., Wang,S.I., Zheng,Z.M., Bose,S., Call,K.M., Tsou,H.C., Peacocke,M., Eng,C., and Parsons,R. (1997). Germline mutations of the PTEN gene in Cowden disease, an inherited breast and thyroid cancer syndrome. Nature Genetics *16*, 64-67.

Lie,D.C., Dziewczapolski,G., Willhoite,A.R., Kaspar,B.K., Shults,C.W., and Gage,F.H. (2002). The adult substantia nigra contains progenitor cells with neurogenic potential. Journal of Neuroscience *22*, 6639-6649.

Liggett,W.H. and Sidransky,D. (1998). Role of the p16 tumor suppressor gene in cancer. J Clin Oncol *16*, 1197-1206.

Ligon,K.L., Alberta,J.A., Kho,A.T., Weiss,J.E.N.N., Kwaan,M.R., Nutt,C.L., Louis,D.N., Stiles,C.D., and Rowitch,D.H. (2004). The Oligodendroglial Lineage Marker OLIG2 Is Universally Expressed in Diffuse Gliomas. Journal of Neuropathology & Experimental Neurology *63*.

Liliental,J., Moon,S.Y., Lesche,R., Mamillapalli,R., Li,D.M., Zheng,Y., Sun,H., and Wu,H. (2000). Genetic deletion of the Pten tumor suppressor gene promotes cell motility by activation of Rac1 and Cdc42 GTPases. Current Biology *10*, 401-404.

Lin,T.X., Chao,C., Saito,S., Mazur,S.J., Murphy,M.E., Appella,E., and Xu,Y. (2005). P53 induces differentiation of mouse embryonic stem cells by suppressing Nanog expression. Nature Cell Biology *7*, 165.

Liu,Q.H., Nguyen,D.H., Dong,Q.H., Shitaku,P., Chung,K., Liu,O.Y., Tso,J.L., Liu,J.Y., Konkankit,V., Cloughesy,T.F., Mischel,P.S., Lane,T.F., Liau,L.M., Nelson,S.F., and Tso,C.L. (2009). Molecular properties of CD133+glioblastoma stem cells derived from treatment-refractory recurrent brain tumors. Journal of Neuro-Oncology *94*, 1-19.

Llaguno,S.A., Chen,J., Kwon,C.H., Jackson,E.L., Li,Y.J., Burns,D.K., Alvarez-Buylla,A., and Parada,L.F. (2009). Malignant Astrocytomas Originate from Neural Stem/Progenitor Cells in a Somatic Tumor Suppressor Mouse Models. Cancer Cell *15*, 45-56.

Lois,C. and Alvarez-Buylla,A. (1994). Long-distance neuronal migration in the adult mammalian brain. Science *264*, 1145-1148.

Lois,C. and Alvarezbuylla,A. (1993). Proliferating Subventricular Zone Cells in the Adult Mammalian Forebrain Can Differentiate Into Neurons and Glia. Proceedings of the National Academy of Sciences of the United States of America *90*, 2074-2077.

Louis,D.N., Ohgaki,H., Wiestler,O.D., Cavenee,W.K., Burger,P.C., Jouvet,A., Scheithauer,B.W., and Kleihues,P. (2007). The 2007 WHO classification of tumours of the central nervous system. Acta Neuropathologica *114*, 97-109.

Lowry,N.A. and Temple,S. (2009). Identifying the Perpetrator in Medulloblastoma: Dorian Gray versus Benjamin Button. Cancer Cell *15*, 83-85.

Lozano,G. (2010). Mouse Models of p53 Functions. Cold Spring Harbor Perspectives in Biology *2*.

Luskin,M.B. (1993). Restricted Proliferation and Migration of Postnatally Generated Neurons Derived from the Forebrain Subventricular Zone. Neuron *11*, 173-189.

Ma,Y.H., Mentlein,R., Knerlich,F., Kruse,M.L., Mehdorn,H.M., and Held-Feindt,J. (2008). Expression of stem cell markers in human astrocytomas of different WHO grades. Journal of Neuro-Oncology *86*, 31-45.

MacKenzie,K.L., Franco,S., Naiyer,A.J., May,C., Sadelain,M., Rafii,S., and Moore,M.A.S. (2002). Multiple stages of malignant transformation of human endothelial cells modelled by co-expression of telomerase reverse transcriptase, SV40 T antigen and oncogenic N-ras. Oncogene *21*, 4200-4211.

Maehama,T. and Dixon,J.E. (1998). The tumor suppressor, PTEN/MMAC1, dephosphorylates the lipid second messenger, phosphatidylinositol 3,4,5-trisphosphate. Journal of Biological Chemistry *273*, 13375-13378.

Maltzman,W. and Czyzyk,L. (1984). Uv Irradiation Stimulates Levels of P53 Cellular Tumor-Antigen in Nontransformed Mouse Cells. Molecular and Cellular Biology *4*, 1689-1694. Genes & Development *14*, 994-1004.

Marino,S.. Vooijs,M., van der Gulden,H., Jonkers,J. and Berns,A. (2000). Induction of medulloblastomas in p53-null mutant mice by somatic inactivation of Rb in the external granular layer cells of the cerebellum. Genes Dev. *14*, 994-1004.

Marino,S., Krimpenfort,P., Leung,C., van der Korput,H.A.G.M., Trapman,J., Camenisch,I., Berns,A., and Brandner,S. (2002a). PTEN is essential for cell migration but not for fate determination and tumourigenesis in the cerebellum. Development *129*, 3513-3522.

Marino,S., Vooijs,M., van der Gulden,H., Jonkers,J., and Berns,A. (2000). Induction of medulloblastomas in p53-null mutant mice by somatic inactivation of Rb in the external granular layer cells of the cerebellum. Genes & Development *14*, 994-1004.

Martens,T., Schmidt,N.O., Eckerich,C., Fillbrandt,R., Merchant,M., Schwall,R., Westphal,M., and Lamszus,K. (2006). A novel one-armed anti-c-met antibody inhibits glioblastoma growth *in vivo*. Clinical Cancer Research *12*, 6144-6152.

Marzesco,A.M., Janich,P., Wilsch-Brauninger,M., Dubreuil,V., Langenfeld,K., Corbeil,D., and Huttner,W.B. (2005). Release of extracellular membrane particles carrying the stem cell marker prominin-1 (CD133) from neural progenitors and other epithelial cells. J Cell Sci *118*, 2849-2858.

Matsumoto,K., Arao,T., Tanaka,K., Kaneda,H., Kudo,K., Fujita,Y., Tamura,D., Aomatsu,K., Tamura,T., Yamada,Y., Saijo,N., and Nishio,K. (2009). mTOR Signal and Hypoxia-Inducible Factor-1 alpha Regulate CD133 Expression in Cancer Cells. Cancer Research *69*, 7160-7164.

Maurer,M.H., Feldmann,R.E., Futterer,C.D., Butlin,J., and Kuschinsky,W. (2004). Comprehensive Proteome expression profiling of undifferentiated versus differentiated neural stem cells from adult rat hippocampus. Neurochemical Research *29*, 1129-1144.

Meletis,K., Wirta,V., Hede,S.M., Nist+¬r,M., Lundeberg,J., and Fris+¬n,J. (2006). p53 suppresses the self-renewal of adult neural stem cells. Development *133*, 363-369.

Mendez,O., Zavadil,J., Esencay,M., Lukyanov,Y., Santovasi,D., Wang,S.C., Newcomb,E., and Zagzag,D. (2010). Knock down of HIF-1alpha in glioma cells reduces migration *in vitro* and invasion *in vivo* and impairs their ability to form tumor spheres. Molecular Cancer *9*, 133.

Merkle,F.T. and Alvarez-Buylla,A. (2006). Neural stem cells in mammalian development. Current Opinion in Cell Biology *18*, 704-709.

Merkle,F.T., Tramontin,A.D., Garc+¡a-Verdugo,J.M., and Alvarez-Buylla,A. (2004). Radial glia give rise to adult neural stem cells in the subventricular zone. Proceedings of the National Academy of Sciences of the United States of America *101*, 17528-17532.

Messier,B., Leblond,C.P., and Smart,I. (1958). Presence of Dna Synthesis and Mitosis in the Brain of Young Adult Mice. Experimental Cell Research *14*, 224-226.

Mikheeva,S., Mikheev,A., Petit,A., Beyer,R., Oxford,R., Khorasani,L., Maxwell,J.P., Glackin,C., Wakimoto,H., Gonzalez-Herrero,I., Sanchez-Garcia,I., Silber,J., Horner,P., and Rostomily,R. (2010). TWIST1 promotes invasion through mesenchymal change in human glioblastoma. Molecular Cancer *9*, 194.

Miller,C.R. and Perry,A. (2007). Glioblastoma. Archives of Pathology & Laboratory Medicine *131*, 397-406.

Miller,S.J., Lavker,R.M., and Sun,T.T. (2005). Interpreting epithelial cancer biology in the context of stem cells: Tumor properties and therapeutic implications. Biochimica et Biophysica Acta-Reviews on Cancer *1756*, 25-52.

Miraglia,S., Godfrey,W., Yin,A.H., Atkins,K., Warnke,R., Holden,J.T., Bray,R.A., Waller,E.K., and Buck,D.W. (1997). A novel five-transmembrane hematopoietic stem cell antigen: Isolation, characterization, and molecular cloning. Blood *90*, 5013-5021.

Mirzadeh,Z., Merkle,F.T., Soriano-Navarro,M., Garcia-Verdugo,J.M., and Alvarez-Buylla,A. (2008). Neural stem cells confer unique pinwheel architecture to the ventricular surface in neurogenic regions of the adult brain. Cell Stem Cell *3*, 265-278.

Mitsui,K., Tokuzawa,Y., Itoh,H., Segawa,K., Murakami,M., Takahashi,K., Maruyama,M., Maeda,M., and Yamanaka,S. (2003). The homeoprotein Nanog is required for maintenance of pluripotency in mouse epiblast and ES cells. Cell *113*, 631-642.

Mizrak,D., Brittan,M., and Alison,M.R. (2008). CD133: molecule of the moment. Journal of Pathology *214*, 3-9.

Mokhtari,K., Paris,S., Aguirre-Cruz,L., Privat,N., Criniere,E., Marie,Y., Hauw,J.J., Kujas,M., Rowitch,D., Hoang-Xuan,K., Delattre,J.Y., and Sanson,M. (2005). Olig2 expression, GFAP, p53 and 1p loss analysis contribute to glioma subclassification. Neuropathology and Applied Neurobiology *31*, 62-69.

Molofsky,A.V., He,S.H., Bydon,M., Morrison,S.J., and Pardal,R. (2005). Bmi-1 promotes neural stem cell self-renewal and neural development but not mouse growth and survival by repressing the p16(Ink4a) and P19(Arf) senescence pathways. Genes & Development *19*, 1432-1437.

Mori,H., Fujitani,T., Kanemura,Y., Kino-Oka,M., and Taya,M. (2007). Observational examination of aggregation and migration during early phase of neurosphere culture of mouse neural stem cells. Journal of Bioscience and Bioengineering *104*, 231-234.

Moulton,T., Samara,G., Chung,W.Y., Yuan,L., Desai,R., Sisti,M., Bruce,J., and Tycko,B. (1995). Mts1/P16/Cdkn2 Lesions in Primary Glioblastoma-Multiforme. American Journal of Pathology *146*, 613-619.

Murat,A., Migliavacca,E., Gorlia,T., Lambiv,W.L., Shay,T., Hamou,M.F., de Tribolet,N., Regli,L., Wick,W., Kouwenhoven,M.C.M., Hainfellner,J.A., Heppner,F.L., Dietrich,P.Y., Zimmer,Y., Cairncross,J.G., Janzer,R.C., Domany,E., Delorenzi,M., Stupp,R., and Hegi,M.E. (2008). Stem Cell-Related "Self-Renewal" Signature and High Epidermal Growth Factor Receptor Expression Associated With Resistance to Concomitant Chemoradiotherapy in Glioblastoma. J Clin Oncol *26*, 3015-3024.

Nigro,J.M., Baker,S.J., Preisinger,A.C., Jessup,J.M., Hostetter,R., Cleary,K., Bigner,S.H., Davidson,N., Baylin,S., Devilee,P., Glover,T., Collins,F.S., Weston,A., Modali,R., Harris,C.C., and Vogelstein,B. (1989). Mutations in the P53 Gene Occur in Diverse Human-Tumor Types. Nature *342*, 705-708.

Nishide,K., Nakatani,Y., Kiyonari,H., and Kondo,T. (2009). Glioblastoma Formation from Cell Population Depleted of Prominin1-Expressing Cells. PLoS ONE *4*.

Nobori,T., Miura,K., Wu,D.J., Lois,A., Takabayashi,K., and Carson,D.A. (1994). Deletions of the Cyclin-Dependent Kinase-4 Inhibitor Gene in Multiple Human Cancers. Nature *368*, 753-756.

Obaya,A.J. and Sedivy,J.M. (2002). Regulation of cyclin-Cdk activity in mammalian cells. CMLS Cellular and Molecular Life Sciences *59*, 126-142.

O'Brien,C.A., Pollett,A., Gallinger,S., and Dick,J.E. (2007). A human colon cancer cell capable of initiating tumour growth in immunodeficient mice. Nature *445*, 106-110.

O'Farrell,P.H. (2001). Triggering the all-or-nothing switch into mitosis. Trends in Cell Biology *11*, 512-519.

Office for national statistics UK. Review of the National Statistician on deaths in England and Wales, 2008.

Ogden,A.T., Waziri,A.E., Lochhead,R.A., Fusco,D., Lopez,K., Ellis,J.A., Kang,J., Assanah,M., McKhann,G.M., Sisti,M.B., McCormick,P.C., Canoll,P., and Bruce,J.N. (2008). Identification of A2b5+Cd133- Tumor-Initiating Cells in Adult Human Gliomas. Neurosurgery *62*, 505-514.

Ohgaki,H. and Kleihues,P. (2007). Genetic pathways to primary and secondary glioblastoma. American Journal of Pathology *170*, 1445-1453.

Ohgaki,H., Dessen,P., Jourde,B., Horstmann,S., Nishikawa,T., Di Patre,P.L., Burkhard,C., Sch++ler,D., Probst-Hensch,N.M., Maiorka,P.C.s., Baeza,N., Pisani,P., Yonekawa,Y., Yasargil,M.G., L++tolf,U.M., and Kleihues,P. (2004). Genetic Pathways to Glioblastoma. Cancer Research *64*, 6892-6899.

Okano,H., Imai,T., and Okabe,M. (2002). Musashi: a translational regulator of cell fate. J Cell Sci *115*, 1355-1359.

Oliver,T.G. and Wechsler-Reya,R.J. (2004). Getting at the root and stem of brain tumors. Neuron *42*, 885-888.

Omerovic,J., Laude,A., and Prior,I. (2007). Ras proteins: paradigms for compartmentalised and isoform-specific signalling. Cellular and Molecular Life Sciences (CMLS) *64*, 2575-2589.

Pan,G.J. and Thomson,J.A. (2007). Nanog and transcriptional networks in embryonic stem cell pluripotency. Cell Research *17*, 42-49.

Parkin,D.M., Bray,F., Ferlay,J., and Pisani,P. (2005). Global Cancer Statistics, 2002. CA Cancer J Clin *55*, 74-108.

Pencea,V., Bingaman,K.D., Freedman,L.J., and Luskin,M.B. (2001). Neurogenesis in the Subventricular Zone and Rostral Migratory Stream of the Neonatal and Adult Primate Forebrain. Experimental Neurology *172*, 1-16.

Penuelas,S., Anido,J., Prieto-Sanchez,R.M., Folch,G., Barba,I., Cuartas,I., Garcia-Dorado,D., Poca,M.A., Sahuquillo,J., Baselga,J., and Seoane,J. (2009). TGF-beta Increases Glioma-Initiating Cell Self-Renewal through the Induction of LIF in Human Glioblastoma. Cancer Cell *15*, 315-327.

Perry,A., Aldape,K.D., George,D.H., and Burger,P.C. (2004). Small cell astrocytoma: An aggressive variant that is clinicopathologically and genetically distinct from anaplastic oligodendroglioma. Cancer *101*, 2318-2326.

Pfaffl,M.W. (2001). A new mathematical model for relative quantification in real-time RT-PCR. Nucleic Acids Research *29*.

Piccirillo,S.G.M., Reynolds,B.A., Zanetti,N., Lamorte,G., Binda,E., Broggi,G., Brem,H., Olivi,A., Dimeco,F., and Vescovi,A.L. (2006). Bone morphogenetic proteins inhibit the tumorigenic potential of human brain tumour-initiating cells. Nature *444*, 761-765.

Pina-Oviedo,S., Leon-Bojorge,B., Cuesta-Mejias,T., White,M.K., Ortiz-Hidalgo,C., Khalili,K., and Del Valle,L. (2006). Glioblastoma multiforme with small cell neuronal-like component: association with human neurotropic JC virus. Acta Neuropathologica *111*, 388-396.

Po,A., Ferretti,E., Miele,E., De Smaele,E., Paganelli,A., Canettieri,G., Coni,S., Di Marcotullio,L., Biffoni,M., Massimi,L., Di Rocco,C., Screpanti,I., and Gulino,A.

(2010). Hedgehog controls neural stem cells through p53-independent regulation of Nanog. EMBO J *29*, 2646-2658.

Quinones-Hinojosa,A. and Chaichana,K. (2007). The human subventricular zone: A source of new cells and a potential source of brain tumors. Experimental Neurology *205*, 313-324.

Read,T.A., Fogarty,M.P., Markant,S.L., McLendon,R.E., Wei,Z.Z., Ellison,D.W., Febbo,P.G., and Wechsler-Reya,R.J. (2009). Identification of CD15 as a Marker for Tumor-Propagating Cells in a Mouse Model of Medulloblastoma. Cancer Cell *15*, 135-147.

Rebetz,J., Tian,D., Persson,A., Widegren,B., Salford,L.G., Englund,E., Gisselsson,D., and Fan,X. (2008). Glial Progenitor-Like Phenotype in Low-Grade Glioma and Enhanced CD133-Expression and Neuronal Lineage Differentiation Potential in High-Grade Glioma. PLoS ONE *3*, e1936.

Reilly,K,M., Loisel,D,A., Bronson,R,T., McLaughlin,M.E. and Jacks,T. (2000) Nf1;Trp53 mutant mice develop glioblastoma with evidence of strain-specific effects. Nature Genetics *26*, 109–113.

Reubinoff,B.E., Pera,M.F., Fong,C.Y., Trounson,A., and Bongso,A. (2000). Embryonic stem cell lines from human blastocysts: somatic differentiation *in vitro*. Nature Biotechnology *18*, 399-404.

Reynolds,B.A. and Rietze,R.L. (2005). Neural stem cells and neurospheres - re-evaluating the relationship. Nature Methods *2*, 333-336.

Reynolds,B.A., Tetzlaff,W., and Weiss,S. (1992). A Multipotent Egf-Responsive Striatal Embryonic Progenitor-Cell Produces Neurons and Astrocytes. Journal of Neuroscience *12*, 4565-4574.

Reynolds,B.A. and Weiss,S. (1992). Generation of Neurons and Astrocytes from Isolated Cells of the Adult Mammalian Central-Nervous-System. Science *255*, 1707-1710.

Ricci-Vitiani,L., Lombardi,D.G., Pilozzi,E., Biffoni,M., Todaro,M., Peschle,C., and De Maria,R. (2007). Identification and expansion of human colon-cancer-initiating cells. Nature *445*, 111-115.

Rich,J.N., Guo,C.H., McLendon,R.E., Bigner,D.D., Wang,X.F., and Counter,C.M. (2001). A genetically tractable model of human glioma formation. Cancer Research *61*, 3556-3560.

Rietze,R.L. and Reynolds,B.A. (2006). Neural Stem Cell Isolation and Characterization. In Methods in EnzymologyAdult Stem Cells, Irina Klimanskaya and Robert Lanza, ed. Academic Press), pp. 3-23.

Roger,L., Jullien,L., Gire,V., and Roux,P. (2010). Gain of oncogenic function of p53 mutants regulates E-cadherin expression uncoupled from cell invasion in colon cancer cells. J Cell Sci *123*, 1295-1305.

Royds,J.A. and Iacopetta,B. (2006). p53 and disease: when the guardian angel fails. Cell Death and Differentiation *13*, 1017-1026.

Sakakibara,S.i. and Okano,H. (1997). Expression of Neural RNA-Binding Proteins in the Postnatal CNS: Implications of Their Roles in Neuronal and Glial Cell Development. Journal of Neuroscience *17*, 8300-8312.

Sauer,B. and Henderson,N. (1988). Site-Specific Dna Recombination in Mammalian-Cells by the Cre Recombinase of Bacteriophage-P1. Proceedings of the National Academy of Sciences of the United States of America *85*, 5166-5170.

Schmitz,M., Temme,A., Senner,V., Ebner,R., Schwind,S., Stevanovic,S., Wehner,R., Schackert,G., Schackert,H.K., Fussel,M., Bachmann,M., Rieber,E.P., and Weigle,B. (2007). Identification of SOX2 as a novel glioma-associated antigen and potential target for T cell-based immunotherapy. Br J Cancer *96*, 1293-1301.

Scott,J.N., Rewcastle,N.B., Brasher,P.M.A., Fulton,D., Hagen,N.A., MacKinnon,J.A., Sutherland,G., Cairncross,J.G., and Forsyth,P. (1998). Long-term glioblastoma multiforme survivors: a population-based study. Canadian Journal of Neurological Sciences *25*, 197-201.

Seri,B., Garcia-Verdugo,J.M., Mcewen,B.S., and Alvarez-Buylla,A. (2001). Astrocytes give rise to new neurons in the adult mammalian hippocampus. Journal of Neuroscience *21*, 7153-7160.

Seri,B., Herrera,D.G., Gritti,A., Ferron,S., Collado,L., Vescovi,A., Garcia-Verdugo,J.M., and Alvarez-Buylla,A. (2006). Composition and organization of the

SCZ: A large germinal layer containing neural stem cells in the adult mammalian brain. Cerebral Cortex *16*, I103-I111.

Shi,Y., Chichung Lie,D., Taupin,P., Nakashima,K., Ray,J., Yu,R.T., Gage,F.H., and Evans,R.M. (2004). Expression and function of orphan nuclear receptor TLX in adult neural stem cells. Nature *427*, 78-83.

Shmelkov,S.V., Butler,J.M., Hooper,A.T., Hormigo,A., Kushner,J., Milde,T., St Clair,R., Baljevic,M., White,I., Jin,D.K., Chadburn,A., Murphy,A.J., Valenzuela,D.M., Gale,N.W., Thurston,G., Yancopoulos,G.D., D'Angelica,M., Kemeny,N., Lyden,D., and Rafii,S. (2008). CD133 expression is not restricted to stem cells, and both CD133(+) and CD133(-) metastatic colon cancer cells initiate tumors. Journal of Clinical Investigation *118*, 2111-2120.

Singec,I., Knoth,R., Meyer,R.P., Maciaczyk,J., Volk,B., Nikkhah,G., Frotscher,M., and Snyder,E.Y. (2006). Defining the actual sensitivity and specificity of the neurosphere assay in stem cell biology. Nature Methods *3*, 801-806.

Singh,S.K., Clarke,I.D., Terasaki,M., Bonn,V.E., Hawkins,C., Squire,J., and Dirks,P.B. (2003). Identification of a cancer stem cell in human brain tumors. Cancer Research *63*, 5821-5828.

Singh,S.K., Hawkins,C., Clarke,I.D., Squire,J.A., Bayani,J., Hide,T., Henkelman,R.M., Cusimano,M.D., and Dirks,P.B. (2004). Identification of human brain tumour initiating cells. Nature *432*, 396-401.

Smith,J.S. and Jenkins,R.B. (2000). Genetic alterations in adult diffuse glioma: Occurrence, significance, and prognostic implications. Frontiers in Bioscience *5*, D213-D231.

Sneddon,J.B. and Werb,Z. (2007). Location, location, location: The cancer stem cell niche. Cell Stem Cell *1*, 607-611.

Song,D.L. and Joyner,A.L. (2000). Two Pax2/5/8-binding sites in Engrailed2 are required for proper initiation of endogenous mid-hindbrain expression. Mechanisms of Development *90*, 155-165.

Sonoda,Y., Ozawa,T., Aldape,K.D., Deen,D.F., Berger,M.S., and Pieper,R.O. (2001). Akt pathway activation converts anaplastic astrocytoma to glioblastoma multiforme in a human astrocyte model of glioma. Cancer Research *61*, 6674-6678.

Soriano,P. (1999). Generalized lacZ expression with the ROSA26 Cre reporter strain. Nature Genetics *21*, 70-71.

Srivastava,S., Zou,Z.Q., Pirollo,K., Blattner,W., and Chang,E.H. (1990). Germ-Line Transmission of A Mutated P53 Gene in A Cancer-Prone Family with Li-Fraumeni Syndrome. Nature *348*, 747-749.

Stiles,B., Groszer,M., Wang,S.Y., Jiao,J., and Wu,H. (2004). PTENless means more. Developmental Biology *273*, 175-184.

Stiles,C.D. and Rowitch,D.H. (2008). Glioma stem cells: A midterm exam. Neuron *58*, 832-846.

Stone,D.M., Hynes,M., Armanini,M., Swanson,T.A., Gu,Q.M., Johnson,R.L., Scott,M.P., Pennica,D., Goddard,A., Phillips,H., Noll,M., Hooper,J.E., deSauvage,F., and Rosenthal,A. (1996). The tumour-suppressor gene patched encodes a candidate receptor for Sonic hedgehog. Nature *384*, 129-134.

Stupp,R., Hegi,M.E., Mason,W.P., van den Bent,M.J., Taphoorn,M.J., Janzer,R.C., Ludwin,S.K., Allgeier,A., Fisher,B., Belanger,K., Hau,P., Brandes,A.A., Gijtenbeek,J., Marosi,C., Vecht,C.J., Mokhtari,K., Wesseling,P., Villa,S., Eisenhauer,E., Gorlia,T., Weller,M., Lacombe,D., Cairncross,J.G., Mirimanoff,R.O. (2009) Effects of radiotherapy with concomitant and adjuvant temozolomide versus radiotherapy alone on survival in glioblastoma in a randomised phase III study: 5-year analysis of the EORTC-NCIC trial. Lancet Oncololgy.10, 459-466

Sutter,R., Yadirgi,G., and Marino,S. (2007). Neural stem cells, tumour stem cells and brain tumours: Dangerous relationships? Biochimica et Biophysica Acta (BBA) - Reviews on Cancer *1776*, 125-137.

Takemura,S., Kayama,T., Kuge,A., Ali,H., Kokubo,Y., Sato,S., Kamii,H., Goto,K., Yoshimoto,T. (2006). Correlation between copper/zinc superoxide dismutase and the proliferation of neural stem cells in aging and following focal cerebral ischemia. Journal of Neurosurgery *104*, 129-136.

Takenaga,K., Nygren,J., Zelenina,M., Ohira,M., Iuchi,T., Lukanidin,E., Sjoquist,M., and Kozlova,E.N. (2007). Modified expression of Mts1/S100A4 protein in C6 glioma cells or surrounding astrocytes affects migration of tumor cells *in vitro* and *in vivo*. Neurobiology of Disease *25*, 455-463.

Tamura,M., Gu,J.G., Matsumoto,K., Aota,S., Parsons,R., and Yamada,K.M. (1998). Inhibition of cell migration, spreading, and focal adhesions by tumor suppressor PTEN. Science *280*, 1614-1617.

Tao,W. and Levine,A,J. (1999). P19(ARF) stabilizes p53 by blocking nucleo-cytoplasmic shuttling of Mdm2. Proceedings of the National Academy of Sciences of the United States of America *96*, 6937–6941.

Tchougounova,E., Kastemar,M., Brasater,D., Holland,E.C., Westermark,B., and Uhrbom,L. (2007). Loss of Arf causes tumor progression of PDGFB-induced oligodendroglioma. Oncogene *26*, 6289-6296.

Thon,N., Damianoff,K., Hegermann,J., Grau,S., Krebs,B., Schnell,O., Tonn,J.r.C., and Goldbrunner,R. (2010). Presence of pluripotent CD133+ cells correlates with malignancy of gliomas. Molecular and Cellular Neuroscience *43*, 51-59.

Toda,M., Iizuka,Y., Yu,W., Imai,T., Ikeda,E., Yoshida,K., Kawase,T., Kawakami,Y., Okano,H., and Uyemura,K. (2001). Expression of the neural RNA-binding protein musashi1 in human gliomas. Glia *34*, 1-7.

Tong,W,M., Ohgaki,H., Huang,H., Granier,C., Kleihues,P. and Wang,Z,Q. (2003). Null Mutation of DNA Strand Break-Binding Molecule Poly(ADP-ribose) Polymerase Causes Medulloblastomas in p53-/- Mice. American Journal of Pathology *162*, 343-352.

Tong,Q.S., Zheng,L.D., Tang,S.T., Ruan,Q.L., Liu,Y., Li,S.W., Jiang,G.S., and Cai,J.B. (2008). Expression and clinical significance of stem cell marker CD133 in human neuroblastoma. World Journal of Pediatrics *4*, 58-62.

Tropepe,V., Sibilia,M., Ciruna,B.G., Rossant,T., Wagner,E.F., and van der Kooy,D. (1999). Distinct neural stem cells proliferate in response to EGF and FGF in the developing mouse telencephalon. Developmental Biology *208*, 166-188.

Tsatmali,M., Walcott,E.C., and Crossin,K.L. (2005). Newborn neurons acquire high levels of reactive oxygen species and increased mitochondrial proteins upon differentiation from progenitors. Brain Research *1040*, 137-150.

Uchida,N. (2000). Cell sorting of human neural stem cells from fetal brain: phenotype, clonal assay, expansion and characterization. European Cytokine Network *11*, 329-330.

Uhrbom,L., Hesselager,G., Nistér,M. and Westermark,B. (1998) Induction of brain tumors in mice using a recombinant platelet-derived growth factor B-chain retrovirus. Cancer Research *58*, 5275-5279.

Uhrbom,L., Kastemar,M., Johansson,F.K., Westermark,B., and Holland,E.C. (2005). Cell type-specific tumor suppression by Ink4a and Arf in kras-induced mouse gliomagenesis. Cancer Research *65*, 2065-2069.

Vander Griend,D.J., Karthaus,W.L., Dalrymple,S., Meeker,A., DeMarzo,A.M., and Isaacs,J.T. (2008). The Role of CD133 in Normal Human Prostate Stem Cells and Malignant Cancer-Initiating Cells. Cancer Research *68*, 9703-9711.

Veeravalli,K.K., Chetty,C., Ponnala,S., Gondi,C.S., Lakka,S.S., Fassett,D., Klopfenstein,J.D., Dinh,D.H., Gujrati,M., and Rao,J.S. (2010). MMP-9, uPAR and Cathepsin B Silencing Downregulate Integrins in Human Glioma Xenograft Cells In Vitro and In Vivo in Nude Mice. PLoS ONE *5*, e11583.

Vercauteren,S.M. and Sutherland,H.J. (2001). CD133 (AC133) expression on AML cells and progenitors. Cytotherapy *3*, 449-459.

Vermeulen,K., Van Bockstaele,D.R., and Berneman,Z.N. (2003) The cell cycle: a review of regulation, deregulation and therapeutic targets in cancer. Cell Prolif *36*, 131-149.

Vescovi,A.L., Galli,R., and Reynolds,B.A. (2006). Brain tumour stem cells. Nature Reviews Cancer *6*, 425-436.

Vescovi,A.L., Reynolds,B.A., Fraser,D.D., and Weiss,S. (1993). Bfgf Regulates the Proliferative Fate of Unipotent (Neuronal) and Bipotent (Neuronal Astroglial) Egf-Generated Cns Progenitor Cells. Neuron *11*, 951-966.

Vorechovsky,I., Tingby,O., Hartman,M., Stromberg,B., Nister,M., Collins,V.P., and Toftgard,R. (1997). Somatic mutations in the human homologue of Drosophila patched in primitive neuroectodermal tumours. Oncogene *15*, 361-366.

Wang,J., Sakariassen,P.O., Tsinkalovsky,O., Immervoll,H., Boe,S.O., Svendsen,A., Prestegarden,L., Rosland,G., Thorsen,F., Stuhr,L., Molven,A., Bjerkvig,R., and Enger,P.O. (2008). CD133 negative glioma cells form tumors in nude rats and give rise to CD133 positive cells. International Journal of Cancer *122*, 761-768.

Ward,J.F. (1985). Biochemistry of Dna Lesions. Radiation Research *104*, S103-S111.

Watt,F.M. and Hogan,B.L.M. (2000). Out of Eden: Stem cells and their niches. Science *287*, 1427-1430.

Wiedemeyer,W,R., Dunn,I,F., Quayle,S,N., Zhang,J., Chheda,M,G., Dunn,G,P., Zhuang,L., Rosenbluh,J., Chen,S., Xiao,Y., Shapiro,G,I., Hahn,W,C. and Chin,L. (2010). Pattern of retinoblastoma pathway inactivation dictates response to CDK4/6 inhibition in GBM. Proceedings of the National Academy of Sciences of the United States of America *107*, 11501-11506.

Weigmann,A., Corbeil,D., Hellwig,A., and Huttner,W.B. (1997). Prominin, a novel microvilli-specific polytopic membrane protein of the apical surface of epithelial cells, is targeted to plasmalemmal protrusions of non-epithelial cells. Proceedings of the National Academy of Sciences of the United States of America *94*, 12425-12430.

Weinberg,R.A. (1995). The retinoblastoma protein and cell cycle control. Cell *81*, 323-330.

Weiss,W,A., Aldape,K., Mohapatra,G., et al. (1997) Targeted expression of MYCN causes neuroblastoma in transgenic mice. EMBO Journal *16*, 2985-2995.

Weiss,W.A., Burns,M.J., Hackett,C., Aldape,K., Hill,J.R., Kuriyama,H., Kuriyama,N., Milshteyn,N., Roberts,T., Wendland,M.F., DePinho,R., and Israel,M.A. (2003). Genetic determinants of malignancy in a mouse model for oligodendroglioma. Cancer Research *63*, 1589-1595.

Weissenberger,J., Steinbach,J,P., Malin,G., Spada,S., Rülicke,T. and Aguzzi,A. (1997) Development and malignant progression of astrocytomas in GFAP-v-src transgenic mice. Oncogene *14*, 2005-2013.

Weissman,I.L., Anderson,D.J., and Gage,F. (2001). Stem and progenitor cells: Origins, phenotypes, lineage commitments, and transdifferentiations. Annual Review of Cell and Developmental Biology *17*, 387-403.

Weng,L.P., Brown,J.L., and Eng,C. (2001). PTEN coordinates G(1) arrest by down-regulating cyclin D1 via its protein phosphatase activity and up-regulating p27 via its lipid phosphatase activity in a breast cancer model. Human Molecular Genetics *10*, 599-604.

Wetmore,C., Eberhart,D,E. and Curran,T. (2001). Loss of p53 but not ARF accelerates medulloblastoma in mice heterozygous for patched. Cancer Research *61*, 513-516.

Wichterle,H., Lieberam,I., Porter,J.A., and Jessell,T.M. (2002). Directed Differentiation of Embryonic Stem Cells into Motor Neurons. Cell *110*, 385-397.

Wilhelmsson,U., Eliasson,C., Bjerkvig,R., and Pekny,M. (0 AD). Loss of GFAP expression in high-grade astrocytomas does not contribute to tumor development or progression. Oncogene *22*, 3407-3411.

Wright,M.H., Calcagno,A.M., Salcido,C.D., Carlson,M.D., Ambudkar,S.V., and Varticovski,L. (2008). Brca1 breast tumors contain distinct CD44(+)/CD24(-) and CD133(+) cells with cancer stem cell characteristics. Breast Cancer Research *10*.

Xiao,A., Wu,H., Pandolfi,P.P., Louis,D.N., and Van Dyke,T. (2002). Astrocyte inactivation of the pRb pathway predisposes mice to malignant astrocytoma development that is accelerated by PTEN mutation. Cancer Cell *1*, 157-168.

Yin,A.H., Miraglia,S., Zanjani,E.D., AlmeidaPorada,G., Ogawa,M., Leary,A.G., Olweus,J., Kearney,J., and Buck,D.W. (1997). AC133, a novel marker for human hematopoietic stem and progenitor cells. Blood *90*, 5002-5012.

Zaidi,H.A., Kosztowski,T., Dimeco,F., and Quinones-Hinojosa,A. (2009). Origins and clinical implications of the brain tumor stem cell hypothesis. Journal of Neuro-Oncology *93*, 49-60.

Zbinden,M., Duquet,A., Lorente-Trigos,A., Ngwabyt,S.N., Borges,I., and Altaba,A.R.I. (2010). NANOG regulates glioma stem cells and is essential *in vivo* acting in a cross-functional network with GLI1 and p53. Embo Journal *29*, 2659-2674.

Zeppernick,F., Ahmadi,R., Campos,B., Dictus,C., Helmke,B.M., Becker,N., Lichter,P., Unterberg,A., Radlwimmer,B., and Herold-Mende,C.C. (2008). Stem cell marker CD133 affects clinical outcome in glioma patients. Clinical Cancer Research *14*, 123-129.

Zhang,H.S., Gavin,M., Dahiya,A., Postigo,A.A., Ma,D., Luo,R.X., Harbour J.W., and Dean D.C. (2000). Exit from G1 and S phase of the cell cycle is regulated by repressor complexes containing HDAC-Rb-hSWI/SNF and Rb-hSWI/SNF. Cell *101*, 79-89.

Zhang,J.K., Schweers,B., and Dyer,M.A. (2004). The first knockout mouse model of retinoblastoma. Cell Cycle *3*, 952-959.

Zhang,S.C., Wernig,M., Duncan,I.D., Brustle,O., and Thomson,J.A. (2001). In vitro differentiation of transplantable neural precursors from human embryonic stem cells. Nature Biotechnology *19*, 1129-1133.

Zheng,H., Ying,H., Yan,H., Kimmelman,A.C., Hiller,D.J., Chen,A.J., Perry,S.R., Tonon,G., Chu,G.C., Ding,Z., Stommel,J.M., Dunn,K.L., Wiedemeyer,R., You,M.J., Brennan,C., Wang,Y.A., Ligon,K.L., Wong,W.H., Chin,L., and DePinho,R.A. (2008). p53 and Pten control neural and glioma stem/progenitor cell renewal and differentiation. Nature *455*, 1129-1133.

Zhu,Y.H., Mao,X.O., Sun,Y.J., Xia,Z.G., and Greenberg,D.A. (2002). p38 mitogen-activated protein kinase mediates hypoxic regulation of Mdm2 and p53 in neurons. Journal of Biological Chemistry *277*, 22909-22914.

Zimmerman,L., Lendahl,U., Cunningham,M., McKay,R., Parr,B., Gavin,B., Mann,J., Vassileva,G., and McMahon,A. (1994). Independent regulatory elements in the nestin gene direct transgene expression to neural stem cells or muscle precursors. Neuron *12*, 11-24.

9 Awards and Publications

Promega UK Young Life Scientist Award for 2009:	Top 20 finalist
UCL Queen Square Symposium 2009:	Runner-up
UCL Graduate School Poster Competition 2009:	Runner-up
MRC Centre for Neuromuscular Diseases London Seminar 2008:	Invited guest speaker
Keystone Symposium S3 Abstract Competition 2008:	Scholarship winner
UCL Queen Square Symposium 2008:	1st Place
Mammalian Genetics & Development Conference 2007:	1st Place
UCL Queen Square Symposium 2007:	1st Place

Thomas S Jacques, Alexander Swales, Monika J Brzozowski, Jacqueline M Linehan, Zaman Mirzadeh, Catherine O'Malley, Heike Naumann, Arturo Alvarez-Buylla, Sebastian Brandner. (2010) Combinations of genetic mutations in the adult neural stem cell compartment determine brain tumour phenotypes. *EMBO Journal, 29 (1): 222-235*.

Alexander Swales, Heike Naumann, Nick Henriquez, Thomas Jacques, Sebastian Brandner. (2008) Determining the Brain Tumour "Cell of Origin": can astrocytes initiate tumourigenesis? *(Poster Presentation) Keystone Symposia on Molecular and Cellular Biology - Stem Cells, Cancer and Aging*, #333, p88. Singapore.

Alexander Swales, Heike Naumann, Pedro Cuadrado, Thomas Jacques, Sebastian Brandner. (2007) Neural stem cells differentially govern tumourigenesis within the brain dependant on their early genetic profile. *(Presentation) Genetics Research (The Genetics Society's 18th Mammalian Genetics and Development Workshop)*, 90, p289.

10 Appendix